ULTRACOLD QUANTUM MATTER IN LOWER DIMENSIONS

A Dissertation

Presented to the Faculty of the Graduate School

of Cornell University

in Partial Fulfillment of the Requirements for the Degree of

Doctor of Philosophy

by

Stefan Baur

August 2011

ULTRACOLD QUANTUM MATTER IN LOWER DIMENSIONS

Stefan Baur, Ph.D.

Cornell University 2011

Rapid progress in the field of ultracold atoms allows the study of many new and old models of quantum many-body physics. In this doctoral dissertation we theoretically explore exotic phases of ultracold quantum gases, with a special focus spin-imbalanced attractive Fermi gases in lower dimensional situations.

Chapter 2 reviews the mean-field theory approach to pairing in two-component Fermi gases. Applications of this theory are illustrated in **Chapter 3**, where we discuss mostly well-known results of mean-field theory applied to imbalanced Fermi gases. Adapted from the author's prior publications, **Chapters 4, 5** use the theory developed in **Chapters 2, 3**.

In **Chapter 6** we discuss the physics of Fermi gases, squeezed into one spatial dimension. In this and **Chapter 7**, we go beyond mean-field theory, approaching the problem through the Bethe ansatz, exact solutions to few-body problems and Fermi-Bose mappings ("fermionization"). We also show results from a joint effort with the experimental group of Randy Hulet at Rice University to experimentally realize and probe a strongly interacting one dimensional paired Fermi gas.

In **Chapter 8**, after a brief introduction to rapidly rotating two dimensional Bose gases, we introduce a new protocol to create few atom fractional quantum Hall states.

Finally, in **Chapter 9** we study the effects of two-body losses on lattice Bose gases with hardcore interactions in one and two spatial dimensions.

BIOGRAPHICAL SKETCH

Stefan Baur was born in Heidelberg, Germany, on December 10, 1982 as the first child of his father Klaus, a mechanical engineer, and his mother Marie-Luise, a pharmacist and nutrition chemist.

Together with his younger brother Jörg, he grew up and went to high school in Weinheim, Germany. After receiving his "Abitur" degree from the Werner-Heisenberg-Gymnasium in Weinheim in 2002, he enrolled the same year at the University of Heidelberg, Germany to study physics. After passing his "Vordiplom" in 2004, he got a fellowship to spend the academic year 2005-2006 as an exchange student at Cornell University. After a very enjoyable year (with an unusually mild winter) at the Cornell Physics department, he successfully enrolled in the Physics Ph.D. program in 2006, where he joined the research group of Prof. Erich Mueller at Cornell's Lab of Atomic and Solid-State Physics. During his Ph.D. studies he witnessed first hand the tremendous progress that was happening in the field of ultracold gases. During this exciting time, he worked on a variety of theoretical problems involving strongly correlated quantum gases. After receiving his Ph.D., he will join the Theory of Condensed-Matter group at the Cavendish Lab, University of Cambridge in the UK as a post-doctoral researcher.

To my parents

ACKNOWLEDGEMENTS

together with Marty and Chris at the Chapter House.

I should also thank my many house mates over the years for making my rent affordable. Thanks to Johannes Heinonen, Hitesh Changlani, Leif Ristroph, Ravishankar Sundararaman, Shivam Ghosh and Kshitij Auluck for sharing a roof and being great friends.

Thanks to my girlfriend Natalia for everything and being patient whenever I had to work on this thesis, and to our various friends among the Chapter House/Big Red Barn regulars: Axel, Mary, Leifur and everyone else, whether icelandic or not.

Finally, I would like to thank my friends from high school and college for welcoming me back whenever I came home to Weinheim and Heidelberg!

TABLE OF CONTENTS

LIST OF TABLES

LIST OF FIGURES

xvii

LIST OF PUBLICATIONS

1. Meera M. Parish, Stefan K. Baur, Erich J. Mueller, David A. Huse, *Quasi-one-dimensional polarized Fermi superfluids*, Physical Review Letters **99**, 250403 (2007).

2. Stefan K. Baur, Kaden R. A. Hazzard, Erich J. Mueller, *Stirring trapped atoms into fractional quantum Hall puddles*, Physical Review A **78**, 061608 (R) (2008).

3. Stefan K. Baur, Sourish Basu, Theja N. De Silva, Erich J. Mueller, *Theory of the Normal/Superfluid interface in population imbalanced Fermi gases*, Physical Review A **79**, 013415 (2009).

4. T. A. Corcovilos, Stefan K. Baur, J. M. Hitchcock, E. J. Mueller, R. G. Hulet, *Detecting antiferromagnetism of atoms in an optical lattice via optical Bragg scattering*, Physical Review A **81**, 013415 (2010).

5. Stefan K. Baur, John Shumway, Erich J. Mueller, *FFLO vs Bose-Fermi mixture in polarized 1D Fermi gas on a Feshbach resonance: a 3-body study*, Physical Review A **81**, 033628 (2010).

6. Yean-an Liao, Ann Sophie C. Rittner, Tobias Paprotta, Wenhui Li, Guthrie B. Partridge, Randall G. Hulet, Stefan K. Baur, Erich J. Mueller, *Spin-Imbalance in a One-Dimensional Fermi Gas*, Nature **467**, 567 (2010).

7. Stefan K. Baur, Erich J. Mueller, *Two-body recombination in a quantum mechanical lattice gas: Entropy generation and probing of magnetic short-range correlations*, Physical Review A **82**, 023626 (2010).

CHAPTER 1

ULTRACOLD BOSE AND FERMI GASES

1.1 What are cold gases good for?

Since the creation of the first Bose-Einstein condensate (BEC), the field of ultracold gases has tremendously enhanced our understanding of quantum many-body physics [1, 2, 3, 4]. One can say that the field is now evolving into what might be called quantum engineering. Toy models, introduced as simplifications of complicated solid state systems that contain only the basic, but non-trivial, physics, are now routinely created in atomic physics labs. These cold quantum gases show an unprecedented degree of tunability and control through the interplay of slow motion combined with the high degree of control of quantum optics [5, 6, 7]. While cold gases in the laboratory naturally interact very little with their environment, we often cannot directly harvest the remarkable properties of these systems. Apart from using cold atoms as sensors, their main applications will probably lie in the combination of quantum mechanics and information processing. An early application of this sort was an experiment by Lene Hau at Harvard, where a beam of light was slowed down to a few meters per second, basically stored in a BEC [8]. More recently, cold gases are starting to be used as a tool to simulate simple quantum many-body theories [9, 10]. Certain materials found in nature display quite unusual and puzzling properties. One of these systems are the high temperature (high-T_c) superconductors, whose strongly correlated nature inhibits our understanding. While theorists have found simple models (called model Hamiltonians) that should capture the basic physics of high-T_c superconductors, these models are still far from fully

understood. The reason for this lack of understanding lies in the enormous size of the possible quantum states (Hilbert space) of a quantum system of even few particles and the general difficulty of simulating fermionic particles (like electrons) on a computer. A quantum simulator would be a physical system representing a given model Hamiltonian H, that would allows for its simulation and, through various probes, would pave the way to understand its physics [11]. For new real complex materials, we envision that once we have made a list of basic candidate Hamiltonians, cold atom quantum simulators will allow us to map out their properties (phases of matter), bypassing the complexity of the original problem. That way a quantum simulator allows us to gain information about nature that was previously inaccessible (when working with hardware governed by classical mechanics).

If we can control quantum mechanical particles and phases at will, this opens up new potential applications. The creation of topologically ordered states, either as analogs of fractional quantum hall states or novel forms of superconductivity, is within reach [12, 13, 14]. Bold proposals to build quantum computers with cold neutral gases do not seem completely impossible anymore [15]. In the long run, quantum information might be the field where ultracold gases will have the most impact.

1.2 Quantum gases

When dilute atomic gases are cooled to ultra-low temperatures, quantum mechanics starts to become important. We can heuristically understand this behavior from simple dimensional analysis. A non-interacting classical gas is de-

scribed by a single length-scale, namely the inter-particle spacing $l \sim n^{-1/3}$, where n is the density of a three-dimensional gas. The classical gas must therefore be scale invariant, without any phase transition as the temperature is lowered. Because of their attractive interactions, most gases that we know from everyday life undergo phase transitions to liquid and solid phases at sufficiently low temperatures. This happens when the characteristic energy scale of the ideal gas, $k_B T$, becomes comparable to their interaction energy E_{int}. In dilute gases, interactions are less important and these systems remain gaseous down to very low temperatures. However, quantum mechanics provides us with a new fundamental constant: Planck's constant h. In addition to the inter-particle spacing, there appears another length-scale (thermal de Broglie wavelength)

$$\lambda_T \sim \frac{h}{\sqrt{mk_B T}}. \tag{1.1}$$

We anticipate quantum mechanics to be important when inter-particle spacing and the de Broglie length become comparable, i.e. when

$$k_B T \sim \frac{h^2}{ml^2} \sim \frac{\hbar^2 n^{2/3}}{m}. \tag{1.2}$$

A surprising consequence of quantum mechanics is that identical particles that technically to do not interact feel each other's presence when their wavefunctions overlap. The quantum mechanical wavefunction for two identical particles $\psi(\mathbf{r}_1, \mathbf{r}_2)$ must have the same magnitude (probability density) when the coordinates of the particles are exchanged

$$\psi(\mathbf{r}_1, \mathbf{r}_2) = e^{i\phi} \psi(\mathbf{r}_2, \mathbf{r}_1) \tag{1.3}$$

When we repeat the exchange we expect to get our original wavefunction back, therefore usually one has either $\phi = 0$ or $\phi = \pi$ for bosons or fermions. The ground state of a non-interacting Bose gas of N particles is the state where all

particles occupy the lowest energy single particle orbital

$$\psi_B(\mathbf{r}_1, \ldots, \mathbf{r}_N) = \phi_1(\mathbf{r}_1) \ldots \phi_1(\mathbf{r}_N) \tag{1.4}$$

whereas the ground state of N (spinless) fermions is

$$\psi_F(\mathbf{r}_1, \ldots, \mathbf{r}_N) = \frac{1}{\sqrt{N!}} \begin{vmatrix} \phi_1(\mathbf{r}_1) & \phi_1(\mathbf{r}_2) & \ldots & \phi_1(\mathbf{r}_N) \\ \phi_2(\mathbf{r}_1) & \phi_2(\mathbf{r}_2) & \ldots & \phi_2(\mathbf{r}_N) \\ \vdots & \vdots & \ddots & \vdots \\ \phi_N(\mathbf{r}_1) & \phi_N(\mathbf{r}_2) & \ldots & \phi_N(\mathbf{r}_N) \end{vmatrix} \tag{1.5}$$

where the single particle orbitals $\phi_i(\mathbf{r})$ are chosen such that their energies ϵ_i are the lowest N single particle energies.

1.3 Bose-Einstein condensation

The ground state Eq. (1.4) is a pure Bose-Einstein condensate, where all particles occupy the lowest single particle eigenstate. At finite temperature $T \equiv (k_B \beta)^{-1}$, one finds that the total particle number of a non-interacting Bose gas is given by

$$N = \sum_i n_i \tag{1.6}$$

where the average occupation number n_i of orbital i are given by Bose-Einstein statistics

$$n_i = \frac{1}{e^{\beta(\epsilon_i - \mu)} - 1}. \tag{1.7}$$

For a gas in a box of size L with periodic boundary conditions, the sum in Eq. (1.6) becomes

$$N = \sum_{\mathbf{k}} n_{\mathbf{k}} = \sum_{\mathbf{k}} \frac{1}{e^{\beta(\epsilon_{\mathbf{k}} - \mu)} - 1} \tag{1.8}$$

with $\epsilon_{\mathbf{k}} = \hbar \mathbf{k}^2/(2m)$ and $k_i = 2\pi/L \times$ integer ($i = x, y, z$). When we convert this summation over wave vectors into an integral we obtain

$$n = \frac{N}{L^3} = \int \frac{d^3k}{(2\pi)^3} \frac{1}{e^{\beta(\epsilon_{\mathbf{k}} - \mu)} - 1} = \frac{1}{\sqrt{2}\pi^2} \left(\frac{m}{\hbar^2}\right)^{3/2} \int_0^\infty d\epsilon \frac{\epsilon^{1/2}}{e^{\beta(\epsilon - \mu)} - 1} \tag{1.9}$$

If we now lower T (i.e. increase β) and fix the density n to a specific value we have to increase the value of the chemical potential $\mu < 0$ in order to satisfy Eq. (1.9). However, the integral over energies in Eq. (1.9) is clearly bounded by its value at $\mu = 0$

$$\int_0^\infty d\epsilon \frac{\epsilon^{1/2}}{e^{\beta(\epsilon - \mu)} - 1} \leq \int_0^\infty d\epsilon \frac{\epsilon^{1/2}}{e^{\beta\epsilon} - 1} = \beta^{-3/2} \frac{\sqrt{\pi}}{2} \zeta(3/2). \tag{1.10}$$

For temperatures $T < T_c$, with

$$k_B T_c = \frac{2\pi\hbar^2 n^{2/3}}{m\zeta^{2/3}(3/2)} \tag{1.11}$$

we cannot satisfy Eq. (1.9). The solution to this apparent contradiction is that at $T = T_c$, a finite fraction of bosons starts to occupy the ground state orbital. As the temperature is lowered further, this fraction increases until all bosons are condensed and the state of the system approaches Eq. (1.4) as $T \to 0$. For typical dilute atomic gases with $n \sim 10^{14} \text{cm}^{-3}$, this transition temperature is of the order of a hundred nano Kelvin [16].

1.4 Ultracold Fermi gases and Feshbach resonances

The non-interacting Fermi gas behaves quite different from the Bose gas at low temperatures. Instead of forming a condensate, identical atoms occupy distinct quantum states due to the Pauli exclusion principle. In three dimensions the lowest energy states for fermions lie within a sphere in momentum space of radius k_F. However, when fermions interact via attractive interactions, they can

pair up to form effective bosons (Cooper pairs) that can again form a conden-
sate, similar to the Bose gas. It was shown by Bardeen, Cooper and Schrieffer
(BCS) that the Fermi sea of a weakly attractive two component Fermi gas is un-
stable towards forming a condensate of pairs [17]. Since the transition temper-
ature for a weakly interacting gas is exponentially small, creating a condensate
of pairs with ultracold atoms requires strong interactions. Strong interactions
occur when the s-wave scattering length a_s (related to the low energy scattering
cross section $\sigma(k \rightarrow 0) = 4\pi a_s^2$), becomes large compared to the inter-particle
spacing l. While neutral atoms are typically weakly interacting (i.e. $l \gg |a_s|$),
many mixtures of atomic species feature scattering resonances when subjected
to an external magnetic field. By tuning magnetic bias fields close to these Fes-
hbach resonances, experimentalists were able to control interactions and reach
regimes of strong many-body interactions [18, 19, 20, 21, 22]. Near a Feshbach
resonance, the atomic scattering length varies as [23, 6]

$$a_s(B) = a_{bg} \left(1 - \frac{\Delta}{B - B_0} \right) \tag{1.12}$$

where a_{bg} is the background scattering length, B_0 is location and Δ is the width
of the resonance.

In this thesis we are mostly interested in a two-species mixture of ^{6}Li, where
the lowest two hyperfine states display a Feshbach resonance at $B =$834 G with
a width of $\Delta = -300$ G and $a_{bg} = -1405$ Bohr [25]. To understand the origin of
this scattering resonance, consider the hyperfine structure of an alkali atom in a
magnetic field, described by

$$H_{hfs} = a_{hf}\mathbf{I} \cdot \mathbf{S} + \left(2\mu_B S_z - \mu_n I_z \right) B_z \tag{1.13}$$

where I (S) is the nuclear (electron) spin, respectively. For ^{6}Li one has $I = 1$
resulting in a hyperfine splitting into states with $F = I + 1/2 = 3/2$ and

6
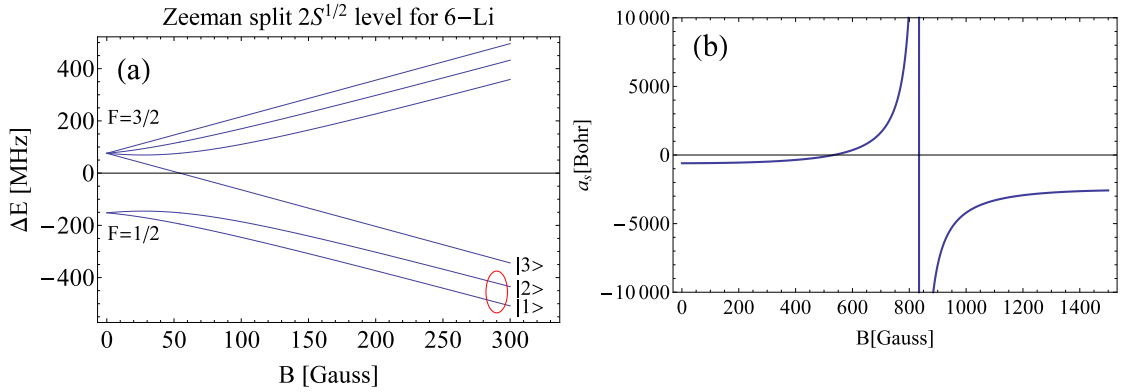
Figure 1.1: (a) shows the hyperfine structure of ^{6}Li as a function of magnetic field B. The lowest two hyperfine states are used in many experiments with ultracold Fermi gases. (b) Scattering length a_s as a function of magnetic field B for collisions between the two lowest hyperfine states $|1\rangle, |2\rangle$ (using the parameterization of Ref. [24]). Notable features are a broad Feshbach resonance at $B = 834$ G (this is where most experiments are performed). Other features special to ^{6}Li are the zero crossing around 500 G and the large negative scattering length at high fields (i.e. the deep BCS limit is inaccessible).

$F = I - 1/2 = 1/2$. In a large magnetic field, the levels Zeeman split according to their electron spin and then, via the nuclear magnetic moment $\mu_n \ll \mu_B$ into $m_I = -1, 0, 1$ as shown in Fig. 1.1. The two lowest hyperfine states in a large magnetic field are therefore approximately the states $|1\rangle \approx |m_s = -1/2, m_I = 1\rangle$ and $|2\rangle \approx |m_s = -1/2, m_I = 0\rangle$ [4]. Regarding the electronic spin, these states are triplet states with some small admixture of states with $m_s = -1/2$ caused by the hyperfine interaction. Typically the interaction potential for alkali atoms is diagonal in the total electron spin, i.e. it can be decomposed into a singlet and triplet potential. Naively one would think the interaction between ^{6}Li atoms should be mostly described by scattering via the triplet potential (which gives rise to the background scattering length a_{bg}). However, because of the hyperfine mixing, whenever a bound-state in the singlet channel coincides with the threshold in the triplet channel, a scattering resonance occurs [26].

A simple model that can serve in many situations as an equivalent description of a Feshbach resonance is the attractive square well potential of depth $V_0 < 0$ and range r_0. In the limit where r_0 is much shorter than the inter-particle spacing (imagine r_0 to be of the order of the size of an atom), low energy scattering of the square well is described by the s-wave scattering length a_s. Tuning the potential depth V_0 allows to change the scattering length from small and negative for low potential depth to small and positive when the potential well is very deep. When the two-body bound state energy crosses zero energy, the s-wave scattering becomes resonant, $a_s = \infty$.

1.5 Appendix A: Effective models for scattering near a Feshbach resonance

A useful effective theory, valid near a Feshbach resonance, is given by the two-channel model where a bosonic molecular state at energy ν is coupled to the continuum via an effective local Feshbach coupling η. This model is most conveniently written in second quantized notation as

$$
\begin{align}
H &= H_a + H_m + H_{am} \tag{1.14}\\
H_a &= \int d^3r \sum_{\sigma=1,2} \psi_\sigma^\dagger(\mathbf{r}) \left(-\frac{\hbar^2 \nabla^2}{2m}\right) \psi_\sigma(\mathbf{r}) \tag{1.15}\\
H_m &= \int d^3r \ \phi^\dagger(x) \left(-\frac{\hbar^2 \nabla^2}{4m} + \nu\right) \phi(x) \tag{1.16}\\
H_{am} &= \eta \int d^3r \ \phi^\dagger(x) \psi_1(x) \psi_2(x) + \text{h.c} \tag{1.17}
\end{align}
$$

where $1, 2$ label the two lowest hyperfine states of ^{6}Li and the bosonic field operator $\phi(x)$ describes a closed channel molecule. On resonance, where $\nu = 0$, the energy of the closed channel molecule is degenerate with the energy of the

incoming atomic channel. While this theory is a convenient effective descrip-
tion of the physics near a Feshbach resonance, often we can use an even simpler
model, effectively integrating out the molecular channel. Such a theory will
be described solely by the s-wave scattering length a_s, instead of the two pa-
rameters η and ν. For degenerate Fermi gases, such a simplification is possible
whenever the scattering length as a function of momentum k does not vary ap-
preciably over a Fermi momentum k_F (often called a broad resonance). For the
broad Feshbach resonance in ^{6}Li, the single channel model, with Hamiltonian

$$H = H_a + H_{int} \tag{1.18}$$

$$H_{int} = g \int d^3r \ \psi_1^\dagger(\mathbf{r})\psi_2^\dagger(\mathbf{r})\psi_2(\mathbf{r})\psi_1(\mathbf{r}) \tag{1.19}$$

is sufficient [27]. This model is equivalent to the attractive square well potential
in the limit of $r_0 \to 0$. The price for using these effective theories, Eqs. (1.14),
(1.18), is that the parameters appearing in the Hamiltonian are effective parame-
ters that have to be matched to observables. For the Hamiltonian Eq. (1.18), we
can calculate the scattering length by solving the Lippmann-Schwinger equa-
tion for the T-Matrix [28]

$$T = V + V G_0^{(+)} T \tag{1.20}$$

where the local interaction V has $V_{\mathbf{k}\mathbf{k}'} = g/L^3$ (L^3 is the volume of space). The
retarded Green's function $G_0^{(+)}$ for the free Hamiltonian H_a is given by

$$\left[G_0^{(+)}\right]_{\mathbf{k}\mathbf{k}'} = \frac{\delta_{\mathbf{k}\mathbf{k}'}}{E - \epsilon_{\mathbf{k}} + i\eta} \tag{1.21}$$

where $\epsilon_{\mathbf{k}} = \hbar^2 \mathbf{k}^2/2\mu$ (with the effective mass $\mu = m/2$). Eq. (1.20) is solved by

$$T_{\mathbf{k}\mathbf{k}'}(E) = \frac{g/L^3}{1 - g\Theta(E)} \tag{1.22}$$

where

$$\Theta(E) = \frac{1}{L^3} \sum_{\mathbf{k}} \frac{1}{E - \epsilon_{\mathbf{k}} + i\eta}. \tag{1.23}$$

9

Formally the real part of the sum Eq. (1.23) diverges at large momenta and should be cut off at some scale Λ. The on-shell T-Matrix is related to the scattering amplitude via [28]

$$f(k) = -\frac{\mu L^3}{2\pi\hbar^2} T(E = \hbar^2 k^2/2m) \tag{1.24}$$

In the limit $k \to 0$ with $f(k) \approx -a_s$ one has

$$g^{-1} = \frac{\mu}{2\pi\hbar^2 a_s} + \theta(E = 0) \tag{1.25}$$

This formula relates the bare coupling strength g to the physical observable scattering length a_s.

BIBLIOGRAPHY FOR CHAPTER 1

[1] M. H. Anderson, J. R. Ensher, M. R. Matthews, C. E. Wieman, and E. A. Cornell, Science **269**, 198 (1995).

[2] C. C. Bradley, C. A. Sackett, J. J. Tollett, and R. G. Hulet, Phys. Rev. Lett. **75**, 1687 (1995).

[3] K. B. Davis, M. O. Mewes, M. R. Andrews, N. J. van Druten, D. S. Durfee, D. M. Kurn, and W. Ketterle, Phys. Rev. Lett. **75**, 3969 (1995).

[4] Immanuel Bloch, Jean Dalibard, and Wilhelm Zwerger, Rev. Mod. Phys. **80**, 885 (2008).

[5] Y. J. Lin, R. L. Compton, K. Jimenez-Garcia, J. V. Porto, and I. B. Spielman, Nature **462**, 628 (2009).

[6] Cheng Chin, Rudolf Grimm, Paul Julienne, and Eite Tiesinga, Rev. Mod. Phys. **82**, 1225 (2010).

[7] Christof Weitenberg, Manuel Endres, Jacob F. Sherson, Marc Cheneau, Peter Schausz, Takeshi Fukuhara, Immanuel Bloch, and Stefan Kuhr, Nature **471**, 319 (2011).

[8] Lene Vestergaard Hau, S. E. Harris, Zachary Dutton, and Cyrus H. Behroozi, Nature **397**, 594 (1999).

[9] Adrian Cho, Science **320**, 312 (2008).

[10] Science **330**, 1605 (2010).

[11] R. P. Feynman, International Journal of Theoretical Physics **21**, 467 (1982).

[12] N. R. Cooper and G. V. Shlyapnikov, Physical Review Letters **103**, 155302 (2009).

[13] N. R. Cooper, Phys. Rev. Lett. **106**, 175301 (2011).

[14] P. Bonderson, S. Das Sarma, M. Freedman, and C. Nayak, ArXiv e-prints (2010).

[15] C. Weitenberg, S. Kuhr, K. Mølmer, and J. F. Sherson, ArXiv e-prints (2011).

[16] M. Vengalattore, J. Guzman, S. R. Leslie, F. Serwane, and D. M. Stamper-Kurn, Phys. Rev. A **81**, 053612 (2010).

[17] J. Bardeen, L. N. Cooper, and J. R. Schrieffer, Phys. Rev. **108**, 1175 (1957).

[18] S. Jochim, M. Bartenstein, A. Altmeyer, G. Hendl, S. Riedl, C. Chin, J. Hecker Denschlag, and R. Grimm, Science **302**, 2101 (2003).

[19] Kevin E. Strecker, Guthrie B. Partridge, and Randall G. Hulet, Phys. Rev. Lett. **91**, 080406 (2003).

[20] M. W. Zwierlein, C. A. Stan, C. H. Schunck, S. M. F. Raupach, A. J. Kerman, and W. Ketterle, Phys. Rev. Lett. **92**, 120403 (2004).

[21] T. Bourdel, L. Khaykovich, J. Cubizolles, J. Zhang, F. Chevy, M. Teichmann, L. Tarruell, S. J. J. M. F. Kokkelmans, and C. Salomon, Phys. Rev. Lett. **93**, 050401 (2004).

[22] C. A. Regal, M. Greiner, and D. S. Jin, Phys. Rev. Lett. **92**, 040403 (2004).

[23] A. J. Moerdijk, B. J. Verhaar, and A. Axelsson, Phys. Rev. A **51**, 4852 (1995).

[24] M. Bartenstein, A. Altmeyer, S. Riedl, R. Geursen, S. Jochim, C. Chin, J. Hecker Denschlag, R. Grimm, A. Simoni, E. Tiesinga, C. J. Williams, and P. S. Julienne, Phys. Rev. Lett. **94**, 103201 (2005).

[25] M. Bartenstein, A. Altmeyer, S. Riedl, S. Jochim, C. Chin, J. Hecker Denschlag, and R. Grimm, Phys. Rev. Lett. **92**, 120401 (2004).

[26] M. Houbiers, H. T. C. Stoof, W. I. McAlexander, and R. G. Hulet, Phys. Rev. A **57**, R1497 (1998).

[27] Roberto B. Diener and Tin-Lun Ho, arXiv:cond-mat/0405174 (2004).

[28] Erich J. Mueller, Ph.D. thesis, University of Illinois at Urbana-Champaign, 2001.

CHAPTER 2

MEAN-FIELD THEORY FOR SUPERFLUID FERMI GASES —

BOGOLIUBOV-DE GENNES EQUATIONS

2.1   General setup

This chapter introduces formal tools to describe superfluid ultracold Fermi gases with attractive interactions. This chapter is self-contained and we will not use any Green's functions or advanced machinery like coherent state path integrals. This approach is very much in the original spirit of de Gennes book [1]. The following two chapters contain various applications of the formalism developed here. We consider a two species Fermi gas, where we label the species spin-$\uparrow$ and -$\downarrow$[1], interacting via an s-wave short range interaction is described by the Hamiltonian

$$H \;\;=\;\; H_0 + H_{int} - \mu_\uparrow N_\uparrow - \mu_\downarrow N_\downarrow \tag{2.1}$$

where the kinetic and interaction parts are given by

$$H_0 \;\;=\;\; \int d^d r \sum_\sigma -\frac{\hbar^2}{2m} \Psi_\sigma^\dagger(\mathbf{r}) \nabla^2 \Psi_\sigma(\mathbf{r}) \tag{2.2}$$

$$H_{int} \;\;=\;\; g \int d^d r \Psi_\uparrow^\dagger(\mathbf{r}) \Psi_\downarrow^\dagger(\mathbf{r}) \Psi_\downarrow(\mathbf{r}) \Psi_\uparrow(\mathbf{r}) \tag{2.3}$$

Here d is the dimension of space, μ_σ are the chemical potentials of the spin-$\uparrow$ and -$\downarrow$ fermions, and $\Psi_\sigma^\dagger(\mathbf{r}), \Psi_\sigma(\mathbf{r})$ are the fermionic creation and annihilation operators satisfying the usual fermionic anti-commutation relations

$$\{\Psi_\sigma(\mathbf{r}), \Psi_{\sigma'}^\dagger(\mathbf{r}')\} = \delta^{(3)}(\mathbf{r} - \mathbf{r}')\delta_{\sigma\sigma'} \quad \{\Psi_\sigma(\mathbf{r}), \Psi_{\sigma'}(\mathbf{r}')\} = 0 \quad \{\Psi_\sigma^\dagger(\mathbf{r}), \Psi_{\sigma'}^\dagger(\mathbf{r}')\} = 0$$

---

[1]When we are talking about cold atoms, these spins are pseudospins representing two distinct hyperfine states. A typical example would be the two lowest hyperfine states of ^{6}Li in a strong magnetic field.

The (bare) coupling constants $g < 0$ describes the strength of the interactions between the different spin components. As described in chapter 1, in cold atom experiments, this coupling strength can be tuned over a wide range of parameters. An analytical solution of the full Hamiltonian Eq. (2.1) is not known[2].

2.2 Mean-field approximation

In the mean-field approximation (sometimes called mean-field decoupling) of the interaction term, one writes

$$\psi_\downarrow(\mathbf{r})\psi_\uparrow(\mathbf{r}) = \underbrace{(\psi_\downarrow(\mathbf{r})\psi_\uparrow(\mathbf{r}) - \langle\psi_\downarrow(\mathbf{r})\psi_\uparrow(\mathbf{r})\rangle)}_{\text{fluctuation}} + \underbrace{\langle\psi_\downarrow(\mathbf{r})\psi_\uparrow(\mathbf{r})\rangle}_{\equiv\Delta(\mathbf{r})/g} \qquad (2.4)$$

and neglects second order terms in the fluctuation of the pairing field $\Delta(\mathbf{r}) = g\langle\psi_\downarrow(\mathbf{r})\psi_\uparrow(\mathbf{r})\rangle$

$$H_{int} \approx \int d^d r \, \Delta^*(\mathbf{r})\psi_\uparrow(\mathbf{r})\psi_\downarrow(\mathbf{r}) + \Delta(\mathbf{r})\psi_\downarrow^\dagger(\mathbf{r})\psi_\uparrow^\dagger(\mathbf{r}) - \frac{1}{g}|\Delta(\mathbf{r})|^2 \qquad (2.5)$$

This Hamiltonian can be diagonalized for fixed $\Delta(\mathbf{r})$ since it is a quadratic form in the creation and annihilation operators. Note that one could also have performed the mean-field coupling in a different channel, combining pairing with Hartree-Fock. Including both, Hartree-Fock and pairing channels, is the Hartree-Fock-Bogoliubov theory described in de Gennes book. We choose not to include Hartree-Fock terms as the bare coupling constant g appears in the resulting equations. In the weak coupling BCS limit $a_s \to 0-$ one may proceed by using the Born approximation $g = 4\pi\hbar^2 a_s/m$. It is not entirely clear how to consistently incorporate Hartree-Fock terms in the unitary limit.

---

[2]In the special case $d = 1$, the quantum mechanical problem of $N_\uparrow$ spin-up and $N_\downarrow$ spin-down fermions, interacting with a contact interaction, can be solved exactly with the Bethe ansatz. The consequences of this solutions will be discussed in the chapters on 1D systems.

In the mean-field approximation (2.5) the Hamiltonian H becomes

$$
\begin{aligned}
H = {} & \int d^d r \left(\Psi_\uparrow^\dagger(\mathbf{r}), \quad \Psi_\downarrow(\mathbf{r}) \right) \begin{pmatrix} -\frac{\hbar^2}{2m}\nabla^2 - \mu_\uparrow & \Delta(\mathbf{r}) \\ \Delta^*(\mathbf{r}) & -\left(-\frac{\hbar^2}{2m}\nabla^2 - \mu_\downarrow\right) \end{pmatrix} \begin{pmatrix} \Psi_\uparrow(\mathbf{r}) \\ \Psi_\downarrow^\dagger(\mathbf{r}) \end{pmatrix} \\
& - \int d^d r \frac{|\Delta(\mathbf{r})|^2}{g} + \text{Tr}\left[-\frac{\hbar^2}{2m}\nabla^2 - \mu_\downarrow \right].
\end{aligned} \tag{2.6}
$$

This Hamiltonian is readily diagonalized by solving the Bogoliubov-de Gennes equations

$$
\begin{pmatrix} -\frac{\hbar^2}{2m}\nabla^2 - \mu & \Delta(\mathbf{r}) \\ \Delta^*(\mathbf{r}) & -\left(-\frac{\hbar^2}{2m}\nabla^2 - \mu\right) \end{pmatrix} \begin{pmatrix} u_n(\mathbf{r}) \\ v_n(\mathbf{r}) \end{pmatrix} = E_n \begin{pmatrix} u_n(\mathbf{r}) \\ v_n(\mathbf{r}) \end{pmatrix}, \tag{2.7}
$$

where we introduced the average chemical potential $\mu = (\mu_\uparrow + \mu_\downarrow)/2$ and the chemical potential difference $h = \mu_\uparrow - \mu_\downarrow$[3]. Note that all eigenvalues E_n come in pairs: if E_n is an eigenvalue, so is $-E_n$. Our convention will be that we denote the positive eigenvalues by $E_n > 0$ and the corresponding eigenvector $\phi_n^{(+)} = (u_n(\mathbf{r}), v_n(\mathbf{r}))^T$. One can then easily see that the orthogonal vector $\phi_n^{(-)} = (-v_n^*(\mathbf{r}), u_n^*(\mathbf{r}))^T$ is an eigenvector with eigenvalue $-E_n$. A set of mutually orthogonal eigenvectors $\phi_n^\pm$ is then complete. The Hamiltonian is expressed in terms of non-interacting[4] Bogoliubov quasiparticles by the transformation

$$
\begin{pmatrix} \Psi_\uparrow(\mathbf{r}) \\ \Psi_\downarrow^\dagger(\mathbf{r}) \end{pmatrix} = \sum_n U_n \begin{pmatrix} \gamma_{\uparrow n} \\ \gamma_{\downarrow n}^\dagger \end{pmatrix} \tag{2.8}
$$

where the unitary matrices U_n are given by

$$
U_n = \begin{pmatrix} u_n(\mathbf{r}) & -v_n^*(\mathbf{r}) \\ v_n(\mathbf{r}) & u_n^*(\mathbf{r}) \end{pmatrix} \tag{2.9}
$$

Note that the U_n would not be unitary in the Bogoliubov theory of bosons. Here these Bogoliubon creation and annihilation operators satisfy Fermi commuta-

---

[3] h is analogous to a Zeeman magnetic field in solid-state system.
[4] Noninteracting within mean-field theory.

tion relations

$$\{\gamma_{\sigma n}, \gamma_{\sigma'n'}^\dagger\} = \delta_{\sigma\sigma'}\delta_{nn'} \quad \{\gamma_{\sigma n}, \gamma_{\sigma'n'}\} = 0 \quad \{\gamma_{\sigma n}^\dagger, \gamma_{\sigma'n'}^\dagger\} = 0 \tag{2.10}$$

This gives

$$H = \sum_{\sigma,n} E_{\sigma n}\gamma_{\sigma n}^\dagger\gamma_{\sigma n} + \sum_n (\epsilon_n - \mu) - \int d^d r \frac{|\Delta(\mathbf{r})|^2}{g} \tag{2.11}$$

with $E_{\sigma n} = E_n + \sigma h$ and $\sum_n \epsilon_n - \mu = \text{Tr}\left[-\frac{\nabla^2}{2m} - \mu\right]^5$. Self-consistency requires

$$\Delta(\mathbf{r}) = g\langle\psi_\downarrow(\mathbf{r})\psi_\uparrow(\mathbf{r})\rangle = g\sum_n u_n^*(\mathbf{r})v_n(\mathbf{r})\left[1 - f(E_{\uparrow n}) - f(E_{\downarrow n})\right] \tag{2.12}$$

Here $f(E) = 1/(1 + e^{E/(k_B T)})$ is the Fermi-Dirac distribution and we have used $\langle\gamma_{\sigma n}^\dagger\gamma_{\sigma'n'}\rangle = f(E_{\sigma n})\delta_{\sigma\sigma'}\delta_{nn'}$. Eq. (2.12) is often also called gap equation. It is worth noting that the superfluid order parameter $\Delta(\mathbf{r})$ is only equal to (twice) the gap in the fermion spectrum when the order parameter field is uniform. A self-consistent solution solves both the BdG equations and the gap equation simultaneously. The equilibrium state of the system is described by the self-consistent solution that has the lowest free energy $\Omega = \langle H \rangle - TS$. A valid numerical approach would be to start with an initial guess for $\Delta(\mathbf{r})$ and then iteratively solve BdG and gap equations until convergence is achieved, and then compute the corresponding free energies. When dealing with phase transitions and competing phases it is more convenient to use a formalism where a we directly calculate and minimize the free energy.

Finally, we note that the number densities are given by

$$n_\sigma(\mathbf{r}) = \langle\psi_\sigma^\dagger(\mathbf{r})\psi_\sigma(\mathbf{r})\rangle \tag{2.13}$$

$$= \sum_n |u_n(\mathbf{r})|^2 f(E_{n\sigma}) + |v_n(\mathbf{r})|^2\left[1 - f(E_{n,-\sigma})\right] \tag{2.14}$$

---

[5]In principle one could also include any external potential, e.g. a trapping potential $V(\mathbf{r})$ into the single particle eigenvalues ϵ_n.

While it is more convenient to do calculations in a grand canonical ensemble at fixed chemical potentials, we often adjust chemical potentials to constrain the directly measurable particle numbers N_σ.

2.3   Variational principle

An alternative but equivalent approach to derive the results of the previous section is to guess a trial Hamiltonian H_T and then use the variational principle. This will also tell us that mean-field theory gives a rigorous upper bound to the groundstate energy (or finite temperature free energy). An educated guess for H_T is

$$H_T = H_0 - \mu_\uparrow N_\uparrow - \mu_\downarrow N_\downarrow + \int d^d r \, \Delta^*(\mathbf{r})\psi_\uparrow(\mathbf{r})\psi_\downarrow(\mathbf{r}) + \Delta(\mathbf{r})\psi_\downarrow^\dagger(\mathbf{r})\psi_\uparrow^\dagger(\mathbf{r}) \quad (2.15)$$

The variational principle for the free energy Ω then states that [2]

$$\Omega \leq \Omega_T + \langle H - H_T \rangle_T = \langle H \rangle_T - TS_T \quad (2.16)$$

When varying the trial order parameter $\Delta(\mathbf{r})$, the best approximation to the free energy is when the functional $\Omega_{MF}[\Delta(\mathbf{r})] = \langle H \rangle_T - TS_T$ is minimal. We calculate

$$\langle H - H_T \rangle_T = -\int d^d r \frac{|\Delta(\mathbf{r})|^2}{g} + g n_\uparrow(\mathbf{r}) n_\downarrow(\mathbf{r}) \quad (2.17)$$

The last term is again the Hartree term and we will neglect this term for the reasons explained previously. The total mean-field free energy is then

$$\Omega_{MF} = \Omega_T - \int d^d r \frac{|\Delta(\mathbf{r})|^2}{g} \quad (2.18)$$

From standard statistical mechanics we know that for a grand canonical partition function $Z_T = \mathrm{Tr}\, e^{-\beta H_T}$, the free energy is given by

$$\Omega_T = -k_B T \log(Z_T) = \sum_n (\epsilon_n - \mu) - k_B T \sum_{\sigma,n} \log\left(1 + e^{-\beta E_{\sigma n}}\right) \quad (2.19)$$

After some simplification we construct the final result of the variational free energy

$$\Omega_{MF}[\Delta(\mathbf{r})] = \frac{1}{2}\sum_{n\sigma}\left(\epsilon_n - \mu - 2k_BT\log\left[2\cosh\frac{\beta E_{n\sigma}}{2}\right]\right) - \int d^d r\frac{|\Delta(\mathbf{r})|^2}{g} \quad (2.20)$$

This formula for the free energy is sometimes attributed to Eilenberger [3, 4]. The beauty of this results is that it expresses the free energy solely in terms of the order parameter $\Delta(\mathbf{r})$ and the energies of the Bogoliubov-de Gennes equation Eq. (2.7). We find the stationary point of the free energy by varying $\Delta(\mathbf{r}) \to \Delta(\mathbf{r}) + \delta\Delta(\mathbf{r})$. Standard first order perturbation theory on the eigenvalues E_n of the BdG equations gives

$$\delta E_n = \left(\phi_n^+, V_{pert}\phi_n^+\right) = \int d^d r\,\delta\Delta(\mathbf{r})u_n(\mathbf{r})v_n^*(\mathbf{r}) + \delta\Delta^*(\mathbf{r})u_n^*(\mathbf{r})v_n(\mathbf{r}) \quad (2.21)$$

with perturbation

$$V_{pert} = \begin{pmatrix} 0 & \delta\Delta(\mathbf{r}) \\ \delta\Delta^*(\mathbf{r}) & 0 \end{pmatrix}. \quad (2.22)$$

The variation of the free energy is

$$\begin{aligned}
\frac{\delta\Omega_{MF}[\Delta(\mathbf{r})]}{\delta\Delta^*(\mathbf{r})} &= -\frac{1}{2}\sum_n \tanh\frac{\beta E_{n\sigma}}{2}\frac{\delta E_{n\sigma}}{\delta\Delta^*(\mathbf{r})} - \frac{1}{g}\Delta(\mathbf{r}) \quad (2.23)\\
&= \sum_n u_n^*(\mathbf{r})v_n(\mathbf{r})\left[f(E_{\uparrow n}) + f(E_{\downarrow n}) - 1\right] - \frac{1}{g}\Delta(\mathbf{r})
\end{aligned}$$

Requiring a stationary free energy we obtain the gap equation Eq. (2.12) derived previously. The explicit formula Eq. (2.23) for the gradient of the free energy is useful for finding a self-consistent numerical solution to the BdG equations. Multivariable minimization algorithms such as the Broyden-Fletcher method can be used when a fast computation of the gradient is possible. Using these methods is in general faster and more stable than simply iterating the gap equation to self-consistency.

2.4 Gradient expansion

When $\Delta(\mathbf{r})$ is small and varies slowly in space, it is valid to expand the free energy in powers of $\Delta(\mathbf{r})$. Expanding to 4th order in $\Delta(\mathbf{r})$ and keeping only the lowest order gradients gives a microscopic derivation of Landau-Ginzburg theory. Here we will derive an approximation to the free energy of the form

$$\Omega_{MF}[\Delta(\mathbf{r})] \approx \int d^d r d^d r' \, \Delta^*(\mathbf{r}) K(\mathbf{r}, \mathbf{r}') \Delta(\mathbf{r}') + \int d^d r \, V[\Delta(\mathbf{r})] \qquad (2.24)$$

The potential $V(\Delta)$ does not include gradient terms and is given by evaluating the free energy density for a homogenous order parameter $V(\Delta) \equiv \Omega_{MF}(\Delta)/L^d$, where L^d stands for the volume space. The kernel of the gradient term is given by the second variation of the free energy [minus the term already included in the homogenous free energy $V(\Delta)$]

$$K(\mathbf{r}, \mathbf{r}') = \underbrace{\frac{\delta^2 \Omega_{MF}[\Delta(\mathbf{r})]}{\delta\Delta(\mathbf{r})\delta\Delta(\mathbf{r}')}}_{K^{(2)}(\mathbf{r},\mathbf{r}')} - V''[\Delta(\mathbf{r})] \Bigg|_{\Delta(\mathbf{r})=0} \qquad (2.25)$$

In order to compute $K(\mathbf{r}, \mathbf{r}')$ we need the correction to the eigenvalues to 2nd order in $\Delta(\mathbf{r})$ (the 1st order term is zero since $\Delta(\mathbf{r}) = 0$ is always a stationary point of Ω_{MF}). When expanding around the free solution, it is more convenient to use a different basis of solutions to the BdG equations

$$\psi_{\mathbf{k}}^p = \frac{1}{L^{d/2}} \begin{pmatrix} 0 \\ 1 \end{pmatrix} e^{i\mathbf{k}\cdot\mathbf{r}} \qquad \psi_{\mathbf{k}}^h = \frac{1}{L^{d/2}} \begin{pmatrix} 1 \\ 0 \end{pmatrix} e^{i\mathbf{k}\cdot\mathbf{r}}. \qquad (2.26)$$

These solutions correspond the particle (p) and hole (h) branches and have energies $\xi_{\mathbf{k}} = \epsilon_{\mathbf{k}} - \mu$ and $-\xi_{\mathbf{k}}$. Second order perturbation theory for the particle

energies gives (note that the scalar product $(\psi_{\mathbf{k}}^{p,h}, V_{pert}\psi_{\mathbf{k}}^{p,h}) = 0$)

$$\delta E_{\mathbf{k}}^{(2)} = \sum_{\mathbf{k}'} \frac{|(\psi_{\mathbf{k}}^{p}, V_{pert}\psi_{\mathbf{k}'}^{h})|^2}{\xi_{\mathbf{k}} + \xi_{\mathbf{k}'}} \tag{2.27}$$

$$= \sum_{\mathbf{k}'} \frac{1}{\xi_{\mathbf{k}} + \xi_{\mathbf{k}'}} \left| \frac{1}{L^d} \int d^d r\, e^{i(\mathbf{k}'-\mathbf{k})\cdot\mathbf{r}} \Delta(\mathbf{r}) \right|^2 \tag{2.28}$$

$$= \sum_{\mathbf{k}'} \frac{|\Delta_{\mathbf{k}-\mathbf{k}'}|^2}{\xi_{\mathbf{k}} + \xi_{\mathbf{k}'}} \tag{2.29}$$

The change in free energy to 2nd order in $\Delta(\mathbf{r})$ (we use again formula (2.23)) is then

$$\delta\Omega_{MF}^{(2)} = \sum_{\mathbf{k},\mathbf{k}'} [f(\xi_{\uparrow\mathbf{k}}) + f(\xi_{\downarrow\mathbf{k}}) - 1] \frac{|\Delta_{\mathbf{k}-\mathbf{k}'}|^2}{\xi_{\mathbf{k}} + \xi_{\mathbf{k}'}} - \frac{1}{g} \int d^d r |\Delta(\mathbf{r})|^2 \tag{2.30}$$

$$= L^d \sum_{\mathbf{q}} K^{(2)}(q) |\Delta_{\mathbf{q}}|^2 \tag{2.31}$$

where we introduced $\xi_{\sigma,\mathbf{k}} = \xi_{\mathbf{k}} + \sigma h$ and

$$K^{(2)}(q) = \frac{1}{L^d} \sum_{\mathbf{k}} \frac{f(\xi_{\uparrow\mathbf{k}+\mathbf{q}/2}) + f(\xi_{\downarrow\mathbf{k}-\mathbf{q}/2}) - 1}{\xi_{\mathbf{k}+\mathbf{q}/2} + \xi_{\mathbf{k}-\mathbf{q}/2}} - \frac{1}{g} \tag{2.32}$$

Note that we shifted momenta $\mathbf{k} \to \mathbf{k}+\mathbf{q}/2$, $\mathbf{k}' \to \mathbf{k}-\mathbf{q}/2$ and used the symmetry $\mathbf{q} \to -\mathbf{q}$ to create a more manifestly symmetric expression. The kernel $K^{(2)}(q)$ can be used to study instabilities of the normal state towards pairing. A negative eigenvalue of the kernel signals an instability, i.e. whenever there exists a $\mathbf{q}$ such that $K^{(2)}(q) < 0$ the normal state is unstable (Thouless criterion [5]). When such an instability happens at finite $\mathbf{q} \neq 0$, the normal state is unstable towards a phase with finite momentum pairing (i.e. the FFLO state [6, 7]) [6]. The advantage of the gradient expansion is that we do not have to solve the complicated BdG equations. The disadvantages are the limited validity of the approach and the lack of information about Bogoliubov quasiparticles.

---

[6]Of course one needs to be careful here. When such a phase transition is first order, this criterion will only give the spinodal line and not the location of the phase transition itself. In this case one has to keep higher orders in $\Delta(\mathbf{r})$

2.5 Summary

In this chapter we developed the basic theory to describe fermion superfluids with spin-imbalance. The important tools are

- A formula for the mean-field free energy in terms of eigenvalues of the BdG equations

$$\Omega_{MF}[\Delta(\mathbf{r})] = \frac{1}{2}\sum_{n\sigma}\left(\epsilon_n - \mu - 2k_BT\log\left[2\cosh\frac{\beta E_{n\sigma}}{2}\right]\right) - \int d^dr \frac{|\Delta(\mathbf{r})|^2}{g}$$

- The gradient of the free energy functional

$$\frac{\delta\Omega_{MF}[\Delta(\mathbf{r})]}{\delta\Delta^*(\mathbf{r})} = \sum_n u_n^*(\mathbf{r})v_n(\mathbf{r})\left[1 - f(E_{\uparrow n}) - f(E_{\downarrow n})\right] + \frac{1}{g}\Delta(\mathbf{r})$$

- A gradient expansion of the free energy

$$\Omega_{MF} \approx \int d^dr\, \Delta^*(\mathbf{r})K^{(2)}(\mathbf{r}-\mathbf{r}')\Delta(\mathbf{r}) + O(\Delta^4) \tag{2.33}$$

In the next chapter we will solve this theory in various limits to illustrate the interplay of pairing and spin-imbalance in strongly interacting Fermi gases.

BIBLIOGRAPHY FOR CHAPTER 2

[1] P. G. de Gennes, *Superconductivity of Metals and Alloys* (W.A. Benjamin, New York, 1966).

[2] R. P. Feynman, Phys. Rev. **97**, 660 (1955).

[3] G. Eilenberger, Z. Physik **184**, 427 (1965).

[4] John Bardeen, R. Kümmel, A. E. Jacobs, and L. Tewordt, Phys. Rev. **187**, 556 (1969).

[5] David J. Thouless, Annals of Physics **10**, 553 (1960).

[6] Peter Fulde and Richard A. Ferrell, Phys. Rev. **135**, A550 (1964).

[7] A. I. Larkin and Yu. N. Ovchinnikov, Sov. Phys. JETP **20**, 762 (1965).

APPLICATIONS OF BOGOLIUBOV-DE GENNES THEORY TO ULTRACOLD ATOMS

3.1 BEC-BCS crossover

The BEC-BCS crossover is parametrized by $k_F a_s$ where $k_F = (3\pi^2 n_0)^{1/3}$ is the Fermi momentum in terms of the number density $n_0 = n_\uparrow + n_\downarrow$, and a_s is the s-wave scattering length. The three different limits that are of interest are

$$k_F a_s \to 0- \qquad \text{BCS}$$

$$k_F a_s \to \pm\infty \quad \text{unitarity}$$

$$k_F a_s \to 0+ \qquad \text{BEC}$$

In the limit of weak attractive interactions $a_s \to 0-$, there is no bound-state in vacuum, and the standard BCS theory of Cooper pairing applies. In the opposite regime of strong attractive interactions $a_s \to 0+$, there exists a deep bound state of $\uparrow$- and $\downarrow$-spin atoms in vacuum and these pairs behave like a weakly interacting gas of bosons. Note that both limits have the same broken gauge symmetry and this suggests that both limits might in fact be part of the same phase. In between, in the regime where $k_F a_s \gg 1$, a weak-coupling description is not possible. This is the so-called unitary limit, where the scattering amplitude reaches the limit dictated by the requirement that the S-matrix has to be unitary and we only consider s-wave scattering[1]. It was realized by Leggett

---

[1]To avoid confusion, we would like to emphasize that this clearly does not mean that there are no cases where interactions are even stronger. For example when considering long-range interactions, scattering channels of all angular momenta become important and the total scattering cross-section can become larger than the contribution from the s-wave channel at unitarity.

that a simple mean-field-theory can capture the qualitative physics over the entire crossover regime at $T = 0$ [1, 2]. Later Nozières, Schmitt-Rink and others, generalized this mean-field theory to include Gaussian fluctuations, which is necessary to obtain a correct description of the finite temperature Bose gas in the BEC limit [3, 4, 5, 6, 7, 8, 9]. In this chapter, we give a short derivation of the mean-field results at $T = 0$. In momentum space, the BdG equations for a uniform superfluid order parameter are

$$
\begin{pmatrix} \xi_{\mathbf{k}} & \Delta_0 \\ \Delta_0 & -\xi_{\mathbf{k}} \end{pmatrix} \begin{pmatrix} u_{\mathbf{k}} \\ v_{\mathbf{k}} \end{pmatrix} = E_{\mathbf{k}} \begin{pmatrix} u_{\mathbf{k}} \\ v_{\mathbf{k}} \end{pmatrix}
$$
(3.1)

The positive eigenvalue and the corresponding normalized eigenvector for the matrix Hamiltonian Eq. (3.1) are

$$
E_{\mathbf{k}} = \sqrt{\xi_{\mathbf{k}}^2 + \Delta_0^2} \; ; \qquad \begin{pmatrix} u_{\mathbf{k}} \\ v_{\mathbf{k}} \end{pmatrix} = \begin{pmatrix} \sqrt{\frac{1}{2} + \frac{\xi_{\mathbf{k}}}{2\sqrt{\Delta_0^2 + \xi_{\mathbf{k}}^2}}} \\ \sqrt{\frac{1}{2} - \frac{\xi_{\mathbf{k}}}{2\sqrt{\Delta_0^2 + \xi_{\mathbf{k}}^2}}} \end{pmatrix}
$$
(3.2)

To find the self-consistent solution we have to solve the gap-equation

$$
\Delta_0 = \frac{g}{L^d} \sum_{\mathbf{k}} \frac{\Delta_0}{2\sqrt{\xi_{\mathbf{k}}^2 + \Delta_0^2}}
$$
(3.3)

As explained in the appendix of chapter 1, in three dimensions we have to replace the bare coupling constant with $1/g \rightarrow m/(4\pi\hbar^2 a_s) - 1/L^3 \sum_{\mathbf{k}} 1/(2\epsilon_{\mathbf{k}})$. This gives a regularized gap equation, where the interactions are parametrized by the experimentally measurable scattering length:

$$
\frac{m}{4\pi\hbar^2 a_s} = \int \frac{d^3 k}{(2\pi)^3} \left(\frac{m}{\hbar^2 k^2} - \frac{1}{2\sqrt{(\epsilon_{\mathbf{k}} - \mu)^2 + \Delta_0^2}} \right)
$$
(3.4)

Since we want to work at fixed particle number we also need to simultaneously solve the number equation

$$
n_0 = \frac{1}{L^3} \sum_{\mathbf{k}} \left(1 - \frac{\xi_{\mathbf{k}}}{E_{\mathbf{k}}} \right) = \int \frac{d^3 k}{(2\pi)^3} \left(1 - \frac{\epsilon_{\mathbf{k}} - \mu}{\sqrt{(\epsilon_{\mathbf{k}} - \mu)^2 + \Delta_0^2}} \right)
$$
(3.5)

24

The pair of equations (3.4), (3.5) can be brought to the dimensionless form

$$F_1(x_0) = -\frac{\pi}{2}\alpha y_0^{1/2} \tag{3.6}$$

$$F_2(x_0) = -\frac{2}{3}y_0^{3/2} \tag{3.7}$$

where $\alpha = (k_F a_s)^{-1}$, $x_0 = \mu/\Delta_0$, $y_0 = E_F/\Delta_0$, and

$$F_1(x_0) = \int_0^\infty dx \left(\frac{x^2}{\sqrt{(x^2 - x_0)^2 + 1}} - 1 \right) \tag{3.8}$$

$$F_2(x_0) = \int_0^\infty dx \, x^2 \left(\frac{x^2 - x_0}{\sqrt{(x^2 - x_0)^2 + 1}} - 1 \right). \tag{3.9}$$

The results from solving gap and number equations numerically as a function
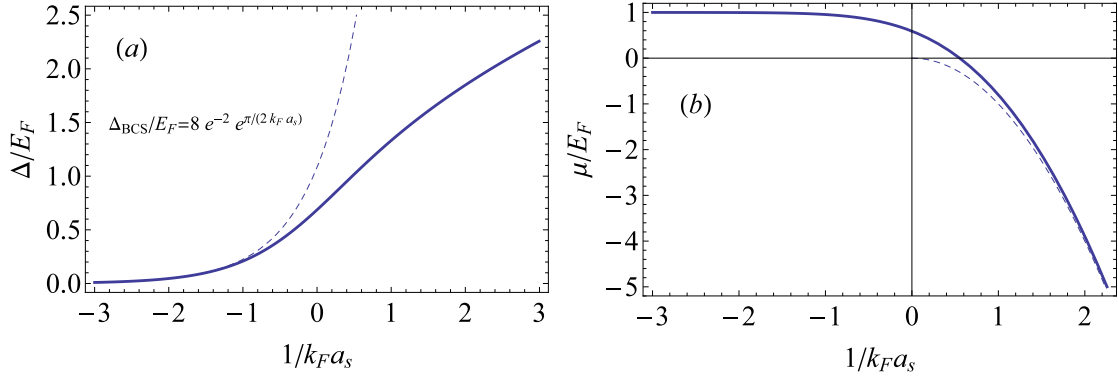
Figure 3.1: Variation of order parameter Δ (a) and chemical potential μ (b) as a function of $1/(k_F a_s)$ from BCS to BEC limit, calculated from mean-field theory. The dashed line in (a) is the BCS limit result for the energy gap $\Delta \sim 8e^{-2}e^{\pi/(2k_F a_s)}$. In (b) we have also plotted $1/2$ of the two-body bound-state energy $\epsilon_B = -\hbar^2/(ma_s^2)$ for $a_s > 0$ (dashed line).

of the crossover parameter $1/(k_F a_s)$ are shown in Fig. 3.1. By construction, this theory must work in the BCS limit, $x_0 \to +\infty$. In this limit, one finds $\mu = E_F$ and the BCS result for the energy gap $\Delta_0 = 8e^{-2}e^{-\pi/(2k_F a_s)}$ [2]. In the opposite limit, $x_0 \to -\infty$, where one has a Bose gas of tightly bound molecules, one has $\mu/E_F = -1/2\epsilon_B/E_F + 2k_F a_s/(3\pi)$ ($\epsilon_B = \hbar^2/(ma_s^2)$ is the two-body binding energy in vacuum). The chemical potential is just half the binding energy plus a correction for the interaction between bosons. Within mean-field theory these

bosons interact with scattering length $a_{BB} = 2a_s$. While this is qualitatively right and the theory gives the correct result in the extreme limit of noninteracting bosons ($a_s = 0+$), a study of the four-body problem showed that actually $a_{BB} = 0.6a_s$ [10]. At temperatures much less than the Bose condensation temperature one can describe the system in the BEC limit with a Gross-Pitaevskii free energy [11, 12]

$$\Omega_{MF} \approx \int d^3r \phi^*(\mathbf{r}) \left[-\frac{\hbar^2 \nabla^2}{4m} - \mu_B \right] \phi(\mathbf{r}) + g_{BB} |\phi(\mathbf{r})|^4 \tag{3.10}$$

where $g_{BB} = 4\pi\hbar^2 a_{BB}/(2m)$, $\mu_B = 2\mu + E_B$, and the density is of pairs given by $n_B(\mathbf{r}) = |\phi(\mathbf{r})|^2$. We note that μ goes negative at $(k_F a_s)^{-1} \approx 0.55$. While there is no phase transition at this point, the minimum of the fermionic excitation spectrum $E(\mathbf{k})$ shifts to $\mathbf{k} = 0$. The gap in the quasi-particle spectrum is given by

$$E_{\text{gap}} = \begin{cases} \Delta_0 & \mu > 0 \\ \sqrt{\Delta_0^2 + \mu^2} & \mu < 0 \end{cases} \tag{3.11}$$

Note that Δ_0 is not equal to the gap in the fermionic excitation spectrum for $\mu < 0$. In the BEC limit the energy gap to creating a (pair of) fermionic excitations is equal to $E_B/2$ (E_B) respectively. To avoid confusion we will call Δ_0 the superfluid order parameter.

Apart from the BCS and BEC limit, most theoretical and experimental work has focused on the strongly interacting unitary limit where $1/(k_F a_s) = 0$. Since a_s is infinite, the scattering cross section at low energies scales as $\sigma \sim 1/k^2$ and the thermodynamics of the system becomes universal [13, 14, 15, 16, 17]. This lack of a length-scale strongly constraints the thermodynamics functions. For example, simple dimensional analysis shows the $T = 0$ energy density ϵ has to
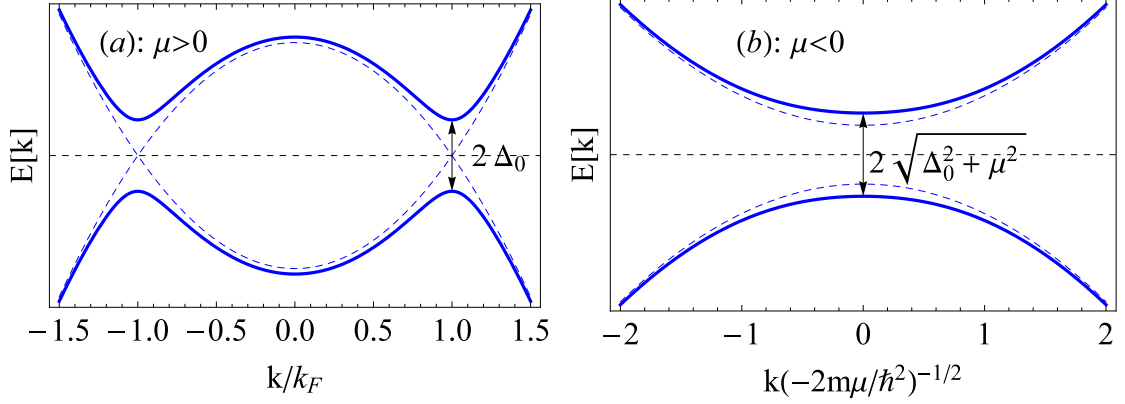
Figure 3.2: Mean-field Bogoliubov excitation spectrum in the BCS (a) and BEC (b) limit (solid lines). Note how the character of the fermionic excitations depends on the sign of $\mu = 0$. The dashed lines are the corresponding noninteracting spectra with $\Delta_0 = 0$.

be proportional to the energy density of a noninteracting Fermi gas ϵ_0 [18]

$$\epsilon = \xi \epsilon_0 \tag{3.12}$$

The proportionality constant ξ is a universal many-body parameter[2] and its precise value has received considerable attention, both in experiments [14, 19, 20, 21] and theoretical calculations [13, 15, 22, 23, 24, 25, 26, 27, 28, 29, 30, 31, 32]. The complete $T = 0$ equation of state is known, once one knows the value of ξ. Mean-field theory gives an upper bound on the parameter ξ, because the variational principle implies $E_{MF} > E$. One finds $\xi_{MF} = 0.6$, whereas Quantum Monte-Carlo calculations give $\xi \approx 0.41 < \xi_{MF}$ [33] [3]. The free energy density $f = \Omega/L^3$ is then expressed as

$$f = \epsilon - \mu n = \xi \epsilon_0 - \xi \frac{\partial \epsilon_0}{\partial n} n = \xi f_0(\mu/\xi) = -\frac{2}{15\pi^2} \left(\frac{2m}{\xi \hbar^2} \right)^{3/2} \mu^{5/2}$$

where we used $f_0 = -2(2m/\hbar^2)^{3/2} \mu^{5/2}/(15\pi^2)$ for the free energy density of a noninteracting two species Fermi gas. The number density $n = n_\uparrow + n_\downarrow$ can be

---

[2]Sometimes we will use instead the equivalent parameter $\beta = \xi - 1$, introduced in [14].
[3]One has $\mu = \xi E_F$, then we can read off $\xi_{MF} = 0.6$ from Fig. 3.1

obtained as

$$n = -\frac{\partial f}{\partial \mu} = \frac{1}{3\pi^2} \left(\frac{2m\mu}{\xi \hbar^2} \right)^{3/2} \tag{3.13}$$

This implies that the density profile of a unitary Fermi gas has the shape at $T = 0$ as that of a noninteracting Fermi gas (up to a scale factor).

3.2   Effect of spin-imbalance — Clogston limit

An interesting tuning knob that is available in experiments with neutral ultracold fermionic atoms is the ability to control spin populations, creating a scenario where $N_\uparrow \neq N_\downarrow$. This is very exciting for several reasons

- In solid state materials, spin imbalance is achieved by putting the sample in a magnetic field, involving both a vector potential (orbital field) and a Zeeman field. For a typical superconductor it is the orbital effect that dominates the physics: either the system expels the field (Meissner phase), the field penetrates the superconductor via vortex lines (Abrikosov flux lattice), or superconductivity is destroyed and the system turns normal. This means it is difficult to study this physics in solid state systems[4].

- How does a paired superfluid respond to spin-imbalance? This is a very old question and many, sometimes exotic, phases have been proposed where Cooper-pairing and magnetism could coexist [38, 39, 40, 41, 42]. Cold atom experiments allow to study this question in different dimensions and lattice configurations, as well as weak and strong coupling.

---

[4]One can suppress the Meissner effect in thin-film or layered or 1D superconductors in a perpendicular magnetic field. In the solid state community such systems have been studied with great interest in recent years (see e.g. [34, 35, 36, 37]).

- The high-energy and nuclear astrophysics communities are interested in understanding the phases of high density QCD which could be relevant to some pulsars. Also neutron-proton pairing in the core of neutron stars has been discussed [43]. These Fermi superfluids, if they exist, are believed to involve asymmetric pairing and strong interactions. Both effects can be simulated in experiments with cold atoms.

In the grand canonical ensemble spin imbalance is achieved by mismatching chemical potentials, i.e. by adding the Zeeman-term

$$H_Z = h \int d^3r \left(n_\uparrow(\mathbf{r}) - n_\downarrow(\mathbf{r}) \right) \tag{3.14}$$

to the Hamiltonian for the balanced gas. We will first discuss what happens in the weak coupling BCS limit. At zero temperature, the free energy of the superfluid is unchanged as long as $h < \Delta_0$, and the system should definitely be magnetized for $h > \Delta_0$, because in this case the system will become magnetized through the creation of Bogoliubov quasiparticles (note that these quasiparticles carry definite spin $\uparrow,\downarrow$). To see whether there is a phase transition for a $h_c < \Delta_0$ we compare the free energy of a noninteracting normal state to that of the superfluid

$$f_N = -\frac{1}{15\pi^2} \left(\frac{2m}{\hbar^2} \right)^{3/2} \left[(\mu + h)^{5/2} + (\mu - h)^{5/2} \right] \approx f_0 - h^2 \frac{mk_F}{2\pi^2\hbar^2} \tag{3.15}$$

When we compare the free energy reduction to the condensation energy Eq. (3.78), we find that both superfluid and polarized normal state have the same energy when $h_c = \Delta_0/\sqrt{2}$. We should expect a first order phase transition (first order because $h_c < \Delta_0$) when the field reaches the critical value $h = h_c$. The point where it becomes more favorable to create a magnetized normal state rather than lowering the energy via Cooper pairing is known as the Clogston-Chandrasekhar or Pauli limit of superconductivity [38, 39]. We can use the

mean-field theory to calculate the phase diagram for an imbalanced gas in the BEC-BCS crossover. For a uniform order parameter $\Delta(\mathbf{r}) = \Delta_0$, the $T = 0$ free energy is given by[5]

$$\Omega_{MF}(\Delta, h) = \frac{1}{2} \sum_{\mathbf{k}, \sigma=\uparrow,\downarrow} \left[\epsilon_{\mathbf{k}} - \mu - |E_{\mathbf{k},\sigma}| - \frac{1}{2\epsilon_{\mathbf{k}}} \right] - \frac{m|\Delta_0|^2}{4\pi a_s \hbar^2} \quad (3.16)$$

The phase diagram Fig. 3.3 can be found by minimizing of the free energy with respect to Δ_0 at fixed μ, h. The choice of normalization is somewhat nontrivial, as the obvious unit for energy, $\hbar^2/(2ma_s^2)$ diverges at unitarity and is symmetric in a_s. A useful way to discuss the global phase diagram was put forward by Son and Stephanov in Ref. [50], were we normalize by the Zeeman field h by the energy gap (in the fermionic spectrum) E_{gap} and work at fixed μ/Δ_0, where Δ_0 is the order parameter for $h = 0$. At $h = 0$, there is then a unique correspondence between μ/Δ_0 and $k_F a_s$. The advantage of this choice of units is that the energy scale that we use to normalize μ and h stays finite throughout the crossover. The free energy difference between the state at $h = 0$ and $h \neq 0$ is given by

$$\delta\Omega(\Delta) = -\sum_{\mathbf{k}} (E_{\mathbf{k}} + h) \, \theta(h - E_{\mathbf{k}}) \quad (3.17)$$

$$= -L^3 \Delta_0^{5/2} \left(\frac{2m}{\hbar^2} \right)^{3/2} \delta^{5/2} F_4(x_0/\delta) \quad (3.18)$$

where we introduced $\delta = \Delta/\Delta_0$, $z_0 = h/\Delta_0$, and

$$F_4(x_0, z_0) = \int_{x_-}^{x_+} dx \, x^2 \sqrt{(x^2 - x_0)^2 + 1} - \frac{z_0}{3} \left(x_+^3 - x_-^3 \right). \quad (3.19)$$

The limits of integration $x_\pm = \sqrt{x_0 \pm \sqrt{z_0^2 - 1}}$ are the real positive solutions for x of the equation $z_0 = \sqrt{(x^2 - x_0)^2 + 1}$. When there is only one positive solution $x_+ > 0$, then $x_- = 0$. In the case where there are no real positive solutions we take $x_+ = x_- = 0$. The total free energy is then given by

$$f(x_0, z_0, \delta) = \frac{\Delta_0^{5/2}}{2\pi^2} \left(\frac{2m}{\hbar^2} \right)^{3/2} \delta^{5/2} \left[F_3(x_0/\delta) + F_4(x_0/\delta, z_0/\delta) - \frac{\alpha\pi}{4} \sqrt{\frac{y_0}{\delta}} \right] \quad (3.20)$$

---

[5]We use Eq. (5.5), with $2\beta^{-1} \log[2 \cosh(\beta E/2)] \to |E|$ as $\beta \equiv 1/(k_B T) \to \infty$.
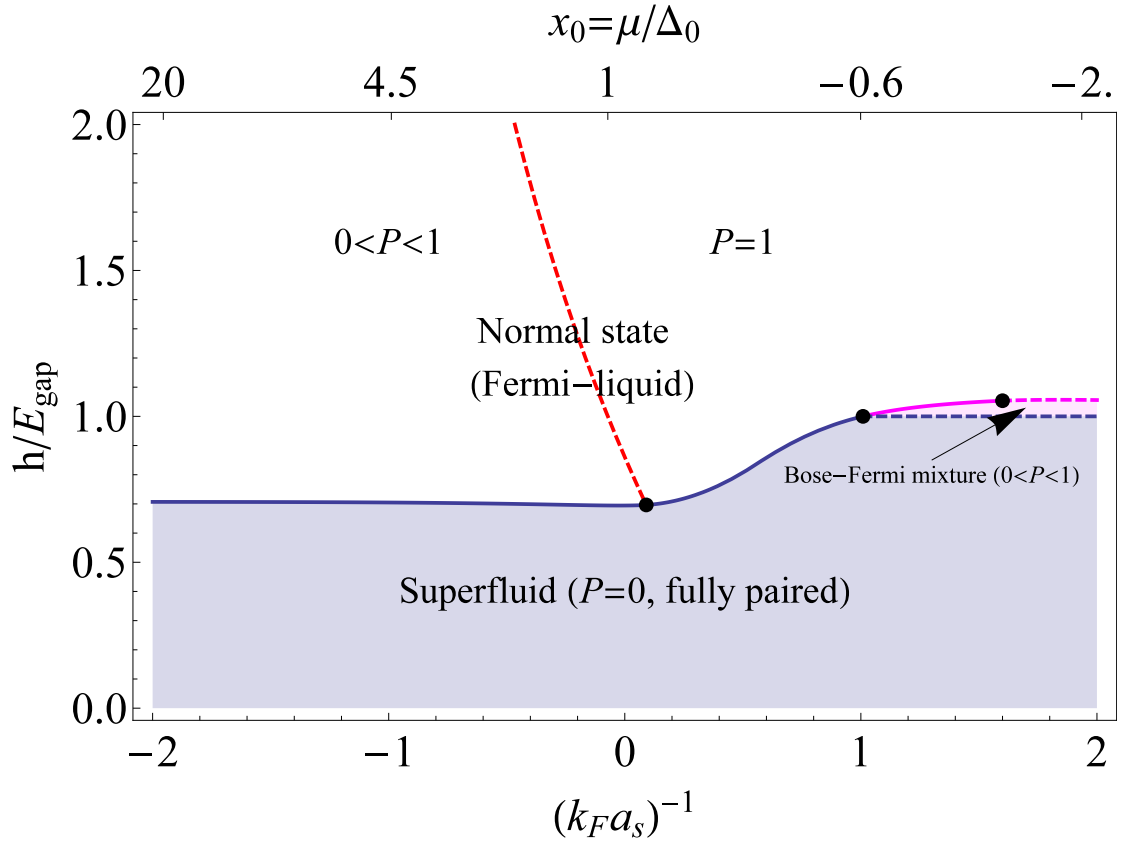
Figure 3.3: Global topology of the mean-field theory phase diagram of the polarized Fermi-gas at $T = 0$ [44, 45, 46, 47, 48, 49, 50, 51, 52]. We plot the phase-diagram in the units of Ref. [50], where we practically work at fixed h, μ and normalize h with the energy gap E_{gap} from Eq. (3.11). Note that we define k_F with reference to the density of the $h = 0$ superfluid. Many qualitative features of this mean-field phase diagram are believed to be correct and have mostly been confirmed in experiments [53, 54, 55]. Including interactions in the normal state shifts the transition line between partially and fully polarized normal to the right (recent QMC calculations suggest that the line is even shifted beyond the critical point where the Bose-Fermi mixture becomes a stable phase [51]). In brackets we indicate whether a phase is polarized [$P = (n_\uparrow - n_\downarrow)/(n_\uparrow + n_\downarrow)$].

with

$$F_3(x_0) = \int_0^\infty dx x^2 \left(x^2 - x_0 - \sqrt{(x^2 - x_0)^2 + 1} \right). \tag{3.21}$$

We plot this free energy in Fig. 3.6 as a function of δ. In the BCS limit the phase diagram features a first order phase transition from the unpolarized superfluid state to a partially polarized Fermi liquid. This picture is still valid at unitarity.

In the BEC limit, the phase diagram of the polarized gas can be understood by mapping the system on a weakly interacting boson-fermion mixture of tightly bound pairs and unpaired excess fermions [56, 57]. The Hamiltonian for a Bose-Fermi mixture is

$$
\begin{aligned}
H_{BF} &= \int d^3x\, \phi_B^\dagger(\mathbf{r}) \left(-\frac{\hbar^2 \nabla^2}{4m} - \mu_B \right) \phi_B(\mathbf{r}) + \int d^3x\, \psi_F^\dagger(\mathbf{r}) \left(-\frac{\hbar^2 \nabla^2}{2m} - \mu_F \right) \psi_F(\mathbf{r}) \\
&+ \frac{g_{BB}}{2} \int d^3x\, \left[\phi_B^\dagger(\mathbf{r}) \right]^2 \left[\phi_B(\mathbf{r}) \right]^2 + g_{BF} \int d^3x\, \phi_B^\dagger(\mathbf{r}) \psi_F^\dagger(\mathbf{r}) \psi_F(\mathbf{r}) \phi_B(\mathbf{r}), \quad (3.22)
\end{aligned}
$$

where $\phi_B^\dagger(\mathbf{r})$ and $\psi_F^\dagger(\mathbf{r})$ are creation operators for the molecules and excess fermions, respectively. A Hartree-Fock mean-field decoupling of the Hamiltonian Eq. (3.22) yields the free energy density

$$
f_{BF} = -\left(\mu_B - \Sigma_B \right) n_B + \frac{g_{BB}}{2} n_B^2 - \frac{(2m)^{3/2}}{15\pi^2\hbar^3} \left(\mu_F - \Sigma_F \right)^{5/2} - g_{BF} n_B n_F. \quad (3.23)
$$

Here the Hartree self-energies are $\Sigma_{B/F} = g_{BF} n_{B/F}$ and the coupling constants are related to scattering lengths as $g_{BF} = 3\hbar^2 a_{BF}/m$, $g_{BB} = 2\hbar^2 a_{BB}/m$. The simple BdG mean-field theory predicts $a_{BF} = 8/3 a_s$, whereas a solution to the three-body problem gives the exact result for the dimer-fermion scattering length $a_{BF} = 1.2 a_s$ [58, 59]. The phase diagram at finite temperature was extensively studied with a self-consistent Hartree-Fock theory by Sourish Basu in his Ph.D. thesis [60]. It turns out that the imbalanced Fermi gas behaves in many ways similar to ^{4}He/^{3}He-3 mixtures [61]. The zero temperature phase diagram[6] is shown in Fig. 3.4. At high densities or strong coupling one has a first order phase transition to a fully polarized (noninteracting) Fermi gas. At the critical point S a polarized superfluid phase emerges. The transition between superfluid and this polarized superfluid is always continuos. Additionally, there is also a tricritical point T where the transition between normal state and superfluid becomes continuous. Before reaching the point S the first order transition

---

[6]Here shown for the accurate parameters for $a_{BB} = 0.6 a_s$, $a_{BF} = 1.2 a_s$. Qualitatively, the mean-field values result in the same phase diagram.

between unpolarized superfluid and fully-polarized normal is found by equating the normal and superfluid free energies $f_S = f_N$, which is equivalent to

$$-\frac{\mu_B^2}{2g_{BB}} = -\left(\frac{2m}{\hbar^2}\right)^{3/2} \frac{\mu_F^{5/2}}{15\pi^2} \tag{3.24}$$

The superfluid state becomes polarized when $\mu_F = g_{BF}n_B$ or

$$\mu_F = g_{BF}\frac{\mu_B}{g_{BB}} \tag{3.25}$$

Both Eqs. (3.24),(3.25) are simultaneously satisfied at the point S, with

$$S = (\mu_B, \mu_F) = \frac{225\pi^4 g_{BB}^2 \hbar^6}{32g_{BF}^5 m^3} \cdot (g_{BB}, g_{BF}). \tag{3.26}$$

To find the tricritical point we approach the problem from low density side where the transition between normal and superfluid is continuos. At the phase transition we have $n_B = 0$ and

$$\frac{\partial f_{BF}}{\partial n_B} = 0 \tag{3.27}$$

Solving for μ_F we get $\mu_F = (\hbar^2/m)(3/4\pi^2\mu_B/g_{BF})^{2/3}$ at the second order transition line. This transition turns first order when

$$\frac{\partial f_{BF}^2}{\partial n_B^2}\bigg|_{n_B=0} = g_{BB} - g_{BF}^2 \sqrt{\frac{\mu_F}{2}} \frac{m^{3/2}}{\pi^2 \hbar^3} = 0 \tag{3.28}$$

The tricritical point is then at

$$T = \frac{2\pi^4 g_{BB}^2 \hbar^6}{g_{BF}^4 m^3} \cdot \left(1, \frac{2g_{BB}}{3g_{BF}}\right). \tag{3.29}$$

3.3 Density profiles and phase diagrams

An important probe in experiments with ultra-cold Fermi gases are in-situ density profiles. These experimental systems are confined by a trapping potential,
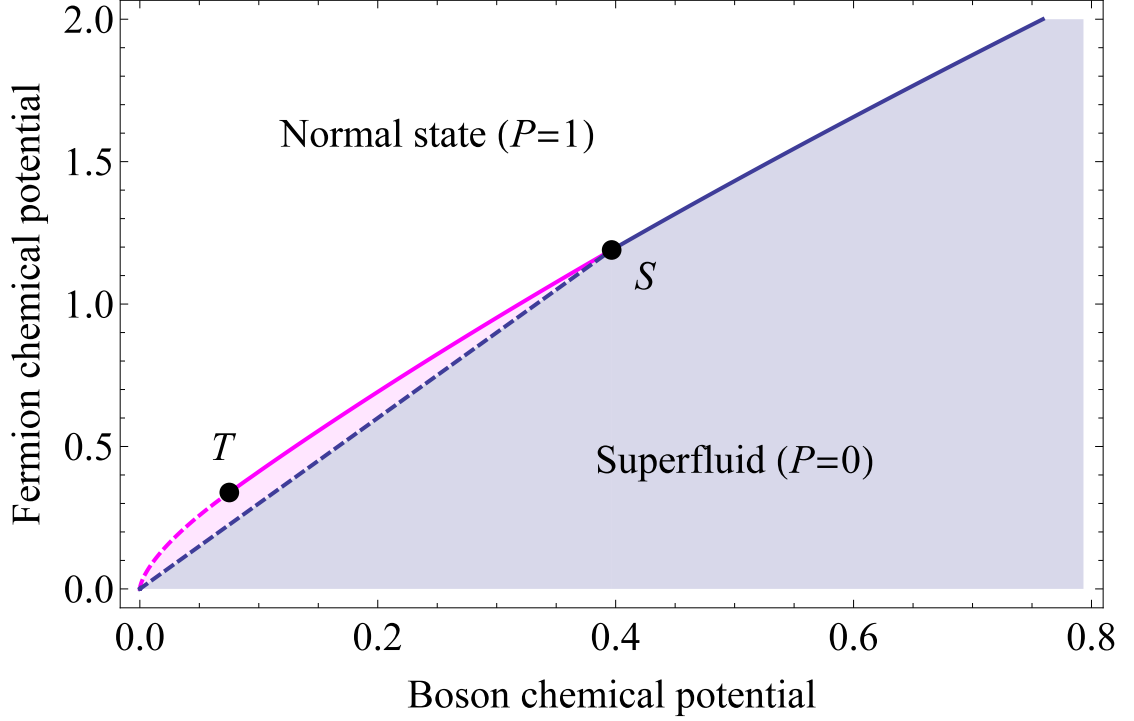
Figure 3.4: Phase diagram of a Bose-Fermi mixture, calculated from the Hartree-Fock free energy Eq. (3.23). The values of the boson-fermion scattering length are $a_{BF} = 1.2a_s$ and $a_{BB} = 0.6a_s$ (these parameters differ from the mean-field results and are appropriate for the imbalanced Fermi gas in the BEC limit) [58, 59, 10]. The boson (fermion) chemical potentials μ_B (μ_F) are normalized by half the binding energy $\epsilon_B/2 = \hbar^2/(2ma_s^2)$ of the pairs.

i.e. experiments probe inhomogeneous systems in an external trapping potential $V(\mathbf{r})$. For theoretical calculations it is more convenient to calculate properties of homogenous systems. Typically $V(\mathbf{r})$ varies on a length scale much longer than the healing length, then a natural assumption is to view the system as locally homogenous and use the homogenous equation of state, with local chemical potential

$$\mu_\sigma(\mathbf{r}) = \mu_\sigma^c - V(\mathbf{r}) \tag{3.30}$$

where $\sigma = \uparrow, \downarrow$ labels the spin components. The chemical potentials at the center μ_σ^c are determined by the total particle numbers

$$N_\sigma = \int d^3r \; n_\sigma(\mu_\uparrow^c - V(\mathbf{r}), \mu_\downarrow^c - V(\mathbf{r})) \tag{3.31}$$

This Thomas-Fermi approximation is also known as local density approximation (LDA) in the ultra-cold atoms community[7]. It can also be derived from the condition of hydrostatic equilibrium of fluids [62]. For a two species Fermi gas it is convenient to display phase diagrams in terms of the effective Zeeman magnetic field $h = (\mu_\uparrow - \mu_\downarrow)/2$ and the average chemical potential $\mu(\mathbf{r}) = (\mu_\uparrow + \mu_\downarrow)/2$. In a trapped system the local Zeeman field is independent of position $h = (\mu_\uparrow^c - \mu_\downarrow^c)/2$, whereas the average chemical potential $\mu(\mathbf{r}) = (\mu_\uparrow^c + \mu_\downarrow^c)/2 - V(\mathbf{r})$ decreases as one goes towards the edge of the cloud. Hence the trapped system lives on a straight line of constant h of the phase diagram plotted in the μ, h-plane. A general feature that can be extracted from experiments is the sequence of phases observed, e.g. by dividing regions into fully polarized, unpolarized or partially polarized [53, 63]. In principle there could be multiple phases with the same density characteristics, but theoretically every phase transition would be visible as a jump (if first order) or singularity (if second order) in the density profile. For the phase diagram of the imbalanced unitary Fermi gas at $T = 0$, two distinct sequences of phases were proposed [44, 64, 27]. If we assume a non-interacting normal state, the location of the first order superfluid to normal phase transition is found by requiring $f_S = f_N$ or

$$(1 + \eta)^{5/2} + \theta(1 - \eta)(1 - \eta)^{5/2} = \frac{2}{\xi^{3/2}} \tag{3.32}$$

where $\eta = h/\mu$ and $\theta(x)$ is the Heaviside step function. When we assume the mean-field theory value $\xi_{MF} = 0.6$, one finds $\eta_c \approx 0.79 < 1$, i.e. the phase

---

[7]So far there are very few known examples where this approximation is not valid. One expects a break down near a second order phase transition (there one has a diverging length-scale).

boundary is between the unpolarized superfluid and a partially polarized normal state. On the other hand we could try to improve upon mean-field theory by using the more accurate QMC value $\xi = 0.42$ [64]. This would imply $\eta_c \approx 1.22 > 1$ and a direct phase transition to the fully polarized normal state with no partially polarized phase. Early experiments by the Rice group seemed to support this "two shell model", whereas the MIT group found three shells including a partially polarized normal phase [21, 65]. QMC calculations relying on the fixed-node approximation for the equation of state of the partially polarized normal state later showed that attractive interactions significantly increase the stability of the normal state [27]. The consequence of these interactions is that there still is a window of stability for the partially polarized normal state, consistent with what was observed in the MIT experiments.

3.4 Stability of the Fulde-Ferrell state in $D = 3$

So far we have not considered any superfluid state that breaks translational symmetry[8]. It turns out that in the BCS limit of the imbalanced Fermi gas, a superfluid with broken translational symmetry appears to be stable [41, 42]. Generically, these Fulde-Ferrell-Larkin-Ovchinnikov (FFLO[9]) states are both polarized and paired at the same time. One should view these states as variational approximations for the gap parameter $\Delta(\mathbf{r})$. The most common approximations are the FF state introduced by Fulde and Ferrell,

$$\Delta_{FF}(\mathbf{r}) = \Delta_0 \, e^{i\mathbf{q}\cdot\mathbf{r}} \tag{3.33}$$

---

[8]A classic example for such a state is the Abrikosov vortex lattice phase.
[9]Some authors also call it the LOFF state.
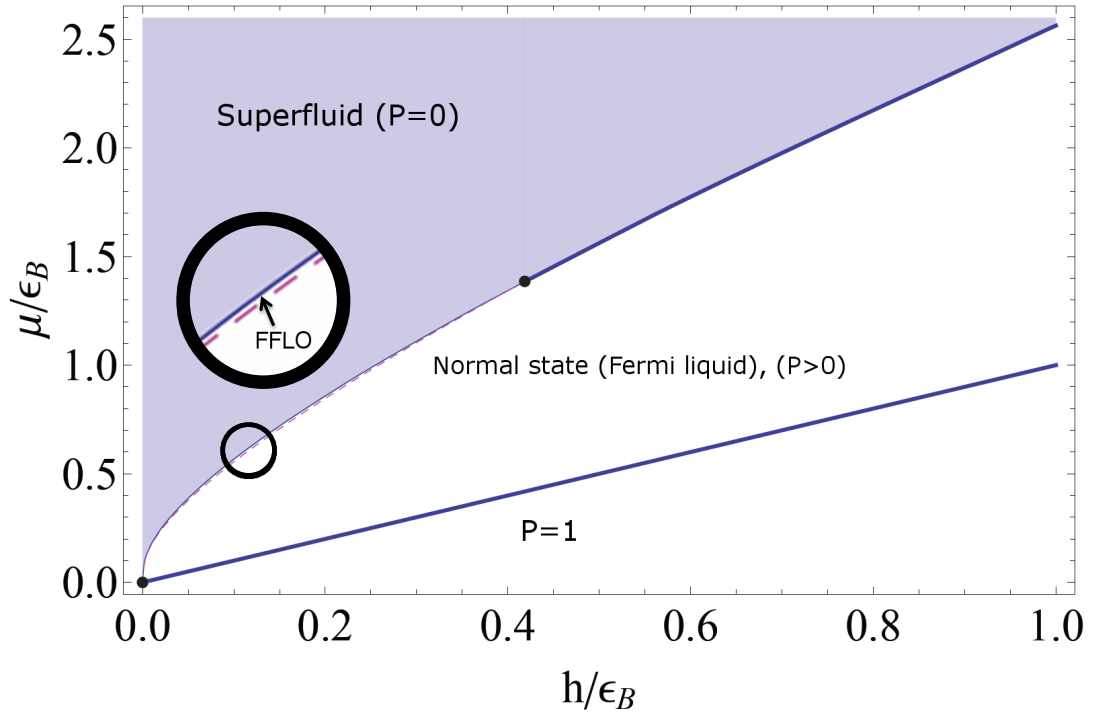
Figure 3.5: Mean-field phase diagram of the imbalanced Fermi gas in the BCS limit (in 3D). There is a tiny sliver of stable FFLO phase, sandwiched between the dashed and solid line. This FFLO phase appears to be stable up to $(h/\epsilon_B, \mu/\epsilon_B) \approx (0.42, 1.39)$ (FFLO is stable for $(k_F a_s)^{-1} \leq -0.56$). The solid (dashed) line represents a first order first (second) order phase transition respectively.

and the LO state first introduced by Larkin-Ovchinnikov,

$$\Delta_{LO}(\mathbf{r}) = \Delta_0 \, cos(\mathbf{q} \cdot \mathbf{r}). \qquad (3.34)$$

Theses states constitute one of the few systems where superfluidity of fermions (Cooper pairing) and magnetism coexists, which makes them particularly intriguing. That such a state should exist can be seen from straightforward stability analysis using the Thouless criterion. The normal state is stable towards
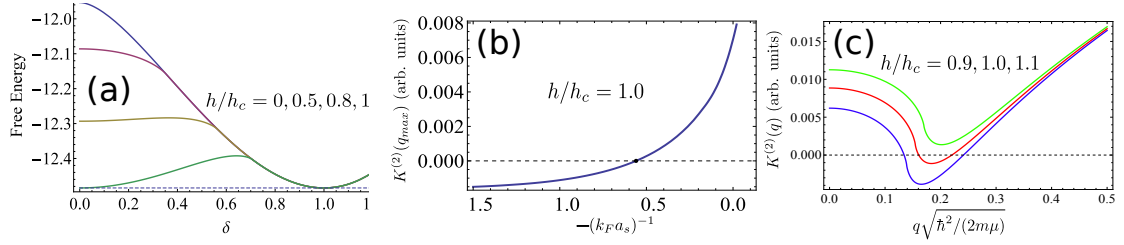
Figure 3.6: (a) Mean-field free energy as a function of the superfluid order parameter $\delta = \Delta/\Delta_0$ for a series of Zeeman magnetic fields $h/h_c = 0, 0.5, 0.8, 1.0$ at $k_F a_s = -1$. Note that at the Clogston limit $h = h_c$ there appears to be a first order phase transition to the normal state when the minima in the free energy are degenerate. (b) Minimum of the kernel $K^{(2)}(q_{\max})$ (related to the pair susceptibility) as a function of interaction strength on the Clogston limit. The normal state becomes unstable towards FFLO around $(k_F a_s)^{-1} \leq -0.56$. (c) $K^{(2)}(q)$ plotted at fixed interaction strength $(k_F a_s)^{-1} = -1$ at, above and below the Clogston limit. (In all figures we have defined k_F always via the unpolarized superfluid state at $h = 0$)

Cooper pairing if the kernel $K^{(2)}(\mathbf{q})$ from Eq. (2.32) has[10]

$$K^{(2)}(\mathbf{q}) > 0 \quad \text{for all} \quad \mathbf{q} \tag{3.35}$$

For $T = 0$ and $h > 0$, $K^{(2)}(q)$ may be evaluated analytically (see S. Basu, Ph.D. thesis [60]). One obtains

$$2\pi \tilde{K}^{(2)}(\mathbf{q}) = 2(1+r) + \frac{f_+^\uparrow + f_-^\uparrow + f_+^\downarrow + f_-^\downarrow}{\tilde{q}} - 2\pi i\zeta - 1/(k_F^\uparrow a_s) \tag{3.36}$$

$$f_\sigma^\uparrow = \left(\frac{\tilde{q}^2}{4} + \zeta^2 - 1 + \sigma\tilde{q}\zeta\right) \log\left(\frac{\tilde{q} - 2 + 2\sigma\zeta}{\tilde{q} + 2 + 2\sigma\zeta}\right)$$

$$f_\sigma^\downarrow = \left(\frac{\tilde{q}^2}{4} + \zeta^2 - r + \sigma\tilde{q}\zeta\right) \log\left(\frac{\tilde{q} - 2r + 2\sigma\zeta}{\tilde{q} + 2r + 2\sigma\zeta}\right)$$

where $\tilde{K}^{(2)} = (4\pi/mk_F^\uparrow)K^{(2)}$, $\tilde{q} = |\mathbf{q}|/k_F^\uparrow$, $r = k_F^\downarrow/k_F^\uparrow$, $\zeta = (1 + r^2)/2 - \tilde{q}^2/4$ and $k_F^{\uparrow,\downarrow} = \sqrt{2m(\mu \pm h)}$, and for brevity we have set $\hbar = 1$. When $\mu_{\uparrow,\downarrow} \leq 0$, one takes $k_F^{\uparrow,\downarrow} \equiv 0$. Note that for $h = 0$, $K^{(2)}(\mathbf{q} \to 0) \to -\infty$. The consequence is that the unpolarized normal state is unstable for an arbitrary weak attractive interaction at T=0 [66]. At finite Zeeman field, the normal state is not always unstable.

---

[10]Note that $K^{(2)}(\mathbf{q}, \mu)$ is related to the many-body T-Matrix via $T^{-1}(\mathbf{q}, \omega) = K^{(2)}(\mathbf{q}, \mu - \omega)$.

To see in what region the partially polarized normal state is unstable, we plot the minimum of $K^{(2)}(q)$ at the Clogston limit $h = h_c$ as a function of $(k_F a_s)^{-1}$ (where k_F is the $h < h_c$ superfluid phase k_F). As can be seen in Fig. 3.6 (b), this minimum crosses zero around $(k_F a_s)^{-1} = -0.56$ (on the BCS side). Below this critical point, the FFLO phase is stable in a thin sliver around the Clogston limit and we find the instability of the normal state by finding the field h_{c1} at which the minimum of $K^{(2)}(q)$ crosses zero. In the deep BCS limit the ratio $h_{c1}/h_c = 1.066$ is maximal [41, 57]. It is generally believed that the transition from the normal state towards FFLO is a second order phase transition and in this case the stability analysis is the same, independent whether the true ground state is the FF or LO state. Typically, the LO state has a slightly lower energy than the FF state[11]. In general the question whether the phase transition from the uniform superfluid to FFLO is first or second order is nontrivial. The FF (and LO) states predict a first order transition of the superfluid towards FFLO, approximately at the Clogston limit (i.e. $h_{c2} = h_c$) [57]. A scenario for a continuous phase transition was investigated by Yoshida and Yip [67]. They estimated the Zeeman field at which a single π-domain wall in the superfluid becomes energetically stable. It was found that this point occurs earlier than the first order transition predicted from the FF state, and the authors concluded that the transition of the superfluid is actually second order starting at polarization $P = 0$ (this was already known to be the case in lower dimensions [68, 69]). While the arguments of Ref. [67] are suggestive of a second order phase transition, there is no proof that the transition within mean-field theory is indeed second order. If domain walls interact via attractive interactions, the transition from uniform superfluid to FFLO would again be first order. Regarding the experimental realization and detection of FFLO we would like to emphasize that the amount of FFLO

---

[11]As we will see it is easier to use the FF state to do calculations.

visible in a trapped system is determined by the region occupied by the phase in the phase diagram plotted in the μ, h-plane. In either scenario this region is extremely small when considering 3D (or 2D) systems. So far, no signature of an FFLO phase has been found in an experiment with imbalanced fermions in 3D. The reason why the FFLO phase in $D > 1$ has such a small region of stability can be understood from an analogy to the Peierls instability of the Fermi gas at $T = 0$. Whenever there is a nesting vector, the normal state is unstable to forming a charge density wave (CDW) for an arbitrarily weak repulsive interaction. In (quasi-)1D there is naturally a momentum vector q such that $k_{F,\downarrow} + q = k_{F,\uparrow}$. The consequence is that then the normal state at $T = 0$ is unstable towards FFLO at any imbalance and for an arbitrarily weak attractive interaction. In higher dimension, there is in general no such nesting vector that allows for pairing of the full Fermi surface at finite momentum and then the normal state will only be unstable for small imbalance. This is similar for the Peierls instability: When there is no nesting vector, a finite interaction strength is required to render the normal state unstable.

3.5 Dark solitons and Andreev boundstates — A toy model for FFLO

In the limit of low population imbalance, a picture for the FFLO phase is an array of well separated π-domain walls [68, 69]. Each of these kinks has a bound-state close to zero energy, analogous to the Caroli-de Gennes-Matricon (CGM) bound states found at the core of vortices in superconductors [70, 71, 72, 73]. An applied Zeeman magnetic field spin-polarizes these Andreev boundstates.
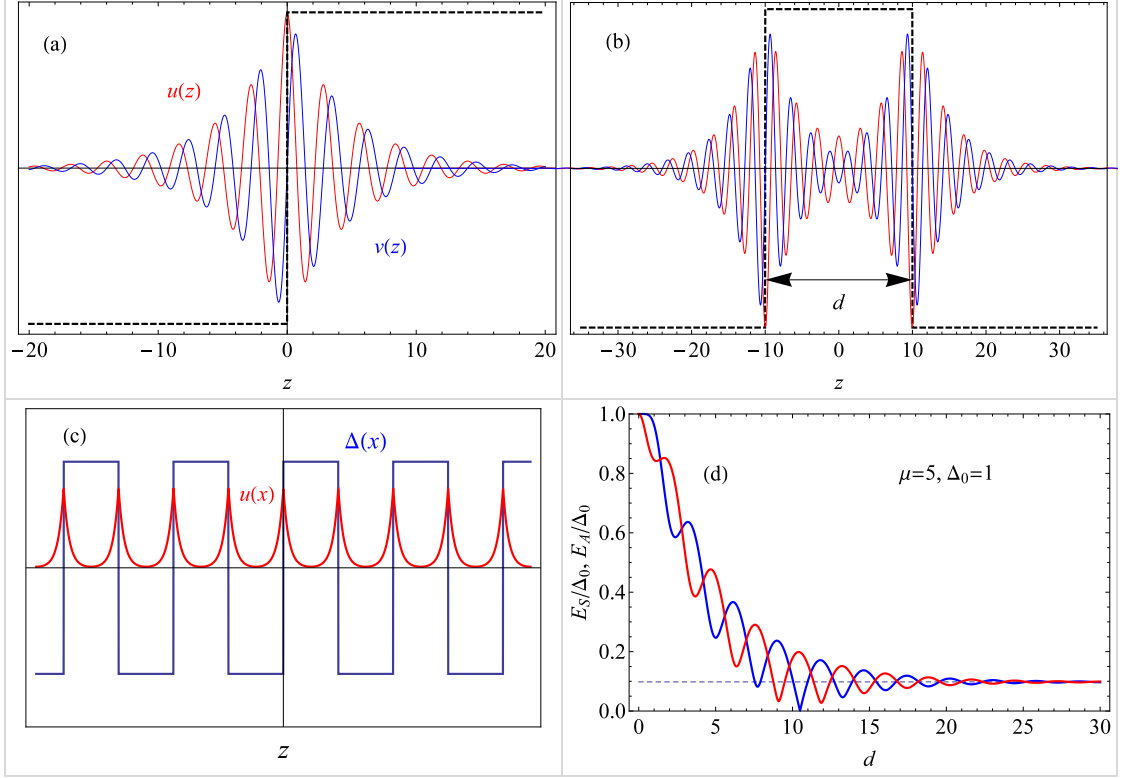
Figure 3.7: Top: Andreev boundstate wavefunctions $(u(z), v(z))^T$ for parameters in the BCS regime (in terms of the dimensionless units described in the text, we used $\Delta_0 = 1$, $\mu = 5$, $d = 20$). (a) Positive energy bound-state solution for a single domain wall $\Delta(z) = \text{sign}(z)\Delta_0$. (b) Symmetric solutions for two domain walls $\Delta(z) = \Delta_0 (\text{sign}(d/2 + z) - \text{sign}(z - d/2) - 1)$. Bottom: (c) Toy model for low polarization density FFLO: An array of weakly interacting sharp domain walls. The boundstates, localized at each domain wall, start to overlap and give rise to a bandstructure. (d) Bound state energies for the configuration of two domain walls in (b), where the distance d between the kinks is varied.

This is the mechanism that allows the superfluid to become polarized in the FFLO phase. A simple model for such a domain wall is a step-function order parameter

$$\Delta(z) = \Delta_0 \ \text{sign}(z) \tag{3.37}$$

It turns out that this model allows for an analytic solution of the Andreev boundstate. This solution will allow us to understand some generic features

41

of the FFLO phase. The Bogoliubov de Gennes equations are ($\hbar^2/2m = 1$)

$$\begin{pmatrix} -\frac{d^2}{dz^2} - \mu & \Delta(z) \\ \Delta^*(z) & -(-\frac{d^2}{dz^2} - \mu) \end{pmatrix} \begin{pmatrix} u_n(z) \\ v_n(z) \end{pmatrix} = E_n \begin{pmatrix} u_n(z) \\ v_n(z) \end{pmatrix} \tag{3.38}$$

Note that the matrix operator

$$\mathcal{P} = \begin{pmatrix} P & 0 \\ 0 & -P \end{pmatrix}, \tag{3.39}$$

where P is the reflection operator with $P\psi(z) = \psi(-z)$, is a symmetry of the Hamiltonian, i.e. $\mathcal{P}H\mathcal{P}^\dagger = H$. The consequence is that we can chose the eigenfunctions of H to be eigenfunctions of $\mathcal{P}$ as well. Therefore the wavefunctions u_n, v_n can be chosen to be symmetric, antisymmetric.

We will now look for possible bound state solutions. Therefore we require $E < \Delta$. The appropriate ansatz for a constant pairing potential is

$$\begin{pmatrix} u(z) \\ v(z) \end{pmatrix} = \begin{pmatrix} u_0 \\ v_0 \end{pmatrix} e^{iwz} \tag{3.40}$$

where w is a c-number. The BdG equations (3.38) for $z > 0$ reduce to

$$\begin{pmatrix} w^2 - \mu & \Delta_0 \\ \Delta_0 & -(w^2 - \mu) \end{pmatrix} \begin{pmatrix} u_0 \\ v_0 \end{pmatrix} = E \begin{pmatrix} u_0 \\ v_0 \end{pmatrix} \tag{3.41}$$

We find for the eigenvalues

$$E_\pm = \pm\sqrt{(w^2 - \mu)^2 + \Delta_0^2} \tag{3.42}$$

and the eigenvectors

$$\psi_\pm = \begin{pmatrix} u_\pm \\ v_\pm \end{pmatrix} \begin{pmatrix} -(w^2 - \mu) \mp \sqrt{(w^2 - \mu)^2 + \Delta_0^2} \\ \Delta_0 \end{pmatrix} \tag{3.43}$$

We consider only solutions with positive energy, so we focus on $E_+ = \sqrt{(w^2 - \mu)^2 + \Delta_0^2}$. Solving for w^2 yields

$$w_{1,2}^2 = \mu \pm i\sqrt{\Delta_0^2 - E^2} \tag{3.44}$$

Using the standard formula for square roots of complex numbers in terms of real imaginary parts

$$\sqrt{x + iy} = \frac{1}{\sqrt{2}}\left\{\sqrt{\sqrt{x^2 + y^2} + x} + i\,\text{sign}(y)\sqrt{\sqrt{x^2 + y^2} - x}\right\} \tag{3.45}$$

we can solve for w

$$
\begin{aligned}
w_{1,2}^\pm &= \pm\frac{1}{\sqrt{2}}\left\{\sqrt{\sqrt{\mu^2 + \Delta_0^2 - E^2} + \mu} \pm i\sqrt{\sqrt{\mu^2 + \Delta_0^2 - E^2} - \mu}\right\} \tag{3.46} \\
&= \pm(\alpha \pm i\kappa) \tag{3.47}
\end{aligned}
$$

The $\pm$ index corresponds to the overall sign, the $1, 2$ index to the second $\pm$ in front of the imaginary part. Using the same convention we write the eigenvectors as

$$\psi_{1,2} = \begin{pmatrix} u_{1,2} \\ v_{1,2} \end{pmatrix} = \begin{pmatrix} E \pm i\sqrt{\Delta_0^2 - E^2} \\ \Delta_0 \end{pmatrix} \tag{3.48}$$

Observing that $|u_{1,2}|^2 = |v_{1,2}|^2 = \Delta_0^2$ we can write up to a (unimportant) constant

$$\psi_{1,2} = \begin{pmatrix} e^{\pm i\phi} \\ 1 \end{pmatrix} \tag{3.49}$$

where $\phi = \arctan\frac{\sqrt{\Delta_0^2 - E^2}}{E}$. By discarding the exponentially increasing solutions as $z \to +\infty$ we find two linear independent solutions for $z > 0$

$$\psi_{1,2}(z) = \begin{pmatrix} e^{\pm i\phi} \\ 1 \end{pmatrix} e^{\pm i\alpha z}e^{-\kappa z} \tag{3.50}$$

We now pick one of the two components antisymmetric, thus we want one of them to be a sine-function ($v(z = 0) = 0$). It turns out that only one of the two

43

possibilities work since the bound state is not degenerate

$$\psi_R(z) = \frac{1}{2i}(\psi_+(z) - \psi_-(z)) = \begin{pmatrix} \sin(\phi + \alpha z) \\ \sin(\alpha z) \end{pmatrix} e^{-\kappa z} \tag{3.51}$$

for the region $z < 0$ we find a similar result

$$\psi_L(z) = \begin{pmatrix} \sin(\phi - \alpha z) \\ \sin(\alpha z) \end{pmatrix} e^{\kappa z} \tag{3.52}$$

The lower component is already continuous as well as its derivative. The upper component is already symmetric, continuous and clearly has a continuous derivative if $u'(z)|_{z=0} = 0$, thus we require

$$\frac{d}{dz}\sin(\phi + \alpha z)e^{-\kappa z}|_{z=0} = 0 \tag{3.53}$$

This is the condition that determines the bound state energy (would we have picked the upper component antisymmetric, i.e. $\phi \to -\phi$, the following equation would have no positive energy solutions). We can solve for the energy E

$$
\begin{aligned}
\alpha\cos(\phi) - \kappa\sin(\phi) &= 0 \\
\tan(\phi) &= \frac{\alpha}{\kappa} \\
\frac{\sqrt{\Delta_0^2 - E_0^2}}{E_0} &= \frac{\sqrt{\sqrt{\mu^2 + \Delta_0^2 - E_0^2} + \mu}}{\sqrt{\sqrt{\mu^2 + \Delta_0^2 - E_0^2} - \mu}} \\
E_0 &= -\frac{\mu}{2} + \sqrt{\frac{\mu^2}{4} + \frac{\Delta_0^2}{2}}
\end{aligned}
$$

The bound state energy is not quite zero, but in the weak interacting limit of small Δ_0 it is

$$E_0 = \frac{\Delta_0^2}{2\mu} + O(\Delta_0^4)$$

When we generalize our solution to $D = 3$, one finds a whole family of bound-states, parametrized by the transverse momentum vector $\mathbf{k}_\perp$. Their energy

eigenvalues are

$$E_{3D}(\mathbf{k}_\perp) = -\frac{\mu - \mathbf{k}_\perp^2}{2} + \sqrt{\frac{(\mu - \mathbf{k}_\perp^2)^2}{4} + \frac{\Delta_0^2}{2}}. \qquad (3.54)$$

This dispersion relation is shown in Fig. 3.8. Qualitatively the dispersion relations behave very differently in the BCS- and BEC-limits. This was noted from a full BdG calculation by the authors of Ref. [74]. What is remarkable, is that the simple step potential solution gives qualitatively a very similar result. In the BCS limit, the energy of the bound state is essentially zero, with a mini-gap of $E_{mg} = \Delta_0(\Delta_0/\mu)/2$ and the transverse effective mass of the Andreev in the domain wall is very large (here $E_{3D}(\mathbf{k}_\perp) \sim E_{mg} + (\mathbf{k}_\perp\Delta_0/\mu)^2/2 + \ldots$, i.e. $m_\perp/m \sim (\mu/\Delta_0)^2 \gg 1$). When the dispersion can be linearized around the Fermi surface (Andreev approximation), the bound state energy is guaranteed to be exactly zero, due to a very general index theorem [75]. Then the bound-states for all $\mathbf{k}_\perp$ would be degenerate at zero energy. In the BEC limit, where a π-soliton would not be stable in equilibrium, $E_{3D}(\mathbf{k}_\perp) \sim -\mu + \mathbf{k}_\perp^2 + \ldots$, i.e. the effective mass is essentially the bare mass $m_\perp \approx m$.

To achieve a finite polarization density in the thermodynamic limit, we need a finite density of domain walls. In such a model for FFLO, the boundstates of these domain walls start to overlap when the length-scale $\xi = \hbar v_F/\Delta_0 \sim d$, where d is the separation between domain walls[12]. This then gives rise to a bandstructure in the tight-binding limit for the excess fermions. To see how this happens we studied the two domain walls depicted in Fig. 3.7. The details of the solution are given in the appendix to this chapter. Here we just note the general features. From the solution of the two domain problem we find that the

---

[12]In units where $\hbar^2/(2m) = 1$, we have $\xi = 2\sqrt{mu}/\Delta_0$. The envelope of $u(z), v(z)$, for the domain wall in Fig. 3.7a decays as $\exp(-\kappa|z|)$, where $\kappa \approx \Delta_0/\sqrt{2\mu}$ (in the BCS limit). Therefore $u(z), v(z) \sim e^{-|z|\sqrt{2}/\xi}$.
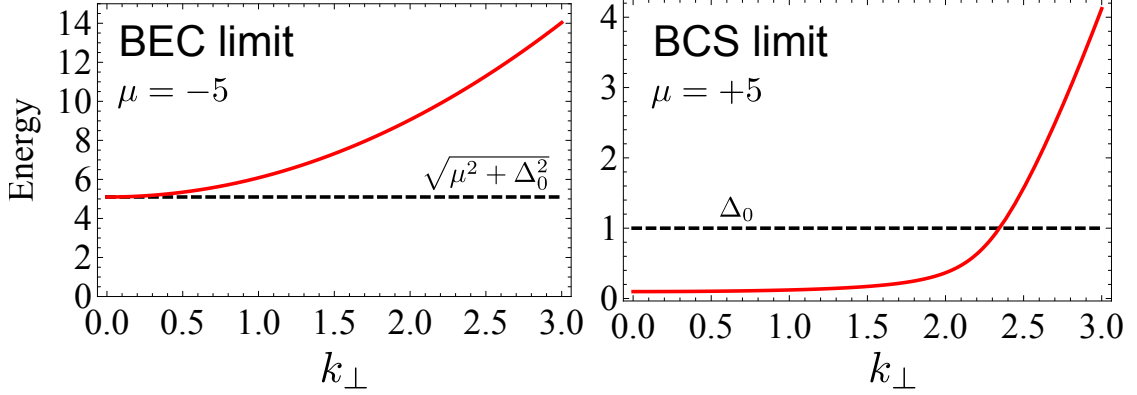
Figure 3.8: Dispersion relation of the Andreev boundstate of a π-domain wall in 2D or 3D (units have $\hbar^2/(2m) = 1$). The dashed line represents the gap to Bogoliubov quasiparticle excitations, E_{gap}.

boundstate solution behaves as

$$E(d) - E_0 \propto \pm 4\alpha\kappa e^{-d\kappa}\sin(\alpha d) + 2\alpha^2 e^{-2d\kappa} \qquad (3.55)$$

where $\kappa \approx \xi/\sqrt{2} = \Delta_0/\sqrt{2\mu}$ and $\alpha \approx k_F = \sqrt{2\mu}$. The bound state energies depend exponentially weak on the separation d, as is naively expected. The leading contribution to the tail oscillates with the Fermi wavevector k_F. This concludes our investigation of a simple toy model for FFLO.

From the toy model we learn that

- Kink domain walls in the superfluid order parameter carry bound states that are close to zero energy in the BCS limit

- Spin polarizing these bound states gives rise to a polarized superfluid state

- An array of domain walls allows for a superfluid with finite polarization density

- The bound states of these domain walls overlap when their separation becomes of order of the coherence length ξ and a band-structure of bound

46

states emerges

- It becomes clear that the 1D FFLO state is a fundamentally distinct phase from the scenario in 2D/3D (assuming the order parameter varies only along a single direction). In 1D, all Andreev boundstates are occupied, and the density of excess fermions is exactly given by the wavevector of the order parameter modulation $q = \pi(n_\uparrow - n_\downarrow)$ (in other words, FFLO is a band insulator for the excess fermions). However in 2D/3D, whatever h, there are always transverse modes crossing the Fermi energy of the excess fermions (David Huse dubbed this situation "incommensurate FFLO"' in order to distinguish it from the 1D "commensurate FFLO" in 1D).

3.6   Fulde-Ferrell versus Larkin-Ovchinnikov in 1D

We mentioned before that typically the LO state has a lower energy than the FF state. In this section we present a study of both states in one spatial dimension at $T = 0$. In general, mean-field theory is not valid in 1D and it turns out that the model described by the Hamiltonian

$$H = \int dz \sum_\sigma \Psi_\sigma^\dagger(z) \left(-\frac{\hbar^2}{2m}\frac{d^2}{dz^2} - \mu_\sigma \right) \Psi_\sigma(z) + g_{1D}\Psi_\uparrow^\dagger(z)\Psi_\downarrow^\dagger(z)\Psi_\downarrow(z)\Psi_\uparrow(z) \tag{3.56}$$

has an exact Bethe ansatz solution [76, 77] (here $g_{1D} = -\hbar^2/(ma) < 0$, with the 1D scattering length $a > 0$). For now this will not bother us and we pretend BdG theory provides a good approximation[13]. Because of a Fermi surface nesting in 1D, the spin imbalanced normal state is always unstable towards FFLO (at $T = 0$). This can be seen from the kernel $K_{1D}^{(2)}$ (pair susceptibility) Eq. (2.32),

---

[13]In fact BdG theory seems to work quite well for certain observables in the weak coupling limit. For an extensive comparison, see e.g. [78].
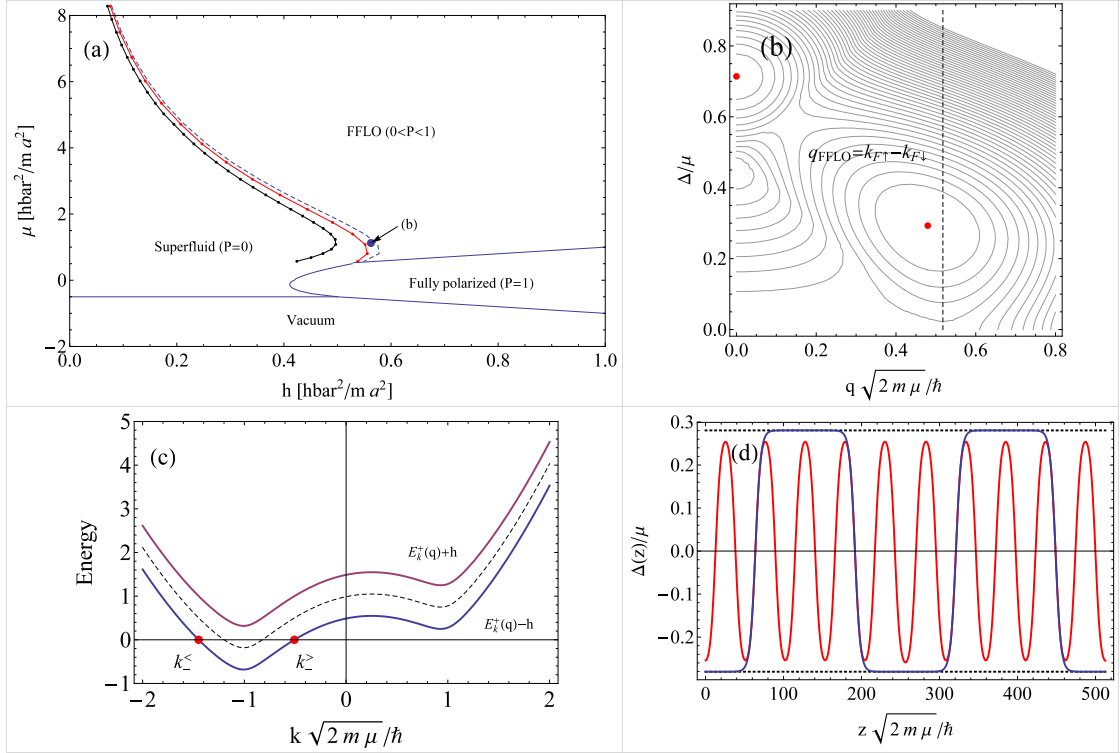
Figure 3.9: Top: (a) Mean-field theory phase diagram of a 1D Fermi gas interacting with attractive interactions with scattering length a (we neglected Hartree shifts). On the black line a π-domain wall has the same energy as the uniform superfluid, indicating an instability of the P=0 superfluid towards FFLO. The red line is the first order phase boundary between superfluid and FF state and the dashed line is the Clogston limit. (b) Free energy of the FF state as a function of Δ_0, q [see Eq. (3.61)] for $(h, \mu) = (0.56, 1.13)\hbar^2/(ma^2)$. Local minima are marked with a red dot. Bottom: (c) Dispersion relation of Bogoliubov quasiparticles for the FF state ansatz $\Delta(z) = \Delta_0 e^{iqz}$ shown here for the parameters of (b). (d) Self-consistent solutions to the 1D BdG equations for different polarization densities at fixed $\mu = 2.25\hbar^2/(ma^2)$. In the limit of low polarization density, the FFLO phase consists of separated domain walls and the order parameter achieves the value of the uniform superfluid in between nodes. At large polarization the magnitude of the order parameter reduces and $\Delta(z)$ becomes sinusiodal. In this limit $\Delta(z)$ closely resembles the LO state.

which evaluates to (for $\mu > h$, $q > 0$)

$$K_{1D}^{(2)}(q) = \frac{m}{\hbar^2} \left[\frac{\text{arctanh}\left(\frac{k_{i+}}{\sqrt{A}}\right) - \text{arctanh}\left(\frac{k_{i-}}{\sqrt{A}}\right) + \text{arctanh}\left(\frac{\sqrt{A}}{k_{o+}}\right)}{\sqrt{A}} \right.$$
$$\left. - \frac{\text{arctanh}\left(\frac{\sqrt{A}}{k_{o-}}\right)}{\sqrt{A}} + \frac{a_{1D}}{2} \right] \qquad (3.57)$$

where $A = \tilde{\mu} - q^2/4$, $k_{i-} = q/2 - \sqrt{\tilde{\mu} - \tilde{h}}$, $k_{o-} = -q/2 - \sqrt{\tilde{\mu} + \tilde{h}}$, $k_{i+} = \min(q/2 + \sqrt{\tilde{\mu} - \tilde{h}}, -q/2 + \sqrt{\tilde{\mu} + \tilde{h}})$, $k_{o+} = \max(q/2 + \sqrt{\tilde{\mu} - \tilde{h}}, -q/2 + \sqrt{\tilde{\mu} + \tilde{h}})$, and $\tilde{\mu}, \tilde{h} = (2m/\hbar^2)\mu, h$. Note that this function has a divergence at $q_{FFLO} = k_{F\uparrow} - k_{F\downarrow} = \sqrt{\tilde{\mu} + \tilde{h}} - \sqrt{\tilde{\mu} - \tilde{h}}$, i.e. mean-field theory predicts that the polarized normal state is always unstable towards pairing at finite momentum.

From this stability analysis we expect three stable equilibrium phases in 1D:

- An unpolarized superfluid state

- A partially polarized phase with pairing at finite momentum (FFLO)

- A fully polarized normal state

The FF state is described by the spatially varying order parameter $\Delta(x) = \Delta\, e^{iqx}$. With the ansatz

$$\begin{pmatrix} u(x) \\ v(x) \end{pmatrix} = \frac{e^{ikx}}{L^{d/2}} \begin{pmatrix} u_k(q)\, e^{iqx/2} \\ v_k(q)\, e^{-iqx/2} \end{pmatrix} \qquad (3.58)$$

the BdG equations become the simple algebraic equations

$$\begin{pmatrix} \xi_{k+q/2} & \Delta \\ \Delta & -\xi_{k-q/2} \end{pmatrix} \begin{pmatrix} u_k(q) \\ v_k(q) \end{pmatrix} = E_k(q) \begin{pmatrix} u_k(q) \\ v_k(q) \end{pmatrix}. \qquad (3.59)$$

Solving the 2×2 eigenvalue problem one finds the eigenvalues

$$E_k^{\pm}(q) = \frac{\xi_{k+q/2} - \xi_{k-q/2}}{2} \pm \sqrt{\left(\frac{\xi_{k+q/2} + \xi_{k-q/2}}{2}\right)^2 + \Delta^2} \qquad (3.60)$$

Since we are using a specific ansatz for $\Delta(x)$, we should variationally minimize the free energy functional Eq. (2.20) as a function of the variational parameters Δ, q. In terms of Δ and q the free energy is given by

$$\Omega(\Delta, q) = \frac{1}{2} \sum_{k,\sigma} \left[\epsilon_k + \epsilon_{q/2} - \mu - |E_k^+(q) + \sigma h| \right] - L\frac{|\Delta|^2}{g_{1D}} \qquad (3.61)$$

The calculation of the free energy is analogous to that of the Sarma phase. When h is larger than the minimum in the dispersion relation $\min_k E_k^+(q)$, the state becomes polarized. In the example from Fig. 3.9 (c), there are two wavevectors, $k_-^\leq > k_-^\geq$, where $h = E_k^+(q)$. The free energy density f is then expressed as the 1D integrals

$$
\begin{aligned}
f(\Delta, q) &= \int_{-\infty}^{k_-^\leq} \frac{dk}{2\pi} \left[\epsilon_k + \epsilon_{q/2} - \mu - E_k^+(q) \right] + \int_{k_-^\geq}^{\infty} \frac{dk}{2\pi} \left[\epsilon_k + \epsilon_{q/2} - \mu - E_k^+(q) \right] \\
&+ \int_{k_-^\leq}^{k_-^\geq} \frac{dk}{2\pi} \left(\epsilon_k + \epsilon_{q/2} - \mu \right) + \frac{1}{2\pi} h \left(k_-^\geq - k_-^\leq \right) + \frac{1}{g_{1D}} |\Delta|^2 \qquad (3.62)
\end{aligned}
$$

We compute these integrals numerically, the results for specific parameters are shown in Fig. 3.9 (b). It turns out that the transition between $P = 0$ superfluid and FF state, shown in Fig. 3.9 (a), is a first order phase transition. To find this transition line we fix $\mu m a^2 / \hbar^2$ and first calculate the energy of the uniform superfluid state at $q = 0$. The energy of the FF state is calculated as a function of the Zeeman field h[14]. The Zeeman field h where the free energy of the FF state matches that of the uniform superfluid marks the location of the first order phase transition. In the weak coupling limit of large density, the asymptotics of the free energy of the FF state can be computed analytically. The critical Zeeman field in this limit is the universal ratio $h_{FF}/\Delta_0 = (1 + \sqrt{3})/4 = 0.683$. We note that, as is the case in 3D, this field is smaller than the Clogston limit

---

[14]To find the finite q minimum of Eq. (3.62) we first perform a line search in Δ along $q = q_{FFLO} = k_{F\uparrow} - k_{F\downarrow}$. With resulting estimates for Δ, q as initial conditions, we use standard minimization algorithms to refine the FF state energy.

$h_c/\Delta_0 = 1/\sqrt{2} = 0.707$ [69].

While the FF state can be used in calculations to find a reasonable approximation to phase boundaries, it is physically distinct from the true mean-field theory FFLO ground state. The main shortcomings of the FF state are

- The excitations of the FF state are gapless Bogoliubov excitations (the true groundstate has gapped Bogoliubov excitations)

- The FF state has the wrong broken symmetries

- A variational calculation with the FF state (or LO state) predicts a first order transition from the SF to normal state. This transition is however believed to be of second order starting with an instability of the superfluid towards forming a single π-soliton.

In 1D it is numerically feasible to directly solve the full system of BdG equations, Eqs. (2.7) and (2.12), self-consistently. The BdG equations in 1D (again neglecting Hartree terms) are given by

$$\begin{pmatrix} -\frac{\hbar^2}{2m}\frac{d^2}{dz^2} - \mu + V(z) & \Delta(z) \\ \Delta^*(z) & -\left(-\frac{\hbar^2}{2m}\frac{d^2}{dz^2} - \mu + V(z)\right) \end{pmatrix} \begin{pmatrix} u_n(z) \\ v_n(z) \end{pmatrix} \tag{3.63}$$

We numerically solve the BdG equations real space by putting the system on a grid with N_g gridpoints and use a box with of length L periodic boundary conditions. The second derivative operator is represented using a pseudospectral representation[15]. The gap equation

$$\Delta(z) = g_{1D} \sum_n u_n^*(z)v_n(z)\left[1 - f(E_{\uparrow n}) - f(E_{\downarrow n})\right] \tag{3.64}$$

---

[15]It turns out that using a pseudospectral representation makes it easier to deal with the UV regularization of the gap equation. Alternatively one could also use a lower order method as we did in Ref. [62], and then match the coupling constant to reproduce the correct order parameter.

needs to be regularized. This is because we work with a finite cutoff, limited by the shortest wavevector or the lattice spacing $\Delta x = L/N_g$ in our simulation, the summation over energies above the cutoff has to be evaluated approximately. This will lead to a correction of the coupling constant g_{1D} [79]. A good approximation is to use a semiclassical approximation for the modes above the momentum cutoff $\Lambda = \pi(N_g - 1)/L$[16]

$$
\begin{aligned}
\sum_{|k|>\Lambda}^{\infty} u_k^*(z)v_k(z) &\approx \sum_{|k|>\Lambda}^{\infty} \frac{\Delta(z)}{2\sqrt{[\epsilon_k - \mu(z)]^2 + |\Delta(z)|^2}} \\
&\approx \Delta(z)\frac{1}{2}\sum_{|k|>\Lambda}^{\infty} \frac{1}{\epsilon_k - \mu(z)} \\
&= \Delta(z)\frac{1}{2\pi}\sqrt{\frac{2m}{\hbar^2\mu(z)}} \operatorname{arctanh}\sqrt{\frac{2m\mu(z)}{\hbar^2\Lambda^2}}
\end{aligned}
$$

where we defined the local chemical potential $\mu(z) = \mu - V(z)$. With this result we can rewrite the gap equation as

$$
\Delta(z) = g_{1D}^R(z) \sum_{n}^{\Lambda} u_n^*(z)v_n(z) \left[1 - f(E_{\uparrow n}) - f(E_{\downarrow n})\right] \tag{3.65}
$$

where the summation is now only over the states included in our numerical simulation (i.e. below the cutoff). The regularized coupling constant g_{1D}^R is related to the bare coupling constant by

$$
\frac{1}{g_{1D}^R(z)} = \frac{1}{g_{1D}} - \frac{1}{2\pi}\sqrt{\frac{2m}{\hbar^2\mu(z)}} \operatorname{arctanh}\sqrt{\frac{2m\mu(z)}{\hbar^2\Lambda^2}}. \tag{3.66}
$$

Similar regularization schemes were used by various authors, see e.g. [79, 78]. Under the assumption of a continuous order phase transition between FFLO and SF we can use the numerical solution to the BdG equations to find the phase boundary. If the phase transition is continuous one expects that at a critical Zeeman field, the free energy of a single domain wall equals the free energy of

[16]We assume an odd number of grid points N_g.

the uniform superfluid. Numerically we find the phase boundary by calculating the free energy of a pair of domain walls. In the self-consistent calculation we seed $\Delta(z)$ with a pair of step potential domain walls and fix h such that all bound states are occupied[17]. The gap equation Eq. (3.65) is subsequently iterated to self-consistency. The energy of the domain wall can be written as $\Omega_{DW} = \Omega_{DW}^{(0)} - h\Delta N$, where the piece $\Omega_{DW}^{(0)}$ includes all eigenvalues in the summation in Eq. (2.20) except for the sub-gap bound states. In terms of the uniform superfluid the critical Zeeman field h_{FFLO} is

$$h_{FFLO} = \frac{\Omega_{DW}^{(0)} - \Omega_{SF}}{\Delta N} \tag{3.67}$$

The black line between SF and FFLO phases in Fig. 3.9 (a) shows $h_{FFLO}(ma^2/\hbar^2)$ as a function of the chemical potential $\mu m a^2/\hbar^2$. Note that this line is always at lower field than the result from the FF ansatz. In the weak coupling limit our result agrees with the analytics of Ref. [69], who predict $h_{FFLO}/\Delta_0 = 2/\pi$. The slope of the SF to FFLO line is opposite of the same transition line in 3D. This can be seen directly from the asymptotic result for the weak coupling mean-field BCS gap $\Delta_0/\mu \sim 8e^{-\pi k_F a}$ which approaches zero as $\mu \to \infty$. In 1D, the high density limit is the weak coupling limit and the low density limit is strongly coupled. One way to understand this behavior is to consider a δ-function impurity in 1D — for any non-zero scattering length, at low energy the reflection probability approaches unity (in 3D it is the other way round, at low energies the scattering rate goes to zero). The implication for experiments with harmonically trapped gases is that at low polarization P, the FFLO phase appears at the *center* of the trap. To illustrate this behavior we have solved the BdG equations for a harmonically trapped 1D system with the results shown in Fig. 3.10.

---

[17]We used a pair of domain-walls to satisfy periodic boundary conditions. This approach works if the separation of the domain walls is much larger than the coherence length.
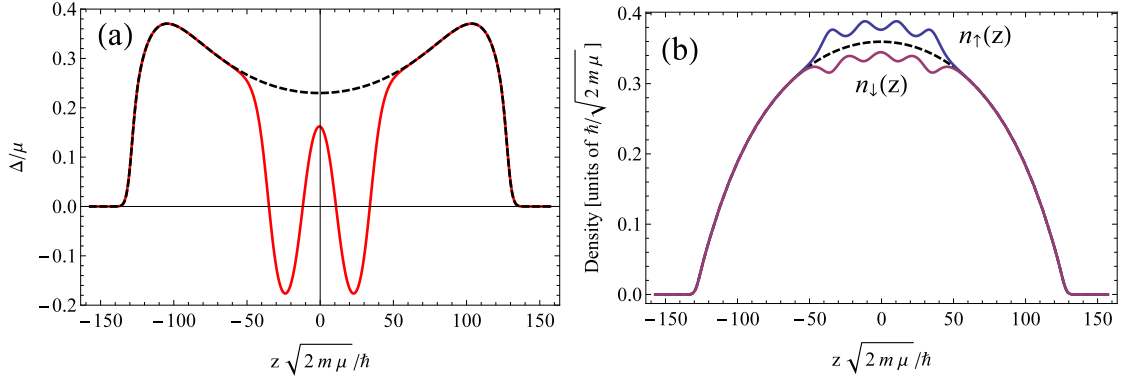
Figure 3.10: Self-consistent solution to the BdG equations in 1D for a harmonically trapped system with $N_\uparrow = 70$, $N_\downarrow = 66$, $\mu(z=0) = 2.25\hbar^2/(ma^2)$. Left: $\Delta(z)$ with and without imbalance. Each node in the order parameter corresponds to one excess fermion. Right: Density of up-spins $n_\uparrow(z)$ (down-spins $n_\downarrow(z)$) respectively. Note that at low polarization the density profile in 1D is inverted with respect to the 3D scenario. The fully paired phase sits on the inside, whereas the FFLO is visible at the trap center.

Finally we would like to emphasize that while the BdG mean-field theory approach described here is a reasonable variational approach in the weak coupling limit, it fails miserably in the limit of strong coupling ($g_{1D} \to -\infty$). At strong coupling the ground state of Eq. (3.56) is, as will be discussed later, a Tonks gas of pairs, whereas mean-field theory would predict a weakly interacting Bose condensate. In that sense we cannot consider the mean-field theory in 1D as an interpolating scheme that interpolates between weakly interacting BEC and BCS limits. A quasi-1D model however, where weak tunneling between tubes is included, does not suffer from these shortcomings. In such a model the low density limit is effectively three dimensional, thus weakly interacting. In the high density limit the Fermi surface of a quasi-1D model becomes one-dimensional, therefore also weakly interacting. These considerations justify our BdG mean-field theory approach for the quasi-1D Fermi gas described in chapter 5.

3.7 Appendix A: Asymptotic expansion for BCS and BEC limit

In this appendix we rederive some basic results for gap and number equation in special limits [8].

3.7.1 BCS limit

In the weak coupling BCS limit, we have $\Delta_0 \to 0$. For small Δ_0, the number equation gives simply the free fermion result

$$n_0 = \frac{1}{3\pi^2} \left(\frac{2m}{\hbar^2} \right)^{3/2} \mu^{3/2} + \cdots \tag{3.68}$$

This means $\mu \approx E_F$. We plug this result into the gap equation and get

$$\frac{\pi}{2k_F a_s} = \int_0^\infty dx \left(1 - \frac{x^2}{\sqrt{(x^2 - 1)^2 + (\Delta_0/E_F)^2}} \right) \tag{3.69}$$

We proceed by computing the integral

$$I_1(\epsilon) = \int_0^\infty dx \left(1 - \frac{x^2}{\sqrt{(x^2 - 1)^2 + \epsilon}} \right) \tag{3.70}$$

as $\epsilon \to 0$. This is a nice textbook exercise in matched asymptotic expansions. If we try to put $\epsilon = 0$, the integral does not converge. This is expected, because we know from BCS theory that the integral should behave as $\log(\epsilon)$. This also means we can't Taylor expand the integrand in ϵ. The integral is sharply peaked around $x = 1$, so we might try approximate the integrand on an interval $(1 - \delta, 1 + \delta)$ around the singularity (where δ is some cutoff)

$$
\begin{aligned}
I_i(\epsilon, \delta) &= \int_{1-\delta}^{1+\delta} dx \left(1 - \frac{x^2}{\sqrt{(x^2 - 1)^2 + \epsilon}} \right) = \int_{-\delta}^{\delta} dy \left(1 - \frac{(1-y)^2}{\sqrt{((1+y)^2 - 1)^2 + \epsilon}} \right) \\
&\approx \int_{-\delta}^{\delta} \left(1 - \frac{1}{\sqrt{4y^2 + \epsilon}} \right) \approx 2\delta - \log \frac{4\delta}{\sqrt{\epsilon}}
\end{aligned}
$$

If we approximate $I \approx I_i$ we get $\Delta/E_F = 4\delta e^{-2\delta} e^{\pi/(2k_F a_s)}$. This is reminiscent of BCS theory, where one typically chooses the Debye frequency as high-energy cutoff. Here we can do a better job since we precisely know the interaction between fermions. We split $I(\epsilon)$ into three parts: two outer regions, and an inner region around the singularity at $x = 1$

$$I_1(\epsilon) = I_o^<(\epsilon, \delta) + I_i(\epsilon, \delta) + I_o^>(\epsilon, \delta) \tag{3.71}$$

In the outer regions we can Taylor expand the integrand in ϵ

$$1 - \frac{x^2}{\sqrt{(x^2-1)^2 + \epsilon}} \approx 1 - \frac{x^2}{|x^2 - 1|} + \frac{x^2 \epsilon}{2\left((x^2-1)^2\right)^{3/2}} + O\left(\epsilon^2\right)$$

The outer integrals

$$I_o^<(\epsilon, \delta) = \int_0^{1-\delta} dx \left(1 - \frac{x^2}{\sqrt{(x^2-1)^2 + \epsilon}}\right) \tag{3.72}$$

$$I_o^>(\epsilon, \delta) = \int_{1+\delta}^{\infty} dx \left(1 - \frac{x^2}{\sqrt{(x^2-1)^2 + \epsilon}}\right) \tag{3.73}$$

can then be done analytically to order ϵ. This approximation is uniformly valid if $\epsilon \ll \delta^2 \ll 1$, so we can e.g take $\delta = \epsilon^{1/3}$ to satisfy this condition as $\epsilon \to 0$. Putting all pieces together and putting $\delta \equiv \epsilon^{1/3}$ we get to leading order in ϵ

$$I_1(\epsilon) \approx 2 + \log(\sqrt{\epsilon}/8) \tag{3.74}$$

This gives the well known analytic result $\Delta/E_F = 8e^{-2} e^{\pi/(2k_F a_s)}$ in the BCS limit. From Fig. 3.1 we see that the formula is a good approximation to the numerical solution of the full mean-field theory already for $k_F a_s \leq -1$. This justifies to some extent why many experiments consider $k_F a_s \sim -1$ to be in the BCS limit. From the asymptotic expansion for the gap equation Eq. (3.74) can be integrated to give an approximation for the energy. For a uniform order parameter, the

mean-field energy is given by

$$\Omega_{MF}(\Delta_0) = \sum_{\mathbf{k}} \left[\epsilon_{\mathbf{k}} - \mu - E_{\mathbf{k}} - \frac{1}{2\epsilon_{\mathbf{k}}} \right] - \frac{m}{4\pi a_s \hbar^2} |\Delta_0|^2 \qquad (3.75)$$

$$\approx E_F \frac{(Lk_F)^3}{2\pi^2} \left[I_2 \left(\frac{\Delta_0^2}{E_F^2} \right) - \frac{\pi}{4k_F a_s} \left(\frac{\Delta_0}{E_F} \right)^2 \right] \qquad (3.76)$$

with

$$I_2(\epsilon) \approx \frac{3}{4}\epsilon + \frac{\epsilon}{2} \log \frac{\sqrt{\epsilon}}{8} - \frac{4}{15} \qquad (3.77)$$

When we evaluate the free energy at its minimum (where $2 + \log(\sqrt{\epsilon}/8) = \pi/(2k_F a_s)$), we get

$$\Omega_{MF}(\Delta_0) - \Omega_{MF}(\Delta_0 = 0) = -\frac{(Lk_F)^3}{8\pi^2} \frac{\Delta_0^2}{E_F} \qquad (3.78)$$

where we subtracted the noninteracting energy of a two-species Fermi gas $\Omega_{MF}(\Delta_0 = 0) = -2E_F(Lk_F)^3/(15\pi^2)$. The energy of the condensed state is lower by an energy gain proportional to Δ_0^2.

3.7.2   BEC limit

In the BEC limit ($|\mu| \gg \Delta_0$; $\mu < 0$), the perturbation expansion of the momentum integrals is non-singular, so we use a Taylor series expansion in $(\Delta_0/\mu)^2$

$$n_0(\mu, \Delta_0) = \left(\frac{-2m\mu}{\hbar^2} \right)^{3/2} \frac{1}{16\pi} \left[\left(\frac{\Delta_0}{\mu} \right)^2 - \frac{3}{32} \left(\frac{\Delta_0}{\mu} \right)^4 + \cdots \right]$$

$$\frac{1}{4\pi a_s} = \frac{1}{4\pi} \left(-\frac{2m\mu}{\hbar^2} \right)^{1/2} \left[1 + \frac{1}{16} \left(\frac{\Delta_0}{\mu} \right)^2 + \cdots \right]$$

We would like to find expansion for μ/E_F in the small parameter $1/k_F a_s$. To do this we write gap and number equations in a dimensionless form with $\epsilon =$

$(\Delta_0/\mu)^2$

$$\left(-\frac{E_F}{\mu}\right)^{3/2} = \frac{3}{16\pi}\left(\epsilon - \frac{3}{32}\epsilon^2 + \cdots\right) \tag{3.79}$$

$$\left(-\frac{\epsilon_B}{2\mu}\right)^{3/2} = 1 + \frac{\epsilon}{16} + \cdots \tag{3.80}$$

where $\epsilon_B = \hbar^2/(ma_s^2)$ is the binding energy of two fermions in vacuum. To leading order we find that $\mu = -\epsilon_B/2$ (or $\mu/E_F \approx -1/(k_F a_s)^2$) which means that for tightly bound dimers, the energy to add one fermion is just half the binding energy, as expected. Solving Eqs. (3.79) and (3.80) perturbatively for $\delta\mu = \mu + \epsilon_B/2$ we find

$$\mu \approx -\epsilon_B/2 + \delta\mu = E_F\left(-\frac{1}{(k_F a_s)^2} + \frac{2}{3\pi}k_F a_s + \cdots\right) \tag{3.81}$$

Similarly one finds

$$\Delta_0 \approx E_F\sqrt{\frac{16}{3\pi}}\frac{1}{(k_F a_s)^{1/2}} + \cdots \tag{3.82}$$

In the deep BEC limit $0 < k_F a_s \ll 1$, mean-field theory describes the tightly bound dimers as a weakly interacting Bose gas. Twice the chemical potential difference $2\delta\mu$ should be interpreted as the boson chemical potential μ_B. For the weakly interacting Bose gas, μ_B is given by

$$\mu_B = \frac{4\pi\hbar^2 a_{BB} n_B}{m_B} = 2\delta\mu = \frac{\pi\hbar^2 a_s n_0}{m} \tag{3.83}$$

Here a_{BB} is the the boson-boson scattering length and $n_B = 2n_0$ $(m_B = 2m)$ is the density (mass) of pairs respectively. From the mean-field theory we obtain the prediction $a_{BB} = 2a_s$[18]

---

[18] As it turns out, this prediction is not quite correct. A solution of the dimer-dimer scattering problem predicts $a_{BB} = 0.6a_s$ [10, 8, 56].

3.8 Appendix B: Andreev boundstates for two domain walls

Here we describe our solution to the BdG equations of two step potential domain walls located at $z = \pm d/2$. This problem serves as a toy model for the FFLO state in 1D. We assume that the nodes of the order parameter are at $z = \pm d/2$ and $\Delta(z) = \Delta_0 > 0$ in between. By reflection symmetry we only need to consider one boundary condition (b.c.) at $z = d/2$ (at $z = -d/2$ the b.c. will automatically be satisfied). There are four linear independent solutions that we choose to be real

$$\psi_1(z) = \begin{pmatrix} \cos(\phi + \alpha z) \\ \cos(\alpha z) \end{pmatrix} e^{-\kappa z} \qquad \psi_2(z) = \begin{pmatrix} \sin(\phi + \alpha z) \\ \sin(\alpha z) \end{pmatrix} e^{-\kappa z}$$

$$\psi_3(z) = \begin{pmatrix} \cos(\alpha z - \phi) \\ \cos(\alpha z) \end{pmatrix} e^{\kappa z} \qquad \psi_4(z) = \begin{pmatrix} \sin(\alpha z - \phi) \\ \sin(\alpha z) \end{pmatrix} e^{\kappa z}$$

First we consider the solutions with even parity. The solutions in the middle region $-d/2 < z < d/2$ are then

$$\psi_{1s}(z) = \psi_1(z) + \psi_3(z) \qquad \psi_{2s}(z) = \psi_2(z) - \psi_4(z)$$

In the region $z > d/2$ we discard the exponentially increasing solutions

$$\phi_1(z) = \begin{pmatrix} \cos(\phi + \alpha(z - d/2)) \\ -\cos(\alpha(z - d/2)) \end{pmatrix} e^{-\kappa(z-d/2)} \qquad \phi_2(z) = \begin{pmatrix} \sin(\phi + \alpha(z - d/2)) \\ -\sin(\alpha(z - d/2)) \end{pmatrix} e^{-\kappa(z-d/2)}$$

Continuity at $z = d/2$ implies

$$A\psi_{1s}(d/2) + B\psi_{2s}(d/2) = C\phi_1(d/2) + D\phi_2(d/2)$$

$$A\psi'_{1s}(d/2) + B\psi'_{2s}(d/2) = C\phi'_1(d/2) + D\phi'_2(d/2)$$

where A, B, C, D are c-number constants. These equations have nontrivial solutions when the determinant of the 4×4 coefficient matrix vanishes. One obtains

the transcendental equation

$$(\alpha\cos(\phi) + \kappa\sin(\phi))(\alpha\cos(\phi) - \kappa\sin(\phi)) = -8e^{-d\kappa}\alpha\kappa\sin(\alpha d) + 4e^{-2d\kappa}\alpha^2 \quad (3.84)$$

For $d \to \infty$ the right hand side is zero and the left hand side is just the product of the equations for the negative and positive single domain wall boundstate energies. Similarly, the eigenvalue equation for odd parity is

$$(\alpha\cos(\phi) + \kappa\sin(\phi))(\alpha\cos(\phi) - \kappa\sin(\phi)) = 8e^{-d\kappa}\alpha\kappa\sin(\alpha d) + 4e^{-2d\kappa}\alpha^2 \quad (3.85)$$

One can extract the asymptotics for large d by expanding the equation on the left hand side around the single domain wall energy E_0 and evaluating the right hand side at $E = E_0$. On the BCS side the solutions oscillate with an exponential decaying envelope $\sim e^{-d\kappa}$, but in the sum of both positive energies the oscillations cancel at large distance and the decay is faster $\sim e^{-2d\kappa}$.

BIBLIOGRAPHY FOR CHAPTER 3

[1] D. M. Eagles, Phys. Rev. **186**, 456 (1969).

[2] A. J. Leggett, in *Modern Trends in the Theory of Condensed Matter*, edited by A. Pekalski and J. Przystawa (Springer-Verlag, Berlin, 1980), p. 14.

[3] Journal of Low Temperature Physics **59**, 195 (1985), 10.1007/BF00683774.

[4] M. Drechsler and W. Zwerger, Annalen der Physik **504**, 15 (1992).

[5] R. Haussmann, **91**, 291 (1993), 10.1007/BF01344058.

[6] C. A. R. Sá de Melo, Mohit Randeria, and Jan R. Engelbrecht, Phys. Rev. Lett. **71**, 3202 (1993).

[7] R. Haussmann, Phys. Rev. B **49**, 12975 (1994).

[8] M. Randeria, in *Bose-Einstein Condensation*, edited by A. Griffin, D. W. Snoke, and S.Stringari (Cambridge University Press, Cambridge, 1995), p. 35.

[9] Y. Ohashi and A. Griffin, Phys. Rev. A **67**, 033603 (2003).

[10] D. S. Petrov, C. Salomon, and G. V. Shlyapnikov, Phys. Rev. Lett. **93**, 090404 (2004).

[11] E. P. Gross, Nuovo Cimento **20**, 454 (1961).

[12] L. P. Pitaevskii, Sov. Phys. JETP **13**, 451 (1961).

[13] Henning Heiselberg, Phys. Rev. A **63**, 043606 (2001).

[14] K. M. O'Hara, S. L. Hemmer, M. E. Gehm, S. R. Granade, and J. E. Thomas, Science **298**, 2179 (2002).

[15] J. Carlson, S.-Y. Chang, V. R. Pandharipande, and K. E. Schmidt, Phys. Rev. Lett. **91**, 050401 (2003).

[16] G. M. Bruun, Phys. Rev. A **70**, 053602 (2004).

[17] Tin-Lun Ho, Phys. Rev. Lett. **92**, 090402 (2004).

[18] G. A. Baker, in *Proceedings of the Tenth International Conference on Recent Progress in Many-Body Theories*, edited by R.F. Bishop et al. (World Scientific, Singapore, 2000).

[19] M. Bartenstein, A. Altmeyer, S. Riedl, S. Jochim, C. Chin, J. Hecker Denschlag, and R. Grimm, Phys. Rev. Lett. **92**, 120401 (2004).

[20] T. Bourdel, L. Khaykovich, J. Cubizolles, J. Zhang, F. Chevy, M. Teichmann, L. Tarruell, S. J. J. M. F. Kokkelmans, and C. Salomon, Phys. Rev. Lett. **93**, 050401 (2004).

[21] Guthrie B. Partridge, Wenhui Li, Ramsey I. Kamar, Yean An Liao, and Randall G. Hulet, Science **311**, 503 (2006).

[22] A. Perali, P. Pieri, and G. C. Strinati, Phys. Rev. Lett. **93**, 100404 (2004).

[23] G. E. Astrakharchik, J. Boronat, J. Casulleras, and S. Giorgini, Phys. Rev. Lett. **93**, 200404 (2004).

[24] S. Y. Chang, V. R. Pandharipande, J. Carlson, and K. E. Schmidt, Phys. Rev. A **70**, 043602 (2004).

[25] J. Carlson and Sanjay Reddy, Phys. Rev. Lett. **95**, 060401 (2005).

[26] Qijin Chen, Jelena Stajic, Shina Tan, and K. Levin, Physics Reports **412**, 1 (2005).

[27] C. Lobo, A. Recati, S. Giorgini, and S. Stringari, Phys. Rev. Lett. **97**, 200403 (2006).

[28] H. Hu, P. D. Drummond, and X.-J. Liu, Nature Phy **3**, 469 (2007).

[29] Martin Y. Veillette, Daniel E. Sheehy, and Leo Radzihovsky, Phys. Rev. A **75**, 043614 (2007).

[30] Yusuke Nishida and Dam Thanh Son, Phys. Rev. A **75**, 063617 (2007).

[31] Peter Arnold, Joaquín E. Drut, and Dam Thanh Son, Phys. Rev. A **75**, 043605 (2007).

[32] R. Haussmann and W. Zwerger, Phys. Rev. A **78**, 063602 (2008).

[33] S. Gandolfi, K. E. Schmidt, and J. Carlson, Phys. Rev. A **83**, 041601 (2011).

[34] X. S. Wu, P. W. Adams, and G. Catelani, Phys. Rev. B **74**, 144519 (2006).

[35] Y. L. Loh, N. Trivedi, Y. M. Xiong, P. W. Adams, and G. Catelani, ArXiv e-prints (2011).

[36] S. Uji, T. Terashima, M. Nishimura, Y. Takahide, T. Konoike, K. Enomoto, H. Cui, H. Kobayashi, A. Kobayashi, H. Tanaka, M. Tokumoto, E. S. Choi, T. Tokumoto, D. Graf, and J. S. Brooks, Phys. Rev. Lett. **97**, 157001 (2006).

[37] H. A. Radovan, N. A. Fortune, T. P. Murphy, S. T. Hannahs, E. C. Palm, S. W. Tozer, and D. Hall, Nature **425**, 51 (2003).

[38] A. M. Clogston, Phys. Rev. Lett. **9**, 266 (1962).

[39] B. S. Chandrasekhar, Applied Physics Letters **1**, 7 (1962).

[40] G. Sarma, J. Phys. Chem. Solids **24**, 1029 (1963).

[41] Peter Fulde and Richard A. Ferrell, Phys. Rev. **135**, A550 (1964).

[42] A. I. Larkin and Yu. N. Ovchinnikov, Sov. Phys. JETP **20**, 762 (1965).

[43] Roberto Casalbuoni and Giuseppe Nardulli, Rev. Mod. Phys. **76**, 263 (2004).

[44] Paulo F. Bedaque, Heron Caldas, and Gautam Rupak, Phys. Rev. Lett. **91**, 247002 (2003).

[45] K. B. Gubbels, M. W. J. Romans, and H. T. C. Stoof, Phys. Rev. Lett. **97**, 210402 (2006).

[46] Masudul Haque and H. T. C. Stoof, Phys. Rev. A **74**, 011602 (2006).

[47] C.-H. Pao, Shin-Tza Wu, and S.-K. Yip, Phys. Rev. B **73**, 132506 (2006).

[48] Daniel E. Sheehy and Leo Radzihovsky, Phys. Rev. Lett. **96**, 060401 (2006).

[49] T. N. De Silva and E. J. Mueller, Phys. Rev. A **73**, 051602 (2006).

[50] D. T. Son and M. A. Stephanov, Phys. Rev. A **74**, 013614 (2006).

[51] S. Pilati and S. Giorgini, Phys. Rev. Lett. **100**, 030401 (2008).

[52] M. Punk, P. T. Dumitrescu, and W. Zwerger, Phys. Rev. A **80**, 053605 (2009).

[53] Yong-Il Shin, Christian H. Schunck, Andre Schirotzek, and Wolfgang Ketterle, Nature **451**, 689 (2008).

[54] Yong-Il Shin, Andre Schirotzek, Christian H. Schunck, and Wolfgang Ketterle, Realization of a strongly interacting Bose-Fermi mixture from a two-component Fermi gas, 2008.

[55] S. Nascimbène, N. Navon, K. J. Jiang, L. Tarruell, M. Teichmann, J. McKeever, F. Chevy, and C. Salomon, Phys. Rev. Lett. **103**, 170402 (2009).

[56] P. Pieri and G. C. Strinati, Phys. Rev. Lett. **96**, 150404 (2006).

[57] Daniel E. Sheehy and Leo Radzihovsky, Ann. Phys. (NY) **322**, 8 (2007).

[58] G.V. Skorniakov and K. A. Ter-Martirosian, Sov. Phys. JETP **4**, 648 (1957).

[59] D. S. Petrov, Phys. Rev. A **67**, 010703 (2003).

[60] Sourish Basu, Ph.D. thesis, Cornell University, 2009.

[61] E. H. Graf, D. M. Lee, and John D. Reppy, Phys. Rev. Lett. **19**, 417 (1967).

[62] Stefan K. Baur, Sourish Basu, Theja N. De Silva, and Erich J. Mueller, Phys. Rev. A **79**, 063628 (2009).

[63] Yean-an Liao, Ann Sophie C. Rittner, Tobias Paprotta, Wenhui Li, Guthrie B. Partridge, Randall G. Hulet, Stefan K. Baur, and Erich J. Mueller, Nature **467**, 567 (2010).

[64] F. Chevy, Phys. Rev. Lett. **96**, 130401 (2006).

[65] Martin W. Zwierlein, Andre Schirotzek, Christian H. Schunck, and Wolfgang Ketterle, Science **311**, 492 (2006).

[66] David J. Thouless, Annals of Physics **10**, 553 (1960).

[67] Nobukatsu Yoshida and S.-K. Yip, Phys. Rev. A **75**, 063601 (2007).

[68] A. I. Buzdin and V. V. Tugushev, Sov. Phys. JETP **58**, 428 (1983).

[69] Kazushige Machida and Hiizu Nakanishi, Phys. Rev. B **30**, 122 (1984).

[70] C. Caroli, P. G. De Gennes, and J. Matricon, Physics Letters **9**, 307 (1964).

[71] P. G. de Gennes, *Superconductivity of Metals and Alloys* (W.A. Benjamin, New York, 1966).

[72] John Bardeen, R. Kümmel, A. E. Jacobs, and L. Tewordt, Phys. Rev. **187**, 556 (1969).

[73] Joel D. Shore, Ming Huang, Alan T. Dorsey, and James P. Sethna, Phys. Rev. Lett. **62**, 3089 (1989).

[74] Mauro Antezza, Franco Dalfovo, Lev P. Pitaevskii, and Sandro Stringari, Phys. Rev. A **76**, 043610 (2007).

[75] Constantine Callias, Communications in Mathematical Physics **62**, 213 (1978), 10.1007/BF01202525.

[76] M. Gaudin, Phys. Lett. **24A**, 55 (1967).

[77] C. N. Yang, Phys. Rev. Lett. **19**, 1312 (1967).

[78] Xia-Ji Liu, Hui Hu, and Peter D. Drummond, Phys. Rev. A **76**, 043605 (2007).

[79] Marcella Grasso and Michael Urban, Phys. Rev. A **68**, 033610 (2003).

CHAPTER 4

DEFORMED CLOUDS OF IMBALANCED FERMIONIC SUPERFLUIDS

4.1 Abstract

We present a series of theoretical studies of the boundary between a superfluid and normal region in a partially polarized gas of strongly interacting fermions. We present mean-field estimates of the surface energy in this boundary as a function of scattering length. We discuss the structure of the domain wall, and use a previously introduced phenomonological model to study its influence on experimental observables. Our microscopic mean-field calculations are not con-sistent with the magnitude of the surface tension found from our phenomono-logical modelling of data from the Rice experiments. We conclude that one must search for novel mechanisms to explain the experiments.

4.2 Introduction

What happens when one tries to polarize a fermionic superfluid? Experiments at MIT and Rice have shown that when the fermions are interacting via resonant short range interactions, the fluid responds by phase separating into a largely unpolarized superfluid region and a less polarized normal region [1, 2, 3, 4, 5].

The Rice experiments [1, 2] show a dramatic distortion of the central super-fluid region in their trapped gas, pointing to significant surface tension in the boundary. Here we present a theoretical study of this boundary and discuss the consequences of surface tension.

The phase separation seen in these experiments arises because a zero temperature conventional s-wave superfluid is unable to accommodate spin polarization: all of the atoms in one spin state ($\uparrow$) are paired with atoms of the opposite spin ($\downarrow$). Changing the density ratio $n_\uparrow/n_\downarrow$ from unity requires adding sufficient energy to break these pairs. Consequently, when excess particles of one spin state are added to a paired atomic cloud, those particles simply float to the surface, forming a normal fluid. Given that there is a sharp boundary between the superfluid and normal region, the order parameter must vary rapidly, producing a surface energy. In section 4.3 we use the Bogoliubov-de-Gennes(BdG) equations as a microscopic theory of this interface, and extract a dimensionless measure of the surface tension η.

In addition to the phase separation scenario seen in experiments, which was essentially predicted by Clogston and Chandrasekhar [6, 7], there have been many theoretical proposals for how the superfluid can accommodate extra spins [8, 9, 10, 11, 12, 13, 14, 15, 16, 17, 18, 19, 20, 21, 22, 23, 24, 25, 26, 27]. We will make some comments on one class of states, the "FFLO" states introduced by Fulde, Ferrell, Larkin and Ovchinnikov [8, 9] where polarization resides in a periodic array of nodes in the superfluid order parameter, or is accommodated by creating supercurrents. Our mean field approach is sufficiently general that if such a phase existed in the parameter regime that we discuss, we could observe it. Like the experiments, and previous mean-field calculations [28], we see no sign

of this phase near unitarity (where the scattering length is infinite). Interestingly, a recent density functional calculation [29] raises the possibility that the mean-field theory may be underestimating the stability of the FFLO state. We anticipate that in the near future more sophisticated numerical techniques will be able to unambiguously address the presence of the FFLO state.

Like other theoretical calculations based upon the Bogoliubov de Gennes equations[30, 31, 32, 33, 34, 35, 36, 37, 38] we find that the order parameter and polarization oscillate in the domain wall separating the two regions. These oscillations, which in no way should be interpreted as an intervening phase [36], are small at unitarity, but become larger as one approaches the BCS limit (small and negative scattering length a). At sufficiently small negative scattering length the decay length of these oscillations diverge, signaling the onset of the bulk FFLO phase. The topology of the phase diagram of polarized fermions [22, 39] at zero temperature features tricritical points in both the BEC ($1/k_f a \gg 1$) and BCS ($-1/k_f a \gg 1$) limit, where the first order phase transition between superfluid and normal state turn second order. As surface tension vanishes at the tricritical points, it reaches a maximum in the crossover region.

In section 4.4 we explore the consequences of surface tension on the shape of the superfluid-normal boundary for a unitary gas in an anisotropic harmonic trap. As in previous work [40, 41, 42] we use a simple elastic model for the boundary. By expanding the shape of the boundary in a Fourier series, we are able to compare its detailed structure with that of experiments. While our model appears to capture a great many of the experimental features, it yields sharper density features. We attribute the discrepancies to the fact that we model the trapping potential as harmonic.

This method complements the approach of Natu and Mueller [42] where the conditions of hydrostatic equilibrium were used to derive a differential equation for the boundary. Like Haque *et al.* [41], we find that as one increases the surface tension, the boundary distorts from an ellipse into a "capsule-like" shape. The most relevant experiments, performed at Rice in 2006 [2], use small numbers of particles in a highly anisotropic trap. Due to the large surface area to volume ratio these experiments observe large distortions, consistent with surface tension which is one order of magnitude larger than predicted by our microscopic arguments. This behavior should be contrasted with experimental studies at MIT [5] which find no observable distortion of the superfluid-normal boundary. Taking into account the much smaller surface area to volume ratio in these experiments, this null observation bounds η to be not much larger than the value we calculate. We have no explanation for this apparent discrepancy. It is undoubtedly related to the fact that the Rice experiment finds a normal fluid whose local polarization is almost 100%, while the normal fluid seen at MIT is always partially polarized, even at the lowest temperatures.

4.2.1 Background

In the experiments of interest, fermionic alkali atoms (typically ^{6}Li) are trapped in a nominally harmonic optical potential. The atoms are transferred into two collisionally stable hyperfine states so that no spin relaxation occurs on the timescale of the experiment: the number of particles in each of the two spin states are separately conserved. Due to the short range nature of the interactions, at sufficiently low temperature scattering is forbidden between two fermions in the same spin state. Hence interactions can be parameterized by

a single scattering length a, which is a function of the applied magnetic field [43, 44].

For $a < 0$ the low energy scattering is attractive, and at low temperature the spin balanced system is a BCS superfluid. For $a > 0$ the low energy scattering is repulsive, however there exists a two-body bound state in vacuum. The low temperature phase in this case is a Bose condensate of pairs. One of the remarkable predictions born out by experiments is that these two superfluid phases are continuously connected to one another [45, 46, 47, 48, 49, 4, 5, ?]. Most interest has focused around the unitary point ($a = \pm\infty$) where the scattering cross-section is maximal and in free space there exists a bound state at threshold. At this point the interactions do not provide a length-scale to the system, leading to universal thermodynamics where all thermodynamic functions can be expressed in terms of a power of the density times a universal function of the density scaled by the thermal wavelength $n\Lambda^3$ and the spin imbalance $n_\uparrow/n_\downarrow$ [50, 51, 52, 53, 54]. In particular, if in the absence of a trap there is a flat phase boundary between a superfluid and a normal region, with equal pressures on each side of the boundary, we showed in [40] that any surface tension can be written as

$$\sigma = \eta \frac{\hbar^2}{2m} n_s^{4/3} \tag{4.1}$$

where n_s is the density on the superfluid side of the boundary. A completely equivalent parameterization was later used by Haque and Stoof [41],

$$\sigma = \eta_s \frac{m}{\hbar^2} \mu^2. \tag{4.2}$$

To convert between the two parameterizations one needs to know the equations of state of the superfluid – which on dimensional grounds has the simple form

$$n_s(\mu) = n_\uparrow + n_\downarrow = \frac{1}{3\pi^2} [\frac{2m}{\hbar^2(1+\beta)}\mu]^{3/2}, \tag{4.3}$$

where μ is the average chemical potential and β is a dimensionless universal many body parameter [50, 51, 53, 54]. According to quantum Monte-Carlo calculations $\beta \approx -0.58$ [52, 55, 56, 57, 58], which gives $\eta = 8.1\eta_s$.

If, as in the experiments, the boundary is curved, one expects to observe a pressure drop related to the curvature [42]. In that case, the dimensional argument leading to Eq. (4.1) yields an extra parameter, and one must take $\eta = \eta(\Delta p/p)$ to be a function of the relative pressure drop. As in all previous treatments, we will neglect the Δp dependence of this parameter.

The presence of a superfluid-normal phase boundary for the trapped gas is understood by examining the finite temperature phase diagram of a uniform Fermi gas, as sketched in figure 4.1(a) in the polarization-temperature plane. At zero temperature the superfluid and normal state are separated by a polarization driven first order phase transition. Since the polarization changes discontinuously, there is a "forbidden region" analogous to the one occurring in the density-temperature phase diagram for a liquid-gas phase transition. The location of the phase boundaries are found by a standard Maxwell construction, where the pressures (free energies) of the two phases are equated. When placed in a fixed volume (or confined by a harmonic trap) this first order phase transition leads to a regime of phase coexistence, just as in the more familiar situation of a liquid-vapor transition.

This first order phase transition is only found at sufficiently low temperatures. There is a tricritical point, above which the boundary becomes a continuous second order line. This behavior is consistent with the standard model of an unpolarized superfluid, which has a temperature driven second order phase transition. This structure was experimentally mapped out in [5].

71
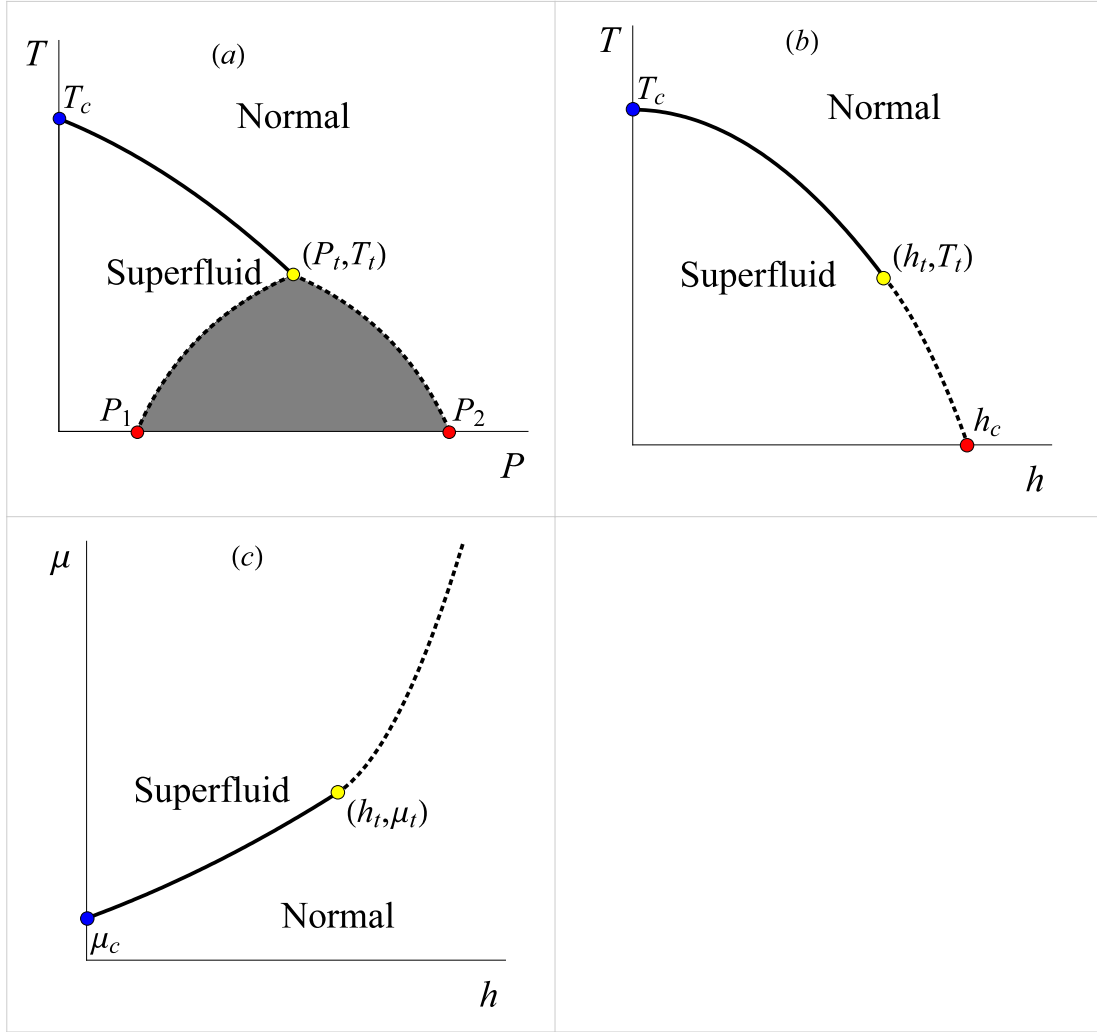
Figure 4.1: Schematic phase diagram of a two component Fermi gas as a function of (a) Temperature $[T]$ - Polarization $[P = (n_\uparrow - n_\downarrow)/(n_\uparrow + n_\downarrow)]$, (b) Temperature $[T]$ - chemical potential difference $[h = (\mu_\uparrow - \mu_\downarrow)/2]$, and (c) chemical potential $[\mu = (\mu_\uparrow - \mu_\downarrow)/2]$ - chemical potential difference $[h = (\mu_\uparrow - \mu_\downarrow)/2]$. The equation of state sets a relationship between P, T, h, and μ, so only three of them are needed to specify the state. Solid lines: continuous phase transitions; dashed lines: discontinuous; these meet at the tricritical point $[P_t, h_t, T_t]$ or $[\mu_t, h_t, T_t]$. The gray region in (a) maps onto the dashed line in (b), and represents a coexistence region. On the BCS side of resonance $a < 0$, and for sufficiently large a, P_1=0 and $0 < P_2 < 1$. When $a > 0$ decreases in magnitude, P_1 and P_2 move to the right, sequentially hitting the maximum allowed value $P = 1$. At unitarity, $a = \infty$, a Wilsonian RG theory[59] predicts $P_t = 0.24$ and $T_t/T_{F,\uparrow} = 0.06$. Monte-Carlo calculations suggest $T_c/T_F = 0.152(7)$[60], and $P_2 = 0.39$[58].

In figure 4.1(c) the same diagram is shown at fixed temperature as a function of the chemical potentials $\mu = (\mu_\uparrow + \mu_\downarrow)/2$ and $h = (\mu_\uparrow - \mu_\downarrow)/2$. As a first approximation, one understands the trapped gas by breaking up the cloud into small pieces, and assuming that at each of these pieces is homogeneous and in local equilibrium. Maintaining equilibrium in the presence of energy transport requires T is constant, allowing momentum transport requires that the pressure obeys $\nabla P = -n\nabla V$, where $V(r)$ is the trapping potential, and allowing particle transport requires $\nabla \mu_j = -\nabla V$ for $j = \uparrow, \downarrow$. This hydrodynamic, *Thomas-Fermi* description allows one to directly read the structure of the trapped gas from the homogeneous phase diagram in figure 4.1(c): h is constant and μ varies from a large value at the center of the cloud to a small value at the edge. The iso-density contours of the cloud follow the iso-potential contours.

Observations at Rice are inconsistent with this local density approximation [61]. As already emphasized, the missing element is that the surface energy described in Eq. (4.1) distorts the cloud. Microscopically, this surface tension arises due to the energy cost of the superfluid-normal boundary, where the order parameter varies rapidly. Depending on the size of the superfluid region it is energetically favorable to either shrink this boundary to reduce its area or, because the surface energy depends on density, shift the boundary to a low density region. In a spherical trap this effect changes the radius (and density) of the superfluid core. In an elongated cloud, one generically expects that the aspect ratio of the superfluid region is reduced. Phenomenological models based on this principle [40, 41], seem to account for the experimental observations.

By fitting various models to experimental density profiles, Haque and Stoof [41] and DeSilva and Mueller [40] both made an estimate of η. The quoted val-

ues of η in [40] were unintentionally scaled by a factor of $\hbar\omega_z/\mu_0$. When corrected for this factor, they found that $\eta \approx 0.6$ for the relatively high temperature data in [1]. Haque and Stoof [41] found $\eta \approx 4.8$ for the lower temperature data in [2]. This is consistent with the expectation that surface tension should drop as one approaches the tricritical point. Here we compare our model with the data in [2], finding $\eta \approx 3$. We attribute the slight discrepancy with Haque and Stoof to trap anharmonicities (which we did not include in our calculation). We emphasize that $\eta \approx 3$ is more than one order of magnitude larger than the value predicted by our microscopic model, $\eta \approx 0.17$.

4.3 Calculation of Surface Tension

In this section we present a calculation of the surface tension in the BEC-BCS crossover. First we give a very crude order of magnitude estimate of the surface tension at $T = 0$ in a unitary gas, then we use a numerical solution to the BdG equations to obtain a more accurate result. In the deep BEC limit, one can use a simpler theory where the free energy is expanded in gradients of the order parameter. We use this theory to test our numerical solution of the BdG equations in the BEC limit.

Related microscopic calculations have been performed by Caldas [62] and Imambekov, Bolech, Lukin and Demler [63].

4.3.1 Order of magnitude

Before presenting a detailed microscopic calculation of the surface tension we give a simple estimate of its magnitude at zero temperature in a unitary gas. In the standard semi-phenomonological model for surface tension, one considers the spatial variation of an order parameter: in this case the superconducting gap $\Delta(\mathbf{r})$. At the first order phase boundary, the free energy has two local minima: one with $\Delta = \Delta_0$ and the other with $\Delta = 0$. Surface tension can be attributed to the fact that in the boundary between the two bulk phases, Δ must pass over a free energy maximum.

The energy cost per unit area of the boundary σ is most simply estimated as the product of the maximum height of the free energy barrier per unit volume $\delta\Omega$ and the thickness of the domain wall ξ. The healing length ξ arises from a competition between the stiffness of the order parameter and the height of the energy barrier, and at unitarity should be of order the interparticle spacing. Within BCS theory (reviewed in detail below), the energy barrier is $\delta\Omega \approx 0.2 \times n_s^{5/3} \hbar^2/2m$. With $\xi \approx n_s^{-1/3}$ this gives $\eta \approx 0.2$. As previously quoted, the full solution of the Bogoliubov de Gennes equations yield $\eta \approx 0.17$.

4.3.2 Mean Field Theory

To calculate the properties of the superfluid-normal boundary, we numerically solve the Bogoliubov de Gennes equations with appropriate boundary conditions. The homogeneous version of these equations is often used to describe the zero temperature BEC-BCS crossover in ultracold fermions. We emphasize however that near unitarity, quantitative predictions of this theory should be
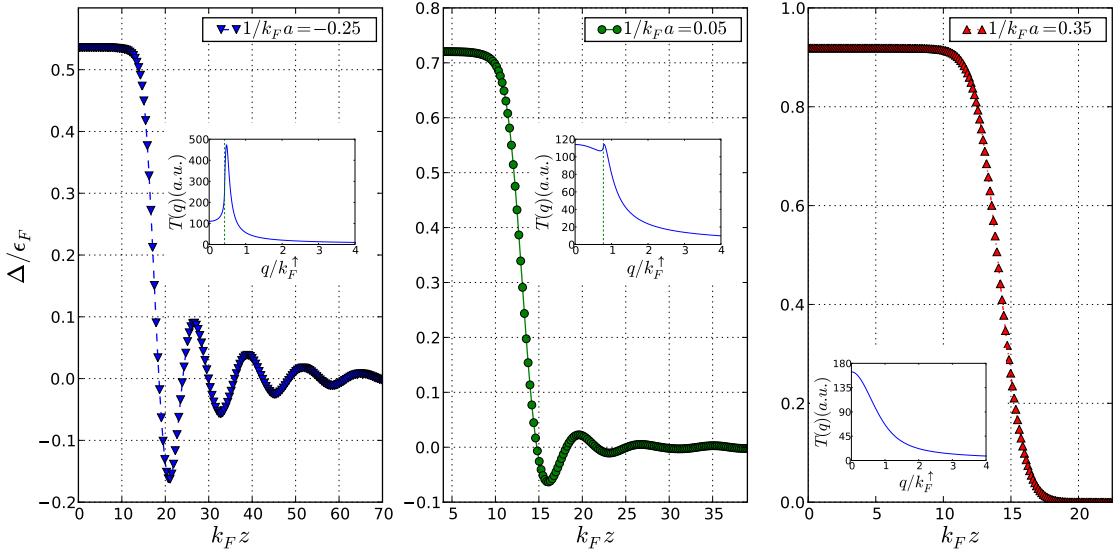
Figure 4.2: Order parameter profiles at the interface between normal and superfluid at critical Zeeman field h_c. Left to right: BCS to BEC side of resonance. Each data point corresponds to a single gridpoint of our real space discretization. Insets: normal state T-matrix (pair susceptibility) as a function of momentum q at the first order phase transition line $h = h_c$ corresponding to the same parameters as the BdG calculations. The Fourier transform of $T(q)$ describes the decay of the superfluid order parameter into the polarized normal state. The vertical line shows $q = k_F^\uparrow - k_F^\downarrow$.

viewed with some skepticism. One could argue that since the mean-field theory overestimates the density discontinuity at the superfluid-normal boundary it should also overestimate η. In this section we review the formal theory, while in the following sections we report results, and describe some simplifying approximations.

Our model consists of a Fermionic system with two different hyperfine states labeled by $\sigma = \uparrow, \downarrow$ in three spatial dimensions. The atoms interact via a point interaction. The system of $N = N_\uparrow + N_\downarrow$ atoms is then described by the Hamiltonian $H = \int d^3\mathbf{r}(H_0 + H_{\text{int}})$, with kinetic ($H_0$) and interaction ($H_{\text{int}}$) energy

densities

$$H_0(\mathbf{r}) = \sum_\sigma \psi_\sigma^\dagger(\mathbf{r})\left(-\frac{\hbar^2}{2m}\nabla^2 - \mu_\sigma\right)\psi_\sigma(\mathbf{r})$$

$$H_{\text{int}}(\mathbf{r}) = -U\psi_\uparrow^\dagger(\mathbf{r})\psi_\downarrow^\dagger(\mathbf{r})\psi_\downarrow(\mathbf{r})\psi_\uparrow(\mathbf{r}) \tag{4.4}$$

where $\psi_\sigma(\mathbf{r})$ are usual Fermionic field operators. Parameters m, and μ_σ are the mass and chemical potential of the atomic species σ respectively. Following convention, we take $\uparrow$ to be the majority species of atoms and use variables $h = (\mu_\uparrow - \mu_\downarrow)/2 \geq 0$ and $\mu = (\mu_\uparrow + \mu_\downarrow)/2$. The bare coupling constant U is renormalized by expressing it through the s-wave scattering length a_s as $1/U = 1/U_R + 1/V \sum_q 1/2\epsilon_q^0$ with $U_R = -4\pi\hbar^2 a_s/m$, $\epsilon_q^0 = \hbar^2 q^2/2m$ where V is the system volume[64].

Performing a mean-field decoupling of the interaction, one writes the Hamiltonian in terms of a gas of Bogoliubov excitations [65],

$$\begin{pmatrix} \Psi_\uparrow(\mathbf{r}) \\ \Psi_\downarrow^\dagger(\mathbf{r}) \end{pmatrix} = \sum_n \begin{pmatrix} u_n(\mathbf{r}) & -v_n^*(\mathbf{r}) \\ v_n(\mathbf{r}) & u_n^*(\mathbf{r}) \end{pmatrix} \begin{pmatrix} \gamma_{\uparrow,n} \\ \gamma_{\downarrow,n}^\dagger \end{pmatrix} \tag{4.5}$$

Excitations with spin $\sigma = \uparrow, \downarrow$ have energies $E_{n,\sigma} = E_n \pm h$, where E_n is the positive energy eigenvalue of the BdG equations

$$\begin{pmatrix} -\frac{\nabla^2}{2m} - \mu & \Delta(\mathbf{r}) \\ \Delta^*(\mathbf{r}) & \frac{\nabla^2}{2m} + \mu \end{pmatrix} \begin{pmatrix} u_n(\mathbf{r}) \\ v_n(\mathbf{r}) \end{pmatrix} = E_n \begin{pmatrix} u_n(\mathbf{r}) \\ v_n(\mathbf{r}) \end{pmatrix} \tag{4.6}$$

The mean-field free energy is then [66, 67]

$$\Omega_{MF} = \sum_n \{\epsilon_n - \mu - \lambda_n\} + \int d^3\mathbf{r}\,\frac{|\Delta(\mathbf{r})|^2}{U} \tag{4.7}$$

$$\frac{\lambda_n}{k_B T} = \log\left(2\cosh\frac{\beta E_{n,\uparrow}}{2}\right) + \log\left(2\cosh\frac{\beta E_{n,\downarrow}}{2}\right)$$

where $\sum_n \epsilon_n - \mu = \text{Tr}\left[-\frac{\nabla^2}{2m} - \mu\right]$ and $\beta = 1/k_B T$. The chemical potentials are

set by the number equations $N_\sigma = \int d^3 r \, n_\sigma(\mathbf{r})$ with

$$n_\sigma(\mathbf{r}) = \left\langle \psi_\sigma^\dagger(\mathbf{r}) \psi_\sigma(\mathbf{r}) \right\rangle \tag{4.8}$$

$$= \sum_n |u_n(\mathbf{r})|^2 f(E_{n,\sigma}) + |v_n(\mathbf{r})|^2 \left[1 - f(E_{n,-\sigma}) \right]$$

where $f(E) = 1/(1 + e^{-\beta E})$. Self-consistency requires that the gap obeys

$$\Delta(\mathbf{r}) = U \left\langle \psi_\uparrow(\mathbf{r}) \psi_\downarrow(\mathbf{r}) \right\rangle$$
$$= U \sum_n u_n(\mathbf{r}) v_n^*(\mathbf{r}) \left[1 - f(E_{n,\uparrow}) - f(E_{n,\downarrow}) \right]. \tag{4.9}$$

It is useful to draw attention to three particular limits of these equations. First, if $\Delta(\mathbf{r}) = 0$ one has just a non-interacting Fermi gas, with free energy

$$\Omega = - \sum_{\mathbf{k},\sigma} k_B T \log \left(1 + e^{-\beta(\epsilon_k - \mu_\sigma)} \right). \tag{4.10}$$

This equation highlights the most significant flaw of the mean-field approach, namely that it yields a noninteracting normal state, overestimating the stability of the superfluid.

As a second useful limit, one can consider the case where $\Delta(\mathbf{r}) = \Delta_0$ is uniform. In that case one can label the eigenstates of (4.6) by momentum and one finds the standard result

$$\Omega_{\text{hom}} = \sum_{\mathbf{k}} \{\epsilon_{\mathbf{k}} - \mu - \lambda_k\} + V \frac{\Delta_0^2}{U} \tag{4.11}$$
$$\frac{\lambda_k}{k_B T} = \log \left(2 \cosh \frac{\beta(E_{\mathbf{k}} + h)}{2} \right)$$
$$+ \log \left(2 \cosh \frac{\beta(E_{\mathbf{k}} - h)}{2} \right)$$

where V is the system volume and $E_{\mathbf{k}} = \sqrt{(k^2/2m - \mu)^2 + \Delta_0^2}$. In this uniform limit one finds that the total particle number $N = N_\uparrow + N_\downarrow$, population imbalance

$\Delta N = N_\uparrow - N_\downarrow$ and gap equation become

$$N = -\frac{\partial\Omega}{\partial\mu} = \sum_{\mathbf{k}}\left(1 - \frac{\epsilon_{\mathbf{k}} - \mu}{2\sqrt{(\epsilon_{\mathbf{k}} - \mu)^2 + \Delta_0^2}}\left\{\tanh\frac{\beta(E_{\mathbf{k}} - h)}{2} + \tanh\frac{\beta(E_{\mathbf{k}} + h)}{2}\right\}\right) \quad (4.12)$$

$$\Delta N = -\frac{\partial\Omega}{\partial h} = \frac{1}{2}\sum_{\mathbf{k}}\left(\tanh\frac{\beta(E_{\mathbf{k}} + h)}{2} - \tanh\frac{\beta(E_{\mathbf{k}} - h)}{2}\right) \quad (4.13)$$

$$0 = \frac{\partial\Omega}{\partial\Delta_0} = -\sum_{\mathbf{k}}\Delta_0\frac{\frac{1}{2}\left(\tanh\frac{\beta(E_{\mathbf{k}}+h)}{2} + \tanh\frac{\beta(E_{\mathbf{k}}-h)}{2}\right)}{\sqrt{(\epsilon_{\mathbf{k}} - \mu)^2 + \Delta_0^2}} + 2V\frac{\Delta_0}{U} \quad (4.14)$$

A third important case is when $\Delta(\mathbf{r})$ is periodic. Prototypical examples are the FF state $\Delta = \Delta_{FF}e^{iqx}$ or the LO state $\Delta = \Delta_{LO}\cos(qx)$. In the BCS limit there is a small window of stability for such a solution. These exotic superfluid states can be described by the BdG approach.

In order to compute the surface tension across the BEC-BCS crossover we numerically solve the BdG equations in Eq. (4.6). We find the parameters such that bulk normal and superfluid have the same free energy and then minimize the free energy functional in Eq. (4.7) with respect to the order parameter for a domain wall between the two phases. A simple way to minimize the free energy functional is to iterate the gap equation Eq. (4.9) to self consistency. We find that it is more computationally efficient to directly minimize Eq. (4.7) with respect to a discretized representation of $\Delta(r)$. For efficiency we calculate the gradient using

$$\frac{\delta\Omega_{MF}[\Delta(\mathbf{r})]}{\delta\Delta(\mathbf{r})} = -\frac{2}{U}\left[\Delta(\mathbf{r}) - \tilde{\Delta}(\mathbf{r})\right] \quad (4.15)$$

$$\frac{1}{U}\tilde{\Delta}(\mathbf{r}) = \sum_{n}u_n(\mathbf{r})v_n^*(\mathbf{r})\left[1 - f(E_{n,\uparrow}) - f(E_{n,\downarrow})\right]$$

where we used $\delta E_n/\delta\Delta(\mathbf{r}) = 2u_n(\mathbf{r})v_n(\mathbf{r})$.

4.3.3 Results ($T = 0$)

The domain wall profiles calculated within the BdG approach are shown in figure 4.2. As can be seen, on the BEC side of resonance the domain wall is largely featureless, while oscillatory structures develop as one approaches the BCS limit. In section 4.3.4 we relate these features to the behavior of the T-matrix, and draw the connection between these oscillations and the FFLO phase.

Due to the contribution from the interface, the energy found in these calculations exceeds that of the bulk superfluid/normal gas. From this excess energy we extract the dimensionless parameter η; our results are summarized in Fig. 4.3. At unitarity we find $\eta \simeq 0.17$. The surface tension drops as one approaches the BCS side of resonance. It grows to a maximum of $\eta \simeq 0.25$ at $1/k_f a \approx 0.4$, then falls as one proceeds towards the BEC limit.

4.3.4 Gradient expansion

A common approximation to the BdG equations is a gradient expansion, where one retains gradients to quadratic in the order parameter. We know that this should be an accurate approximation in the BEC limit, where the superfluid can be described with a Gross-Pitaevskii theory [**?**]. We make us of the result Eq. (2.24) and approximate the free energy as

$$\Omega[\Delta(\mathbf{r})] \approx \frac{1}{V} \sum_q \left[K^{(2)}(q) - K^{(2)}(0) \right] |\Delta_q|^2 + \int d^3r \, f_{hom}(\Delta(\mathbf{r})), \qquad (4.16)$$

where $\Delta(\mathbf{r}) = V^{-1} \sum_q e^{i\mathbf{q}\cdot\mathbf{r}} \Delta_q$ and the function $f_{hom}(\Delta)$ is the mean-field free energy density for a uniform order parameter. We calculate the surface energy
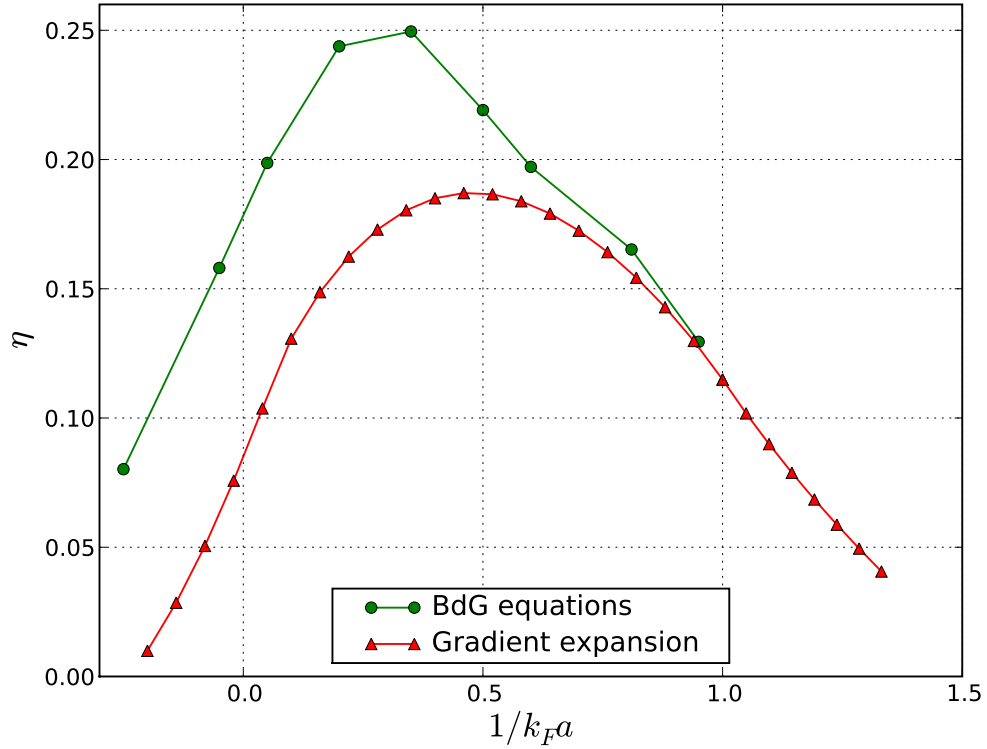
Figure 4.3: Dimensionless surface tension $\eta = 2\hbar^{-2}mn_s^{-4/3}\sigma$ as a function of $(k_Fa)^{-1}$ at $T = 0$. When $(k_Fa)^{-1} > 1.01$ the superfluid state is partially polarized. Triangles: calculation using the full BdG equations as described in 4.3.3, circles: gradient expansion approximation to this solution from 4.3.4. The lines are a guide to the eye.

from (4.16) by employing the variational ansatz

$$\Delta(z) = \Delta_0(\text{erf}(4z/W_{\text{dw}}) + 1)/2 \tag{4.17}$$

and minimizing Ω with respect to W_{dw}, which is a measure of the width of the domain wall. This ansatz is particularly convenient, because the erf-function has the simple and well behaved Fourier transform

$$\text{erf}(z) = \int_{-\infty}^{\infty} \frac{dq}{2\pi} \frac{2ie^{-(q/2)^2}}{q - i\epsilon} e^{iqz}, \tag{4.18}$$

which allows for efficient numerical optimization.

Comparing these gradient expansion results to the full solution to the BdG equations at $T = 0$, we find that the agreement becomes better in the deep BEC limit (see Fig. 4.3). In this limit, $K^{(2)}(q) - K^{(2)}(0)$ is well approximated by a parabola, and f_{hom} can be truncated at quartic order in Δ. Minimizing the resulting free energy results in a Gross-Pitaveskii equation [68]. Recently, Sheehy [69] has discussed the role of quantum fluctuations near the tricritical point. At unitarity ($a_s^{-1} = \infty$), the gradient expansion predicts a dimensionless surface tension of $\eta \sim 0.1$. The discrepancy between this result and the full BdG equations can be attributed to the neglect of gradient terms which are higher order in Δ.

Proximity effect

On the normal side of the domain wall, where $\Delta(z)$ is small, the free energy can be expanded to quadratic order in Δ. To find the asymptotic behavior of Δ in the domain wall one minimizes the quadratic approximation, $\Omega \approx (1/V) \sum_{\mathbf{q}} K^{(2)}(\mathbf{q})|\Delta_{\mathbf{q}}|^2$ with the constraint that $\Delta(z = 0) = \bar{\Delta}$ is nonzero. By symmetry, $\Delta_{\mathbf{q}} = \Delta_{q_z}$, and one finds

$$K^{(2)}(q_z)\Delta_{q_z} - \lambda = 0, \tag{4.19}$$

where λ is a Lagrange multiplier. Consequently, for large z, the order parameter is proportional to the *one dimensional* Fourier transform of the T-Matrix $T(q) = 1/K^{(2)}(q)$

$$\Delta(z) \propto \int \frac{dq}{2\pi} e^{iqz} T(q). \tag{4.20}$$

This result is confirmed in figure 4.2, where insets show the behavior of $T(q)$ as a function q. For example, on the BEC side of resonance the T-matrix is peaked at $q = 0$, yielding a monotonically decaying order parameter. On the BCS side,

the T-matrix is peaked at finite $q \approx k_F^\uparrow - k_F^\downarrow$, and one observes oscillations of $\Delta(z)$ with this wave-vector.

One can make a simple analogy, noting that the q-dependence of the T-matrix is reminiscent of the frequency dependence of a driven damped harmonic oscillator. The spatial dependence of the order parameter domain wall would then be analogous to the temporal dependence of the oscillator's position once the drive is turned off. The BEC/BCS sides of resonance then map on to overdamped/underdamped oscillators.

4.4 Effect of surface tension on density profiles

Having explored the microscopic theory of the domain wall separating the superfluid and normal regions, we now investigate how the surface energy in this boundary affects the shape of a trapped gas. We will assume that the zero temperature population imbalanced atomic system is phase separated into two regions: a central superfluid core surrounded by a normal shell. We will take the normal state to be fully polarized (with $n_\downarrow = 0$) and the superfluid state to be fully paired (with $n_\uparrow = n_\downarrow$). As discussed in the introduction, this is an approximation. Remarkably, the experiments at Rice university[1, 2] are largely consistent with this ansatz, which was first introduced by Chevy [70]. As seen in figures 4.4-4.5, in these elongated clouds there is no experimental evidence of a partially polarized normal region between the fully paired superfluid and fully polarized normal regions. The absence of this phase is significant: a partially polarized normal state is seen in experiments at MIT [3, 4, 5] and in more sophisticated theoretical calculations of the bulk phase diagram [58, **?**, 29]. The
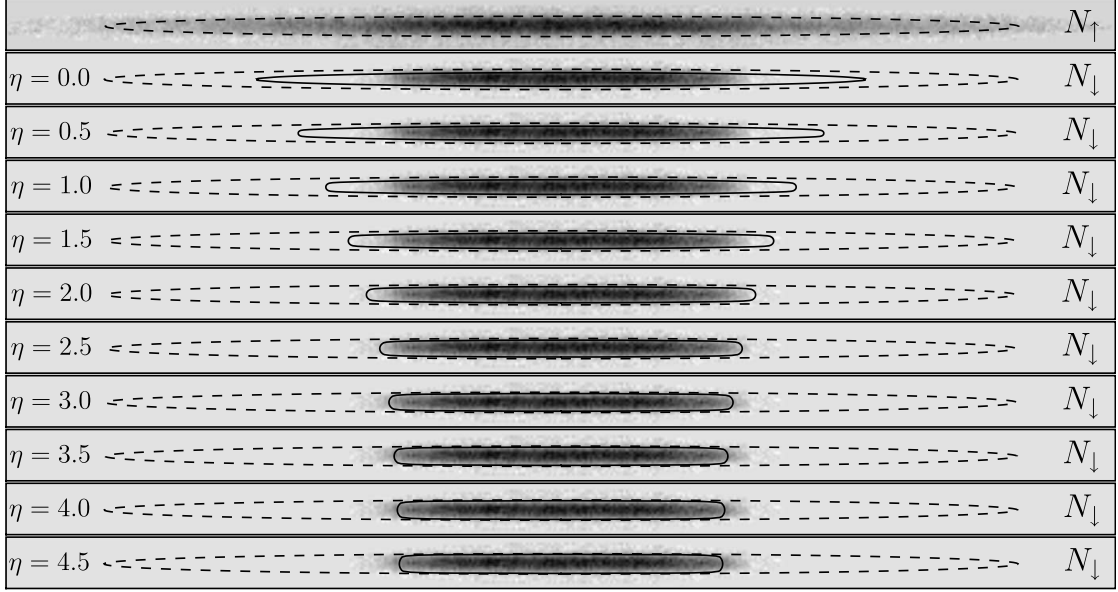
Figure 4.4: Experimental two-dimensional column densities (black denotes high density) for $P = 0.38$ with theoretically calculated boundaries for different surface tensions η (fixing the number of particles to be constant). Top: majority atoms $N_\uparrow$; Bottom: minority atoms $N_\downarrow$. The dotted line is the ellipse with semi-major and semi-minor axes Z_{TF} and R_{TF} respectively, while the solid line is the superfluid-normal boundary in the presence of surface tension. As η is increased, the superfluid-normal boundary deforms from an elliptical iso-potential surface, but the boundary becomes increasingly insensitive to surface tension with increasing η. $N_c = 15$ Fourier components were chosen for equation (4.24). Data corresponds to Fig. 1(c) in Ref. [2], used with permission. Data outside of an elliptical aperture has been excluded. This truncation of the data leads to a slight discrepancy in P compared to the value quoted in [2]. Each panel is $1.4\text{mm} \times 0.06\text{mm}$, and shows the true aspect ratio of the cloud.

unexplained behavior seen at Rice is presumably related to the small numbers of particles and the high aspect ratio of the cloud, but other considerations, such as the kinetics of spin transport, may also be important [36, 38, 71].

We will restrict our discussion to unitarity, where physics is universal and the superfluid and surface energy densities between the superfluid and normal regions have simple forms. The equation of state of the central superfluid shell
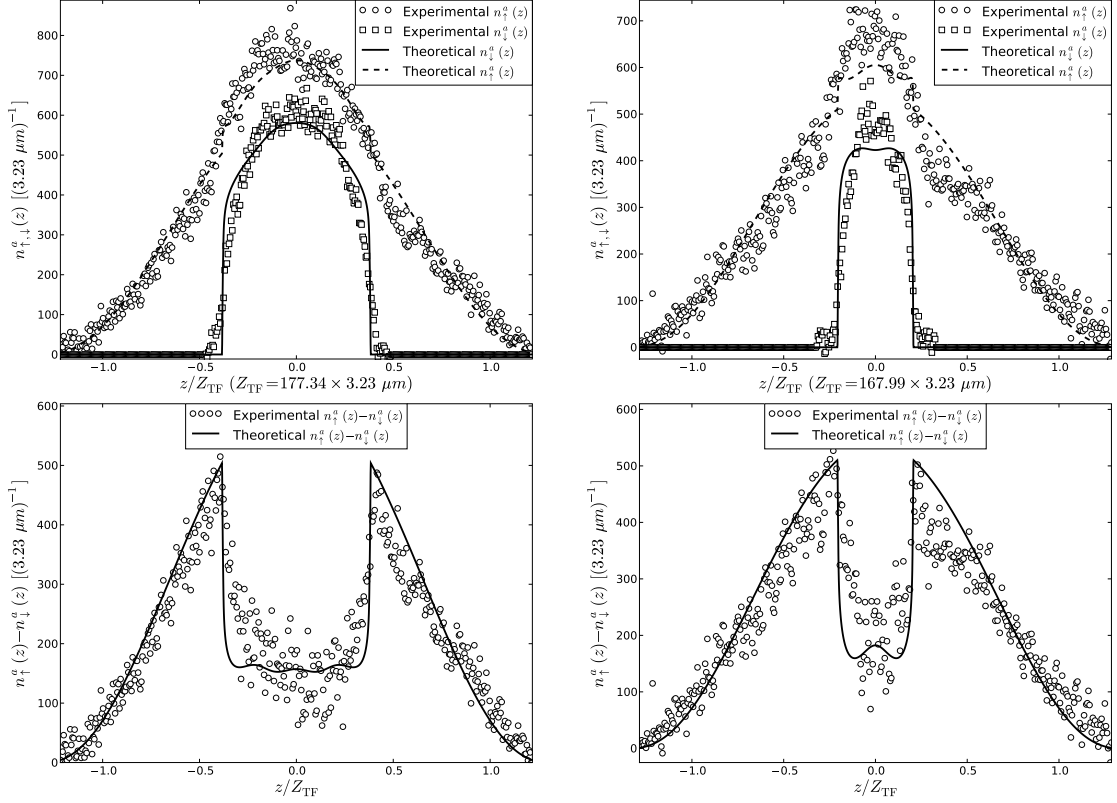
Figure 4.5: Axial densities. Symbols: experimental one-dimensional ^{6}Li spin densities and density differences for $P = 0.39$ ($N_\uparrow = 155,000, N_\downarrow = 68,500$) (left column) and $P = 0.63$ ($N_\uparrow = 123,600, N_\downarrow = 28,000$) (right column), from Ref. [2], with permission. Lines: theoretical curves for $\eta = 2.83$, taking a cigar shaped harmonic trap with small oscillation frequencies $\omega_z = (2\pi)7.2$Hz and $\omega_r = (2\pi)325$ Hz. Oscillations in the density difference within the superfluid region are artifacts of our ansatz (4.24). To minimize noise, only experimental data inside an elliptical window was considered (see text). This aperture is visible in figure 4.4.

is given at $T = 0$ by eq. (4.3), while the outer fully polarized normal shell obeys

$$n_n(\mathbf{r}) = n_\uparrow = \frac{1}{6\pi^2}\left[\frac{2m\mu_n(\mathbf{r})}{\hbar^2}\right]^{3/2}. \tag{4.21}$$

The free energy densities of the bulk phases $f_{s,n} = -\int n_{s,n}d\mu$ can be written as

$$f_{s,n}(\mathbf{r}) = -\frac{2}{15\pi^2}\left(\frac{2m}{\hbar^2}\right)^{3/2}\zeta_{s,n}\mu_{s,n}^{5/2}(\mathbf{r}) \tag{4.22}$$

where $\zeta_s = 1/(1 + \beta)^{3/2}$, $\zeta_n = 1/2$. Then we calculate the total bulk energies $\Omega_{S,N} = \int_{s/n} d^3\mathbf{r} f_{s,n}[\mu(\mathbf{r}), h]$ by integrating the bulk energy densities over

85

the superfluid/normal regions. As previously introduced, we model the surface energy density $\sigma[\mu(\mathbf{r}), h] = \eta(\hbar^2/2m)n_s^{4/3}$, where η is the dimensionless constant calculated in the previous section. We calculate the total surface energy $E_{dw} = \int d^2r\sigma[\mu(\mathbf{r}), h]$ by integrating the surface energy density over the superfluid-normal boundary. Away from the superfluid-normal boundary, we assume that the system is locally homogenous and the external harmonic trapping potential $V_{trap}(\mathbf{r}) = b_\perp\rho^2 + b_zz^2 = m\omega_z^2(\lambda^2\rho^2 + z^2)/2$ is treated in the LDA by introducing a local chemical potential $\mu(\mathbf{r}) = \mu_0 - V_{trap}(\mathbf{r})$. Given that the experimental traps are formed by focussed laser beams, describing it via a harmonic potential should be viewed as an approximation.

4.4.1 Calculation of boundary

We make a completely general ansatz for the domain wall, only assuming rotational symmetry about the long axis of the trap. We parameterize the boundary in terms of coordinates f and θ, which are related to the cylindrical coordinates ρ and z by

$$\rho(\theta, f) = R_{TF}f\cos\theta$$
$$z(\theta, f) = Z_{TF}f\sin\theta$$

(4.23)

where $R_{TF} = \sqrt{\mu_0/b_\perp}$, $Z_{TF} = \sqrt{\mu_0/b_z}$. The boundary is described by the function $f = F(\theta)$. As shown in appendix 4.8, the two-dimensional integrals for the free energy can then be simplified to one dimensional integrals, which can be performed numerically.

The optimal shape is found by minimizing the free energy functional $\Omega_T = \Omega_S + \Omega_N + E_{DW}$ on the space of functions $F(\theta)$ at fixed $N_\uparrow$ and $N_\downarrow$. The constraints

are imposed using Lagrange multipliers.

We expand $F(\theta)$ as

$$F(\theta) = \sum_{n=0}^{\infty} a_n \cos(2n\theta) \tag{4.24}$$

which is compatible with the boundary conditions imposed by the symmetry of the problem, $F'(0) = F'(\pi/2) = 0$. We truncated this series at a finite number of Fourier components N_c and numerically minimized Ω_T with respect to $a_0, a_1, \ldots, a_{N_c}$. We find that we need to include more terms in this series when η is larger, but for all values of η, the profiles become insensitive to N_c for $N_c \gtrsim 15$.

In figure 4.4 we plot the boundary $F(\theta)$ that minimizes Ω_T for different values of η. The boundary becomes almost insensitive to η for high surface tension. This behavior has two sources: (i) For large η the ends become increasingly flat, so surface tension plays an increasingly insignificant role, (ii) the edges along the minor axis touch the edge of the majority cloud, at which point the superfluid-normal boundary changes to a superfluid-vacuum boundary and surface tension ceases to be important. Due to this "saturation" of the boundary shape with high η, and the difficulty of defining the boundary from noisy 2-D data, we find it convenient to follow references [40, 41] and find η by fitting our theoretical model to the 1-D axial densities, defined by $n_{\uparrow,\downarrow}^{(a)}(z) = \int dx\, dy\, n(x, y, z)$. As illustrated in Fig. 4.4, we improve signal to noise by excluding data outside of an elliptical window [1]. We find that $\eta \simeq 3$ gives an axial density difference profile most closely matching the experimental density from Ref. [2] for $P = 0.38$ and $P = 0.63$. As seen in figure 4.5, the overall quality

---

[1]We discarded all data outside of an ellipse which was chosen so that by eye only pixels with no particles in them were excluded. The ellipse was chosen independently for each spin state and each data set. This windowing increased the signal to noise while reducing significant systematic biases due to the background. For example by this measure the $P = 0.39$ data has $N_\uparrow = 155,000$, $N_\downarrow = 68,500$, while without windowing $N_\uparrow = 166,000$, $N_\downarrow = 88,000$.

of the fit is quite good. There are however distinct differences between the predictions of the model and the observed profiles. These can largely be attributed to trap anharmonicities whose modelling is not reported here.

We also believe that the δp dependence of η may be important for capturing the exact shape of the domain wall. Generically one would expect that this dependence would reduce η at the ends of the boundary, increasing the curvature of the end-caps and making a smoother axial density. This effect would also lead to an apparent polarization and number dependence of η. Finally, we found some sensitivity to how we treat the background in each image. For example, if we fit the axial density difference at $P = 0.6$ without windowing the data, we find that $\eta = 1$ provides a better fit. This sensitivity can be attributed to structure in the background which persist throughout the image, even far from the cloud.

Since they are based upon identical models (just using different ansatz's for the boundary shape), the quality of our fits are very similar to the ones found by Haque and Stoof when investigating a large number of similar profiles [41]. Converting to our units, Haque and Stoof found $\eta = 4.8 \pm 1.2$. Their result is slightly higher than ours. We attribute this difference to differences in fitting procedures (such as windowing the data) and to modeling of the trap. Haque and Stoof used a more sophisticated Gaussian model for the trap, while we assumed it was harmonic.

The authors of Ref. [5] from the MIT experiment find no visible distortion of the superfluid cloud and quote an uncertainty of about 2% for this null observation. We studied how surface tension would affect this experiment. As evident from figure 4.6, a distortion of less than 2% implies $\eta \lesssim 1$. Thus their null-

observation is consistent with a value of surface tension on the same order as what we find in our microscopic calculation. Figure 4.6 shows that the surface tension needed to fit [2], $\eta \simeq 3$, would cause a distortion more than 10% in the MIT experiment (as was already pointed out in [5]), well above their threshold of detection.
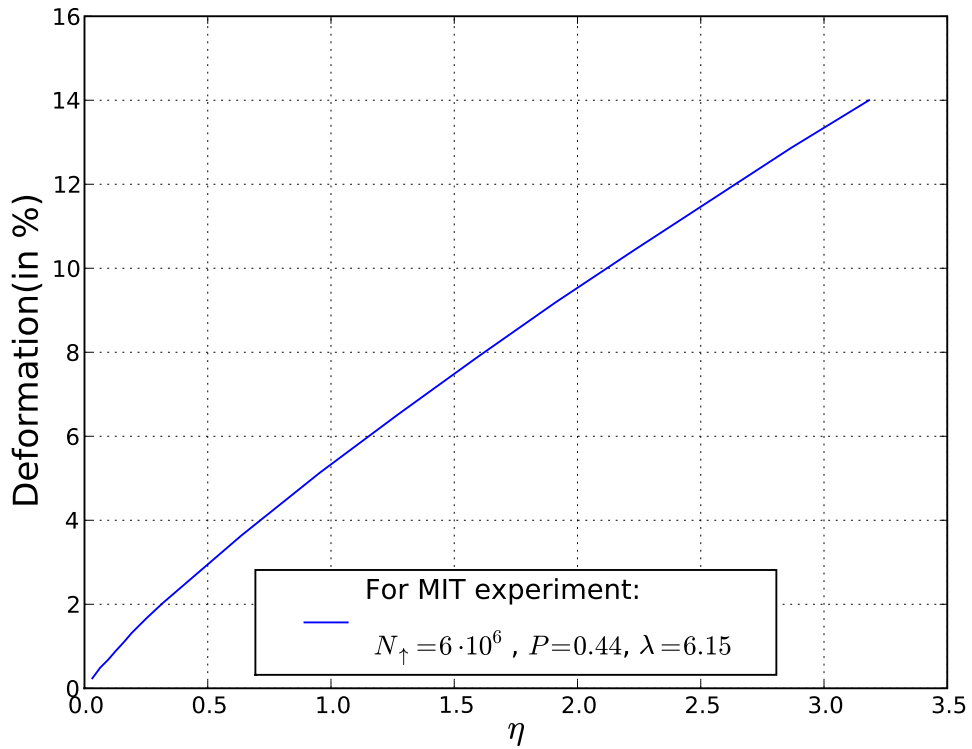
Figure 4.6: Distortion of superfluid core aspect ratio ($= 1 - F(\pi/2)/F(0)$) in % as a function of the dimensionless surface tension η for parameters of Ref [5], where λ is the aspect ratio of the harmonic trap.

4.5 Summary and Conclusions

We presented a microscopic calculation of surface tension at a superfluid-polarized boundary in a polarized two-component Fermi gas, finding a value of the dimensionless surface tension η which is consistent with an ϵ-expansion [72]. We argue that η vanishes in both the BEC and BCS limits, with a peak on the BEC side of resonance near unitarity.

We compared our microscopic calculation of η to experimental estimates extracted by fitting a phenomenological model to axial density data. We find that our microscopic predictions of $\eta = 0.17$ at unitarity are an order of magnitude smaller than our best fits to the experimental data from Rice [2] ($\eta \sim 3$). On the other hand, phenomenological modeling of the the MIT experiment [5] bound η to be somewhere between zero and a few times larger than our microscopic predictions. We think that additional theoretical insight, as well as more experimental data, would be needed to resolve these discrepancy.

Despite the differences in the magnitude of η, we find that the experimental observations at Rice [2] show all of the appropriate hallmarks of surface tension. Using our phenomenological model, we presented a short study of how surface tension distorts the shape of the superfluid core in a harmonically trapped cloud of atoms. We reproduce both the observed double peak structure[1] in the axial density difference profile and the distorted shape of the superfluid/normal boundary[2].

We find that with increasing surface tension (figure 4.4), the superfluid/normal boundary attains a "limiting" shape significantly different from the isopotential contours that are predicted by the Thomas Fermi approxima-

tion. As the temperature increases, the system moves closer to the tricritical point in figure 4.1, and as a result the surface tension decreases and disappears at the tricritical point. As a result, surface tension-induced distortion of the superfluid core must be absent if the temperature of the atomic trap is maintained above the tricritical point; indeed, this behavior is observed in [2]. We would argue that thermal effects are not responsible for the differences between experiments at Rice [2, 1] and MIT [3, 4, 5]. The strongest evidence that temperature is not the issue, is the excellent agreement between zero temperature Monte-Carlo results[58] and the MIT experiments [5].

Sensarma *et al* [36], and more recently Tezuka and Ueda[38], attempt to understand the deformation of the superfluid core by studying a microscopic model of the entire atomic cloud. They solved the BdG equations for a relatively small number of particles (a few thousand) in an axially symmetric system. While these calculations do give more insight into the properties of these systems, it is difficult to extract quantitative information from them. In particular, the small particle numbers lead to a much larger surface area to volume ratio than in experiments, and artificially amplifies the role of surface tension. We believe that those calculations do not "explain" the inconsistencies which we observe between the magnitude of surface tension in our microscopic BdG calculations and our phenomenological modeling of the experimental data. It is possible that larger simulations of that sort might be more useful in this regard.

4.6 Acknowledgments

4.7 Appendix A: Cutoff dependence of the BdG calculations

In order to compute the surface tension across the BEC-BCS crossover we used a numerical calculation based on the BdG equations (4.6). Here we give details about our numerical approach, showing that we have used sufficiently large cutoffs to produce unbiased results.

We find parameters such that bulk normal and superfluid have the same free energy and then minimize the functional (4.7) with respect to the order parameter for a configuration with a domain wall between the two phases. The excess free energy of this configuration is attributed to the domain walls, and allows us to extract a surface tension.

We assume that the order parameter varies only along the z-direction. In the simulation we discretize this one dimensional space on a uniform grid with N grid points and approximate the gradients through a fourth order finite difference matrix. We find it convenient to use periodic boundary conditions in the z-direction, simulating two domain walls. We have verified that the interaction between the two walls is negligible.

Translational invariance in the directions perpendicular to the interface (i.e. x- and y-axes) implies that the u and v's are of the form

$$u(\mathbf{r}) = e^{i\mathbf{k}_\perp \mathbf{r}_\perp} u_n(z) \qquad v(\mathbf{r}) = e^{i\mathbf{k}_\perp \mathbf{r}_\perp} v_n(z) \qquad (4.25)$$

One has to solve a $2N \times 2N$ matrix eigenvalue problem for each $k_\perp = |\mathbf{k}_\perp|$. The coupling constant U depends on the UV-cutoff and was fixed by renormalizing $\Omega_{MF}(\Delta_0)$ through the result from a direct calculation (4.11) where a uniform order parameter was assumed. We found that when seeded with an order parameter profile with two domain walls the minimization algorithm converges to a local minimum with two domain walls. This solution correctly obeys the self-consistent gap equation.

We systematically increased N to check the convergence of the order parameter profiles and surface tension (see Fig. 4.7). In the deep BEC limit, the gradient expansion becomes a good approximation to the BdG equations, enabling us to check our BdG calculation. In that limit we found excellent agreement between these theories, giving us confidence in the accuracy of our numerical methods. The largest number of grid points N and transverse modes N_k we used were $N = 400$ and $N_k = 400$; these were, for example, used to obtain Fig 4.3. We feel that any residual errors from our finite gridpoints/cutoffs are much smaller than the errors introduced through the mean field approximation.

4.8   Appendix B: Evaluation of phenomenological Free energy

This appendix gives the analytic expressions used to calculate the free energy of an arbitrary domain wall. We parameterize the boundary by $f = F(\theta)$, in
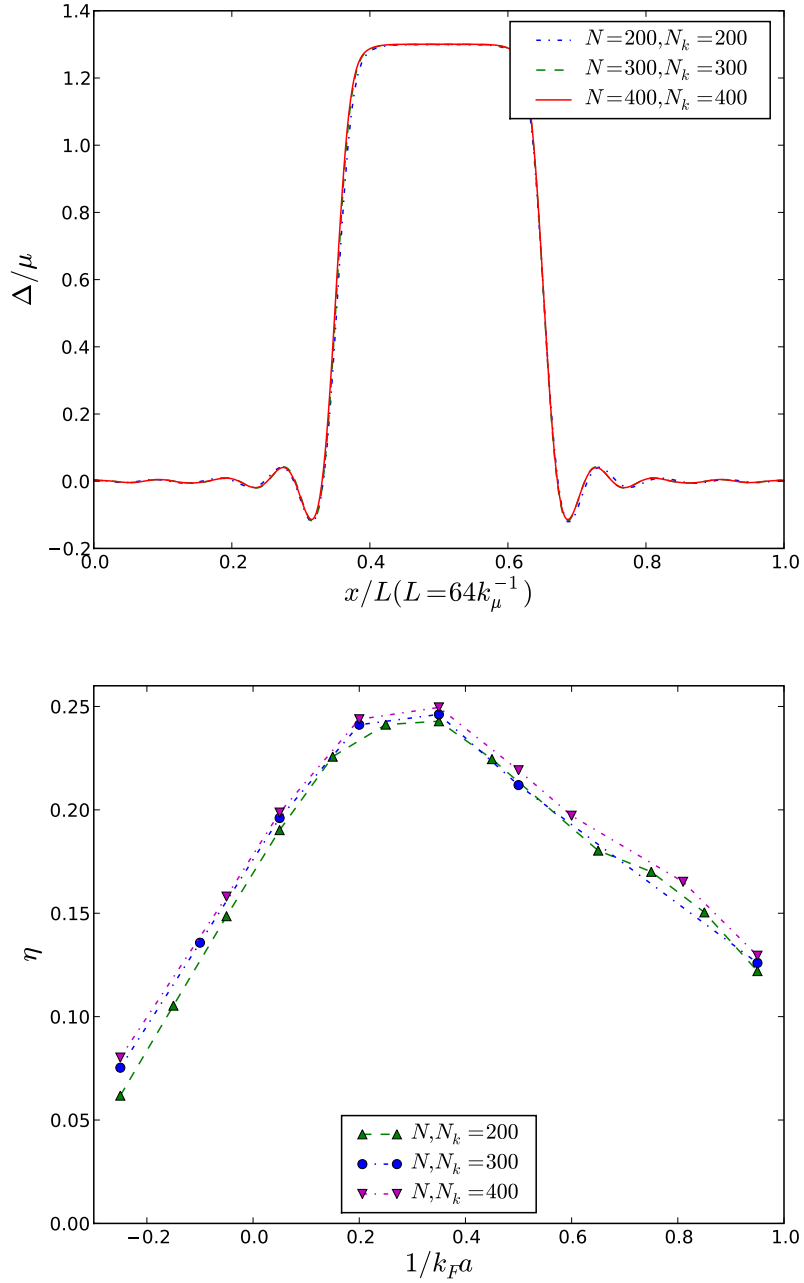
Figure 4.7: **Top:** Representative order parameter profiles for different cutoffs computed using the BdG equations at $1/k_F a = 0.05$. For better visibility a line connecting the data points is displayed. **Bottom:** Dimensionless surface tension constant η for different cutoffs as a function of $1/k_F a$.

terms of which the coordinates of the boundary are $\rho(\theta, f) = R_{TF} f \cos \theta$ and

$z(\theta, f) = Z_{TF} f \sin \theta$. The surface energy is

$$
\begin{aligned}
E_{DW} &= A_{dw} \int \left(1 - \frac{\rho^2}{R_{TF}^2} - \frac{z^2}{Z_{TF}^2} \right)^2 d^2 r \\
&= 2 A_{dw} \int_0^{\pi/2} d\theta F(\theta) \cos \theta \\
&\quad \times [F'(\theta) \cos \theta - F(\theta) \sin \theta] \times [1 - F(\theta)^2]^2 \\
&\quad \times \sqrt{1 + \left(\frac{Z_{TF}}{R_{TF}} \right)^2 \left(\frac{F'(\theta) \sin \theta + F(\theta) \cos \theta}{F'(\theta) \cos \theta - F(\theta) \sin \theta} \right)^2}
\end{aligned}
\tag{4.26}
$$

where we define the coefficient

$$
A_{dw} = \hbar \omega_z R_{TF}^2 Z_{TF} \left[\frac{2m}{\hbar^2} \right]^{3/2} \left[\frac{\eta \pi \mu_0^{3/2}}{(1 + \beta)^2 (3\pi^2)^{4/3}} \right].
\tag{4.27}
$$

We write the free energy of the superfluid core as

$$
\begin{aligned}
\Omega_S &= A_s \int_s \rho \, d\rho \, dz \left(1 - \frac{\rho^2}{R_{TF}^2} - \frac{z^2}{Z_{TF}^2} \right)^{5/2} \\
&= 2 A_s \int_0^{\pi/2} d\theta \cos \theta \int_0^{F(\theta)} df \, f^2 (1 - f^2)^{5/2} \\
&= 2 A_s \int_0^{\pi/2} d\theta \, G_1 [F(\theta)] \cos \theta
\end{aligned}
\tag{4.28}
$$

$$
A_s = -\zeta_s R_{TF}^2 Z_{TF} \left[\frac{2m}{\hbar^2} \right]^{3/2} \left[\frac{4\mu_0^{5/2}}{15\pi} \right]
\tag{4.29}
$$

$$
\begin{aligned}
G_1(x) &= \frac{1}{384} \Big[x\sqrt{1 - x^2} \left(-15 + 118 x^2 - 136 x^4 + 48 x^6 \right) \\
&\quad + 15 \sin^{-1}(x) \Big]
\end{aligned}
\tag{4.30}
$$

Similarly, the free energy of the fully polarized normal shell, $\Omega_N = A_n \int_n \rho \, d\rho \, dz (1 + \gamma - \rho^2/R_{TF}^2 - z^2/Z_{TF}^2)^{5/2}$, is:

$$
\Omega_N = 2 A_n (1 + \gamma)^4 \left[\frac{5\pi}{256} - \int_0^{\pi/2} d\theta \, G_1 \left[\frac{F(\theta)}{\sqrt{1 + \gamma}} \right] \cos \theta \right]
$$

$$
A_n = -\zeta_n R_{TF}^2 Z_{TF} \left[\frac{2m}{\hbar^2} \right]^{3/2} \left[\frac{4\mu_0^{5/2}}{15\pi} \right].
\tag{4.31}
$$

The total number of atoms in the two phases are given by

$$N_s = 2B_s \int_0^{\pi/2} d\theta \cos \theta G_2[F(\theta)]$$

$$N_n = 2B_n(1+\gamma)^3 \left[\pi/32 - \int_0^{\pi/2} d\theta \cos \theta G_2 \left[\frac{F(\theta)}{\sqrt{1+\gamma}} \right] \right]$$

(4.32)

where

$$B_{s,n} = \zeta_{s,n} \frac{2}{3\pi} \left[\frac{2m\mu_0}{\hbar^2} \right]^{3/2} R_{TF}^2 Z_{TF}$$

$$G_2(x) = \frac{1}{48} \left[x\sqrt{1-x^2}(-3 + 14x^2 - 8x^4) + 3\sin^{-1}(x) \right].$$

(4.33)

Thus both the free energy, and the constraints of fixed N and P reduce to one dimensional integrals.

BIBLIOGRAPHY FOR CHAPTER 4

[1] Guthrie B. Partridge, Wenhui Li, Ramsey I. Kamar, Yean An Liao, and Randall G. Hulet, Science **311**, 503 (2006).

[2] G. B. Partridge, Wenhui Li, Y. A. Liao, R. G. Hulet, M. Haque, and H. T. C. Stoof, Phys. Rev. Lett. **97**, 190407 (2006).

[3] Martin W. Zwierlein, Andre Schirotzek, Christian H. Schunck, and Wolfgang Ketterle, Science **311**, 492 (2006).

[4] M. W. Zwierlein, A. Schirotzek, C.H. Schunk, and Wolfgang Ketterle, Nature **442**, 54 (2006).

[5] Yong-Il Shin, Christian H. Schunck, Andre Schirotzek, and Wolfgang Ketterle, Nature **451**, 689 (2008).

[6] A. M. Clogston, Phys. Rev. Lett. **9**, 266 (1962).

[7] B. S. Chandrasekhar, Applied Physics Letters **1**, 7 (1962).

[8] Peter Fulde and Richard A. Ferrell, Phys. Rev. **135**, A550 (1964).

[9] A. I. Larkin and Yu. N. Ovchinnikov, Sov. Phys. JETP **20**, 762 (1965).

[10] Elena Gubankova, W. Vincent Liu, and Frank Wilczek, Phys. Rev. Lett. **91**, 032001 (2003).

[11] Bimalendu Deb, Amruta Mishra, Hiranmaya Mishra, and Prasanta K. Panigrahi, Phys. Rev. A **70**, 011604 (2004).

[12] E. Gubankova, E. G. Mishchenko, and F. Wilczek, Phys. Rev. Lett. **94**, 110402 (2005).

[13] Igor Shovkovy and Mei Huang, Phys. Lett. B **564**, 205 (2003).

[14] R. Combescot, Europhys. Lett. **55**, 150 (2001).

[15] U. Lombardo, P. Nozières, P. Schuck, H.-J. Schulze, and A. Sedrakian, Phys. Rev. C **64**, 064314 (2001).

[16] Heron Caldas, Phys. Rev. A **69**, 063602 (2004).

[17] Armen Sedrakian, Jordi Mur-Petit, Artur Polls, and Herbert Müther, Phys. Rev. A **72**, 013613 (2005).

[18] D. T. Son and M. A. Stephanov, Phys. Rev. A **74**, 013614 (2006).

[19] Lianyi He, Meng Jin, and Pengfei Zhuang, Phys. Rev. B **73**, 214527 (2006).

[20] W. Yi and L.-M. Duan, Phys. Rev. A **73**, 031604 (2006).

[21] Hui Hu and Xia-Ji Liu, Phys. Rev. A **73**, 051603 (2006).

[22] M. M. Parish, F. M. Marchetti, A. Lamacraft, , and B. D. Simons, Nature Physics **3**, 124 (2007).

[23] K. B. Gubbels, M. W. J. Romans, and H. T. C. Stoof, Phys. Rev. Lett. **97**, 210402 (2006).

[24] M. Iskin and C. A. R. Sá de Melo, Phys. Rev. Lett. **97**, 100404 (2006).

[25] Kun Yang, arXiv:cond-mat/0508484 (2005).

[26] Chih-Chun Chien, Qijin Chen, Yan He, and K. Levin, Phys. Rev. Lett. **98**, 110404 (2007).

[27] Meera M. Parish, Stefan K. Baur, Erich J. Mueller, and David A. Huse, Phys. Rev. Lett. **99**, 250403 (2007).

[28] Nobukatsu Yoshida and S.-K. Yip, Phys. Rev. A **75**, 063601 (2007).

[29] Aurel Bulgac and Michael McNeil Forbes, Phys. Rev. Lett. **101**, 215301 (2008).

[30] K. Machida, T. Mizushima, and M. Ichioka, Phys. Rev. Lett. **97**, 120407 (2006).

[31] T. Mizushima, K. Machida, and M. Ichioka, Phys. Rev. Lett. **94**, 060404 (2005).

[32] T. Mizushima, M. Ichioka, and K. Machida, J. Phys. Soc. Jpn. **76**, 104006 (2007).

[33] Xia-Ji Liu, Hui Hu, and Peter D. Drummond, Phys. Rev. A **75**, 023614 (2007).

[34] J. Kinnunen, L. M. Jensen, and P. Törmä, Phys. Rev. Lett. **96**, 110403 (2006).

[35] L. M. Jensen, J. Kinnunen, and P. Törmä, Phys. Rev. A **76**, 033620 (2007).

[36] Rajdeep Sensarma, William Schneider, Roberto B. Diener, and Mohit Randeria, arXiv:0706.1741v1 (2007).

[37] Paolo Castorina, Marcella Grasso, Micaela Oertel, Michael Urban, and Dario Zappalà, Phys. Rev. A **72**, 025601 (2005).

[38] M. Tezuka and M. Ueda, arXiv:0811.1650 (2008).

[39] Daniel E. Sheehy and Leo Radzihovsky, Ann. Phys. (NY) **322**, 8 (2007).

[40] Theja N. De Silva and Erich J. Mueller, Phys. Rev. Lett. **97**, 070402 (2006).

[41] Masudul Haque and H. T. C. Stoof, Phys. Rev. Lett. **98**, 260406 (2007).

[42] Stefan S. Natu and Erich J. Mueller, arXiv:0802.2083 (2008).

[43] Herman Feshbach, Annals of Physics **5**, (1958).

[44] U. Fano, Phys. Rev. **124**, 1866 (1961).

[45] C. A. Regal, M. Greiner, and D. S. Jin, Phys. Rev. Lett. **92**, 040403 (2004).

[46] M. W. Zwierlein, C. A. Stan, C. H. Schunck, S. M. F. Raupach, A. J. Kerman, and W. Ketterle, Phys. Rev. Lett. **92**, 120403 (2004).

[47] C. Chin, M. Bartenstein, A. Altmeyer, S. Riedl, S. Jochim, J. Hecker Denschlag, and R. Grimm, Science **305**, 1128 (2004).

[48] T. Bourdel, L. Khaykovich, J. Cubizolles, J. Zhang, F. Chevy, M. Teichmann, L. Tarruell, S. J. J. M. F. Kokkelmans, and C. Salomon, Phys. Rev. Lett. **93**, 050401 (2004).

[49] J. Kinast, S. L. Hemmer, M. E. Gehm, A. Turlapov, and J. E. Thomas, Phys. Rev. Lett. **92**, 150402 (2004).

[50] Henning Heiselberg, Phys. Rev. A **63**, 043606 (2001).

[51] K. M. O'Hara, S. L. Hemmer, M. E. Gehm, S. R. Granade, and J. E. Thomas, Science **298**, 2179 (2002).

[52] J. Carlson, S.-Y. Chang, V. R. Pandharipande, and K. E. Schmidt, Phys. Rev. Lett. **91**, 050401 (2003).

[53] G. M. Bruun, Phys. Rev. A **70**, 053602 (2004).

[54] Tin-Lun Ho, Phys. Rev. Lett. **92**, 090402 (2004).

[55] G. E. Astrakharchik, J. Boronat, J. Casulleras, , and S. Giorgini, Phys. Rev. Lett. **93**, 200404 (2004).

[56] S. Y. Chang, V. R. Pandharipande, J. Carlson, and K. E. Schmidt, Phys. Rev. A **70**, 043602 (2004).

[57] J. Carlson and Sanjay Reddy, Phys. Rev. Lett. **95**, 060401 (2005).

[58] C. Lobo, A. Recati, S. Giorgini, and S. Stringari, Phys. Rev. Lett. **97**, 200403 (2006).

[59] K. B. Gubbels and H. T. C. Stoof, Phys. Rev. Lett. **100**, 140407 (2008).

[60] E. Burovski, N. Prokof'ev, B. Svistunov, and M. Troyer, Phys. Rev. Lett. **96**, 160402 (2006).

[61] T. N. De Silva and E. J. Mueller, Phys. Rev. A **73**, 051602 (2006).

[62] Heron Caldas, Journal of Statistical Mechanics: Theory and Experiment **2007**, P11012 (2007).

[63] Adilet Imambekov, C. J. Bolech, Mikhail Lukin, and Eugene Demler, Phys. Rev. A **74**, 053626 (2006).

[64] Y. Ohashi and A. Griffin, Phys. Rev. A **67**, 033603 (2003).

[65] P. G. de Gennes, *Superconductivity of Metals and Alloys* (W.A. Benjamin, New York, 1966).

[66] John Bardeen, R. Kümmel, A. E. Jacobs, and L. Tewordt, Phys. Rev. **187**, 556 (1969).

[67] G. Eilenberger, Z. Physik **184**, 427 (1965).

[68] P. Pieri and G. C. Strinati, Phys. Rev. Lett. **96**, 150404 (2006).

[69] Daniel E. Sheehy, arXiv:0807.0922 (2008).

[70] F. Chevy, Phys. Rev. Lett. **96**, 130401 (2006).

[71] Meera M. Parish and David A. Huse, Phys. Rev. A **80**, 063605 (2009).

[72] Andrei Kryjevski, Phys. Rev. A **78**, 043610 (2008).

CHAPTER 5

QUASI-ONE-DIMENSIONAL POLARIZED FERMI SUPERFLUIDS

5.1 Abstract

We calculate the zero temperature ($T = 0$) phase diagram of a polarized two-component Fermi gas in an array of weakly-coupled parallel one-dimensional (1D) "tubes" produced by a two-dimensional optical lattice. Increasing the lattice strength drives a crossover from three-dimensional (3D) to 1D behavior, stabilizing the Fulde-Ferrell-Larkin-Ovchinnikov (FFLO) modulated superfluid phase. We argue that the most promising regime for observing the FFLO phase is in the quasi-1D regime, where the atomic motion is largely one-dimensional but there is weak tunneling in the other directions that stabilizes long range order. In the FFLO phase, we describe a phase transition where the quasiparticle spectrum changes from gapless near the 3D regime to gapped in quasi-1D.

5.2 Introduction

Recent experiments on ultracold ^{6}Li have probed polarized, two-component Fermi gases as a function of interatomic interaction strength and spin population imbalance [1, 2, 3, 4, 5, 6]. These experiments have focussed on the unitarity

regime, where the s-wave scattering length is large and the scattering properties are universal. At low temperatures they have seen phase separation between an unpolarized or weakly polarized superfluid phase and a highly polarized normal phase. Future experiments hope to observe the elusive FFLO spatially-modulated superfluid phase, first predicted to occur in magnetized superconductors over 40 years ago [7, 8]. While the FFLO phase is expected to exist in trapped 3D gases for small polarizations and weak attractive interactions [9], it is predicted to occupy only a small part of the $T = 0$ phase diagram [10], and this region is only further diminished with increasing T [11, 12]. Here we theoretically explore how a two-dimensional (2D) optical lattice can enlarge the region of stability of the FFLO phase, paving the way for its observation.

Although it has been shown that a 3D simple cubic optical lattice enhances the FFLO phase [13], we argue that a 2D optical lattice, which permits free motion in one direction, is more effective. The instability of the normal state to the FFLO phase is due to a Fermi surface "nesting", which is enhanced in 1D. The situation is similar to the Peierls instability that leads to the formation of charge density waves(CDWs) in quasi-1D metals([14] and references therein). By increasing the intensity of the optical lattice, one can continuously tune the single atom dispersion from 3D to 1D.

As revealed by the Bethe *ansatz* [15, 16], the exact $T = 0$ phase diagram of the 1D polarized Fermi gas displays four phases: unpolarized superfluid, FFLO, fully-polarized normal, and vacuum, characterized by the densities of the two species and by algebraic order. Unlike 3D, in 1D all of the phase transitions are continuous and the FFLO phase occurs at *all* non-zero partial polarizations for *any* strength attractive interaction [16]. Furthermore, the polarized FFLO super-

fluid is denser than the unpolarized superfluid (SF) in 1D, while the opposite is true in 3D. In a trap, the spatial structure is therefore inverted: in 1D one expects to find a central FFLO region surrounded by SF. During the crossover from 1D to 3D we find a regime where FFLO is found both at the center and edge of the cloud, with an intervening SF shell.

5.3 Model

We consider two species of fermionic atoms (labeled by pseudospin $\sigma = \uparrow, \downarrow$ or $\sigma = \pm 1$) confined by a smooth potential $V(\mathbf{r})$ and a square optical lattice which breaks the cloud into an array of tubes aligned along the z-direction. The spatial variation of the lattice intensity, $I(\mathbf{r})$, and of the trapping potential, $V(\mathbf{r})$, will be modeled by a local density approximation, where the properties at location $\mathbf{r}$ depend on the local lattice intensity and the local chemical potentials $\mu_\sigma(\mathbf{r}) \equiv \mu_\sigma - V(\mathbf{r})$ in the same way that the uniform system depends on I and μ_σ. The spatially varying pattern of phases in a trap can be read off from the uniform phase diagram by tracing the spatial variation of $\mu \equiv (\mu_\uparrow + \mu_\downarrow)/2$ and the lattice parameters. In the special case of uniform I, only μ varies in space.

To produce the uniform phase diagram we study the untrapped system in a uniform lattice with $N_x \times N_y$ tubes. For a sufficiently low density and strong enough lattice, the xy motion is well approximated by a one-band tight-binding model with single-atom dispersion:

$$\epsilon_\mathbf{k} = \frac{k_z^2}{2m} + 2t[2 - \cos(k_x b) - \cos(k_y b)] , \tag{5.1}$$

where t is the hopping, b is the lattice spacing, m is the mass, and we use $\hbar = 1$. The Brillouin zone of the xy motion is $|k_x|, |k_y| \leq \pi/b$, while k_z is unconstrained.

For energies well above the xy bandwidth $\epsilon_\mathbf{k} \gg 8t$, the dispersion is 1D-like. For low energies $\epsilon_\mathbf{k} \ll t$, the dispersion is 3D-like, and can be made isotropic if we rescale the momenta $\{k_x, k_y, k_z\} \mapsto \{b\sqrt{2t}k_x, b\sqrt{2t}k_y, k_z/\sqrt{m}\}$. This single-band, tight-binding regime is accessed experimentally by working in a regime with $t, \varepsilon_{F\sigma} \ll \sqrt{U/mb^2}$, where U is the depth of the optical potential, and $\varepsilon_{F\sigma} = (3\pi^2 n_\sigma)^{2/3}/2m$ is the Fermi energy for each species of density n_σ.

Since the ^{6}Li experiments use highly dilute gases with a wide Feshbach resonance, the interactions can be modeled by a contact interaction, giving a Hamiltonian,

$$\hat{H} - \mu_\uparrow \hat{N}_\uparrow - \mu_\downarrow \hat{N}_\downarrow = \sum_\mathbf{k} \sum_{\sigma=\uparrow,\downarrow} (\epsilon_\mathbf{k} - \mu_\sigma) c_{\mathbf{k}\sigma}^\dagger c_{\mathbf{k}\sigma}$$

$$+ \frac{g}{L_z N_x N_y} \sum_{\mathbf{k},\mathbf{k}',\mathbf{q}} c_{\mathbf{k}\uparrow}^\dagger c_{\mathbf{k}'\downarrow}^\dagger c_{\mathbf{k}'+\mathbf{q}\downarrow} c_{\mathbf{k}-\mathbf{q}\uparrow} . \quad (5.2)$$

The system has length L_z in the z-direction. The coupling constant g can be expressed in terms of the three-dimensional s-wave scattering length a [17]:

$$\frac{1}{g} = \frac{ma_{1D}}{2} \equiv \frac{ma_\perp}{2}\left(\frac{a_\perp}{a} - C\right) \quad (5.3)$$

where $a_\perp = \sqrt{1/m\omega_\perp}$ is the oscillator length in the xy-direction within one tube of the optical lattice and $C \simeq 1.0326$. Thus, we have an attractive 1D interaction when $a_\perp/a < C$. Defining the 1D two-body binding energy $\varepsilon_B = g^2 m/4$, we can fully parameterize the $T = 0$ phase diagram of the uniform system with three dimensionless quantities: t/ε_B, μ/ε_B and h/ε_B, where $h \equiv \mu_\uparrow - \mu_\downarrow$ [1].

---

[1] Only 2 parameters are needed in 3D, e.g. μ/h, $1/a\sqrt{2mh}$.

5.4 Phase diagram

We calculate the $T = 0$ phase diagram within mean-field theory, which captures most of the qualitative features of the phase diagram as we move between the 1D and 3D regimes. We know by comparison to the exact solution that this mean-field approximation does miss some features of the 1D limit, as we note below.

We begin at $h = 0$ where there are only two phases: the unpolarized superfluid and the vacuum (see Fig. 5.1). In the 1D limit (small t) the attractive interaction leads to a two-atom bound state with binding energy E_B. These bosonic pairs enter the system and form a Bose-Einstein condensate (BEC) for $\mu > -E_B/2$. Increasing the density further brings the system through a density-driven BEC-BCS crossover, similar to excitonic systems [18]. Making the system more three-dimensional, by increasing t, reduces both E_B and the BEC regime. For $t/\varepsilon_B > 0.2066$ there is no two-atom bound state and thus only the BCS regime. Weak coupling BCS behavior is found when either μ or t is large compared to ε_B.

At finite h we must also consider the FFLO superfluid phase where the Cooper pairs condense with nonuniform pairing order parameter (gap) $\Delta(z) = -g/(L_z N_x N_y) \sum_{\mathbf{k},q_z} e^{iq_z z} \langle c_{-\mathbf{k}+q_z\hat{\mathbf{z}}/2\downarrow} c_{\mathbf{k}+q_z\hat{\mathbf{z}}/2\uparrow} \rangle = -g/(N_x N_y) \sum_l u_{l,\mathbf{k}_\perp}(z) v^*_{l,\mathbf{k}_\perp}(z) f(E_{l,\mathbf{k}_\perp})$, where $f(x)$ is the zero-temperature Fermi function, $\mathbf{k}_\perp$ is the momentum in the xy direction, l labels the quasiparticle modes, and the energies/coherence factors obey the Bogoliubov-de Gennes (BdG) equations [19]

$$\begin{pmatrix} h_{0\uparrow} - \mu & \Delta(z) \\ \Delta^*(z) & -h_{0\downarrow} + \mu \end{pmatrix} \begin{pmatrix} u_{l,\mathbf{k}_\perp}(z) \\ v_{l,\mathbf{k}_\perp}(z) \end{pmatrix} = E_{l,\mathbf{k}_\perp} \begin{pmatrix} u_{l,\mathbf{k}_\perp}(z) \\ v_{l,\mathbf{k}_\perp}(z) \end{pmatrix} \tag{5.4}$$
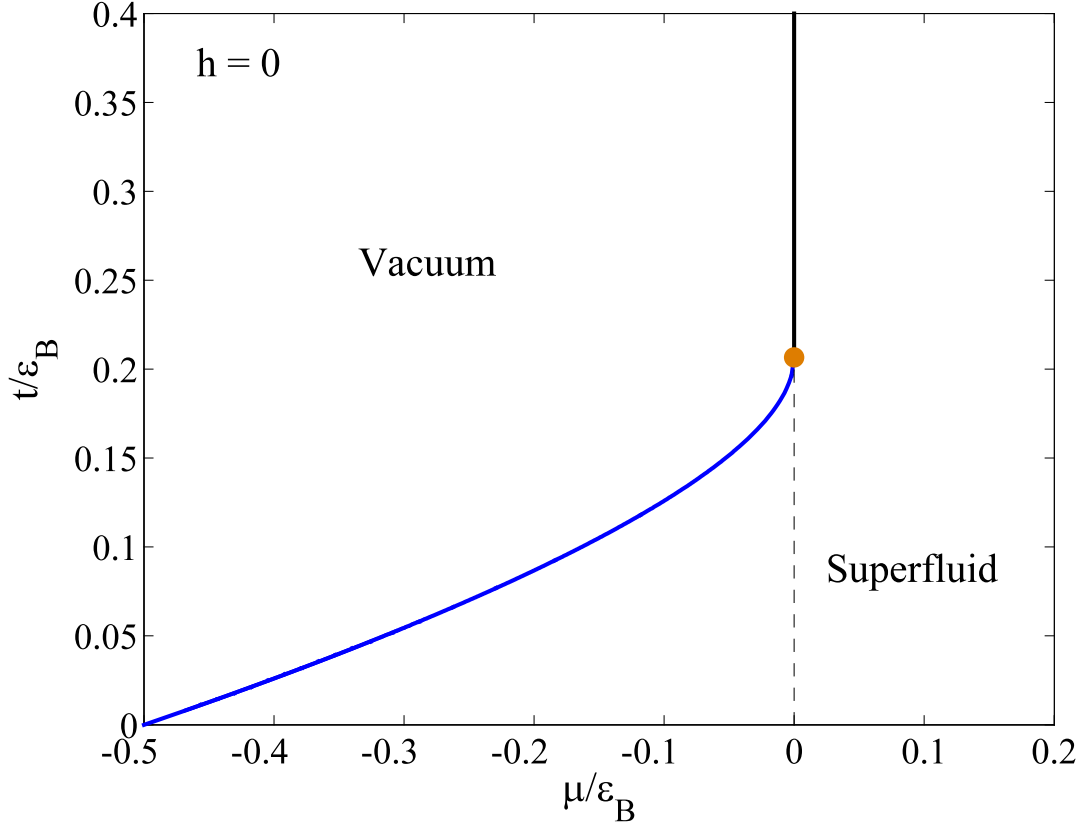
Figure 5.1: (Color online) Phase diagram for $h = 0$. For t/ε_B below the filled circle, there is a two-atom bound state, and the resulting bosonic pairs enter the system as a Bose condensate as μ is increased through the solid line. For t/ε_B above the filled circle we are always in the BCS regime.

with $h_{0\sigma} = -\frac{\partial_z^2}{2m} + 2t[2 - \cos(k_x b) - \cos(k_y b)] + gn_{-\sigma}(z)$. The densities in the Hartree term are $n_\uparrow(z) = (1/N_x N_y) \sum_{l,\mathbf{k}_\perp} |u_{l,\mathbf{k}_\perp}(z)|^2 f(E_{l,\mathbf{k}_\perp})$ and $n_\downarrow(z) = (1/N_x N_y) \sum_{l,\mathbf{k}_\perp} |v_{l,\mathbf{k}_\perp}(z)|^2 f(-E_{l,\mathbf{k}_\perp})$. The thermodynamic potential is [20, 21]

$$\Omega = \text{Tr}[\frac{1}{2}(h_{0,\uparrow} + h_{0,\downarrow}) - \mu] + \frac{1}{2} \sum_{l,\mathbf{k}_\perp,\sigma} (E_{l,\mathbf{k}_\perp} + \sigma h) f(E_{l,\mathbf{k}_\perp} + \sigma h)$$

$$- N_x N_y \int dz [\frac{|\Delta(z)|^2}{g} + gn_\uparrow(z)n_\downarrow(z)]. \quad (5.5)$$

The simplest ansatz for the FFLO phase is Fulde and Ferrell's one-plane

107

wave state $\Delta(z) = \Delta_{FF} e^{iqz}$ [7]. Here, the energy eigenvalues $E_{l,\mathbf{k}_\perp}$ reduce to $E_{\mathbf{k}\pm} = \sqrt{(\epsilon_\mathbf{k} + \frac{q^2}{8m} - \mu + \frac{g}{2}(n_\uparrow + n_\downarrow))^2 + \Delta^2} \pm (\frac{k_z q}{2m} + \frac{g}{2}(n_\uparrow - n_\downarrow))$ and we can then minimize Eq. (5.5) directly. This state is a good approximation in the limit $\Delta_{FF} \to 0$. Indeed, one can show that the second-order transition to the normal phase occurs at single wavevector q when

$$-\frac{1}{g} = \frac{1}{N_x N_y L_z} \sum_\mathbf{k} \frac{1 - f(\xi_+^\uparrow) - f(\xi_-^\downarrow)}{\xi_+^\uparrow + \xi_-^\downarrow}, \tag{5.6}$$

where $\xi_\pm^\sigma = \epsilon_{\mathbf{k}\pm q\hat{\mathbf{z}}/2} - \mu_\sigma + g n_{-\sigma}$. In Fig. 5.2 we illustrate the locus of this transition with a dotted-dashed line.

Larkin and Ovchinnikov [8] showed that the energy is lower if the Cooper pairs condense in a standing wave, with $\Delta(z) = \Delta_{LO} \cos(qz)$ when the gap is small. More generally, $\Delta(z)$ is a real periodic function of z. When the coherence length ξ is small compared to $1/q$, this state consists of well-separated domain walls between domains where Δ is alternately positive and negative. The polarized cores of these domain walls result from occupying the spin-up Andreev bound states on each wall.

To determine the stability of the unpolarized superfluid (SF) to the FFLO state we self-consistently solve Eq. (5.4) to find the h where the energy of a single domain wall vanishes. If the domain walls interact repulsively, the transition is continuous and lies at this h, otherwise this determines the spinodal of a first-order transition (which in this case is likely to be near the true phase boundary). The transition is continuous in 1D [22], and has been argued to be so in 3D [23, 24]: in weak coupling the critical fields are respectively $h = (2/\pi)\Delta_0(= 0.64\Delta_0)$, and $0.67\Delta_0$, where Δ_0 is the gap in the SF phase. We are unaware of a strong coupling 3D calculation of the sign of the domain wall interaction.

Fig. 5.2 shows a representative slice of the mean-field phase diagram at fixed
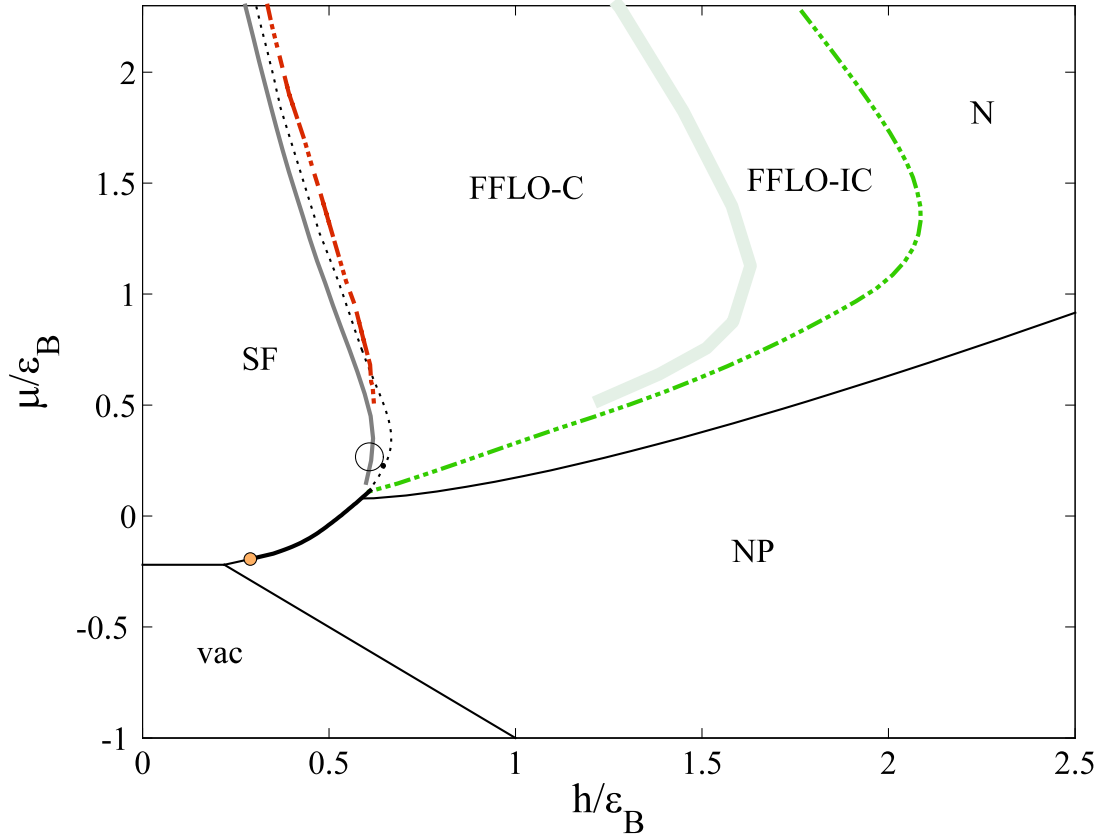
Figure 5.2: (Color online) Slice of the mean-field phase diagram taken at $t/\varepsilon_B = 0.08$. The phases shown include the unpolarized superfluid (SF), partially-polarized normal (N), and fully-polarized normal (NP). The FFLO phase is divided into gapped 'commensurate' (C) and ungapped 'incommensurate' (IC) phases. The filled circle marks the tricritical point; near it, but not visible here is a tiny region of SF_M phase, a remnant of the 3D BEC regime. The SF-NP and SF-N transitions are first-order for μ/ε_B above the tricritical point, along the solid heavy line. The SF-FFLO transition (solid line) is estimated from the domain wall calculation. The transition from FFLO to normal (dotted-dashed line) is assumed to be second-order. The large circle marks the region of FFLO where Δ/ε_F is largest, so the phase is likely most robust to $T > 0$ here. The dashed line near the SF-FFLO transition shows where the wave vector of the FFLO state is stationary as a function of μ: $dq/d\mu = 0$ (this is calculated using the FF approximation).

$t/\varepsilon_B = 0.08$ (if one can neglect the spatial variation of ϵ_B and t, this slice corresponds to a fixed optical lattice intensity). Near the vacuum at small filling (low μ) is the 3D BEC regime, including a very small region of the SF_M magnetized superfluid phase where the excess fermions form a Fermi liquid within the BEC. As μ and thus the filling is increased, the system crosses over towards 1D. Here, the FFLO phase appears and occupies a large portion of the phase diagram. Both the unpolarized SF phase and the FFLO phase become re-entrant: in the 1D regime the FFLO phase is at a higher μ and thus a higher density than SF, while in the 3D regime this density relation is reversed. Thus, we see that the "inverted" phase separation in 1D trapped gases is connected to the standard phase separation of 3D via an intermediate pattern of phases where SF forms a shell surrounded by polarized phases. As t/ε_B is further reduced, the 3D regime becomes smaller, with the re-entrance of the SF phase moving to lower μ, while the FFLO phase grows and the sliver of N phase between FFLO and NP is diminished. In the limit $t = 0$ this phase diagram matches fairly well to that obtained from the exact solution in 1D (e.g., Fig. 1 of Ref. [15]). The main feature that the mean-field approximation misses at $t = 0$ is the multicritical point where the four phases, SF, FFLO, NP and vacuum, all meet at $h = -\mu = \varepsilon_B/2$. In the mean-field approximation, the FFLO phase never extends all the way down to zero density; instead it is preempted by a first-order SF-to-NP transition.

A new $T = 0$ phase transition occurs within the FFLO phase as one moves from 3D to 1D by increasing the intensity of the 2D optical lattice. In 3D the FFLO state has a Fermi surface, and is therefore gapless. In 1D the spectrum of BdG quasiparticles is fully gapped in the FFLO state. The gapped, commensurate FFLO state (FFLO-C), contains exactly one excess spin-up atom per 1D tube per domain wall. This commensurability means $q = \pi(n_\uparrow^{(1)} - n_\downarrow^{(1)})$, where $n_\sigma^{(1)}$

is the 1D density of that species in one tube of the optical lattice. By contrast, the number of excess up spins in the ungapped, incommensurate FFLO state (FFLO-IC) is not constrained.

The transition between FFLO-C and FFLO-IC can be understood from the band structure of the Andreev bound states on the domain walls. In FFLO-C the chemical potential lies in a gap in the quasiparticle spectrum. Thus the superfluid FFLO-C phase is a band insulator for the *relative* motion of the unpaired atoms and the condensate of pairs. As the optical lattice intensity is decreased, the 3D bands broaden and may overlap the chemical potential, opening up a Fermi surface. We approximate the IC-C transition within the FF *ansatz* by examining the $k_z > 0$ half of the Fermi surface to see if it is fully gapped. In the limit $\mu/t \gg 1$, the transition occurs when $\Delta \sim 8th/\mu$.

5.5 Experimental considerations

We now address the question of what are the best conditions for experimentally producing, detecting and studying the FFLO phase. Ideally one might use *in situ* imaging to directly observe the spatial density and magnetization modulations in this phase. In a 3D gas, producing the FFLO phase may be problematic, for it occurs for only restricted values of μ and h [10]. Thus only a thin shell in a trap will be in the FFLO phase. Moreover, imaging the modulations will be complicated by their 3D nature (e.g., they may form an onion-like pattern). The 1D limit also has problems. Although in 1D the FFLO phase occurs in a large region of the $T = 0$ phase diagram, it has no true long-range order, only power-law correlations. Further, the transition temperature of this 1D superfluid is

zero. We mention that in quasi-1D materials that undergo a Peierls instability it is important that they are not strictly 1D, but have sufficient interchain hopping to supress fluctuations [14]. Also, for $t = 0$ (strictly 1D) we have an array of independent parallel 1D clouds whose density modulations will be out of phase with one another, reducing the observed signal.

Given these concerns, we believe that the optimal conditions for observing FFLO are likely to be in the quasi-1D regime where the 2D optical lattice is at an intermediate intensity that is strong enough to make the Fermi surface 1D-like (and hence enhance the instability towards FFLO), but weak enough that the atoms are still able to hop between the parallel tubes and thus introduce strong inter-tube correlations in the optical lattice. The resulting 3D long-range order can then survive to nonzero T.

Although we have only performed a $T = 0$ calculation, we can crudely estimate the transition temperature from the size of the gap Δ. For small Δ, superfluid phases have transition temperatures $T_c \propto \Delta$, however when Δ approaches ε_F, the transition temperature saturates. Thus the observability of a superfluid phase such as FFLO is enhanced if the gap is increased to of order ε_F, but there is not likely to be an advantage to increasing the gap to much larger values. In 3D the maximum T_c/ε_F of the unpolarized SF occurs on the BEC side of the Feshbach resonance, well away from the FFLO phase [25]. However, as we move towards 1D in our phase diagram, the FFLO phase extends more and more into the regime of strong pairing where the gap is of order ε_F, and thus we expect a large T_c. For a given t/ε_B, we find that the gap in the FFLO phase is the largest fraction of ε_F at the SF-FFLO phase boundary near its point of reentrance, where h on the SF-FFLO boundary reaches its maximum (see Fig. 2).

We also find that within mean-field theory this fraction Δ/ε_F increases as we reduce the hopping t. At sufficiently low t the system crosses over from quasi-1D to 1D and our mean-field theory becomes unreliable. In the 1D limit T_c must vanish, so the maximum value of T_c/ε_F within the FFLO phase must occur in the quasi-1D regime at some small but nonzero hopping t.

Another consideration that may complicate the detection of the FFLO phase within a trap is the fact that μ varies spatially both within and between tubes. This means that the local wavenumber q of the modulation will vary through the cloud, making the modulations more difficult to detect. This variation can be minimized if one works near a point where $dq/d\mu = 0$. We find such points do exist in the quasi-1D regime (see Fig. 5.2); in 3D, $dq/d\mu$ is always negative so such points do not exist. Note that in the 1D limit ($t = 0$) there is even a point in the exact phase diagram near strong coupling where $d^2q/d\mu = dq/d\mu = 0$ that should be a real "sweet spot" for having a uniform q over a fairly large fraction of a trap, and that this feature should survive to small t.

BIBLIOGRAPHY FOR CHAPTER 5

[1] G. B. Partridge, W. Li, R. I. Kamar, Y. Liao, and R. G. Hulet, Science **311**, 503 (2006a).

[2] M. W. Zwierlein, A. Schirotzek, C. H. Schunck, and W. Ketterle, Science **311**, 492 (2006a).

[3] M. W. Zwierlein, C. H. Schunck, A. Schirotzek, and W. Ketterle, Nature **442**, 54 (2006b).

[4] Y. Shin, M. W. Zwierlein, C. H. Schunck, A. Schirotzek, and W. Ketterle, Phys. Rev. Lett. **97**, 030401 (2006).

[5] G. B. Partridge, W. Li, Y. A. Liao, R. G. Hulet, M. Haque, and H. T. C. Stoof, Phys. Rev. Lett. **97**, 190407 (2006b).

[6] C. H. Schunck, Y. Shin, A. Schirotzek, M. W. Zwierlein, and W. Ketterle, Science **316**, 867 (2007).

[7] P. Fulde and R. A. Ferrell, Phys. Rev. **135**, A550 (1964).

[8] A. I. Larkin and Y. N. Ovchinnikov, Sov. Phys. JETP **20**, 762 (1965).

[9] T. Mizushima, K. Machida, and M. Ichioka, Phys. Rev. Lett. **94**, 060404 (2005).

[10] D. E. Sheehy and L. Radzihovsky, Phys. Rev. Lett. **96**, 060401 (2006).

[11] R. Casalbuoni and G. Nardulli, Rev. Mod. Phys. **76**, 263 (2004).

[12] M. M. Parish, F. M. Marchetti, A. Lamacraft, and B. D. Simons, Nature Phys. **3**, 124 (2007).

[13] T. Koponen, T. Paananen, J.-P. Martikainen, and P. Torma, cond-mat/0701484.

[14] R. Thorne, Physics Today p. 42 (1996).

[15] G. Orso, Phys. Rev. Lett. **98**, 070402 (2007).

[16] H. Hu, X.-J. Liu, and P. D. Drummond, Phys. Rev. Lett. **98**, 070403 (2007).

[17] M. Olshanii, Phys. Rev. Lett. **81**, 938 (1998).

[18] C. Comte and P. Nozières, J. Physique **43**, 1069 (1982).

[19] P. G. de Gennes, *Superconductivity of Metals and Alloys* (Westview Press, 1999).

[20] J. Bardeen, R. Kümmel, A. E. Jacobs, and L. Tewordt, Phys. Rev. **187**, 556 (1969).

[21] G. Eilenberger, Z. Physik **184**, 427 (1965).

[22] K. Machida and H. Nakanishi, Phys. Rev. B **30**, 122 (1984).

[23] S. Matsuo, S. Higashitani, Y. Nagato, and K. Nagai, J. Phys. Soc. Jpn **67**, 280 (1998).

[24] N. Yoshida and S.-K. Yip, Phys. Rev. A **75**, 063601 (2007).

[25] C. A. R. Sá de Melo, M. Randeria, and J. R. Engelbrecht, Phys. Rev. Lett. **71**, 3202 (1993).

THEORY AND EXPERIMENTS WITH IMBALANCED FERMI GASES IN ONE DIMENSION

6.1 Trapped Fermi gases in one dimension

Cold atom experiments offer a natural opportunity to study quantum physics in lower dimensions. Attractively interacting two component Fermi gases are particularly interesting as they could offer a unique opportunity to study the elusive FFLO phase [1, 2, 3]. One dimensional systems, cold atom analogues of quantum wires, have been created in atom-chip experiments and also in arrays of two dimensional optical lattices [4]. When these 2D lattice potentials are very strong, one may consider each lattice site as an independent harmonic 1D waveguide. To be concrete we consider the site at $x = y = 0$ for the 2D optical lattice potential $V(x, y) = V_0[\sin^2(kx) + \sin^2(ky)]$, described by the lattice strength V_0 and wavenumber $k = 2\pi/\lambda$ (λ is the wavelength of the lattice laser). When $V_0 \gg E_R = \hbar^2 k^2/(2m)$, we may approximate the sinusoidal potential as

$$V(x, y) = V_0 \left[\sin^2(kx) + \sin^2(ky)\right] \approx V_0 k^2 \left(x^2 + y^2\right) = \frac{1}{2}m\omega_\perp(x^2 + y^2), \quad (6.1)$$

where $\omega_\perp = k\sqrt{2V_0/m}$. This waveguide is characterized by the harmonic oscillator length $a_\perp = \sqrt{\hbar/(m\omega_\perp)}$.

We will now review the theory of the 1D BEC-BCS crossover [5, 6]. Intuition about the physics of interacting two component fermions in such a waveguide is obtained by separately considering the molecule and fermion limits, $\pm a_s/a_\perp \gg 1$ (a_s is the usual 3D scattering length of the unconfined gas). In the fermion limit, a weakly attractively interacting Fermi gas is confined to a

harmonic waveguide. We can assume that only the lowest transverse mode is occupied and approximate the fermion creation operator $\psi_\sigma^\dagger(\mathbf{r})$ as

$$\psi_\sigma^\dagger(\mathbf{r}) \approx \phi_0(x,y)\psi_\sigma^\dagger(z), \tag{6.2}$$

where $\psi_\sigma^\dagger(z)$ is a 1D fermion creation operator and $\phi_0(x,y) = e^{-(x^2+y^2)/(2a_\perp^2)}/(a_\perp\sqrt{\pi})$ is the ground state wavefunction of the transverse harmonic oscillator potential. Using this replacement in the Hamiltonian Eq. (2.1) for the 3D gas and replacing the coupling g with its Born approximation value $g \to 4\pi\hbar^2 a_s/m$, we integrate over the transverse degrees of freedom and obtain the purely 1D Hamiltonian Eq. (3.56)

$$H = \int dz \sum_\sigma \psi_\sigma^\dagger(z)\left(-\frac{\hbar^2}{2m}\frac{d^2}{dz^2}\right)\psi_\sigma(z) + g_{1D}\psi_\uparrow^\dagger(z)\psi_\downarrow^\dagger(z)\psi_\downarrow(z)\psi_\uparrow(z), \tag{6.3}$$

with

$$g_{1D} = \frac{4\pi\hbar^2 a_s}{m}\int dxdy|\phi_0(x,y)|^4 = \frac{2\hbar^2 a_s}{ma_\perp^2} \equiv -\frac{2\hbar^2}{ma_{1D}}. \tag{6.4}$$

As mentioned before, this 1D theory is the exactly solvable Gaudin-Yang model [7, 8]. For the balanced gas, the set of Bethe ansatz equations for the ground state are given by

$$
\begin{aligned}
\sigma(k) &= \frac{1}{\pi} - \frac{2/a_{1D}}{\pi}\int_{-K}^{K} dk'\frac{\sigma(k')}{(2/a_{1D})^2 + (k-k')^2} \\
\frac{E}{L} &= 2\int_{-K}^{K} dk\,\frac{\hbar^2 k^2}{2m}\sigma(k) - \frac{1}{2}\epsilon_B\frac{N}{L} \\
\frac{N}{L} &= \frac{N_\uparrow + N_\downarrow}{L} = 2\int_{-K}^{K} dk\,\sigma(k)
\end{aligned} \tag{6.5}
$$

where the two body binding energy is $\epsilon_B = \hbar^2/(ma_{1D}^2)$. From the solution to these equations the zero temperature equation of state $n(\mu)$ (and consequently Thomas-Fermi density profiles) can be obtained from a Legendre transformation.

We will now consider the opposite limit, where $a/a_\perp \gg 1$. In this BEC limit, the spin-up and spin-down fermions form tightly bound bosonic molecules with 3D binding energy $E_B = \hbar^2/(ma^2)$. When this boson of mass $2m$ is placed in a waveguide we can approximate the boson creation operator $\phi^\dagger(\mathbf{r})$ as

$$\phi^\dagger(\mathbf{r}) = \tilde{\phi}_0(x, y)\phi^\dagger(z) \tag{6.6}$$

where $\phi^\dagger(z)$ is the 1D boson creation operator and $\tilde{\phi}_0(x, y) = e^{-(x^2+y^2)/a_\perp^2} 2/(\sqrt{\pi}a_\perp)$ is the groundstate harmonic oscillator wavefunction for the center of mass coordinate of the pair. These bosons can be described with the Hamiltonian of the 1D Bose gas

$$H = \int dz \sum_\sigma \phi^\dagger(z) \left(-\frac{\hbar^2}{4m} \frac{d^2}{dz^2} \right) \phi(z) + \frac{g_{1D}^{BB}}{2} \phi^\dagger(z)\phi^\dagger(z)\phi(z)\phi(z), \tag{6.7}$$

with $g_{1D}^{BB} = 2\hbar^2 a_s^{BB}/(ma_\perp^2) \equiv -2\hbar^2/(ma_{1D}^B B)$ and from Petrov's solution to the four-body problem we know that $a_s^{BB} = 0.6a_s$ [9]. The 1D Bose gas can also be solved exactly by the Lieb-Liniger solution [10]. For this bosonic case the Bethe ansatz equations are

$$\rho(\lambda) = \frac{1}{2\pi} - \frac{2/a_{1D}^{BB}}{\pi} \int_{-\Lambda}^{\Lambda} d\lambda' \frac{\rho(\lambda')}{(2/a_{1D}^{BB})^2 + (\lambda - \lambda')^2},$$

$$\frac{E_{boson}}{L} = \int_{-\Lambda}^{\Lambda} d\lambda \, \hbar^2 \lambda^2 2m\rho(\lambda), \quad \frac{N_{boson}}{L} = \int_{-\Lambda}^{\Lambda} d\lambda \, \rho(\lambda), \tag{6.8}$$

What is very surprising is that if we rescale

$$k = \lambda/2, \quad \rho(\lambda) = \sigma(k)/2, \quad a_{1D}^B B \to a_{1D}/2, \tag{6.9}$$

Eqs. (6.8) and Eqs. (6.5) become identical (up to the binding energy E_B that should be subtracted from E_{boson} to obtain the fermion energy E) [5]. What is even more surprising and the key observation of the authors of Refs. [5, 6] is that the theories of BEC and BCS limits can be smoothly connected via the strongly interacting regime at $|a_{1D}| = |a_{1D}^{BB}| = \infty$, where the Lieb-Liniger theory

and the Gaudin-Yang model both describe a Tonks gas of bosons. This resulting theory is universal in the sense that the equation of state only depends on a single dimensionless parameter

$$\gamma^{-1} = (na_\perp)^{-1}\chi(a_\perp/a_s) \tag{6.10}$$

where $\chi(x)$ is a dimensionless universal function and $n = (N_\uparrow + N_\downarrow)/L$ is the total density. This is surprising because basically one has two different dimensionless parameters, na_s and $na_\perp$ available, and it is not immediately obvious why one should drop out. In terms of the parameter γ, the Bethe ansatz equations Eqs. (6.8), (6.5) can be written as [6]

$$
\begin{aligned}
\sigma(k) &= \frac{1}{\pi} + \frac{1}{\pi}\int_{-K}^{K} dq\, \frac{n\gamma\sigma(q)}{(n\gamma)^2 + (k-q)^2} \\
E_0/L &= 2\int_{-K}^{K} dk\, \frac{\hbar^2 k^2}{2m}\sigma(k) - nE_B/2 \\
N/L &= 2\int_{-K}^{K} dk\, \sigma(k),
\end{aligned}
\tag{6.11}
$$

where γ is

$$
\gamma^{-1} =
\begin{cases}
\frac{\hbar^2 n}{g_{1D}^{BB}m} = \frac{a_s}{1.2na_\perp^2} & \text{BEC limit} \\[2mm]
\frac{\hbar^2 n}{g_{1D}m} = \frac{a_s}{2na_\perp^2} & \text{BCS limit}
\end{cases}
\tag{6.12}
$$

Olshanii has solved the general two-body scattering problem in a harmonic waveguide for all values of a_s [11]. His result is that the low energy 1D scattering amplitude can be reproduced with a δ-function interaction of coupling strength

$$g = 2\hbar\omega_\perp \frac{a_s}{1 - Aa_s/a_\perp}, \tag{6.13}$$

where $A = -\zeta(1/2)/\sqrt{2} \approx 1.03$. This formula holds for scattering at momenta with $ka_\perp \ll 1$. The point where $a_\perp/a_s = A \sim 1$ is called the confinement induced resonance (CIR). At the CIR the coupling the one dimensional Bose

gas becomes hardcore, i.e. one has a Tonks-Girardeau gas [12]. Note that this contact interaction description *does not* work for the two-body bound state. This is because the short range physics of the confinement become important when the pair shrinks to size of order $a_\perp$. The bound state energy in a one dimensional waveguide is [13]

$$\zeta(1/2, -E_B/(\hbar\omega_\perp) + 1/2) = -\sqrt{2}\frac{a_\perp}{a_s} \tag{6.14}$$

where $\zeta(s, a)$ is the generalized ζ-function as defined in Ref. [13]. As shown in Fig. 6.8 this function is a smooth function of $a_\perp/a_s$. Eq. (6.13) suggests an extrapolation scheme for the universal function $\chi(x)$ into the strong coupling regime $|a_s| \gg a_\perp$ [6]. Coming from the BEC limit, we can try to extrapolate (6.12) into the strong coupling regime by using Olshanii's formula for the molecules

$$g_{1D}^{BB} = \frac{1.2\hbar^2 a_s}{ma_\perp^2} \frac{1}{1 - 0.6\sqrt{2}Aa_s/a_\perp} \tag{6.15}$$

Similarly, it seems reasonable to extrapolate from the BCS limit as

$$g_{1D} = \frac{2\hbar^2 a_s}{ma_\perp^2} \frac{1}{1 - Aa_s/a_\perp} \tag{6.16}$$

The authors of Ref. [6] then combine these formulas by matching the CIR at $a_\perp/a_s = A$ $(0.6\sqrt{2} = 0.85 \to 1$ in Eq. (6.15)). The universal function $\chi(x)$ is then

$$\chi(x) = \begin{cases} x(A - 1/x)/2 & x < 1/A \\ x(A - 1/x)/1.2 & x > 1/A \end{cases}. \tag{6.17}$$

While this is clearly only an approximation for $\chi(x)$, the true location of the CIR can in principle be obtained from a solution of the four-body problem in a waveguide. At the moment, the true location of this CIR in the 1D BEC-BCS crossover problem is still somewhat controversial [14, 15].

One could wonder why the 1D Fermi gas described by the Hamiltonian Eq. (3.56) fails to describe the full 1D BEC-BCS crossover. After all, a single channel

model is able to capture the entire crossover in 3D. The deeper reason is that in the limit of tightly bound fermions (where $g_{1D} \to -\infty$), these pairs *must* interact via a hardcore interaction in 1D[1]. Therefore the weakly interacting Bose gas limit is completely absent. A simple solution to this problem is to add an extra boson channel and consider the 1D two channel (or Bose-Fermi resonance) model with Hamiltonian [16]

$$
\begin{aligned}
H \;=\; & \int dz \sum_\sigma \psi_\sigma^\dagger(z) \left(-\frac{\hbar^2}{2m} \frac{d^2}{dz^2} \right) \psi_\sigma(z) + \phi^\dagger(z) \left(-\frac{\hbar^2}{4m} \frac{d^2}{dz^2} + \nu \right) \phi(z) \\
& + \; \eta \int dz \; \left[\psi_\uparrow^\dagger(z) \psi_\downarrow^\dagger(z) \phi(z) + \psi_\downarrow(z) \psi_\uparrow(z) \phi(z) \right],
\end{aligned}
\tag{6.18}
$$

where $\phi(z)$ is the bosonic creation operator for the molecular channel, η is the Feshbach coupling and ν is the detuning. Here $\nu \to \infty$ corresponds to the BCS limit, where one can integrate out the bosons to obtain the 1D Fermi gas Hamiltonian Eq. (3.56), and the limit $\nu \to -\infty$ is the BEC limit where we can integrate out the fermions to get the 1D Bose gas Hamiltonian (6.7). In Ref. [16], it was shown that this model can also be mapped onto the 1D Bethe ansatz solution Eq. (6.11). This means the 1D Bose-Fermi resonance model is equivalent to the BEC-BCS crossover problem in a harmonic waveguide. As we argue in chapter 7, a generalization of the model will also provide a *qualitative* description of the BEC-BCS crossover of the imbalanced gas.

Finally we note that a Fermi gas in a harmonic waveguide can be considered 1D if the effective chemical potential of the dimers $\tilde{\mu} = \mu + E_B/2$ and the temperature T satisfy

$$
\tilde{\mu}, T \ll \hbar\omega_\perp
\tag{6.19}
$$

An upper bound on $\tilde{\mu}$ can be obtained by noting that the effective chemical po-

---

[1]By symmetry dimers interact in the even scattering channel, and the Pauli principle requires a node at the origin of the relative wavefunction.

tential of an attractive gas is always less than free Fermi gas value $\tilde{\mu} = \epsilon_F$ (this value is achieved in the deep BCS limit). Therefore $\epsilon_F, T \ll \hbar\omega_\perp$ is always sufficient for the gas to be considered one dimensional. When the 1D gas is created from a 2D optical lattice, one needs to additionally ensure that the tunneling matrix element t between lattice sites is sufficiently small.

6.2 The spin imbalanced case

As we have seen from the mean-field theory calculation of chapter 3, the attractive Fermi gas in 1D is expected to feature a large region of stability for the exotic FFLO phase. The prospect for observing and realizing the FFLO phase is what makes the spin imbalanced gas in 1D particularly exciting. Gaudin and Yang also derived a Bethe ansatz solution for the Hamiltonian Eq. (3.56) when the spin populations are imbalanced [7, 8]. Since this is a solution for the 1D Fermi gas Hamiltonian, it is rigorously only valid in the BCS limit ($-a_s/a_\perp \gg 1$). While the phase diagram of the imbalanced Fermi gas for the entire BEC-BCS crossover is currently poorly understood, we gained insight into this important problem from a study of the three-particle problem, described in chapter 7.

In the BCS limit, the energy scale for breaking a pair in the unpolarized gas is not simply the two-body binding energy ϵ_B, but twice a spin-gap Δ_s [2], whose quantitative value is renormalized by many-body effects (this spin-gap quickly approaches ϵ_B in the strong coupling limit and is calculated in Ref. [6]). When an applied Zeeman field h exceeds this spin-gap, the system enters a polar-

---

[2]Here we adopt Kun Yang's definition of Δ_s analogous to the BCS gap where 2Δ is the energy required to break a Cooper pair [17]. Other authors [6, 1], define Δ as the energy required to break a pair, i.e. $2\Delta_s$.

ized phase, analogous to the mean-field transition to a soliton lattice. Recently, the full ground state phase diagram was obtained from a solution to the Bethe ansatz equations by Orso, and independently Hu *et al.* [1, 2]. In the imbalanced case these Bethe ansatz equations are a set of coupled integral equations [18]

$$
\begin{aligned}
\sigma(k) &= \frac{1}{\pi} + \int_{-B}^{B} a_2(k - k')\sigma(k')dk + \int_{-Q}^{Q} a_1(k - k')\rho(k')dk', \\
\rho(k) &= \frac{1}{2\pi} + \int_{-B}^{B} a_1(k - k')\sigma(k)dk, \\
N_\downarrow/L &= \int_{-B}^{B} dk\, \sigma(k), \quad (N_\uparrow - N_\downarrow)/L = \int_{-Q}^{Q} dk\, \rho(k), \\
E/L &= \int_{-Q}^{Q} dk\, \frac{\hbar^2 k^2}{2m}\rho(k) + 2\int_{-B}^{B} dk\, \frac{\hbar^2 k^2}{2m}\sigma(k) - n_\downarrow \epsilon_B,
\end{aligned}
\tag{6.20}
$$

with the integral kernel

$$
a_\nu(k) = \frac{1}{\pi}\frac{\nu/a_{1D}}{k^2 + (\nu/a_{1D})^2},
\tag{6.21}
$$

where $\nu = 1, 2, 3\ldots$. The exact phase diagram of the imbalanced gas Fig. 6.1 is qualitatively similar to the mean-field phase diagram Fig. 3.9. It features a partially polarized phase, an unpolarized fully paired phase and a noninteracting fully polarized normal gas [1]. The phase transition from the unpolarized to polarized phase occurs at a critical Zeeman field that is identical to the spin gap $h_{c1} \equiv \Delta_s$. As we will argue later, the partially polarized phase features FFLO correlations with an oscillating superfluid correlation function with the wavevector q of these oscillations set by the imbalance $q = \pi(n_\uparrow - n_\downarrow)$. In strictly 1D, however, these correlations decay as a power law at zero temperature as required by the Mermin-Wagner theorem [19]. Note that all phase transitions in 1D become crossovers at finite temperatures, smearing out the phase boundaries [20]. A very interesting observation is made in Ref. [1], about the limit of strong coupling ($c' = \infty$, i.e. the multicritical point in Fig. 6.1): In this limit the total energy is just the energy of a noninteracting Fermi gas of pairs of mass $2m$

and a noninteracting Fermi gas of excess fermions

$$E/L \approx E_B + E_F - nE_B/2 = \frac{\hbar^2 \pi^2 n_\downarrow^3}{12m} + \frac{\hbar^2 \pi^2 (n_\uparrow - n_\downarrow)^3}{6m} - nE_B/2. \qquad (6.22)$$

For the unpolarized gas this result is not surprising, because it is known that a hardcore Bose gas can be mapped onto a non-interacting Fermi gas via a Jordan Wigner transformation. The wavefunction for a hardcore Bose gas $\psi_B(z_1, \ldots, z_N)$ is then related to the free fermion wavefunction $\psi_F(z_1, \ldots, z_N)$ simply as [12]

$$\psi_B(z_1, \ldots, z_N) = |\psi_F(z_1, \ldots, z_N)|. \qquad (6.23)$$

On the other hand, we felt that it is very peculiar that there appears to be no interaction energy between the excess fermions and the pairs, even though this is the limit of strong coupling and the system should be in the correlated FFLO phase. We explain this behavior in 6.4 where we describe a generalization of the Jordan-Wigner transform that applies to strongly interacting imbalanced fermions in 1D. Our mapping allows for the calculation of correlations functions and explicitly demonstrates the FFLO oscillations in the pair correlation function.

For experiments, a few key features of the Bethe ansatz phase diagram are worth noting [1, 2, 21, 3]

- The inverted phase sequence predicted by the BdG mean-field theory still occurs in the exact solution. This can be seen from the negative slope of the superfluid to FFLO boundary in Fig. 6.1. Below a critical polarization, a trapped system features an unpolarized outer shell [illustrated in Fig. 6.2 (a)]
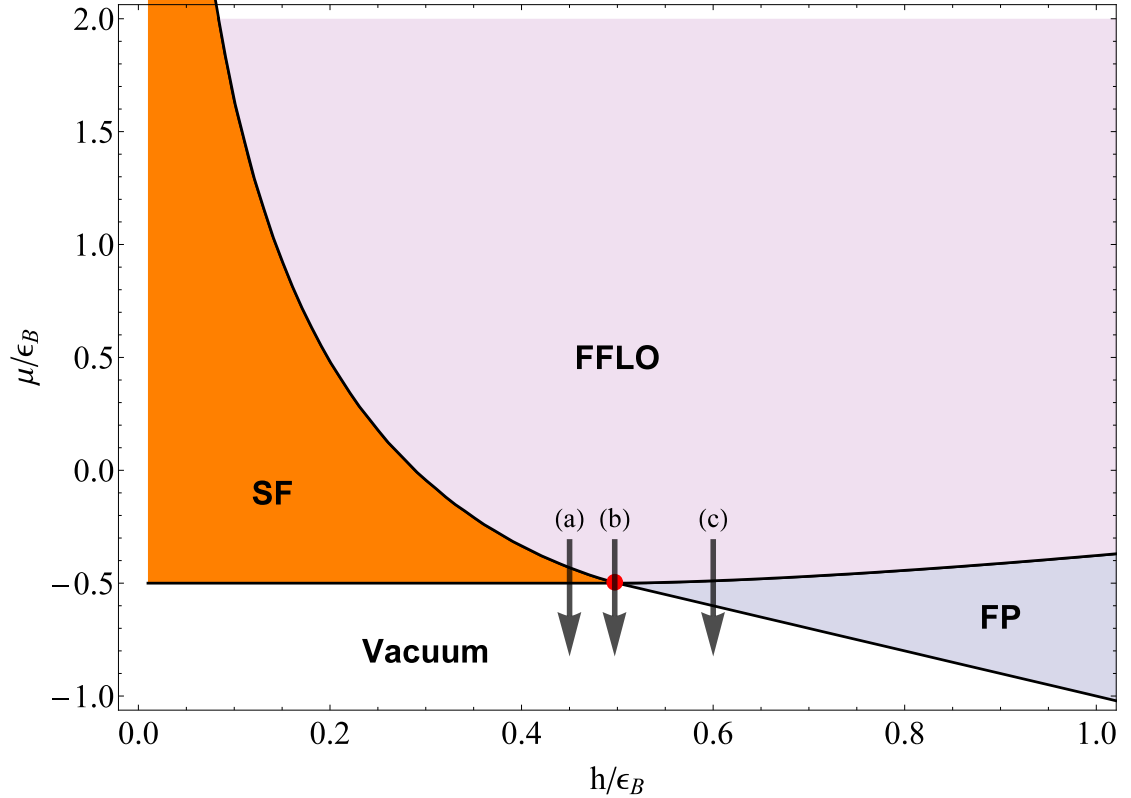
Figure 6.1: Phase diagram of the 1D attractive Fermi gas Eq. (3.56) as calculated from a solution to the Bethe ansatz integral equations (6.20) (chemical potentials are scaled by the two-body binding energy $\epsilon_B = \hbar^2/(ma_{1D}^2)$). The SF region is an unpolarized ($n_\uparrow = n_\downarrow$) and fully paired phase. The 1D FFLO phase has $n_\uparrow > n_\downarrow > 0$, featuring spatially modulated superfluid correlations. At large Zeeman field h the gas becomes fully polarized, here labeled FP. The arrows correspond to the ranges of μ, h of the (trapped system) density profiles shown in Fig. 6.2. Note that for a trapped imbalanced gas, three distinct phase sequences are possible [(a) $\rightarrow$ FFLO/SF, (b) $\rightarrow$ FFLO, (c) $\rightarrow$ FFLO/FP], as shown in Fig. 6.2.

- There is a multicritical point at strong coupling at $(\mu/\epsilon_B, h/\epsilon_B) = (-0.5, 0.5)$, where all phases meet. When tuned to this point, a trapped system is completely in the partially polarized FFLO phase and minority and majority Thomas-Fermi radii are equal [see Fig. 6.2 (b)].

- Surprisingly one finds that at moderate polarizations, the density difference remains almost uniform across the FFLO phase in a trapped system [see Fig. 6.2 (c)]. This implies the FFLO phase is paired at the same
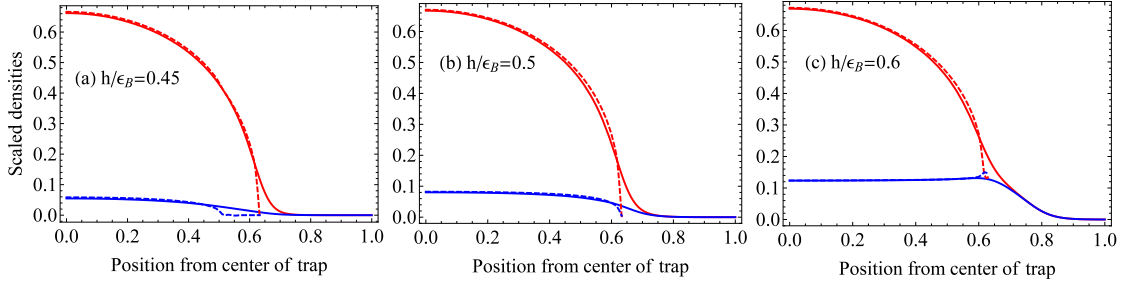
Figure 6.2: Density profiles at zero (dashed lines) and finite temperature $T/\epsilon_B = 0.03$ (solid lines) for a 1D imbalanced Fermi gas in a harmonic trap. The red curves show the total density na_{1D} and the blue curves the density difference $(n_\uparrow - n_\downarrow)a_{1D}$. The densities were calculated from a solution to the Bethe ansatz integral equations and using local density approximation. The central chemical potential is the same for all plots ($\mu_{central}/\epsilon_B = -0.3$). Position z along the tubes is scaled by the factor a_z^2/a_{1D}, where a_z is the harmonic oscillator of the harmonic trapping potential. Note that in the moderate imbalanced regime shown in (c), the density difference in the FFLO phase varies only by a few percent, thus making a detection of FFLO feasible even in an inhomogeneous trap.

wavevector $q = \pi(n_\uparrow - n_\downarrow)$ and detection schemes that measure the trap averaged pair momentum distribution will display a peak at finite momentum, just as a uniform gas would.

6.3   Extensions to finite temperature

Experiments with ultracold atoms are always performed at finite temperatures $T > 0$ and understanding the effects of finite temperature is crucial to interpreting data, particularly in lower dimensions. Achieving reliable thermometry is very challenging in cold gases, essentially because whenever a strongly correlated system is realized, its properties are usually poorly understood. Possible solutions include adiabatic ramps from a weakly interacting system (then one knows that final and initial state have same entropy) or putting the system
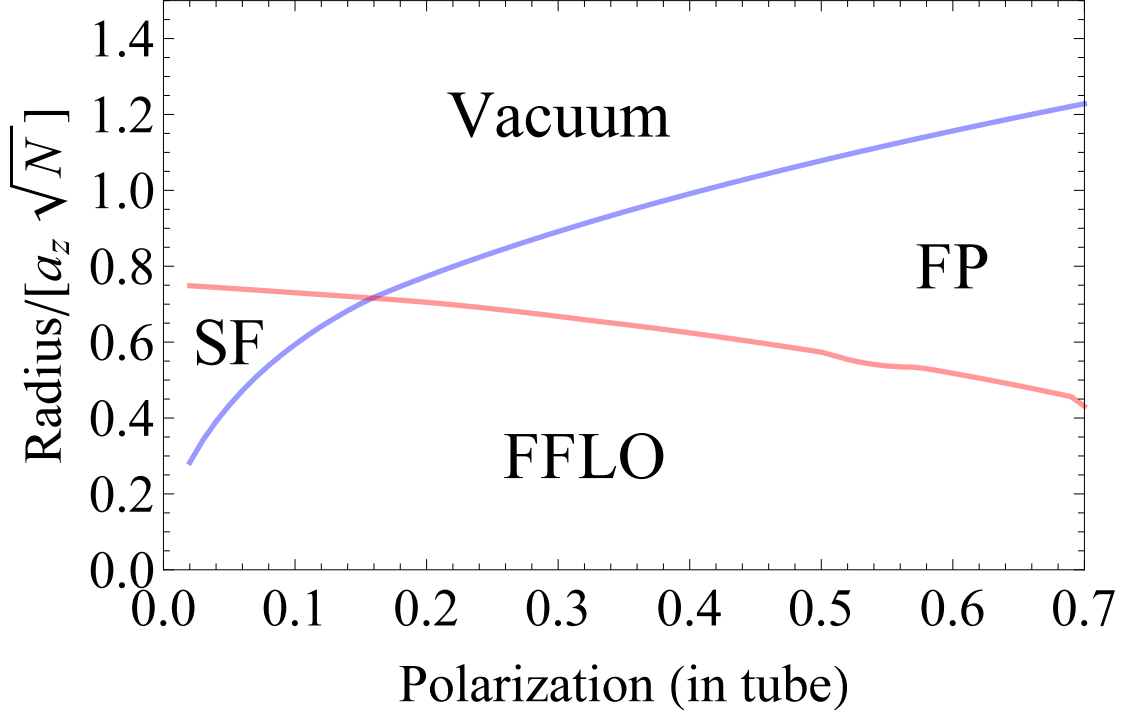
Figure 6.3: An in-trap version of the ($T = 0$) phase diagram Fig. 6.1, where we show the more easily experimentally accessible quantities of minority (red) and majority (blue) Thomas-Fermi radii for a harmonically trap gas (see [1, 22]). The radii are normalized by $a_z\sqrt{N}$, where a_z is the 1D harmonic oscillator length for the trapping potential. Note that the minority- and majority-radius cross around 15% polarization (when the edge of the cloud hits the multicritical point). When plotted in these variables, the phase diagram is not universal anymore in the sense that it still has a (weak) dependence on the ratio between Fermi energy and binding energy $\kappa = (\hbar\omega N/2)/\epsilon_B = N a_{1D}^2/a_z^2$ [1]. Here the plot is shown for typical parameters of the Rice experiments, $\kappa = N a_{1D}^2/a_z^2 \approx 0.26$ (where $N \approx 170$, $a_{1D} = 0.11\mu$m, $a_z = 2.83\mu$m).

into contact with a non-interacting gas, serving as a thermometer [23, 24, 25].

Since the 1D BEC-BCS crossover problem is exactly solvable, one has the unique

opportunity to study a both strongly correlated *and* exactly solvable problem

where one could in principle hope to do thermometry based on the exact equa-

tion of state at finite temperature. The thermodynamic Bethe ansatz (TBA) in-

troduced by Yang and Yang in Ref. [26], is a generalization of the approach of

Lieb-Liniger to finite temperature. In the BEC limit we therefore know that the

gas will described by Yang-Yang thermodynamics with Bethe ansatz equations $(k_B = 1)$ [26]

$$
\begin{aligned}
\epsilon(\lambda) &= \frac{\hbar^2 \lambda^2}{4m} - \mu_{boson} + \frac{2T}{\pi a_{1D}^{BB}} \int_{-\infty}^{\infty} d\lambda' \frac{c}{(2/a_{1D}^{BB})^2 + (\lambda - \lambda')^2} \log\left(1 + e^{-\epsilon(\lambda')/T}\right) \\
\rho(\lambda) &= \left(1 + e^{\epsilon(\lambda)/T}\right)^{-1} \left[\frac{1}{2\pi} + \frac{2/a_{1D}^{BB}}{\pi} \int_{-\infty}^{\infty} \frac{\rho(\lambda')d\lambda'}{(2/a_{1D}^{BB})^2 + (\lambda - \lambda')^2}\right] \\
N_{boson}/L &= \int_{-\infty}^{\infty} d\lambda \, \rho(\lambda), \quad \Omega/L = -T \int_{-\infty}^{\infty} \frac{dk}{2\pi} \log\left(1 + e^{-\epsilon(k)/T}\right)
\end{aligned}
\tag{6.24}
$$

The non-linear integral equation for $\epsilon(\lambda)$ may be solved by iteration (as suggested in the original paper, Ref. [26]). Once $\epsilon(\lambda)$ is known, we have to solve a linear integral equation analogous to the zero temperature Lieb-Liniger equations (6.8). An obvious question, having seen the solution for the zero temperature 1D BEC-BCS crossover, is whether we can generalize the solution of Fuchs *et. al* [6] to finite temperature, by employing the mapping Eq. (6.9). To our knowledge this question has not yet been discussed in the literature. In the BCS limit, the TBA solution was found by Takahashi [27]. While the 1D Bose gas is described by the fairly simple set of equations (6.24), Takahashi's solution for the Fermi gas is much more complicated (for the sake of completeness we quote his equations in the appendix). In fact, just numerically solving the infinite set of coupled TBA integral equations for fermions is quite challenging (see e.g. [28]). What we argue in Appendix 6.6 is that under the most relevant experimental circumstances, where one is interested in a range of temperatures that have $T \ll E_B$ and $na_{1D} \ll 1$, the infinite set of TBA equations can be truncated to reduce to the naive expectation where one can simply transform according to Eq. (6.9). This means the equation of state for the 1D BEC-BCS crossover at

finite temperature is described by the set of equations

$$
\begin{aligned}
\epsilon(k) &= 2\left[\frac{\hbar^2 k^2}{2m} - \mu - E_B/2\right] - \frac{T}{\pi}\int_{-\infty}^{\infty} dq \frac{n\gamma}{(n\gamma)^2 + (k-q)^2}\log\left(1 + e^{-\epsilon(q)/T}\right) \\
\sigma(k) &= \left(1 + e^{\epsilon(k)/T}\right)^{-1}\left[\frac{1}{\pi} + \frac{1}{\pi}\int_{-K}^{K} dq\,\frac{n\gamma\rho(q)}{(n\gamma)^2 + (k-q)^2}\right] \\
E_0/L &= 2\int_{-K}^{K} dk\,\frac{\hbar^2 k^2}{2m}\rho(k) - nE_B/2 \\
N/L &= 2\int_{-K}^{K} dk\,\rho(k).
\end{aligned}
\tag{6.25}
$$

This is the generalization of the zero temperature result of Refs. [5, 6] to finite temperature (with the caveat that these equations are valid as long as $T \ll \Delta_s = h_{c,1}$, where Δ_s is the gap to breaking a pair, i.e. the spin-gap).

Similarly, in the regime of validity of the 1D model Eq. (6.3), we can use a truncated set of Bethe ansatz equations, to obtain the equation of state at finite temperature for the imbalanced system (see Appendix 6.6 for details). In Ref. [22] we used the results from this TBA theory for the imbalanced gas to model the data from the Rice experiment.

6.4   Correlations of the paired state

6.4.1   Simple strong coupling theory

In this section we will give an intuitive explanation for the 1D FFLO phase by showing how to calculate correlation functions of the 1D Gaudin-Yang model close to the multicritical strong coupling point, where $n_\uparrow a_{1D}, (n_\downarrow - n_\uparrow)a_{1D} \ll 1$. Even though there is the exact Bethe ansatz solution for the Gaudin-Yang model, calculating correlation functions is extremely challenging. Apart from large

scale numerical simulations such as Quantum Monte-Carlo and DMRG, the asymptotics of correlation functions can often be extracted using bosonization methods, especially when combined with Bethe ansatz solutions [29, 21, 30]. The technique we are using is a variation of the Bose-Fermi Jordan-Wigner mapping for hardcore lattice bosons (see e.g. [31]). This mapping allows us to express correlation functions as Toeplitz determinants that can be efficiently evaluated numerically. The result from Orso's paper that at strong coupling in the 1D attractive Fermi gas the energy is that of two noninteracting Fermi gases suggests we can map the Gaudin-Yang model on two non-interacting Fermi gases. The trick is that while the pairs and fermions have no interaction energy, the wavefunction still picks up a phase shift of π whenever we exchange a pair and fermion (illustrated in Fig. 6.4). Basically nature still knows that we are exchanging two fermions (due to the truly one dimensional nature of the model), even though one is tightly bound into a molecule and naively shouldn't interact with the excess fermion. This is somewhat reminiscent to the topological Berry phase a particle picks up when a charged particle is transported around a magnetic flux, even though it there is apparently no interaction[32]. The three fermion problem has been extensively discussed by Mora *et al.* in Ref. [33, 34], where it was found that the scattering length in the antisymmetric pair-fermion scattering channel is infinite in the Bethe ansatz model (3.56) (which is equivalent to a phase shift of π). Our model for a strong coupling FFLO state is a gas of hardcore bosons and free fermions on a 1D lattice with the additional ingredient that exchanging a boson and a fermion gives a π phase shift. The way this is accomplished is by applying a Jordan-Wigner transformation to the bosons and include a π phase shift each time a boson and a fermion pass each other as
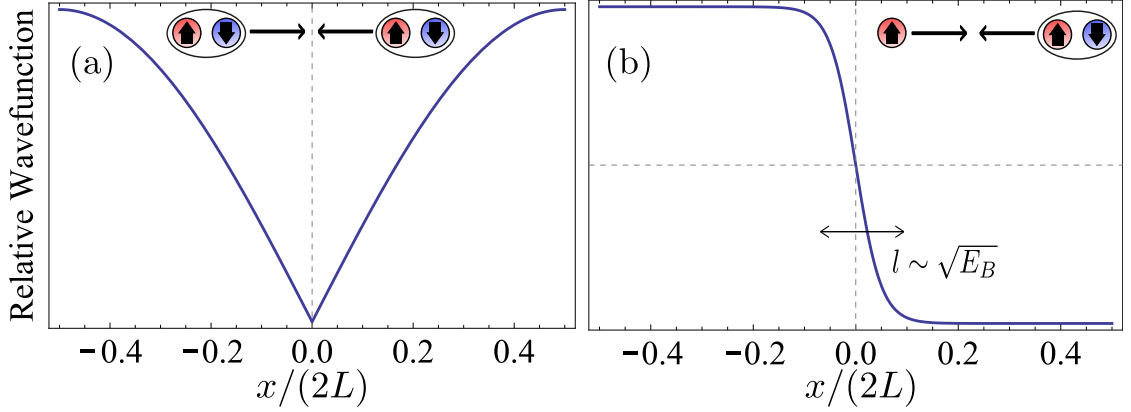
Figure 6.4: Strong coupling limit of Gaudin-Yang model: Here we sketch the relative wavefunction between pairs (bosons) (a) and a pair and excess fermion (b) in the strong coupling/low density limit as a function of the relative coordinate x in a fictitious box of length L with the boundary condition that the derivative vanishes at $x = \pm L/2$. The interaction between bosons becomes hardcore at low density. What is remarkable is that the pair-fermion interaction vanishes apart from a phase shift of π.

$$
\begin{aligned}
\bar{\psi}_B(i) &= (-1)^{N_B(i)}(-1)^{N_F(i)}\psi_B(i) = \exp(i\pi\left[N_B(i) + N_F(i)\right])\psi_B(i) \\
\bar{\psi}_F(i) &= (-1)^{N_B(i)}\psi_F(i) = \exp(i\pi N_B(i))\psi_F(i)
\end{aligned}
$$

where

$$
\begin{aligned}
N_B(j) &= \sum_{i<j}\psi_B^\dagger(i)\psi_B(i) = \sum_{i<j}\bar{\psi}_B^\dagger(i)\bar{\psi}_B(i) \\
N_F(j) &= \sum_{i<j}\psi_F^\dagger(i)\psi_F(i) = \sum_{i<j}\bar{\psi}_F^\dagger(i)\bar{\psi}_F(i)
\end{aligned}
$$

$N_B(j)(N_F(j))$ count the number of bosons (fermions) to the left of lattice site j. $\bar{\psi}_F(i), \bar{\psi}_B(i)$ are annihilation operators for two noninteracting lattice Fermi gases. It is easy to verify that these operators satisfy Fermi statistics provided $\psi_B(i)$ ($\psi_F(i)$) are boson (fermion) operators plus with a hardcore constraint for having two bosons on the same site. We are interested in the Bose correlation function

$$
\begin{aligned}
C(i,j) &= \langle\psi_B^\dagger(i)\psi_B(j)\rangle = \langle\bar{\psi}_B^\dagger(i)(-1)^{N_B(i)}(-1)^{N_B(j)}\bar{\psi}_B(j)\rangle\langle(-1)^{N_F(i)}(-1)^{N_F(j)}\rangle \\
&= C_B(i,j)C_F(i,j) \tag{6.26}
\end{aligned}
$$

131

with

$$C_B(i,j) = \langle \bar{\psi}_B^\dagger(i)(-1)^{N_B(i)}(-1)^{N_B(j)}\bar{\psi}_B(j)\rangle \qquad (6.27)$$

$$C_F(i,j) = \langle (-1)^{N_F(i)}(-1)^{N_F(j)}\rangle \qquad (6.28)$$

$C(i,j)$ simply factors into the correlation function of an unpolarized hard-core Bose gas $C_B(i,j)$ and a contribution that comes from the excess fermions ($C_F(i,j)$). There is a standard framework for calculating precisely correlation functions of this type in the free fermion representation using Toeplitz determinants. An advantage of this formalism is that it is straight forward to extend it to finite temperature and inhomogeneous systems [35]. For a homogenous system one finds that at large distances[3] $R \gg 1$

$$C_B(R) \sim \frac{1}{\sqrt{R}} \qquad (6.29)$$

$$C_F(R) \sim \frac{\cos(\pi n_f a R)}{\sqrt{R}} \qquad (6.30)$$

From the explicit numerical calculation of these function we have demonstrated this scaling in Fig. 6.5. In terms of the 1D BEC-BCS crossover one is in this case on the critical point between a finite momentum quasi condensate and or just a power law cusp at finite momentum in the pair momentum distribution (at this point the momentum distribution has a $\log$-divergence at finite momentum). We will now outline the calculation of the correlation function $C_F(R)$ following Ref. [31] (where the authors calculate $C_B(R)$). We have

$$
\begin{aligned}
C_F(R) &= \langle (-1)^{\sum_{j=i}^{j=i+R-1} \bar{\psi}_F^\dagger(j)\bar{\psi}_F(j)}\rangle \\
&= \langle \left(\bar{\psi}_F(i) - \bar{\psi}_F^\dagger(i)\right)\left(\bar{\psi}_F(i) + \bar{\psi}_F^\dagger(i)\right)\dots \\
&\quad \dots \left(\bar{\psi}_F(i+R-1) - \bar{\psi}_F^\dagger(i+R-1)\right)\left(\bar{\psi}_F(i+R-1) + \bar{\psi}_F^\dagger(i+R-1)\right)\rangle \\
&= \langle B_i A_i B_{i+1} A_{i+1} \dots B_{i+R-1} A_{i+R-1}\rangle
\end{aligned}
$$

---

[3]The result for $C_B(R)$ is well known [31]. For the result for $C_F(R)$ we do not have a proof, but we verified that it describes the leading asymptotics of numerical simulations.
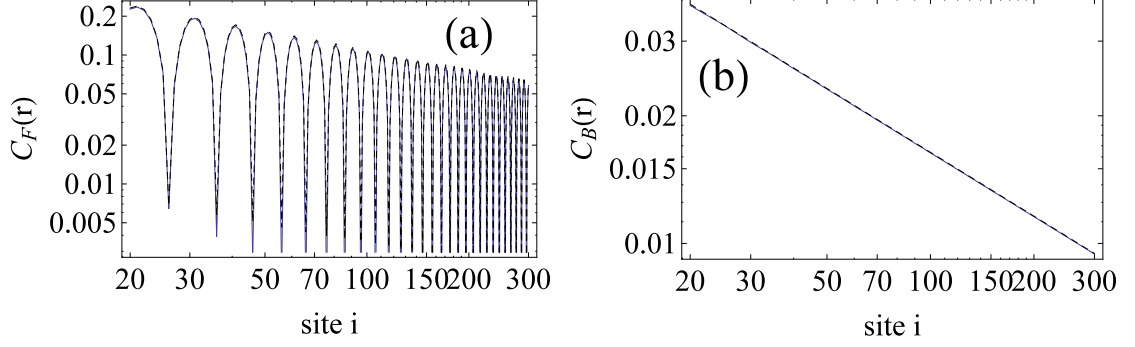
Figure 6.5: Long distance properties of $C_F(R)$ (shown in (a) for filling $\nu_F = \pi n_f a = 0.1$ and the hardcore Bose correlation function $C_B(R)$ for $\nu_B = 0.2$ (b), both shown as a function of lattice site index $i = R$ on a log-log plot(solid blue lines). The dashed lines are fits to the asymptotic expressions, Eqs. (6.29) for (a)[(6.30) for (b)].

where we used the relation $(-1)^{\bar{\psi}_F^\dagger(i)\bar{\psi}_F(i)} = \left(\bar{\psi}_F(i) - \bar{\psi}_F^\dagger(i)\right)\left(\bar{\psi}_F(i) + \bar{\psi}_F^\dagger(i)\right)$ and introduced

$$A_i = \bar{\psi}_F(i) + \bar{\psi}_F^\dagger(i)$$

$$B_i = \bar{\psi}_F(i) - \bar{\psi}_F^\dagger(i)$$

Contractions of these operators in the free Fermi sea give (see Ref. [31])

$$\langle A_i B_j \rangle = G(i-j)$$

$$\langle A_i A_j \rangle = \langle B_i B_j \rangle = 0$$

with the free fermion Green's function

$$G(l) = \frac{2}{\pi}\frac{\sin(\pi n_F a l)}{l} - \delta_{0,l}$$

Note that this function needs to be modified when considering a trapped system or finite temperature. We evaluate expectation value of the string of A_i, B_i

133

operators using Wick's theorem

$$C_F(R) = \begin{vmatrix} G_0 & G_1 & \dots & G_{R-2} \\ G_{-1} & G_0 & \dots & G_{R-3} \\ \vdots & \vdots & \ddots & \\ G_{2-R} & G_{3-R} & & G_0 \end{vmatrix}$$

This $(R-1) \times (R-1)$ determinant can be efficiently evaluated numerically to calculate this correlation function on a lattice. We can recover the continuum limit by taking the lattice spacing to zero. In time-of-flight experiments when atoms are suddenly released from a trap and interactions between pairs are suddenly switched off (e.g. by ramping to the BEC limit) one measures the pair momentum distribution

$$n_B(k) = \sum_k C(R) e^{-ikR} \tag{6.31}$$

We show sample results for the correlation functions $C(R)$ and the pair momentum distribution in Fig. 6.6. The peak at finite momentum in the pair momentum distribution of the FFLO phase in 1D is not a δ-function singularity as one would expect for true long range order, but a $\log$-singularity at strong coupling. Note that at any finite temperature this singularity gets smoothed out, therefore very low temperatures are needed for a signature to be visible in experiments.

6.4.2 Predictions from weak coupling bosonization

Bosonization theory is a non-perturbative method that enables us to calculate long distance properties of correlation functions in many one dimensional systems. For the imbalanced Fermi gas, the standard bosonization approach as described in [17, 36], applies when we are in the regime where $h \ll \epsilon_F$, i.e. we
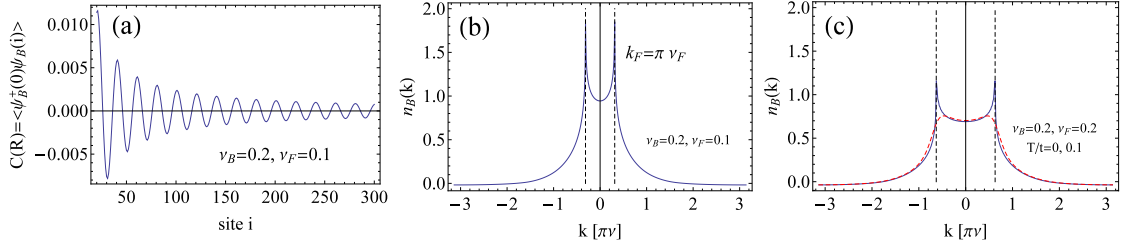
Figure 6.6: (a) Bose correlation function $C(R)$ calculated from the mapping on non-interacting fermions described in the text (here shown for fillings $\nu_B = 0.2$, $\nu_F = 0.1$). (b), (c): Fourier transforms of $C(R)$ (time-of-flight momentum distributions) for two different filling factors. The peaks at the FFLO pairing vector $k_F = \pi\nu_F$ have a $\log$-singularity (this is because we are in the strong coupling limit. For weaker interactions one would see a cusp singularity). In (c) the dashed curve shows the effect of finite temperature. Here $T/t = 0.1$, where t is the boson/fermion hopping (that we arbitrarily took to be the same).

can linearize around the Fermi surface and Fermi velocities satisfy $v_{F\uparrow} \approx v_{F\downarrow}$ (basically when we can neglect band curvature at low polarizations, or always when we are in the weak coupling limit). In this section we will not go into the details of bosonization, but mainly quote well-known results (for a detailed discussion of the bosonization method see e.g. [36]). Bosonization begins by expressing Fermi operators in terms of effective boson fields as (for two species of fermions labelled by the index σ)

$$\psi_\sigma(x) = \psi_{\sigma,-}(x)e^{-ik_f x} + \psi_{\sigma,+}(x)e^{ik_f x} \tag{6.32}$$

$$\psi_{\sigma,\tau}(x) = K_{\sigma,\tau}e^{-i\theta_\sigma(x)+i\tau\phi_\sigma(x)} \tag{6.33}$$

where one treats the different Fermi point (labelled $\pm$) as distinct fermions. The boson field $\phi_\sigma(x)$ simply is a counting operator that counts all particles of spin σ to the left of a location x and $\theta_\sigma(x)$ is something analogous to a superconducting phase. For the formalism on how this theory is quantized we refer the reader to the literature[?]. In this limit one has the so called spin-charge separation, where the system can be described by a theory of independent charge and spin

degrees of freedoms

$$H = H_c + H_s + H_z$$

$$H_c = \frac{\hbar v_c}{2\pi} \int dx \left[K_c \left(\frac{\partial \theta_c(x)}{\partial x} \right)^2 + \frac{1}{K_c} \left(\frac{\partial \phi_c(x)}{\partial x} \right)^2 \right]$$

$$H_s = \frac{\hbar v_s}{2\pi} \int dx \left[K_s \left(\frac{\partial \theta_s(x)}{\partial x} \right)^2 + \frac{1}{K_s} \left(\frac{\partial \phi_s(x)}{\partial x} \right)^2 \right] + V \cos(\sqrt{8}\phi_s(x))$$

$$H_z = (\mu_\uparrow - \mu_\downarrow) \sqrt{2} \int dx \partial_x \phi_s(x)$$

and the new (charge/spin) fields are related to the original ones by

$$\phi_{c,s} = \frac{1}{\sqrt{2}} (\phi_\uparrow(x) \pm \phi_\downarrow(x))$$

$$\theta_{c,s} = \frac{1}{\sqrt{2}} (\theta_\uparrow(x) \pm \theta_\downarrow(x))$$

We emphasize again that this spin-charge separation holds for the Gaudin-Yang model only at low polarization or weak interactions. There is a very involved general method based on a generalization of this weak coupling approach that allows for calculation of correlation functions beyond spin-charge separation [37, 30, 38]. While the charge Hamiltonian is already just a non-interacting phonon theory, the spin Hamiltonian has this cosine (called backscattering) term. This term gives rise to Cooper pairing for attractive interactions when $V \sim g < 0$ and is RG irrelevant for repulsive interactions (i.e. after renormalization of K_s, v_s it may be put to zero). In the repulsive case this will then give independent gapless spin/density sound modes. In the attractive case the term is RG relevant and grows under rescaling causing the spin sector to become gapped. This gap is the same spin-gap Δ_s we found from the Bethe ansatz solution. It simply means that breaking singlet pairs requires a finite energy cost. In this model the low energy spin excitations are solitions or π slips in the ϕ_s

field [17]. When the system becomes polarized at a Zeeman field $h > \Delta_s$, a finite density of solitions forms a lattice (i.e. our FFLO phase). Therefore we are interested in the superconducting correlation function

$$C_{SC}(x) = \langle \psi_{\uparrow+}^\dagger(x)\psi_{\downarrow-}^\dagger(x)\psi_{\downarrow-}(0)\psi_{\uparrow+}(0)\rangle$$

The operator $O(x) = \psi_{\uparrow+}^\dagger(x)\psi_{\downarrow-}^\dagger(x) \sim e^{i\sqrt{2}(\theta_c(x)-\phi_s(x))}$ creates a Cooper pair made out of a $\uparrow$-spin fermion from the right-mover Fermi point and a $\downarrow$-spin fermion from the left-mover Fermi point. In the unpolarized case $h < \Delta_s$, a consequence of the gapped spin sector is that the spin counting field is locked, $\phi_s(x) \equiv 0$. Again, without going into details, one finds

$$C_{SC}(x) \sim \frac{1}{x^{1/K_c}} \tag{6.34}$$

The $\sim$ means that bosonization tells us only long distance properties (i.e. we only get the leading order term for large x, without prefactor). The parameter K_c can be obtained for any point in the 1D BEC-BCS crossover from the Bethe ansatz (via the compressibility) and is calculated in Ref. [6]. When one is near the Tonks-Girardeau regime for the pairs, then $K_c \approx 2$

$$C_{SC}(x) \sim \frac{1}{\sqrt{|x|}} \tag{6.35}$$

in agreement with the Jordan-Wigner approach [31]. Now we focus on the FFLO phase $h > \Delta_s$. Following Ref. [17] we ungap the spin sector by introducing a harmonic Hamiltonian for the FFLO soliton lattice

$$\phi_s(x) = \pi n_{sol}x/\sqrt{2} + \phi_{sol}(x)/\sqrt{2}$$

with $n_{sol} = n_\uparrow - n_\downarrow$ is the density of excess (or unpaired) fermions. The soliton field is described by a free phonon Hamiltonian

$$H_{sol} = \frac{\hbar v_{sol}}{2\pi} \int dx \left[K_{sol} \left(\frac{\partial \theta_{sol}(x)}{\partial x}\right)^2 + \frac{1}{K_{sol}} \left(\frac{\partial \phi_{sol}(x)}{\partial x}\right)^2 \right]$$

One finds [17]

$$C_{SC}(x) \sim \frac{1}{x^{1/K_c + K_{sol}/2}} \cos(\pi n_{sol} x) \tag{6.36}$$

At low polarization one can assume the solitions as weakly interacting fermions with $K_{sol} = 1$. Then we see that this correlation function agrees with our Fermi mapping from the previous section in the strong coupling limit for $K_c = 2$, as expected. This correlation function translates into finite momentum peaks in the pair momentum distribution (at $T = 0$)

$$n_{pair}(q) = \int dx e^{iqx} C_{SC}(x) \sim \text{const.} \pm \text{const.} \times |q \pm \pi n_{sol}|^{1/K_c + K_{sol}/2 - 1} \tag{6.37}$$

The bosonization result is valid only in the vicinity around $q_{FFLO} = \pi n_{sol}$. For typical parameters of the Gaudin-Yang model, $1 < K_{sol} < 2$, $2 > K_c > 1$, this means one has a power law cusp (rather than a divergence) in the pair momentum distribution at q_{FFLO}. In principle there is a quantum phase transition to a state with a finite momentum quasi-condensate FFLO phase as one goes towards the BEC side (when $1/K_c + K_{sol}/2 < 1$), but it could be preempted by a transition to a Bose-Fermi mixture phase with no finite momentum peaks [39]. Experiments that want to detect these FFLO peaks, should probably try to go as far to the BEC side as possible to take advantage of the appearance of a quasi-condensate for $K_c > 2$. In the unpolarized case one has always a divergence (quasi condensate) in the zero T pair correlation function at zero momentum in the 1D BEC-BCS crossover. At any finite temperature these singularities in the momentum distribution, whether power law cusp or divergence, are smoothed out.

6.4.3 Strong coupling bosonization

Around the strong coupling point, one can use a slightly modified version of the previous bosonization theory. The system is described by independent sectors for the pairs and excess fermionic excitations. This is different from the previous weak coupling/low polarization approach where spin and charge were decoupled and it is more appropriate to cold atomic gases where one typically has tightly bound dimers. The Hamiltonians for pairs and excess fermions phonons are

$$H_B = \frac{\hbar v_B}{2\pi} \int dx \left[K_B \left(\frac{\partial \theta_B(x)}{\partial x} \right)^2 + \frac{1}{K_B} \left(\frac{\partial \phi_B(x)}{\partial x} \right)^2 \right] \tag{6.38}$$

$$H_F = \frac{\hbar v_F}{2\pi} \int dx \left[K_F \left(\frac{\partial \theta_F(x)}{\partial x} \right)^2 + \frac{1}{K_F} \left(\frac{\partial \phi_F(x)}{\partial x} \right)^2 \right] \tag{6.39}$$

In the strong coupling limit, $K_B = K_F = 1$ and v_B, v_F are set by the slope of the noninteracting dispersion relations at the Fermi level. The FFLO correlations come in when expressing the bare boson and fermion operators in terms of the phonon fields

$$\psi_B(x) \sim e^{-i\theta_B(x)} \cos(qx + \phi_F(x)) \tag{6.40}$$

$$\psi_F(x) \sim e^{-i\theta_F(x)} \left(K_+ e^{i[qx+\phi_F(x)+\pi n_B x+\phi_B(x)]} + K_- e^{-i[qx+\phi_F(x)+\pi n_B x+\phi_B(x)]} \right)$$

In this theory the correlation functions are

$$C_B(x) = \langle \psi_B^\dagger(x)\psi_B(0) \rangle \sim \frac{\cos(qx)}{x^{K_F/2+1/(2K_B)}} \tag{6.41}$$

$$C_E(x) = \langle \psi_F^\dagger(x)\psi_F(0) \rangle \sim \frac{\cos((q+\pi n_B)x)}{x^{(1/K_F+K_F)/2+K_B/2}} \tag{6.42}$$

Note that this agrees with results given in Ref. [38] for a charge mixing parameter $\xi = 1$. As they point out, the scaling of the excess fermion Green's function $C_E(x)$ comes out right only when spin charge mixing is included. In the vicin-

ity of the strong coupling point, spin and charge are mixed such that one has independent pair and fermion modes.

6.5 Experimental probes of the 1D imbalanced Fermi gas

In a collaboration with the experimental group of Randy Hulet at Rice University, we provided theoretical understanding for an experimental realization of the paired imbalanced Fermi gas in 1D. Beyond the possible realization of a 1D analogue of the FFLO state, this experiment also provides one of the first benchmarks for (analog) quantum simulation. Quantum simulation with ultracold gases is the idea to simulate a strongly correlated model Hamiltonian, such as the Fermi Hubbard model, and obtain information about its phase diagram using experiments with ultracold gases. This research project was funded by the DARPA Optical Lattice emulator program, where the first goal was to simulate a strongly correlated system where the theory is known. This allows to identify possible problems and tests the practicability of the approach. While we are able to demonstrate good agreement between predictions from the exact Bethe ansatz theory and experimental data, FFLO correlations of the partially polarized paired phase were not probed directly in the experiment.

6.5.1 Experimental setup

In the experiment of the Rice group, a 2D optical lattice is used to split a two-component Fermi gas of ^{6}Li atoms into an ensemble of 1D tubes (see Fig. 6.7). The original trap is a crossed beam trap consisting of two perpendicular red

(a) Crossed beam trap

(b)

Position (units of lattice spacing)
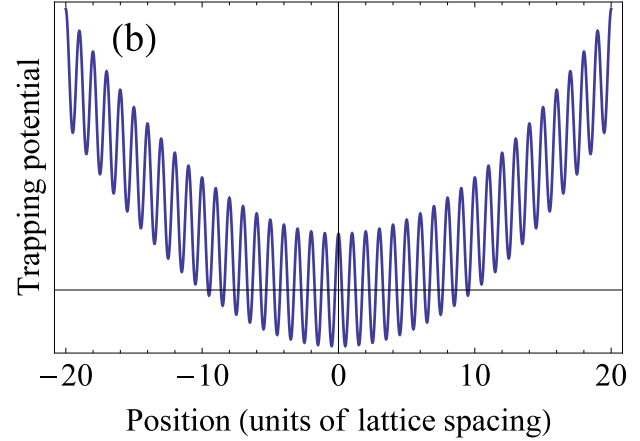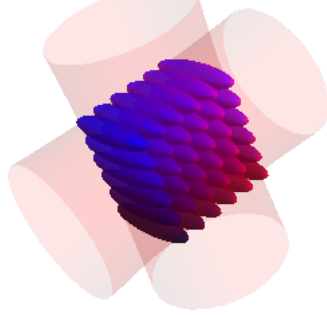
Figure 6.7: (a) Illustration of the crossed beam trap in the Rice experiment. It creates a harmonic potential plus a tight 2D lattice for the atomic cloud, confining the atoms to 1D tubes. (b) Perpendicular to the 1D tubes, the potential is a superposition between a harmonic trap and a lattice potential of the form $V_0 \sin^2(kz)$, where $k = 2\pi/\lambda$, $\lambda = 1064$ nm is the laser wavelength.

detuned Gaussian laser beams[4]. The AC stark shift of the laser beams creates a trapping potential $V(\mathbf{r})$ for the atoms that is proportional to laser intensity as [4]

$$V(\mathbf{r}) = \frac{3\pi c^2}{2\omega_0^3} \frac{\Gamma}{\Delta} I(\mathbf{r}) \tag{6.43}$$

where $I(\mathbf{r})$ is the laser intensity, Γ is the decay rate of the excited state, Δ the detuning and ω_0 is the transition frequency[5]. In the experiment, that we are concerned with, one uses a crossed beam trap made from elliptical beams. For a single beam one has an intensity profile of the form[6]

$$I(x, y, z) = \frac{2P}{\pi w_0 w_1} e^{-2\left(x^2/w_0^2 + y^2/w_1^2\right)} \tag{6.44}$$

In the crossed beam trap of the Rice experiment, each beam is retro-reflected (with polarization rotated by 90°), so the total power P for each direction is the

---

[4]Experimentalists give these beams slightly different wavelengths to avoid interference.

[5]In practice this formula would be too simple, as it was derived for a far detuned laser beam for a two-level atom. The fact that potential strength is proportional to laser beam intensity is also true for a real atom.

[6]For a crossed beam trap we can take the Rayleigh length to ∞.

141

sum of the retro-reflected and incident beam $P = P_i + P_r$ (no interference for orthogonal polarizations). The total intensity for the crossed beam trap is then

$$I_{tot}(x,y,z) = I_1(x,y,z) + I_2(x,y,z) = \frac{2P}{\pi w_0 w_1}e^{-2(x^2/w_0^2 + z^2/w_1^2)} + \frac{2P}{\pi w_0 w_1}e^{-2(y^2/w_0^2 + z^2/w_1^2)}$$

In a tightly bound trap we may expand the intensity around the center $x = 0$, $z = 0$. The intensity in the harmonic approximation is

$$I_{tot}(x,y,z) = \frac{2P}{\pi w_0 w_1}\left(2 - \frac{2x^2}{w_0^2} + \frac{2y^2}{w_0^2} + \frac{4z^2}{w_1^2}\right) \tag{6.45}$$

The trapping potential is then

$$V(\rho,z) = -V_{trap}\left(1 - \frac{\rho^2}{w_0^2} - \frac{2z^2}{w_1^2}\right) = -V_{trap} + \frac{1}{2}m\omega_\rho^2\rho^2 + \frac{1}{2}m\omega_z z^2 \tag{6.46}$$

with $\omega_\rho = \sqrt{\frac{2V_{trap}}{mw_0^2}}$ and $\omega_z = \sqrt{\frac{4V_{trap}}{mw_1^2}}$. If the beam would be circular $\omega_z = \sqrt{2}\omega_\rho$, but here $\omega_z = \omega_\rho\sqrt{2}w_0/w_1$. Using elliptical beams allows for a softer potential along the z-axis. In the Rice experiment $w_0 = 54\mu$m, $w_1 = 236\mu$m so

$$\text{Aspect ratio} = \frac{\omega_\rho}{\omega_z} = \frac{236}{54\sqrt{2}} = 3.1 \tag{6.47}$$

This is the aspect ratio of the 3D trap. Now we consider the optical lattice case. The lattice is turned on by tilting the polarization and interfering the incident and retro-reflected beam. For a each beam one has an E-field of

$$E(x,y,z) = e^{-x^2/w_0^2 - y^2/w_1^2}\left(E_i e^{ikz} + E_r e^{-ikz}\right) \tag{6.48}$$

$$= e^{-x^2/w_0^2 - y^2/w_1^2}\left((E_i - E_r)e^{ikz} + 2E_r\cos(kz)\right) \tag{6.49}$$

where $k = 2\pi/\lambda$ is the wavevector of the laser beam. The intensity is proportional to

$$I(x,y,z) \propto |E|^2 = \frac{1}{2}e^{-2x^2/w_0^2 - 2y^2/w_1^2}\left(E_i^2 + E_r^2 + 2E_i E_r\cos(2kz)\right) \tag{6.50}$$

For a red detuned beam, lattice sites are intensity maxima, so for positions that are lattice sites $z = 0, \pm\pi, \pm 2\pi, \ldots$

$$I(x,y,z) \propto e^{-2x^2/w_0^2 - 2y^2/w_1^2}\left(E_i + E_r\right)^2 \tag{6.51}$$

142

When we define the difference in power between retro reflected and incoming beam as a $A = P_r/P_i$, we may write the total intensity (on lattice sites) as

$$I_{tot}(x,y,z) = \frac{2P}{\pi w_0 w_1}\left(2 - \frac{2x^2}{w_0^2} + \frac{2y^2}{w_0^2} + \frac{4z^2}{w_1^2}\right) \tag{6.52}$$

but now in the lattice $P_L = P_i(1 + \sqrt{A})^2$ (without lattice we had $P = P_i + P_r = P_i(1 + A)$). The ratio of trapping potentials is then (assuming laser power stays constant and only polarizations of the retro-reflected beam is rotated by $90°$)

$$\delta^2 = \frac{V_{trap,L}}{V_{trap,3D}} = \frac{(1+\sqrt{A})^2}{(1+A)} \approx 2. \tag{6.53}$$

The numerical value is for an assumed $A = 0.6$. Then $\delta = \sqrt{2} \approx 1.4$, so the trapping frequencies rescale as $\omega_{\rho,z}^{3D} \rightarrow \omega_{\rho,z}^{1D} = \delta \times \omega_{\rho,z}^{3D} = \sqrt{2}\omega_{\rho,z}^{3D}$. Note that the aspect ratio is unchanged. We finally note that the (small oscillation) frequency of each lattice well is obtained from a Taylor expansion of Eq. (6.50) around the site at $z = 0$

$$I_{tot}(z) = \frac{2P_L}{\pi w_0 w_1}\left(1 - \frac{(2kz)^2}{2}\right) \tag{6.54}$$

The ratio between the small oscillation frequency $\omega_\perp$ and the trapping frequency ω_ρ is then

$$\frac{\omega_\perp}{\omega_\rho} = \sqrt{\frac{4\sqrt{A}}{(1+A)}}(kw_0). \tag{6.55}$$

In practice these frequencies are not calculated from the beam parameters, but directly measured. When the potential is modulated at twice the trap frequency atoms can be resonantly excited to higher harmonic oscillator states. Experimentalists then observe a loss feature when monitoring the density as a function of modulation frequency. For the Rice experiments of Ref. [22], we had

$$\omega_z \approx (2\pi)200 \text{ Hz}; \quad \omega_\perp \approx (2\pi)200 \text{ kHz} \tag{6.56}$$

What do experiments measure?

In the Rice experiments, the main probe are in-situ images that provide a direct measure of the column density. By appropriate detunings it is possible to image each spin component individually. So the measured quantity is

$$n_c^\sigma(x, z) = \int_{-\infty}^{\infty} dy \; n_{3D}^\sigma(x, y, z) \tag{6.57}$$

where $\sigma = \uparrow, \downarrow$. From now on we label the coordinates along the laser beams of the crossed-beam trap x, y and along the tubes z. Note that because of an axially symmetric trapping potential, the density $n_\sigma(x, y, z)$ is really only a function of the radial coordinate $\rho = \sqrt{x^2 + y^2}$. These images were taken perpendicular to the array of tubes (the long axis on the image is along the tubes). Sample column density images are shown in Fig. 6.9. Note that the current experimental resolution is nowhere close to resolving individual tubes.

6.5.2   Theory model

Interaction parameters for ^{6}Li

The Rice experiments were performed with a two species ^{6}Li gas close to the broad Feshbach resonance at 890 Gauss, with a small oscillation frequency $\omega_\perp = 200(2\pi)$ kHz in the 2D optical lattice (this corresponds to a lattice of strength $V_0 \approx [(\hbar\omega_\perp)/(2E_R)]^2 \approx 12E_R$). When we use Olshanii's formula for the 1D scattering length a_{1D} in terms of the 3D scattering length a_s, we find

$$a_{1D} = a_\perp \left(1 - A a_s/a_\perp\right)/(a_s/a_\perp) \approx 1.1\mu\mathrm{m} \tag{6.58}$$

with $a_s(B = 890G) = -9145$ Bohr and $a_\perp \approx 0.09\mu$m. While this is well on the BCS side of the confinement induced resonance (see Fig. 6.8), it still is in the strong coupling regime. This can be seen from

$$na_{1D} \sim 2k^0_{F\downarrow}a_{1D}/\pi = \sqrt{2/\pi}\sqrt{E^0_{F\downarrow}/\epsilon_B} = \sqrt{2/\pi}\sqrt{\hbar\omega_z N_\downarrow/\epsilon_B} \approx 0.23 < 1 \quad (6.59)$$

where $E^0_F \approx 1.5\mu$K (we used the noninteracting gas formula to estimate Fermi energy and central density and took $N_\downarrow = 150$). The (actual) binding energy at this field can be calculated using Olshanii's Eq. (6.14), to give about

$$E_B \approx 4.8\mu K \quad (6.60)$$

These numbers put the system well into the 1D regime since

$$E^0_F \ll \hbar\omega_\perp = 10\mu K \quad (6.61)$$

Furthermore temperature estimates from the Bethe ansatz show that

$$T \ll E^0_F \ll \hbar\omega_\perp \quad (6.62)$$

i.e. that we can assume that no transverse modes are occupied by thermal excitations and the gas is quantum degenerate.

Local density approximation

Using the Bethe ansatz equation of state as input, we would like to calculate density profiles for parameters of the Rice experiment. When the lattice potential is sufficiently deep one may consider each well as an independent one dimensional system with particle numbers N_σ and longitudinal trapping frequency ω_z. When constructing a model for the ensemble, one could hope that
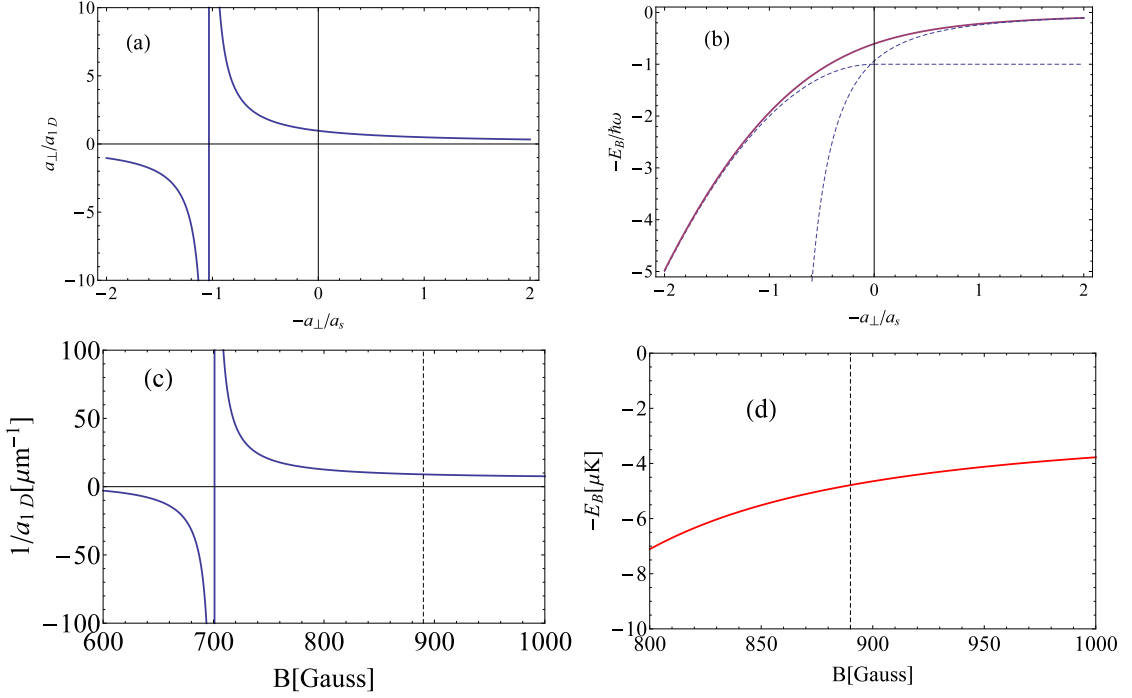
Figure 6.8: (a),(b): Scattering length and binding energy for atoms confined to 1D as a function of the ratio between s-wave scattering length a_s and harmonic oscillator length $a_\perp$ of the transverse confinement (from Ref. [11, 13]). In (b) the dashed lines show how the binding energy approaches the value of the binding energy of a 1D contact interaction in the BCS limit [with scattering length from (a)] and how E_B approaches the molecular limit $\hbar^2/(ma^2) - \hbar\omega_\perp$. (c), (d) show results for the specific parameters of the two lowest hyperfine states of ^{6}-Li and the lattice of the Rice experiment ($V_0/E_R = 12$). The experiment of Ref. [22] was performed at 890 Gauss (indicated by the dashed vertical line) near the Feshbach resonance at 835 Gauss, which is is well on the BCS side of the 1D confinement induced resonance.

the bundle of tubes is in thermal and chemical equilibrium, i.e. that a local density approximation holds also between tubes and the local chemical potential is just given by

$$\mu_{i,j}^\sigma(z) = \mu_{center}^\sigma - \frac{1}{2}m\omega_\rho^2 l^2(i^2 + j^2) - \frac{1}{2}m\omega_z^2 z^2 \tag{6.63}$$

where i, j label lattice sites. Erich Mueller showed that the integrated axial profiles $n_a^\sigma(z) = \int dx\, n_c^\sigma(x, z)$ across the bundle of tubes is simply proportional to

146
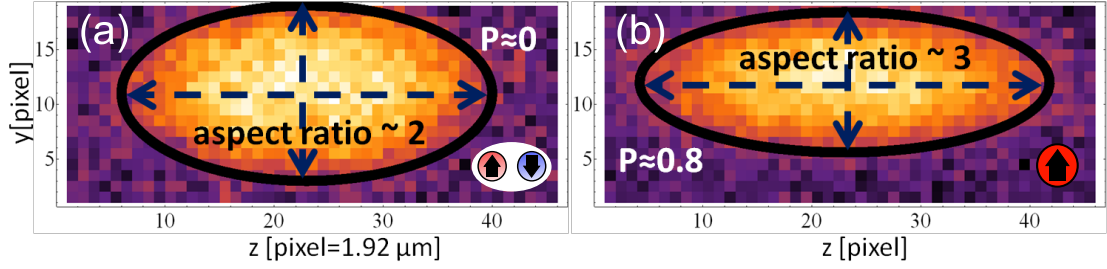
Figure 6.9: (a), (b) show experimental column densities from the Rice group. (a) shows an unpolarized data set, where all atoms are expected to be paired. The observed aspect ratio of ~ 2 is different from the Thomas-Fermi expectation of 3. We attribute this difference to a radial density distribution that froze in at some point while the atoms were loaded into the 2D lattice. (b) shows a column density of spin-up atoms at high polarization $P \approx 0.8$. The unbound free atoms have a higher tunneling rate than the pairs and appear to equilibrate on experimental time scales.

pressure (or grand potential) P of the central tube[7]. The only input parameter for a theory would then be the particle numbers $N_{tot,\uparrow}$, $N_{tot,\downarrow}$ of the entire ensemble (and trapping frequencies and lattice spacing). However, when the experiment was performed, it became clear that in a deep lattice pairs do not equilibrate and this local density approximation is too simplistic. The effect is illustrated in Fig. 6.9, where it is clear that the aspect ratio of the fully paired strongly deviates from the equilibrium value of 3, whereas unpaired fermions (with a much faster hopping rate) display an aspect ratio very close to the equilibrium expectation. To still be able to theoretically model the experimental density profile, we have to obtain knowledge of the particle number of each tube as a function of radius, $N_\sigma(\rho)$, where $\rho = \sqrt{x^2 + y^2}$. Fortunately, reconstructing $N_\sigma(\rho)$ from axially symmetric column density profile is a well-known problem in the field of image reconstruction. When we integrate the column density

---

[7]This result only holds for harmonic traps.

along z, we obtain the radial profile

$$n_r^\sigma(x) = \int dz dy\; n_{3D}^\sigma(x, y, z) = \frac{1}{l^2} \int dy\; N_\sigma(\sqrt{x^2 + y^2}) \qquad (6.64)$$

where $l = \lambda/2$ is the lattice spacing of the 2D optical lattice potential and we used $N_\sigma(\rho) = l^2 \int dz\; n_{3D}^\sigma(\rho = \sqrt{x^2 + y^2}, z)$. The integration (6.65) is known in mathematics as the Abel transform. Because this Abel transform has an inverse, we can reconstruct the function $N(\rho)$ from the radial profile n_r^σ. According to wikipedia a pair of Abel transforms is given by

$$F(y) = 2 \int_y^\infty \frac{f(\rho)\rho}{\sqrt{\rho^2 - y^2}} \quad \left[= \int_{-\infty}^\infty dx f(\sqrt{x^2 + y^2}) \right] \qquad (6.65)$$

$$f(\rho) = \frac{1}{\pi} \int_\rho^\infty \frac{dF}{dy} \frac{dy}{\sqrt{y^2 - \rho^2}} \qquad (6.66)$$

For discrete, noisy input data $F(y)$, it is a non-trivial problem to find the optimal inverse Abel transform $f(\rho)$, because Eq. (6.66) contains a numerical derivative. In practice we fit input data (radial densities) using a simple ansatz for $F_T(\rho)$, such as

$$F_T(\rho) = A(1 - \rho^2/B^2)^\nu \qquad (6.67)$$

with the inverse Abel transform

$$f_T(y) = \frac{A}{B} \frac{\nu \Gamma(\nu)}{\Gamma(\nu + 1/2)} \left[1 - \left(\frac{\rho}{B} \right)^2 \right]^{\nu - 1/2} \qquad (6.68)$$

where $\Gamma(\nu)$ is the usual Gamma function. ν could be fixed to a value that provides a reasonable description of the density profile and one of the two parameters A, B can be fixed by matching the total density, while the other is a fit parameter. The ansatz Eq. (6.67) is sensible because it can describe a $T = 0$ non-interacting or unitary Fermi gas Thomas-Fermi profile in either 1D or 3D. If ν is allowed to vary, we can also obtain a Gaussian or Maxwell-Boltzmann

distribution, by sending $B, \nu \to \infty$ while keeping B^2/ν constant. In Fig. 6.10, we illustrate this approach for a typical fully paired data set.

Once $N_\sigma(\rho)$ is known one can use the Thomas-Fermi approximation and Bethe ansatz equation of state $n_\sigma(\mu_\uparrow, \mu_\downarrow)$ in each tube, with tube central chemical potentials $\mu_{center}^\sigma(\rho)$ chosen such that

$$N_\sigma(\rho) = \int_{-\infty}^{\infty} dz \; n_\sigma \left[\mu^\uparrow(\rho, z), \mu^\downarrow(\rho, z) \right], \tag{6.69}$$

with

$$\mu^\sigma(\rho, z) = \mu_{center}^\sigma(\rho) - \frac{1}{2} m \omega_z^2 z^2. \tag{6.70}$$

The 3D density at location ρ, z is then given by

$$n_{3D}^\sigma(\rho, z) = \frac{1}{l^2} n_\sigma \left[\mu^\uparrow(\rho, z), \mu^\downarrow(\rho, z) \right] \tag{6.71}$$

From this 3D density we can calculate column- and axial-density profiles that can be compared with experiments.

Extracting Thomas-Fermi radii from experimental data

We also extracted the axial Thomas-Fermi radii $R_\uparrow$, $R_\downarrow$ from the experimental column densities. These radii can be compared to results from the exact solution because we have access to the central tube particle number $N(\rho = 0) = N_\uparrow(0) + N_\downarrow(0)$ and polarization $P(\rho = 0) = [N_\uparrow(0) - N_\downarrow(0)]/[N_\uparrow(0) + N_\downarrow(0)]$ from the inverse Abel transform. Then we can in principle plot the data in the variables of Fig. 6.3. While a simple estimation of these radii works well enough to obtain rough agreement between $T = 0$ theory and the Rice experiments, the extraction of Thomas-Fermi radii from noisy finite temperature data is very subtle. At finite temperatures all phase boundaries smooth out in 1D, there is no
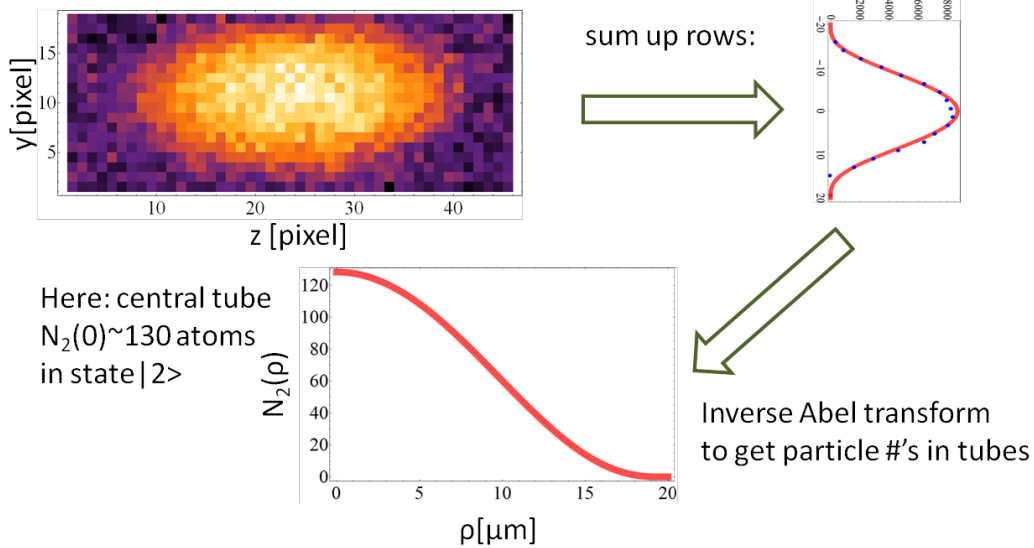
Figure 6.10: Here we illustrate how we can still extract the distribution of particle numbers from column density profiles using the an inverse Abel transformation. We sum up the rows of the density profiles to obtain the axial profile. This axial profile is then modeled using a simple functional form and inverse Abel transformed to in order to obtain $N_2(\rho) \equiv N_\downarrow(\rho)$

thermodynamic singularity (such as a jump in the density, as for the 3D imbalanced Fermi gas) and the concept of a Thomas-Fermi radius is strictly speaking only well defined at zero temperature. For example identifying the multicritical point where the profile changes from FFLO $\rightarrow$ fully paired to FFLO $\rightarrow$ fully polarized becomes ambiguous (see e.g. Fig. 6.2). Additionally, the large noise level in experimental data looks similar to effects of finite temperature. In any consistent consistent comparison between theory and experiment, one has to compare the exact same observables if we expect to obtain quantitative agreement. When analyzing the data of the Rice experiment we played with three different approaches to measure the Thomas-Fermi radii

- Fit a reasonable functional form to data and theory, then locate boundary

- Introduce a cutoff slightly above noise level and estimate where the data crosses a threshold

- Measure the radii by visual inspection

The method that gave the least fluctuations in the radii for a large number of data sets at different polarizations, was to measure the radii by hand from looking at the column density profiles (in random order to avoid bias). This simple approach gave the best results because mechanized approaches based on non-linear fits that tend to show poor convergence for high noise level. We attempted to estimate the Thomas-Fermi radii by fitting the entire column density profile for majority/minority to an inverted parabola and extrapolating this fit to the boundary. The problem with this approach is that it is very sensitive to the choice of the functional form of the fit function and also it converged well only for a fraction of data sets. The third method that we attempted was to define the Thomas-Fermi radii as the point where majority/minority density crosses a low threshold (of order noise level) . This method gave results similar to the manual extraction of radii (though one could think of this method as inconsistent as one does not actually probe the edge of the atomic cloud anymore). We compared the experimentally extracted radii to radii extracted from an ensemble of theory density profiles with same nominal parameters[8]. After modeling these effects of finite temperature and experimental noise, we found excellent agreement between the TBA predictions and the experimental data, as can be seen in Fig. 6.11.

---

[8]To be able to directly compare theory and experiment, we added random noise with the same statistics as the noise from the experimental shot to the theory column density before we extracted radii.
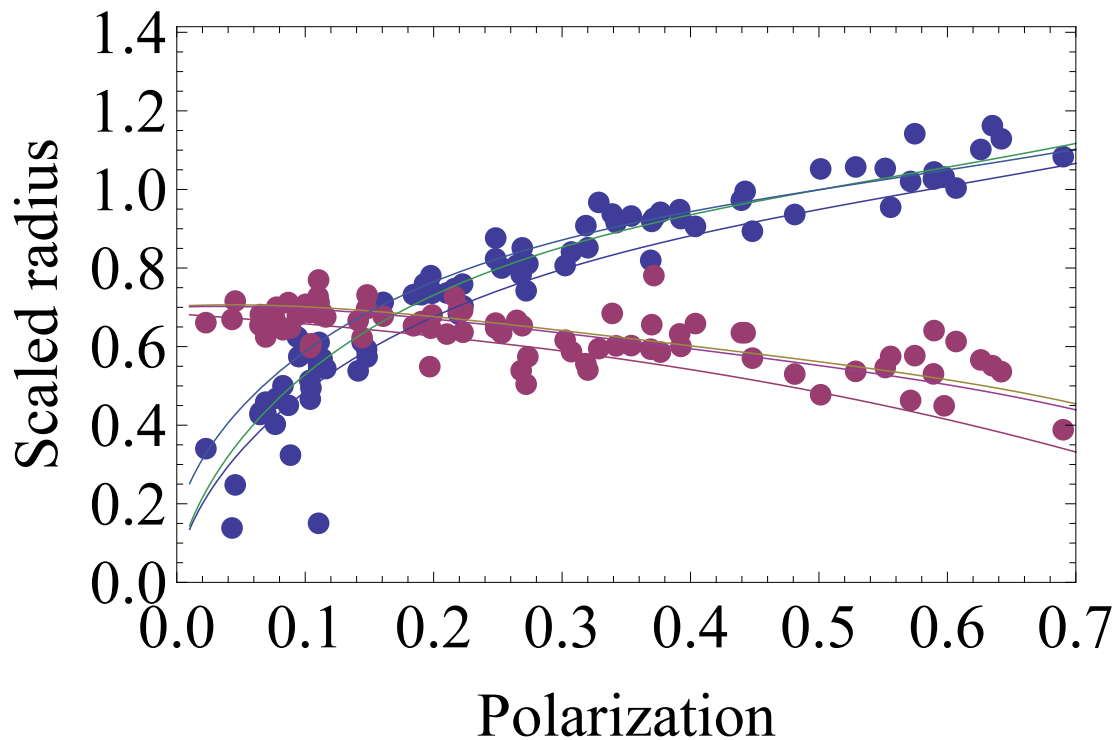
Figure 6.11: Thomas-Fermi radii of the central tube, extracted from an ensemble of experimental data sets for the 1D attractive imbalanced Fermi gas (dots). Each radius is scaled by the factor $a_z \sqrt{N}$ and the polarization refers to the central tube (N, P are found via an inverse Abel transform). The solid lines are theory curves corresponding to $T = 0, 175, 200$nK (where the $T = 175$nK curve was the best fit obtained through interpolation). The theory radii were obtained from column density profiles with the same extraction method as the experimental ones.

6.6   Appendix A: Truncation of TBA equations

Here we briefly discuss how one can truncate the infinite set of TBA equations for the Gaudin-Yang model in the limit where $T/\epsilon_B \ll 1$. Takahashi originally derived the TBA equations for the Gaudin-Yang model [27] in 1971. They consist of an infinite set of non-linear integral equations for a set of functions

(quoted from Takahashi's book Ref. [18])

$$\epsilon = 2(k^2 - c'^2 - \mu) + Ta_2 * \log(1 + e^{-\epsilon/T}) + Ta_1 * \log(1 + e^{-\kappa/T})$$

$$\kappa = k^2 - \mu - h + Ta_1 * \log(1 + e^{-\epsilon/T}) - T\sum_{n=1}^{\infty} a_n * \log(1 + e^{-\epsilon_n/T})$$

$$\epsilon_n = 2nh + Ta_n * \log(1 + e^{-\kappa/T}) + T\sum_{m=1}^{\infty} T_{nm} * \log(1 + e^{-\epsilon_m/T}) \qquad (6.72)$$

where $n = 1, 2, 3, \ldots$ and

$$a_n(k) = \frac{n|c'|}{(n|c'|)^2 + k^2} \quad a_0(k) = \delta(k)$$

$$T_{nm}(k) = \begin{cases} a_{|n-m|}(k) + 2a_{|n-m|+2} + 2a_{|n-m|+4}(k) + \ldots + 2a_{n+m-2}(k) + a_{n+m}(k) \\ \qquad\qquad\qquad \text{for } n \neq m \\ 2a_2(k) + 2a_4(k) + \ldots + 2a_{2n-2}(k) + a_{2n}(k) \\ \qquad\qquad\qquad \text{for } n = m \end{cases}$$

.

Here $*$ stands for the convolution $g*f = \int_{-\infty}^{\infty} dx' g(x - x') f(x')$. Once the "dressed energies" $\epsilon(k)$, $\kappa(k)$ and $\epsilon_n(k)$ are known, one has a set of linear integral equations similar to the zero temperature Bethe ansatz equations

$$\frac{1}{\pi} = \sigma'\left(1 + e^{-\epsilon/T}\right) + a_2 * \sigma' + a_1 * \rho \qquad (6.73)$$

$$\frac{1}{2\pi} = \rho\left(1 + e^{-\kappa/T}\right) + a_1 * \sigma' + \sum_{n=1}^{\infty} a_n * \sigma_n \qquad (6.74)$$

$$a_n * \rho = \left(1 + e^{-\epsilon_n/T}\right) + \sum_{m=1}^{\infty} T_{nm} * \sigma \qquad (6.75)$$

The bulk thermodynamic quantities are given by

$$p = -\frac{\Omega}{L} = T\int \frac{dk}{\pi} \log(1 + e^{-\epsilon(k)/T}) + T\int \frac{dk}{2\pi} \log(1 + e^{-\kappa(k)/T}) \quad (6.76)$$

$$N/L = (N_\uparrow + N_\downarrow)/L = \int [\rho(k) + 2\sigma'(k)] \qquad (6.77)$$

$$N_\downarrow/L = \int \left[\sigma'(k) + \sum_{n=1}^{\infty} n\sigma_n(k)\right] dk \qquad (6.78)$$

153

Takahashi derived these equations for the Hamiltonian

$$H' = -\sum_{i,\sigma} \frac{\partial^2}{\partial x_{i\sigma}^2} + 4c' \sum_{i,j} \delta(x_{i\uparrow} - x_{j\downarrow}) \tag{6.79}$$

For reference we note that H' maps onto the Hamiltonian Eq. (6.3) under the rescaling of units

$$c' = -\frac{\hbar}{\sqrt{2m}a_{1D}} \quad x_{i\sigma} = \sqrt{\frac{2m}{\hbar^2}} z_{i\sigma} \tag{6.80}$$

and momenta rescale with a factor of $\sqrt{\hbar^2/(2m)}$.

Directly solving the infinite set of non-linear integral equations is essentially a hopeless task. This is because of the contributions of the string solutions (giving rise to the equations for the ϵ_n), which were absent in the bosonic case [18]. These string solutions come from the presence of broken pairs at finite T. In order to understand when we can truncate the infinite set of integral equations, we first consider the unpolarized case $h = 0$. Intuitively we expect that whenever $T \ll \Delta_s$, pairs cannot be broken, therefore all spin excitations must be exponentially suppressed. At very low temperatures, we note that because of the inequality $\epsilon_n(k) > 0$, as $T \to 0$ one is left with just two equations [18]

$$\epsilon(k) = 2(k^2 - c'^2 - \mu) - \int_{-K}^{K} dk' a_2(k - k')\epsilon(k) - \int_{-Q}^{Q} dk' a_1(k - k')\kappa(k)$$

$$\kappa(k) = k^2 - h - \mu - \int_{-K}^{K} dk' a_1(k - k')\epsilon(k) \tag{6.81}$$

Where K, Q have to found self-consistently such that $\epsilon(K) = 0$, $\kappa(Q) = 0$. At $T = 0$ and for $h < h_{c1} = \Delta_s$, it turns out that the minimum of $\kappa(k)$ (at $k = 0$) is simply the spin gap Δ_s. Solving these equations is also a convenient method to calculate the phase boundaries of the $T = 0$ phase diagram in 6.1. Because of this gap it is valid to neglect the term involving $\kappa(k)$ in the limit of small $h, T \ll \Delta_s$ in the equation for $\epsilon(k)$ in the set of Eqs. (6.72). On the other hand,

when the gas becomes polarized, one has $h \gtrsim \Delta_s$ and we see that the ϵ_n satisfy

$$\epsilon_n > 2hn \gtrsim 2\Delta_s n \gg T \tag{6.82}$$

In this case, it is clear that contributions of the ϵ_n are negligible (because they are of order $e^{-\Delta_s/T}$ or smaller) in the equations for $\kappa(k)$, and we conclude that for low temperatures $T \ll \Delta_s$ it is valid to use the truncated set of TBA equations

$$
\begin{aligned}
\epsilon(k) &= 2(k^2 - c'^2 - \mu) + \int dk' a_2(k - k') \log(1 + e^{-\epsilon(k')/T}) \\
&+ \int dk' a_1(k - k') \log(1 + e^{-\kappa(k')/T}) \\
\kappa(k) &= k^2 - h + \mu - \int dk' a_1(k - k') \log(1 + e^{-\epsilon(k')/T}) \tag{6.83}
\end{aligned}
$$

and

$$
\begin{aligned}
\frac{1}{\pi} &= \sigma' \left(1 + e^{-\epsilon/T}\right) + a_2 * \sigma' + a_1 * \rho \\
\frac{1}{2\pi} &= \rho \left(1 + e^{-\kappa/T}\right) + a_1 * \sigma' \tag{6.84}
\end{aligned}
$$

In the experiments we were interested in, the binding energy of the pairs was always by far the largest energy scale (while at the same time $T \ll \epsilon_F$). In this relative strong coupling and low temperature regime, the truncation to two coupled integral equations is essentially exact. We note that a similar and even simpler approximation scheme (that however only works in the regime of strong coupling) was put forward in Ref. [40]. Numerically solving these coupled integral equations is still not entirely trivial, because the functions live on an infinite domain and a sharp feature occurring at the "Fermi" moment of the dressed energies. When solving these equations numerically, we first mapped the infinite domain $(-\infty, \infty)$ on the open interval $(-1, 1)$ using the substitution function

$$g(u) = \frac{u}{1 - u^2} \tag{6.85}$$
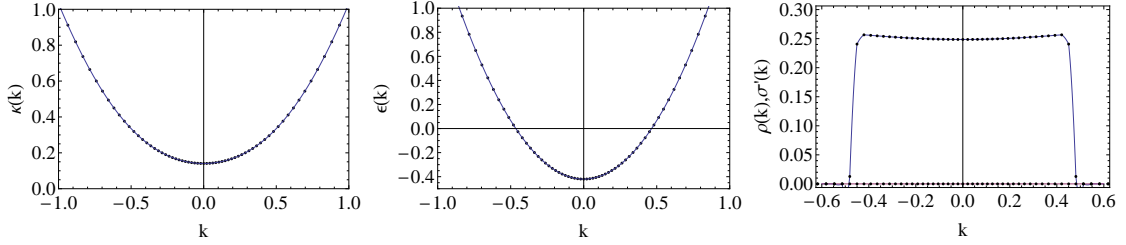
Figure 6.12: Sample dressed energies $\epsilon(k)$, $\kappa(k)$ at $T = 0.01$ ($c' = -0.5$) and $\mu = h = 0$ (for these parameters, the gas is practically unpolarized, so $\rho(k) \approx 0$). The gap in $\kappa(k)$ is basically equal to the spin gap Δ_s.

Then we discretized the domain $(-1, 1)$ using a Gauss-Legendre grid (see e.g. [41] for a description of this method). The non-linear integral equations (6.83) are then solved using iteration with initial $\epsilon_0(k) = 2(k^2 - c'^2 - \mu)$ and $\kappa_0(k) = k^2 - \mu - h$. In practice we found this procedure to be very stable. Then the linear integral equations (6.84) become a matrix equation that is straightforward to solve numerically. We then tabulated at fixed temperature T the densities $n_\sigma(\mu, h)$ as a function of μ, h over a large range of relevant parameters. At not too low temperature, the singularity at the Fermi edge is smeared over a range of momenta on the order of T and usually ramping up the grid size worked well to go to reasonably low temperatures[9]. For example we used $N = 151$ grid points, over a range of temperature of $T = 0.005, \ldots, 0.03$ (in units where $c' = -0.5$). For the lowest temperatures, artifacts (ripples in the density as a function of μ) appeared at high density[10]. We show sample dressed energies and distribution functions σ', ρ in Fig. 6.12.

---

[9]We also used a method were we first used a small grid to approximately bracket the location of the singularity and then in a second step used an adaptive grid with a customized substitution function to better resolve the Fermi edge at low temperatures. Such a method worked very well in the unpolarized case. It is however difficult to implement in the polarized case where one has to deal with two singularities and two different discretizations.

[10]This is not really a problem in practice because there the zero temperature equation of state is already valid

156

BIBLIOGRAPHY FOR CHAPTER 6

[1] G. Orso, Phys. Rev. Lett. **98**, 070402 (2007).

[2] Hui Hu, Xia-Ji Liu, and Peter D. Drummond, Phys. Rev. Lett. **98**, 070403 (2007).

[3] Meera M. Parish, Stefan K. Baur, Erich J. Mueller, and David A. Huse, Phys. Rev. Lett. **99**, 250403 (2007).

[4] Immanuel Bloch, Jean Dalibard, and Wilhelm Zwerger, Rev. Mod. Phys. **80**, 885 (2008).

[5] I. V. Tokatly, Phys. Rev. Lett. **93**, 090405 (2004).

[6] J. N. Fuchs, A. Recati, and W. Zwerger, Phys. Rev. Lett. **93**, 090408 (2004).

[7] M. Gaudin, Phys. Lett. **24A**, 55 (1967).

[8] C. N. Yang, Phys. Rev. Lett. **19**, 1312 (1967).

[9] D. S. Petrov, C. Salomon, and G. V. Shlyapnikov, Phys. Rev. Lett. **93**, 090404 (2004).

[10] Elliott H. Lieb and Werner Liniger, Phys. Rev. **130**, 1605 (1963).

[11] M. Olshanii, Phys. Rev. Lett. **81**, 938 (1998).

[12] M. Girardeau, J. Math. Phys. **1**, 516 (1960).

[13] T. Bergeman, M. G. Moore, and M. Olshanii, Phys. Rev. Lett. **91**, 163201 (2003).

[14] C. Mora, A. Komnik, R. Egger, and A. O. Gogolin, Phys. Rev. Lett. **95**, 080403 (2005).

[15] D. Blume and D. Rakshit, Phys. Rev. A **80**, 013601 (2009).

[16] A. Recati, J. N. Fuchs, and W. Zwerger, Phys. Rev. A **71**, 033630 (2005).

[17] Kun Yang, Phys. Rev. B **63**, 140511 (2001).

[18] Minoru Takahashi, *Thermodynamics of one-dimensional solvable models* (Cambridge University Press, Cambridge, 1999).

[19] N. D. Mermin and H. Wagner, Phys. Rev. Lett. **17**, 1133 (1966).

[20] L. van Hove, Physica **16**, 137 (1950).

[21] A. E. Feiguin and F. Heidrich-Meisner, Phys. Rev. B **76**, 220508 (2007).

[22] Yean-an Liao, Ann Sophie C. Rittner, Tobias Paprotta, Wenhui Li, Guthrie B. Partridge, Randall G. Hulet, Stefan K. Baur, and Erich J. Mueller, Nature **467**, 567 (2010).

[23] Le Luo and J. Thomas, Journal of Low Temperature Physics **154**, 1 (2009), 10.1007/s10909-008-9850-2.

[24] S. Nascimbène, N. Navon, K. J. Jiang, F. Chevy, and C. Salomon, Nature **463**, 1057 (2010).

[25] D McKay and B DeMarco, New Journal of Physics **12**, 055013 (2010).

[26] C. N. Yang and C. P. Yang, Journal of Mathematical Physics **10**, 1115 (1969).

[27] Minoru Takahashi, Progress of Theoretical Physics **46**, 1388 (1971).

[28] C. J. Bolech and N. Andrei, Phys. Rev. B **71**, 205104 (2005).

[29] Michele Casula, D. M. Ceperley, and Erich J. Mueller, Phys. Rev. A **78**, 033607 (2008).

[30] Erhai Zhao and W. Vincent Liu, Phys. Rev. A **78**, 063605 (2008).

[31] D M Gangardt and G V Shlyapnikov, New Journal of Physics **8**, 167 (2006).

[32] Y. Aharonov and D. Bohm, Phys. Rev. **115**, 485 (1959).

[33] C. Mora, R. Egger, A. O. Gogolin, and A. Komnik, Phys. Rev. Lett. **93**, 170403 (2004).

[34] C. Mora, R. Egger, and A. O. Gogolin, Phys. Rev. A **71**, 052705 (2005).

[35] Belen Paredes, Artur Widera, Valentin Murg, Olaf Mandel, Simon Folling, Ignacio Cirac, Gora V. Shlyapnikov, Theodor W. Hansch, and Immanuel Bloch, Nature **429**, 277 (2004).

[36] T. Giamarchi, *Quantum Physics in One Dimension* (Oxford University Press, New York, USA, 2004).

[37] K. Penc and J. Sólyom, Phys. Rev. B **47**, 6273 (1993).

[38] T. Vekua, S. I. Matveenko, and Shly, arXiv:0807.4185v1 (2008).

[39] Stefan K. Baur, John Shumway, and Erich J. Mueller, Phys. Rev. A **81**, 033628 (2010).

[40] Erhai Zhao, Xi-Wen Guan, W. Vincent Liu, M. T. Batchelor, and Masaki Oshikawa, Phys. Rev. Lett. **103**, 140404 (2009).

[41] H. W. Press, S. A. Teukolsky, W. T. Vetterling, and B. P. Flannery, *Numerical Recipes* (Cambridge University Press, New York, 1986).

CHAPTER 7

FFLO VS BOSE-FERMI MIXTURE IN POLARIZED 1D FERMI GAS ON A FESHBACH RESONANCE: A 3-BODY STUDY

*This chapter was adapted from "Fulde-Ferrell-Larkin-Ovchinnikov vs Bose-Fermi mixture in polarized 1D Fermi gas on a Feshbach resonance: a 3-body study" by Stefan K. Baur, John Shumway and Erich J. Mueller, published in Physical Review A **81**, 033628 (2010).*

7.1 Abstract

We study the three-fermion problem within a 1D model of a Feshbach resonance in order to gain insight into how the Fulde-Ferrell-Larkin-Ovchinnikov(FFLO)-like state at small negative scattering lengths evolves into a Bose-Fermi mixture at small positive scattering lengths. The FFLO state possesses an oscillating superfluid correlation function, while in a Bose-Fermi mixture correlations are monotonic. We find that this behavior is already present at the three-body level. We present an exact study of the three-body problem, and gain extra insights by considering world lines of a path-integral Monte Carlo calculation.

7.2 Introduction

Trapped ultracold clouds of fermions such as ^{6}Li provide unique insights into the superfluidity of neutral fermions and have opened up new directions for inquiry. By considering the three-body problem, here we theoretically address

the properties of a one-dimensional (1D) superfluid gas of spin-imbalanced fermions (where $n_\uparrow > n_\downarrow$) when the interactions are tuned via a Feshbach resonance. We find a change in symmetry of the ground-state wave function as a function of system parameters, and connect this symmetry change with properties of the many-body state. Our conclusions come from (i) the scattering lengths calculated from an exact solution of the 3-body problem and (ii) the off-diagonal elements of the pair density matrix calculated with path-integral Monte Carlo. In the latter formulation the symmetry change in the wave function emerges from a competition between two classes of topologically distinct imaginary-time world lines. Our conclusions are relevant to experiments on ^{6}Li atoms trapped in an array of very elongated traps, formed from a two-dimensional optical lattice [1]. When such a lattice is sufficiently strong, one has an array of independent 1D systems, and experiments probe ensemble-averaged quantities including the momentum distribution of pairs.

Similar experiments in three dimensions (3D) have demonstrated a crossover between BCS superfluidity of loosely bound pairs to a Bose-Einstein condensation (BEC) of molecules, finding particularly rich physics (mostly involving phase separation) when the gas is spin polarized [2]. One dimension brings a new set of phenomena, driven by quantum fluctuations and the topology of the Fermi surface.

Of particular interest, Fermi surface nesting in 1D stabilizes [3] a version of the Fulde-Ferrell-Larkin-Ovchinnikov (FFLO) phase in the spin-imbalanced gas [4]. FFLO phases, which occupy an extremely small region of the 3D phase diagram [5], are characterized by a coexistence of magnetic and superfluid order, typically coupled together with a spin-density wave. An intuitive example is

given by a quasi-1D spin-imbalanced BCS superfluid, where one finds an array of π-domain walls in the superfluid order parameter, with the excess unpaired atoms residing near the nodes [6]. At higher polarizations the domain walls merge, and the order parameter becomes sinusoidal. We are interested in the truly 1D limit, where there is no long range order: Instead, one can introduce an operator $b(x)$ which annihilates a pair at position x, finding the analogy of FFLO state is that $\langle b^\dagger(x)b(0)\rangle \sim \cos(2\pi n_F x)/|x|^\delta$ where $n_F = n_\uparrow - n_\downarrow$ is the density of excess fermions and the exponent δ depends on interactions [7].

When the interactions are weak, a sufficiently dilute and cold gas of ^{6}Li atoms in an elongated trap (with transverse dimension $d = \sqrt{\hbar/m\omega_\perp}$) can be modeled as a 1D Fermi gas interacting through a short-range 1D potential [8]. This mapping requires that the 3D scattering length is negative with $|a|/d \ll 1$, and both the thermal energy $k_B T$ and the chemical potential μ are small compared to the transverse confinement energy $\hbar\omega_\perp$. Like Refs. [9, 10], we will consider stronger interactions. The breakdown of the mapping onto a 1D Fermi gas is illustrated by the situation where the 3D scattering length is small and positive, hence producing a deeply bound molecular state. The correct description of the unpolarized system in this limit is a weakly interacting gas of these bosons: a model which is not equivalent to a 1D gas of fermions with point interactions.

If one spin imbalances the system in this BEC limit, one does not produce a FFLO state, but rather the excess fermions only mildly perturb the bosonic pairs, and the correlation function $\langle b^\dagger(x)b(0)\rangle \sim 1/|x|^{\delta'}$ is monotonic [11]. Here we study the three-body problem to address the key question of how a spin-imbalanced gas evolves between this fluctuating "BEC" limit and the fluctuat-

ing "BCS" limit already described. How does the correlation function go from monotonic to oscillatory? We find that in the three-body problem the transition occurs due to a level crossing.

To this end, we consider the minimal 1D model of a Feshbach resonance [12, 13], which can capture the relevant physics,

$$
\begin{aligned}
H &= \sum_{k,\sigma} \frac{\hbar^2 k^2}{2m} c^\dagger_{k,\sigma} c_{k,\sigma} + \sum_k \left(\frac{\hbar^2 k^2}{4m} + \nu \right) b^\dagger_k b_k \\
&+ \frac{g}{\sqrt{L}} \sum_{q,Q} b^\dagger_Q c_{Q/2+q,\downarrow} c_{Q/2-q,\uparrow} + h.c.,
\end{aligned} \tag{7.1}
$$

where L is the length of the system and $c^\dagger_{k,\sigma}$, $c_{k,\sigma}(b^\dagger_k, b_k)$ are fermionic(bosonic) creation/annihilation operators. The parameter g describes the coupling strength between the bosonic and fermionic channel and ν is the detuning with $\nu \to \infty$ ($\nu \to -\infty$) being the BCS (BEC) limit. We will use units in which $\hbar^2/m = 1$. [1]

7.3 Qualitative Structure

Figure 7.1 shows a cartoon depiction of the lattice version of this model. One can represent the model in terms of two 1D channels, represented as the legs of a ladder. Fermions move on the lower leg, while bosons move on the upper. As shown at (1) and (2), pairs of fermions can hop from the lower leg to the upper, becoming a boson and vice versa.

In the BCS limit, $\nu \gg g^{4/3}$, the atoms mainly sit on the lower leg, making

---

[1]Following submission of this paper a numerical study of the many-body problem of a similar model was carried out by the authors of [F. Heidrich-Meisner, A. E. Feiguin, U. Schollwöck, and W. Zwerger, Phys. Rev. A **81**, 023629 (2010)] finding results consistent with those reported here.
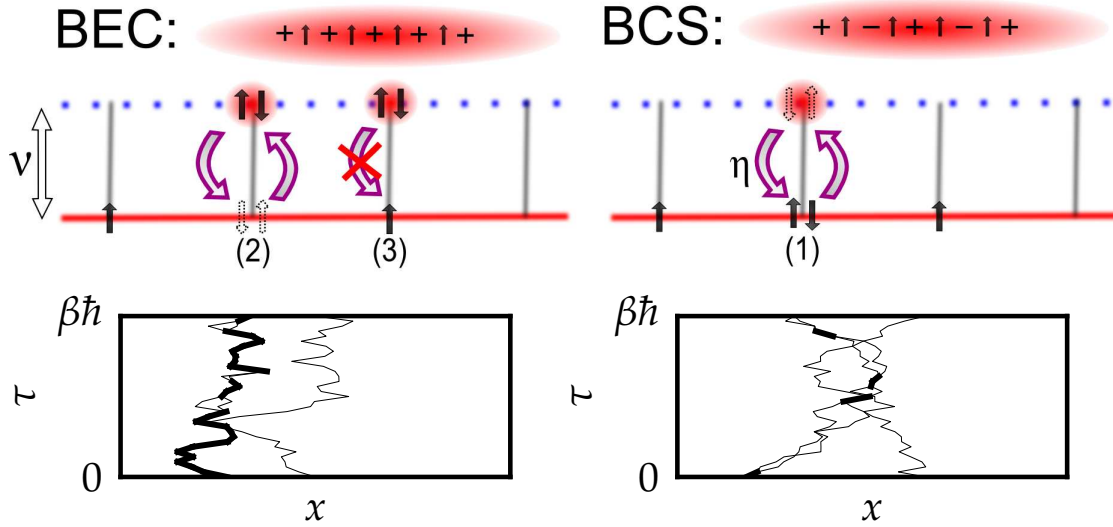
Figure 7.1: (Color online) Cartoon depictions of the physics of Eq. (7.1) in the BEC (left) and BCS (right) limits. (Top) Symmetry of Bose wave function: in the BCS limit the wave function changes sign whenever a pair passes a (spin-up) fermion. (Middle) Depiction of lattice model which is used for developing intuition about Eq. (1). (Bottom) Typical world lines illustrating interaction of a boson (heavy line) and fermion (thin line) with space along the horizontal axis and imaginary-time along the vertical axis.

virtual transitions to the bosonic leg. These virtual transitions lead to a weak local attraction between fermions, $U = -g^2/\nu$. The figure on the bottom right illustrates typical world lines for three fermions.

In the BEC limit, $-\nu \gg g^{4/3}$, the atoms mainly sit on the upper leg. They make virtual transitions to the lower leg. As illustrated at (3), a boson cannot make a virtual transition if an excess fermion sits at that location. This leads to a repulsive interaction between the bosons and fermions of strength g^2/ν. Unlike the BCS limit, the world-lines of the fermions and bosons cross.
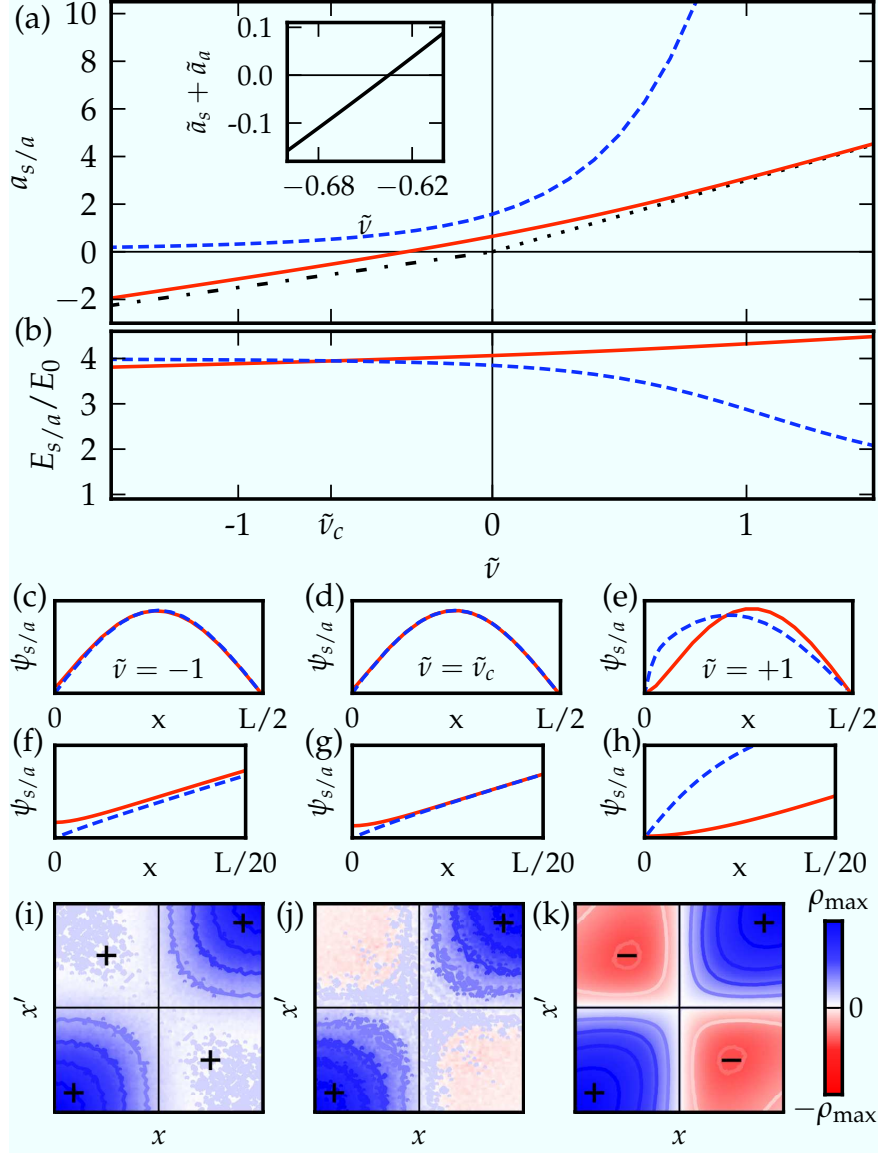
Figure 7.2: (Color online) The dimensionless 1D scattering lengths $\tilde{a}_{s/a} = a_{s/a}g^{2/3}$ for the symmetric (solid red line)/antisymmetric (dashed blue line) channel plotted vs the dimensionless detuning $\tilde{\nu} = \nu/g^{4/3}$. The dotted (dashed dotted) line is the asymptotic result for a_s, $a_s = 3\nu/g^2$ ($a_s = (3/2)\nu/g^2$) in the BCS limit (BEC limit); (cf [10]). (Inset) Sum $\tilde{a}_s + \tilde{a}_a$ (solid line) crosses zero at $\tilde{\nu} \approx -0.635$, marking the change in symmetry of the ground state. (c)-(e) Lowest-energy symmetric (solid line)/antisymmetric (dashed line) wave function $f_{s/a}(x) = L^{-1/2} \sum_Q e^{iQx} f_{s/a,Q}$, in a hard-wall box of size $L \approx 160/g^{2/3}$, where x represents the relative separation of the boson and fermion. Left to right: $\tilde{\nu} = -1, -0.635, 1$. (f)-(h) Wave function near the origin. Finite range of the effective interaction is apparent from the nonsinusoidal shape of f for small x. (i)-(k) Reduced density-matrix $\rho(x, x')$ defined in the text before Eq. (7.6) for $\beta = 100/g^{4/3}$ calculated with QMC. Blue/red represents positive/negative weight. Quadrants with predominant positive/negative weight are labeled with "+"/"−".

165

7.4 Wave functions

To gain insight into how this symmetry change occurs, we study the eigenstates of Eq. (7.1) for the case of three particles. Mora *et al.* [10] carried out a similar study for a more sophisticated model of fermions confined to a harmonic waveguide. The simpler nature of our model, which only includes the most relevant degrees of freedom, makes the physics more transparent.

We study what the symmetry of the ground state is as a function of the dimensionless parameter $\tilde{\nu} = \nu/g^{4/3}$. Given that the three-body wave function can be written

$$|\Psi\rangle = \left(\sum_K f_K b_K^\dagger c_{-K,\uparrow}^\dagger + \sum_{k,K} g_{K,k} c_{K,\downarrow}^\dagger c_{k-K/2,\uparrow}^\dagger c_{-k-K/2,\uparrow}^\dagger \right) |0\rangle , \qquad (7.2)$$

we ask what the symmetry of f_K is under switching the relative position of the boson and the fermion (i. e. $K \to -K$). We find that the ground state f switches from odd (consistent with FFLO) to even (consistent with a Bose-Fermi mixture) as ν is increased from large negative values.

To arrive at this result, we integrate out the three-fermion part of the wave function [14], deriving an integral equation for the two-particle wave function f_K,

$$\mathcal{L}(Q,E)f_Q = -\frac{g^2}{L} \sum_{K'} \frac{f_{K'}}{K'^2 + QK' + Q^2 - E}, \qquad (7.3)$$

where

$$\mathcal{L}(Q,E) = 3Q^2/4 + \nu - E - g^2/(2\sqrt{3Q^2/4 - E}) \qquad (7.4)$$

For details, see Appendix 7.8.

The low-energy symmetric and antisymmetric scattering states have the form $\psi_s(x) \propto \sin[k(|x| - a_s)]$ and $\psi_a(x) \propto \sin[k(x + \text{sign}(x)a_a)]$ for large $|x|$.

166

By imposing hard-wall boundary conditions, $f(x = \pm L/2) = 0$, one sees that the ground state will be symmetric when $a_s > -a_a$, and antisymmetric otherwise. Figure 7.2(a) shows these scattering lengths as a function of ν, revealing that the symmetry of the wave function changes at $\tilde{\nu} \approx -0.635$, where the two solutions are degenerate. Figures 7.2(b)-(h) shows the structure of the lowest energy symmetric and antisymmetric wave functions with these boundary conditions. Note that on the BCS side of resonance, where $-a_a > a_s$, the Bose-Fermi interaction cannot be described by a local potential, rather it is a more general kernel [10]. The off-diagonal nature of the interaction allows the system to violate the standard theorem that the ground-state wave function of a nondegenerate system has no nodes. The level crossing between the states of differing symmetry suggests one of several scenarios for the many-body system, with the most likely candidates being a first-order phase transition or a crossover. Similar behavior was seen by Kestner and Duan [15] in their investigation of the three-body problem in a 3D harmonic trap.

7.5   Quantum Monte Carlo (QMC)

We developed a QMC algorithm to calculate thermodynamic quantities in this model and to give alternative ways of thinking about the underlying physics. We calculate the thermal density matrix

$$\rho(x, x') = Z^{-1} \operatorname{Tr} \left[e^{-\beta H} b^\dagger(x) c_\uparrow^\dagger(0) c_\uparrow(0) b(x') \right], \tag{7.5}$$

where $b(x) = L^{-\frac{1}{2}} \sum_k e^{ikx} b_k$, $c_\sigma(x) = L^{-\frac{1}{2}} \sum_k e^{ikx} c_{k,\sigma}$, $\beta = 1/k_B T$, and Z is the partition function. Figures 7.2(i)-(k) shows a density plot of this correlation function. The FFLO phase is distinguished from the Bose-Fermi mixture by the

sign of ρ in the top left and bottom right quadrants. The boundary between these behaviors occurs roughly where $-a_a = a_s$.

Considering first the fermionic sector, with two spin-up and one spin-down fermions, we discretize imaginary time into $\mathcal{N}$ slices, writing

$$\rho(x_{\mathcal{N}}^{1\uparrow}, x_{\mathcal{N}}^{2\uparrow}, x_{\mathcal{N}}^{\downarrow};\ x_0^{1\uparrow}, x_0^{2\uparrow}, x_0^{\downarrow};\ \beta) = \frac{1}{2Z}\left[\int_I \prod_j dx_j^{1\uparrow} dx_j^{2\uparrow} dx_j^{\downarrow} e^{-S} - \int_X \prod_j dx_j^{1\uparrow} dx_j^{2\uparrow} dx_j^{\downarrow} e^{-S}\right]$$

(7.6)

as integrals over the positions of the up-spins $x^{i\uparrow}$ and the down-spin $x^{\downarrow}$ at imaginary times $\tau_j = j\beta/\mathcal{N}$, with discretized action S. For appropriately chosen S, this expression converges to the exact thermal expectation value as $\mathcal{N} \to \infty$. Two separate boundary conditions account for the fermionic statistics: $\int_I$ has $x_{\mathcal{N}}^{1\uparrow} = x_{\mathcal{N}}^{1\uparrow}$ and $x_{\mathcal{N}}^{2\uparrow} = x_{\mathcal{N}}^{2\uparrow}$ while $\int_X$ has $x_{\mathcal{N}}^{1\uparrow} = x_{\mathcal{N}}^{2\uparrow}$ and $x_{\mathcal{N}}^{2\uparrow} = x_{\mathcal{N}}^{1\uparrow}$ The integrals are performed by a Monte Carlo algorithm, treating e^{-S} as a probability measure. Details of our choice of discretized action and the resulting Monte Carlo rules are given in Appendix 7.9.

While path-integral QMC techniques are well established [16], the present situation is novel because two fermions can bind and form a boson. We implement this feature by introducing extra variables that record the slices at which two fermions are bound, and requiring that when two fermions are bound (say $x_j^{1\uparrow}$ and $x_j^{\downarrow}$) then their positions must be equal. The moves in our Markov process are as follows: moving a particle in one time slice, binding two unbound fermions of opposite spin into a boson, and unbinding two fermions. In all cases the probabilities of the move in slice j only depends on the positions at time slices $j - 1$ and $j + 1$. Sampling new positions from a Gaussian centered about weighted average of the particle's position in the previous and last slice optimizes the acceptance rate. As described in Appendix 7.9, we find the rules

Table 7.1: Gaussian sampling widths and Metropolis acceptance rule, $\mathcal{A} = \min(1, e^{-\Delta S}T_R/T_F)$, for moves in Figs. 7.3 (a)-(d). Moves for bead $x'_j \rightarrow x_j$ are sampled from a Gaussian of width σ_F centered about $\bar{x}_j$; while the reverse moves $x_j \rightarrow x'_j$ sample a Gaussian of width σ_R.

Move	$\bar{x}_j$	σ_F	σ_R	$e^{-\Delta S}T_R/T_F$
(a) Fermion	$\frac{x^{\uparrow}_{j+1} - x^{\uparrow}_{j-1}}{2}$	$\sqrt{\Delta\tau/2}$	$\sqrt{\Delta\tau/2}$	1
(b) Boson	$\frac{x_{j+1} - x_{j-1}}{2}$	$\sqrt{\Delta\tau/4}$	$\sqrt{\Delta\tau/4}$	1
(c) Close$\rightarrow$open	$\frac{x_{j+1} - x_{j-1}}{2}$	$\sqrt{\Delta\tau/2}$	$\sqrt{\Delta\tau/4}$	$\exp(\nu\,\Delta\tau)\big/ g^2\,\Delta\tau^2\sqrt{8\pi\,\Delta\tau}$
(d) Zip$\rightarrow$unzip	$\frac{x^{\uparrow}_{j+1} + x^{\uparrow}_{j+1} - 2x_{j-1}}{4}$	$\sqrt{\Delta\tau/2}$	$\sqrt{\Delta\tau/4}$	$\exp\left(\nu\Delta\tau + \frac{\left|x^{\uparrow}_{j+1} - x^{\downarrow}_{j+1}\right|^2}{8\Delta\tau}\right)\big/\sqrt{2}$
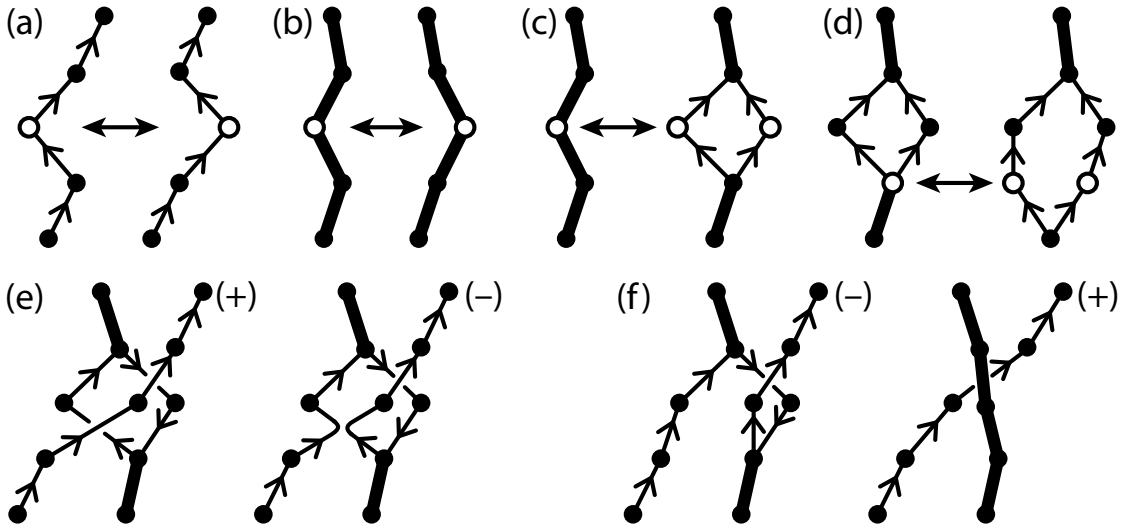
Figure 7.3: Illustrative moves in our QMC algorithm. Fermions are designated by thin lines with arrows representing the spin, bosons by thick lines, and moving beads are white: (a) Moving a fermion, (b) moving a boson, (c) opening/closing, and (d) zipping/unzipping. (e) Crossing of same-spin fermions is always canceled by an equal weight path of opposite sign. (f) Bosons enable paths with both negative and positive weight that do not cancel.

summarized in Table 7.1 and illustrated in Figs. 7.3(a)-(d), which let (7.6) converge to the exact density matrix as $\mathcal{N} \rightarrow \infty$. Specifying these Markov rules is equivalent to specifying S.

Since the density matrix involves adding up terms with different signs, at low temperatures or large particle numbers the efficiency can suffer; this is the

"fermion sign problem." For three particles the variance remains small enough that we can produce reasonably accurate results with the algorithm already described. To make further improvements, we use of the fact that paths cancel when world lines for identical fermions cross in 1D, a well-known technique for eliminating the sign problem in 1D[2]. For example, Fig. 7.3(e) illustrates two paths for which e^{-S} has the same value, but which contribute to ρ with opposite signs. We therefore throw away both sets of paths. In a purely 1D system of fermions one could thereby eliminate all paths with one sign or the other, depending on the relative ordering of the particles at the beginning and end. Here the cancellation is incomplete. Figure 7.3(f) illustrates paths of opposite sign which have no term of the opposite sign to cancel. When the exchanges are dominated by paths with positive weights (such as the RHS of Fig. 3(f)) one has a Bose-Fermi mixture; otherwise one has an FFLO-like state.

7.6   Realization/Detection

We studied the simplest model for the BEC-BCS crossover of spin-polarized fermions in harmonic waveguides, a many-body system realizable by spin imbalancing the array of 1D tubes created in [1]. In such an experiment one could distinguish FFLO from a Bose-Fermi mixture by either using an interferometric probe [17] or measuring the pair momentum distribution, e.g. by sweeping to the BEC side followed by time-of-flight expansion. The signature of the FFLO phase is a peak at finite momentum $q = \pi n_F$ set by the density of excess fermions $n_F = n_\uparrow - n_\downarrow$ [18]. This peak should be absent in a Bose-Fermi

---

[2]Note that our model is not purely 1D as the boson channel provides a mechanism for fermions to move past one-another.

mixture with monotonically decaying superfluid correlations. Another probe, based on correlations in the atomic shot noise after time-of-flight expansion, has been suggested in [19]. Additionally, there has recently been effort in studying the BEC-BCS crossover in few-body clusters [20]. By creating ensembles of elongated clusters one can directly realize and study the three-body system considered here: tuning interactions using a photoassociation or a Feshbach resonance [12, 21].

7.7   Acknowledgments

7.8   Appendix A: Solution of the 3-body problem

Applying the Hamiltonian Eq. 7.1 to $|\Psi\rangle$ gives a pair of coupled Schrödinger equations

$$
\left(k^2 + \frac{3}{4}K^2 - E \right) g_{K,k} - \frac{g \left(f_{k+K/2} - f_{-k+K/2} \right)}{2\sqrt{L}} = 0
$$
$$
\left(\frac{3}{4}K^2 + \nu - E \right) f_K - 2\frac{g}{\sqrt{L}} \sum_k g_{K/2+k,3K/4-k/2} = 0.
$$

In the first equation we antisymmetrized the second term in k to ensure manifest antisymmetry of $g_{K,k}$. Eliminating $g_{K,k}$ from the last equation gives an integral

171

equation for f_K

$$\left(\frac{3}{4}K^2 + \nu - E\right)f_K = \frac{g^2}{L}\sum_k \frac{f_K - f_{k-K/2}}{k^2 + 3K^2/4 - E} \tag{7.7}$$

After performing the integral $\int_{-\infty}^{\infty} dk/\left[2\pi(k^2 + 3K^2/4 - E)\right] = 1/(2\sqrt{3K^2/4 - E})$ this simplifies to (we relabeled K to Q)

$$\mathcal{L}(Q,E)f_Q = -\frac{g^2}{L}\sum_{K'}\frac{f_{K'}}{K'^2 + QK' + Q^2 - E} \tag{7.8}$$

with $\mathcal{L}(Q,E) = 3Q^2/4 + \nu - E - g^2/(2\sqrt{3Q^2/4 - E})$. The solution E_B of the equation $\mathcal{L}(0, E_B) = 0$ is the two-body bound state energy [12],[3] and $\mathcal{L}(Q, E_Q) = 0$ is solved by $E_Q = 3Q^2/4 + E_B$. Equation (7.8) can be converted into a Lippmann-Schwinger equation for the scattering amplitude $F(Q,K)$ using the ansatz [10],

$$f_Q = 2\pi\delta(K - Q) + iF(Q,K)\sum_{\pm} 1/(K \pm Q + i\epsilon), \tag{7.9}$$

which gives

$$2iF(Q,K)K = -V(Q,K,K) - i\frac{1}{L}\sum_{K',\pm}\frac{F(K',K)}{K \pm K' + i\epsilon}V(Q,K',K) \tag{7.10}$$

where we introduced the effective boson fermion potential

$$V(Q,K',K) = g^2\frac{K^2 - Q^2}{\mathcal{L}(Q,E_K)(K'^2 + QK' + Q^2 - E_K)} \tag{7.11}$$

At low energies(small momentum K^4) one has $F(Q,K) \approx -1 + iKa_s + iQa_a$ [10] where $a_s(a_a)$ is the scattering length for the symmetric(antisymmetric) channel. To extract the low-energy scattering properties, we numerically solve the integral equation Eq. (7.10) at fixed small K and compute the scattering length from

---

[3]Solving $L(0, E_B) = 0$ gives $E_B = \nu/(3\xi) - \xi$ with $\xi = \left(27g^4 + 8\nu^3 + 3g^2\sqrt{81g^4 + 48\nu^3}\right)^{1/3}$. The asymptotics are $E_B \sim \nu$ for $\nu \to -\infty$(BEC limit) and $E_B \sim -g^4/4\nu^2$ for $\nu \to +\infty$(BCS limit) [12].

[4]What we mean here is that the typical size of a pair $r = 1/\sqrt{-E_B}$ is much smaller than the interparticle spacing $r_i = 1/n_p$(n_p is the density of pairs). In cold atom system not too far on the BCS side of the resonance, this condition can typically be achieved.

the limits

$$a_s = \lim_{K \to 0} \text{Im}[F(K, K) + F(-K, K)]/2K, \tag{7.12}$$

$$a_a = \lim_{K \to 0} \text{Im}[F(K, K) - F(-K, K)]/2K. \tag{7.13}$$

7.9 Appendix B: Derivation of the path integral action and Monte Carlo rules

The partition function Z corresponding to the Hamiltonian [Eq. (7.1)] can be expressed as a path integral. The path-integral formulation is useful both as a computational tool, but also provides insights from a different point of view. We formulate the path integral in real space (position basis) and imaginary time, $0 \leq \tau \leq \beta$. We discretize imaginary time into discrete steps $\Delta\tau = \beta/\mathcal{N}$, where $\mathcal{N}$ is the Trotter number. The path integral is equivalent to Eq. (7.1) in the limit $\mathcal{N} \to \infty$, which is taken by extrapolating our numerical results to $\Delta\tau \to 0$, following the high-accuracy method of Schmidt and Lee [22] .

To construct the path integral, we start from the imaginary time propagators

(a) x (b)   (c)   (d)

   x'

$$G_f(x \uparrow, x' \uparrow; \Delta\tau) \quad G_f(x \downarrow, x' \downarrow; \Delta\tau) \quad G_b(x, x'; \Delta\tau) \quad -g\,\Delta\tau$$
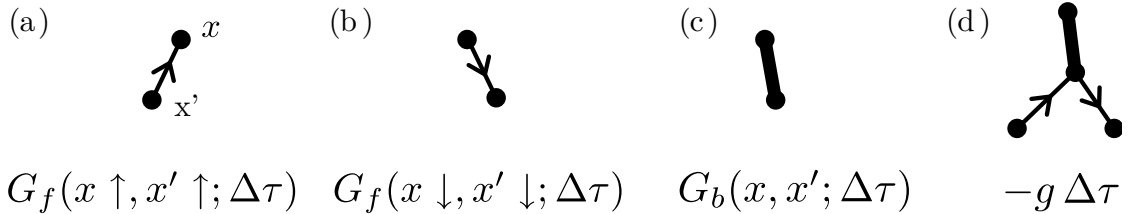
Figure 7.4: Propagators and interaction vertex for discretized path-integral model of Eq. (7.1). (a) Spin-up free fermion, Eq. (7.14), (b) spin-down free fermion, Eq. (7.14), (c) free boson, Eq. (7.15), and (d) interaction vertex with extra weight $-g\,\Delta\tau$.

for free fermions,

$$G_f(x\sigma, x'\sigma'; \Delta\tau) = \langle 0|c_\sigma(x)e^{-\Delta\tau H}c_\sigma^\dagger(x')|0\rangle = \delta_{\sigma\sigma'}\exp\left(-\frac{|x-x'|^2}{2\Delta\tau}\right)\bigg/\sqrt{2\pi\,\Delta\tau},$$

(7.14)

and for free bosons,

$$G_b(x, x'; \Delta\tau) = \langle 0|b(x)e^{-\Delta\tau H}b^\dagger(x')|0\rangle = \exp\left(-\frac{|x-x'|^2}{\Delta\tau} - \nu\,\Delta\tau\right)\bigg/\sqrt{\pi\,\Delta\tau}.$$

(7.15)

These propagators are illustrated in Fig. 7.4. To represent the interaction, we weigh a vertex [Fig. 7.4(d)] with $-g\,\Delta\tau$. The action S for a path configuration, used in Eq.(7.6), is then given by the negative of the log of the product of the propagators and interaction vertices that make up the path.

To sample the path, we use the Metropolis algorithm, in which the acceptance of a move is given by

$$\mathcal{A} = \min(1, e^{-\Delta S}T_R/T_F),$$

(7.16)

where T_F and T_R are the forward and reverse probabilities of attempting a particular move. For example, consider the move illustrated in Fig. 7.3(c), where a bead on a bosonic path is split to form a fermionic pair (a bubble). For the forward move, we sample the two fermion positions $x_j^\uparrow$ and $x_j^\downarrow$ from a Gaussian of width $\sigma_F = \sqrt{\Delta\tau/2}$ centered about $\bar{x}_j = (x_{j+1} + x_{j-1})/2$ where x_{j-1} and x_{j+1} are the stationary boson positions immediately before and after the sampled slice. For the reverse move, we sample the recombined boson position x_j from a Gaussian of width $\sigma_R\sqrt{\Delta\tau/4}$ centered about $\bar{x}_j$. We find

$$e^{-\Delta S}\frac{T_R}{T_F} = \frac{G_f(x_{j+1}, x_j^\uparrow)G_f(x_j^\uparrow, x_{j-1})G_f(x_{j+1}, x_j^\uparrow)G_f(x_j^\uparrow, x_{j-1})(g\,\Delta\tau)^2}{G_b(x_{j+1}, x_j)G_b(x_j, x_{j-1})}$$

$$\times \frac{e^{-\frac{|x_j-\bar{x}_j|^2}{2\sigma_R}}(2\pi\sigma_R^2)^{-\frac{1}{2}}}{e^{-\frac{|x_j^\uparrow-\bar{x}_j|^2}{2\sigma_F}}e^{-\frac{|x_j^\downarrow-\bar{x}_j|^2}{2\sigma_F}}(2\pi\sigma_F^2)^{-1}} = \frac{\exp(\nu\,\Delta\tau)}{g^2\,\Delta\tau^2\sqrt{8\pi\,\Delta\tau}}.$$

(7.17)

This rule and the rules for the other moves illustrated in Figs. 7.3(a)-(d) are summarized in Table 7.1.

BIBLIOGRAPHY FOR CHAPTER 7

[1] H. Moritz *et al.*, Phys. Rev. Lett. **94**, 210401 (2005).

[2] G. B. Partridge *et al.*, Science **311**, 503 (2006); M. W. Zwierlein *et al.*, Science **311**, 492 (2006).

[3] G. Orso, Phys. Rev. Lett. **98**, 070402 (2007); H. Hu, X.-J. Liu, and P. D. Drummond, Phys. Rev. Lett. **98**, 070403 (2007); M. M. Parish *et al.*, Phys. Rev. Lett. **99**, 250403 (2007).

[4] P. Fulde and R. A. Ferrell, Phys. Rev. **135**, A550 (1964); A. I. Larkin and Y. N. Ovchinnikov, Sov. Phys. JETP **20**, 762 (1965).

[5] D. E. Sheehy and L. Radzihovsky, Phys. Rev. Lett. **96**, 060401 (2006); M. M. Parish *et al.*, Nat. Phys. **3**, 124 (2007).

[6] A. I. Buzdin and V. V. Tugushev, Sov. Phys. JETP **58**, 428 (1983); K. Machida and H. Nakanishi, Phys. Rev. B **30**, 122 (1984).

[7] K. Yang, Phys. Rev. B **63**, 140511 (2001); M. Rizzi *et al.*, Phys. Rev. B **77**, 245105 (2008); A. E. Feiguin and F. Heidrich-Meisner, Phys. Rev. B **76**, 220508 (2007); M. Tezuka and M. Ueda, Phys. Rev. Lett. **100**, 110403 (2008); E. Zhao and W. V. Liu, Phys. Rev. A **78**, 063605 (2008).

[8] M. Olshanii, Phys. Rev. Lett. **81**, 938 (1998).

[9] J. N. Fuchs, A. Recati, and W. Zwerger, Phys. Rev. Lett. **93**, 090408 (2004); I. V. Tokatly, Phys. Rev. Lett. **93**, 090405 (2004); C. Mora *et al.*, Phys. Rev. Lett. **95**, 080403 (2005); D. Blume and D. Rakshit, Phys. Rev. A 80, 013601 (2009).

[10] C. Mora *et al.*, Phys. Rev. Lett. **93**, 170403 (2004); C. Mora, R. Egger, and A. O. Gogolin, Phys. Rev. A **71**, 052705 (2005).

[11] A. Imambekov and E. Demler, Phys. Rev. A **73**, 021602 (2006).

[12] A. Recati, J. N. Fuchs, and W. Zwerger, Phys. Rev. A **71**, 033630 (2005).

[13] D. E. Sheehy and L. Radzihovsky, Phys. Rev. Lett. **95**, 130401 (2005); R. Citro and E. Orignac, Phys. Rev. Lett. **95**, 130402 (2005); S. Sachdev and K. Yang, Phys. Rev. B **73**, 174504 (2006).

[14] A. O. Gogolin, C. Mora, and R. Egger, Phys. Rev. Lett. **100**, 140404 (2008); M. Jona-Lasinio, L. Pricoupenko, and Y. Castin, Phys. Rev. A **77**, 043611 (2008).

[15] J. P. Kestner and L.-M. Duan, Phys. Rev. A **76**, 033611 (2007).

[16] D. M. Ceperley, Rev. Mod. Phys. **67**, 279 (1995).

[17] V. Gritsev, E. Demler, and A. Polkovnikov, Phys. Rev. A **78**, 063624 (2008).

[18] M. Casula, D. M. Ceperley, and E. J. Mueller, Phys. Rev. A **78**, 033607 (2008).

[19] A. Lüscher, R. M. Noack and A. M. Läuchli, Phys. Rev. A **78**, 013637 (2008).

[20] N. Gemelke *et al.*, in *Proceedings of the XXI International Conference on Atomic Physics, Storrs, 2008*, edited by R. Côté, P. L. Gould, M. Rozman and W.W. Smith(World Scientific, 2009), p. 240

[21] For a harmonic waveguide on a Feshbach resonance our argument that $a_s = -a_a$ for the symmetry change of the three-body wave function still holds. We estimate the transition at $d/a = 1.7$[10].

[22] K. E. Schmidt and M. A. Lee, Phys. Rev. E **51**, 5495 (1995).

CHAPTER 8

ROTATING BOSE GASES AND FRACTIONAL QUANTUM HALL STATES

*This chapter was adapted from "Stirring trapped atoms into fractional quantum Hall puddles" by Stefan K. Baur, Kaden R. A. Hazzard and Erich J. Mueller, published in Physical Review A **78**, 061608 (2008) (R).*

8.1   Motivation — Rapidly rotating Bose gases

Typically correlated states of quantum matter emerge at low temperatures when kinetic and interaction energy in a system become comparable. In cold quantum gases this may be achieved using optical lattices, where the bandwidth limits kinetic energy and the interactions are increased due to the localization of the Wannier orbitals. Alternatively, Feshbach resonances allow tuning interactions and allow for reaching strongly correlated regimes with Fermi and Bose gases.

A third and novel type of strong correlation may be achieved in rotating Bose gases (for a review article, see [14]). Rotation plays the role of an external magnetic field for neutral atoms, and as for electrons in semiconductors, fast rotating Bose gases should feature an analogue of the fermionic quantum hall state. To understand when interactions become important, we consider a particle in a harmonic 2D ("pancake") trap. In the frame rotating with frequency Ω the single particle Hamiltonian is

$$H = H_0 - L_z \Omega \tag{8.1}$$

where $L_z = (\mathbf{r} \times \mathbf{p})_z$ is the z-component of the angular momentum operator and

$$H_0 = -\frac{1}{2}\left(\partial_x^2 + \partial_y^2\right) + \frac{1}{2}\omega^2\left(x^2 + y^2\right) \tag{8.2}$$

178
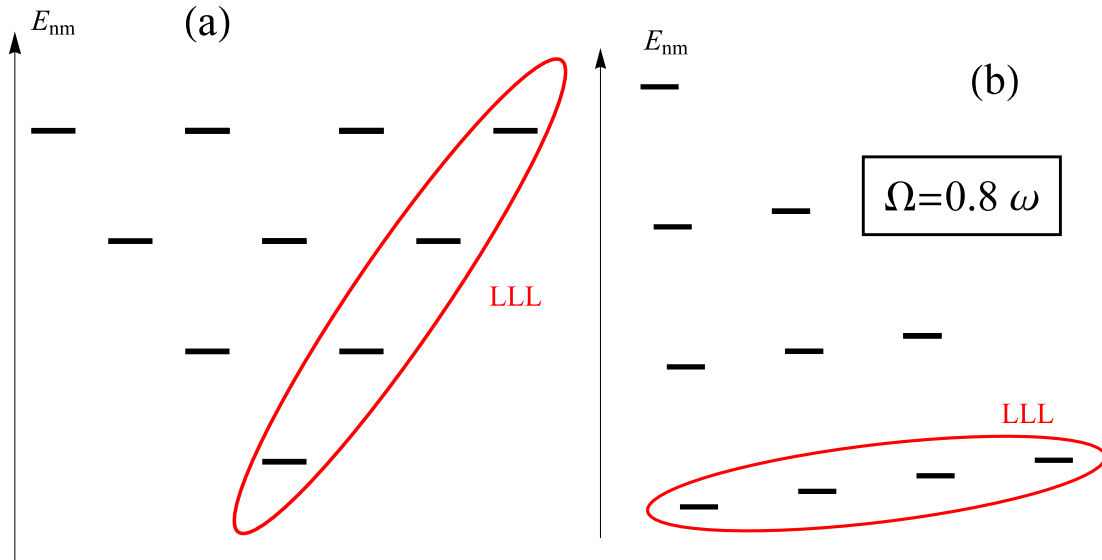
Figure 8.1: In the frame rotating with $\Omega \approx \omega$ the 2D harmonic oscillator states (a) form degenerate manifolds at energies $E = 0, 2\omega, 4\omega, \ldots$. The lowest of these manifolds are the lowest Landau level (LLL) states, here marked with a red circle.

is the Hamiltonian in the lab frame (for convenience we put $\hbar = m = 1$). L_z commutes with H_0, because we assumed an isotropic trap. Therefore the eigenfunction of H are just the eigenfunction of H_0 in the angular momentum basis $|nm\rangle$ with the well-known energies

$$E_{nm} = \omega(2n + |m| + 1) - m\Omega. \tag{8.3}$$

Here $m = 0, \pm 1, \pm 2, \ldots$ ($n = 0, 1, 2, \ldots$) are the angular momentum (radial) quantum numbers. The spectrum in the rotating frame is simply obtained by tilting the spectrum in the lab frame. As the rotation frequency approaches the trapping frequency, the so called Landau levels become degenerate. Often we may assume, that the chemical potential μ of the gas is much less than the spacing ω between Landau levels. Then we can effectively consider only the lowest Landau level (LLL) states with $n = 0$, $m \geq 0$ and use these states as our basis. Quantum fluctuations become important when the interaction energy U

becomes comparable to the splitting of LLL states. When Ω is very close ω, the interacting ground state has total angular momentum $L = N(N-1)$, where N is the number of particles. This state is the well known $\nu = 1/2$ Laughlin wavefunction for the bosonic fractional quantum hall state. There are various problems in experimentally creating this quantum hall state, for one thing one has to achieve the LLL regime, the trapping potential vanishes (or is very small) when $\Omega \approx \omega$, the stirring process causes heating (and very low temperatures might be required when the gas becomes very dilute and spread out and fast rotation). Also, in order to specifically create the Laughlin-state, ω has to be tuned less than Ω, basically with a precision that scales as $1/N$, making it not very feasible to realize the Laughlin state large bosonic condensate. A way out of this dilemma was proposed in Ref. [3], where small puddles of $N = 2, \ldots, 6$ particles were considered. Motivated by experiments by Steven Chu's group at Stanford, who attempted to realize this proposal [13], we studied a new protocol that could allow for the realization and detection of few atom quantum hall states.

8.2   Abstract

We theoretically explore the generation of few-body analogs of fractional quantum Hall states. We consider an array of identical few-atom clusters ($n = 2, 3, 4$), each cluster trapped at the node of an optical lattice. By temporally varying the amplitude and phase of the trapping lasers, one can introduce a rotating deformation at each site. We analyze protocols for coherently transferring ground state clusters into highly correlated states, producing theoretical fidelities (probability of reaching the target state) in excess of 99%.

8.3 Introduction

Cold atom experiments promise to produce unique states of matter, allowing controllable exploration of exotic physics. For example, since rotation couples to neutral atoms in the same way that a uniform magnetic field couples to charged particles, many groups are excited about the possibility of producing analogs of fractional quantum hall states [1, 2, 3, 4]. In particular, if a two dimensional harmonically trapped gas of bosons is rotated at a frequency Ω sufficiently close to the trapping frequency ω, then the ground state will have vortices bound to the atoms – an analog of the binding of flux tubes to electrons in the fractional quantum hall effect. The ground state will be topologically ordered and possess fractional excitations. Technically, the difficulty with realizing this goal experimentally has been that it requires Ω to be tuned to a precision which scales as $1/n$, where n is the number of particles. Responding to this impediment, several authors [2, 3, 4] have proposed studying clusters with $n \lesssim 10$. Such puddles possess many of the features of a bulk quantum hall liquid, and producing them would be a great achievement. Here we propose and study protocols for producing strongly correlated clusters of rotating atoms.

The issue prompting this investigation is that in such clusters there are very few mechanisms for dissipating energy, and hence experimentally producing the ground state of a rotating cluster is nontrivial. First, the small number of particles results in a discrete spectrum, and leaves few kinetic paths. Second, in the strongly correlated states of interest the atoms largely avoid each other, further blocking the kinetics. On these grounds, one should not expect to be able to cool into the ground state. Instead we advocate a dynamical process where one coherently *drives* the system into the strongly correlated state through a well-

planned sequence of rotating trap deformations. This approach is based upon an analogy between the states of these atomic clusters, and the energy levels of a molecule. By deforming the harmonic trap, and rotating the deformation, one couples the many-body states in much the same way that an oscillating electric field from a laser couples molecular states. We consider a number of pulse sequences, finding that one can rapidly transfer atoms to a strongly correlated state with nearly unit efficiency. Following a proposal by Popp *et al.* [3], experimentalists at Stanford have achieved considerable success with a related procedure, where one slowly increases the rate of rotation, adiabatically transferring bosonic atoms from an initially non-rotating state, to an analog of the Laughlin state [5]. One could also imagine implementing more sophisticated protocols such as rapid adiabatic passage [6].

To achieve sufficient signal to noise, any experimental attempt to study small clusters of atoms must employ an ensemble of identical systems: for example by trapping small numbers of atoms at the nodes of an optical lattice. When formed by sufficiently intense lasers, this lattice will isolate the individual clusters, preventing any "hopping" from one node to another. We will not address the very interesting question of what would happen if the barriers separating the clusters were lowered. By using filtering techniques, one can ensure that the same number of atoms sit at each node [5]. A rotating deformation of each *microtrap* can be engineered through a number of techniques. For example, if the intensity of the lattice beams forming a triangular lattice are modulated in sequence, then a rotating quadrupolar deformation is be produced. A more versatile technique is to modulate the phases between counter-propagating lattice beams. Changing these phases uniformly translates the lattice sites. If one moves the lattice sites around faster than the characteristic times of atomic mo-

tion ($10^{-5}s$) but slow compared to the times for electronic excitations (10^{-15}s) then the atoms see a time averaged potential. This technique, which is closely related to the time orbital potential traps pioneered at JILA [7], can produce almost arbitrary time dependent deformations of the individual traps which each of the clusters experiences [5]. Each cluster feels the same potential.

Once created, the ensemble of clusters can be experimentally studied by a number of means. *In situ* probes such as photoassociation [8] and RF spectroscopy [9] reveal details about the interparticle correlations. In the regime of interest, time-of-flight expansion, followed by imaging, spatially resolves the ensemble averaged *pre-expansion* density. This result follows from the scaling form of the dynamics of lowest Landau level wavefunctions [4].

8.4   Methods and Results

We model a single cluster as a small number of two-dimensional harmonically trapped bosonic atoms. The two dimensionality can be ensured by increasing the intensity of the lattice beams in the perpendicular direction. Neglecting the zero-point energy, one finds that in the frame rotating with frequency Ω, the single particle harmonic oscillator eigenstates have the form $E_{jk} = \hbar(\omega - \Omega)k + \hbar(\omega + \Omega)j;\ (j, k = 0, 1, \ldots)$. In typical lattices, the interaction energy $U/\hbar \sim$10 kHz is small compared to the small oscillation frequency $\omega \sim$100 kHz [10]. Therefore the many-body state will be made up of single particle states with $j = 0$: the lowest Landau level, with wavefunctions of the form

$$\psi_k(x, y) \quad = \quad (\pi k!)^{-1/2} z^k e^{-z^* z/2},\qquad\qquad (8.4)$$

183

where $z = (x + iy)/d$ with $d = \sqrt{\hbar/M\omega}$ is the complex representation of the coordinate in the plane measured in units of the oscillator length, where M is the atomic mass. Including interactions, the many-body Hamiltonian for a single cluster is then

$$H_{LLL} = \sum_j j\hbar(\omega - \Omega)a_j^\dagger a_j + \sum_{jklm} V_{jklm}a_j^\dagger a_k^\dagger a_l a_m \tag{8.5}$$

where a_m is the annihilation operator for the single particle state ψ_m. For point interactions the interaction kernel is

$$V_{jklm} = \frac{U}{2}\delta_{j+k-l-m}2^{-(j+k)}\frac{(j+k)!}{\sqrt{j!k!l!m!}}, \tag{8.6}$$

where $U = \sqrt{2/\pi}\,\hbar^2 a/(Md_z d^2)$ is the on-site interaction between two particles in the same well, a is the three dimensional s-wave scattering length and d_z is the oscillator length in the transverse direction. As has been explored in depth by previous authors [1, 2, 3, 4], for a given total number of particles n, and angular momentum projection L, the Hamiltonian (8.5) is a finite matrix which is readily diagonalized. Example spectra are shown in figures 8.2 through 8.4. We plot the spectra as energy versus angular momentum, with $\Omega = \omega$. Spectra at other rotation speeds are readily found by "tilting" the graphs – the energy of a state with angular momentum projection L is simply shifted up by $\hbar(\omega - \Omega)L$.

We imagine applying to each cluster a rotating single particle potential (in the lab frame) of the form

$$H_S(r, t) = V_p(t)\left[z^m e^{im\Omega_p t} + (z^*)^m e^{-im\Omega_p t}\right], \tag{8.7}$$

where m determines the symmetry of the deformation (e.g. $m = 2$ is a quadrupolar deformation), the envelope function $V_p(t)$ is the time-dependent amplitude of the deformation, and Ω_p is the frequency at which the perturbation rotates. We will mainly focus on the case $m = 2$. When restricted to the lowest
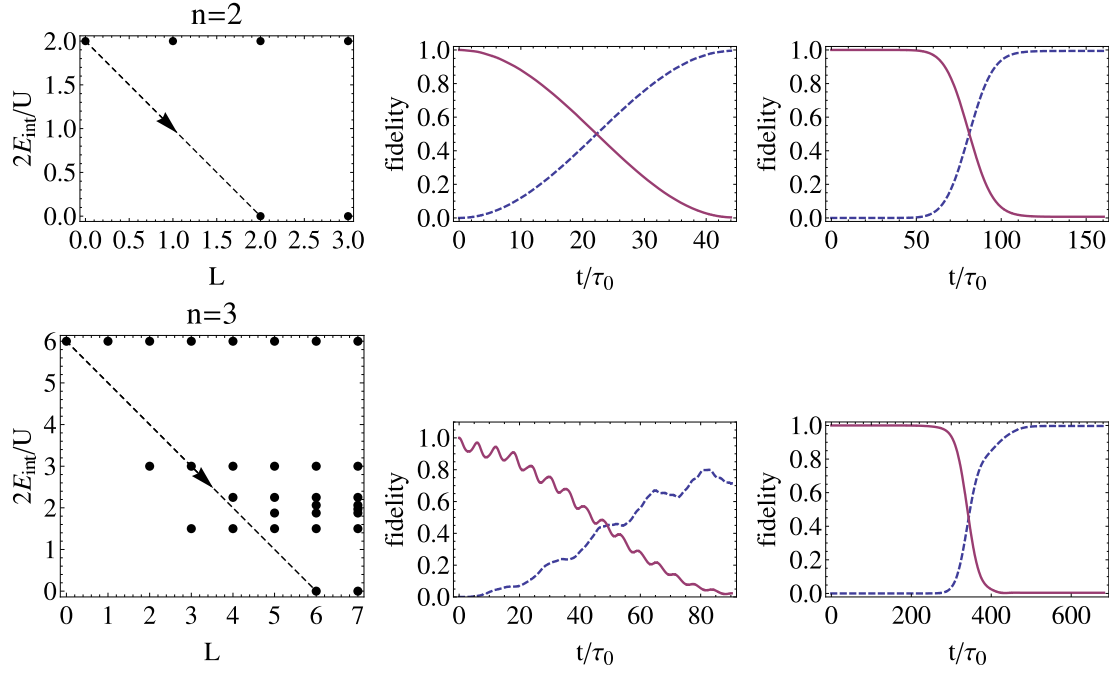
Figure 8.2: Transferring small clusters from non-rotating ground state to $\nu = 1/2$ Laughlin state using rotating quadrupolar ($m = 2$) deformations. Left: Interaction energy (in units of $U/2$) of quantum states of harmonically trapped two dimensional clusters as a function of total angular momentum projection L in units of $\hbar$. Excitation paths are shown by arrows. Central: squared overlap (fidelity) of $|\psi(t)\rangle$ with the initial (solid) and final (dashed) states as a function of the duration of a square pulse. Right: Fidelities as a function of time for an optimized Gaussian pulse of the form $e^{-(t-t_0)^2/\tau^2}$. Time is measured in units of $\tau_0 = \hbar/U \sim 10^{-4}$s. For $n = 2$, the peak perturbation amplitude is $V_p = 0.05(U/2)$, $\omega - \Omega_p = 2.0(U/2)$, and a Gaussian pulse time of $\tau = 24\tau_0$. For $n = 3$, $\tau = 102\tau_0$ and $\omega - \Omega_p = 2.046(U/2)$ and $2.055(U/2)$ for the Gaussian and square cases, respectively. For $n = 3$, nonlinear effects (coupling with near-resonant levels) shifted the optimal frequency away from the linear response expectation, $\omega - \Omega_p = 2(U/2)$.

Landau level, this potential generates a coupling between the many-body states which in the rotating frame is expressed as

$$H_S = V_p(t) \sum_l v_{lm} \left(e^{im(\Omega_p - \Omega)t} a^\dagger_{l+m} a_l + \text{H.C.} \right) \tag{8.8}$$

with $v_{lm} = 2^{-m/2}(l+m)!/\sqrt{l!(l+m)!}$. As such it only couples states whose total angular momentum projection differs by m. For our calculation will work in

185

the co-rotating frame with $\Omega = \Omega_p$, where the only time dependence is given by $V_p(t)$.

We wish to implement a π-pulse, where the amplitude $V_p(t)$ is engineered so that after the pulse, a cluster is transferred from its initial state to a target state of our choosing. If the perturbation coupled only two states, this would be a straightforward procedure. The frequency Ω_p is selected so that the initial and target state are degenerate in the rotating frame. For any finite V_p, the system Rabi flops between the two coupled states, and by turning off the perturbation at the right time one ends up in the target state with unit probability. The present example is more complicated, as there are many states coupled by the perturbation. The basic idea however remains sound: one still chooses Ω_p to make the initial and final state degenerate. The time dependence of $V_p(t)$ should be tailored to minimize the coupling to unwanted states. These stray couplings could be particularly disastrous, because the coupling between the initial and target state are generically quite high order in V_p. As a particularly relevant example, we consider transfering clusters from the ground state (with $L = 0$) to the the $\nu = 1/2$ Laughlin state $\psi_L(z_1, \cdots z_n) = \prod_{i<j}(z_i - z_j)^2 \exp(-\sum_j |z_j|^2/4l_B^2)$, which has angular momentum $n(n-1)$. Using a perturbation with $m = 2$, this requires a $n(n-1)/2$-order process. A picturesque way of thinking about the dynamics in the presence of the perturbation is to map the problem onto the motion of a particle on a complicated "lattice". The states of the unperturbed system are analogous to "lattice sites", while the perturbation produces a "hopping" between sites. The goal is to engineer a time-dependent hopping which efficiently moves the "particle" from a known starting position to a desired ending position. The transfer efficiency is measured by the probability that the system is in the target state ψ_T at the end of the time evolution: we plot this probability –

known as the fidelity – as a function of time, given by $f(t) = |\langle\psi_T|\psi(t)\rangle|^2$.

As this analogy emphasizes, the problem of transfering a quantum system from one state to another is generic. Müller, Chiow, and Chu [11] recently considered how one can optimize pulse shapes to produce high order Bragg diffraction, while avoiding transfering atoms into unwanted momentum states. These authors developed a formalism for calculating the fidelity by adiabatically eliminating the off-resonant states. They found that Gaussian pulse shapes greatly outperformed simple square pulses. This result is natural, as the smoother pulses have a much smaller bandwidth.

We numerically solve the time dependent Schrödinger equation, truncating our Hilbert space at finite total angular momentum $L = n(n-1) + 4$ for $n = 2, 3$ and $L = n(n-1) + 8$ for $n = 4$. We have numerically verified that changing this cutoff to higher values has negligible effects. Figure 8.2 shows f in the case of $n = 2$ and $n = 3$ for square and Gaussian pulses. For the square pulse the fidelity is shown as a function of pulse length. For the Gaussian pulse, a fixed pulse duration is used, and the fidelity is shown as a function of time. For $n = 2$, where only two states are involved, the pulse shape is irrelevant. For $n = 3$, where there is a near-resonant state with $L = 4$, the Gaussian pulse shape greatly outperforms the square pulse, producing nearly 100% transfer efficiency in 10's of ms, even for a very weak perturbation.

For $n > 3$ we find that these high order processes become inefficient. For $m = 2$ the coupling between the initial and final state scale as $(V_p/U)^{n(n-1)/2}$, making transfer times unrealistically long unless one drives the system into a highly nonlinear regime. As illustrated in figure 8.3, this difficulty can be mitigated by using perturbations with higher m. There, for illustration, we consider exciting
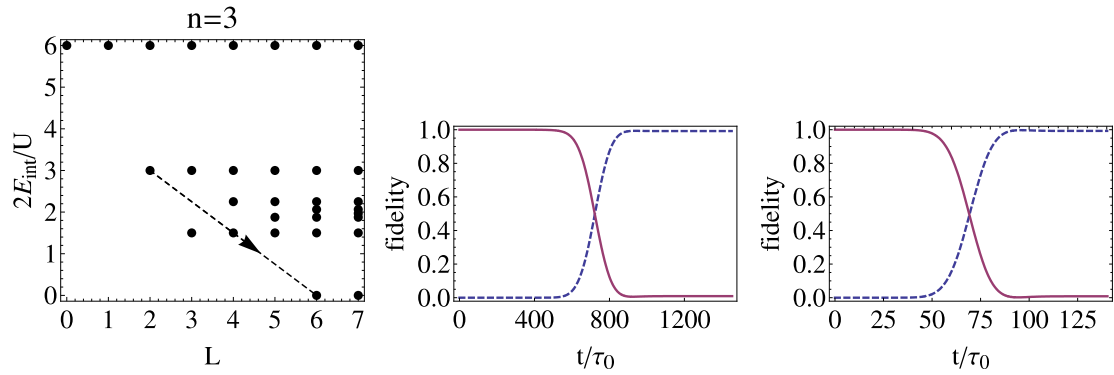
Figure 8.3: Using a rotating m-fold symmetric perturbation to drive $n = 3$ particle clusters from $L = 2$ to the $\nu = 1/2$ Laughlin state. Left:path on the energy level diagram. Center: second-order process coming from a deformation with $m = 2$. Right: direct transition produced with $m = 4$. Solid (dashed) lines are fidelities with the initial (Laughlin) state. In both cases the peak deformation is $V_p = 0.05(U/2)$. Both use a Gaussian pulse. The frequencies and pulse times τ we used for $m = 2, 4$ were $\omega - \Omega_p = (3.00/2)(U/2), 3.035(U/2)$ and $\tau/\tau_0 = 218, 21$. Note how much more rapid the direct process is.

a 3-particle cluster from the lowest energy $L = 2$ state to the $L = 6$ Laughlin state. The second order $m = 2$ pulse requires much longer than the first order $m = 4$ pulse. An interesting aside is that one would naively have expected that the resonant $l = 4$ state would make the second-order process extremely inefficient. It turns out that the coupling to that state is fortuitously zero.

Further improved scaling can be arranged by using a sequence of π pulses. One transfers the cluster from one long-lived state to another. Since the number of pulses scales as the angular momentum, the transfer time is then quadratic in the angular momentum, rather than exponential. One can also tailor the path to maximize the fidelity of each step. Some two-pulse sequences are shown in figure 8.4. The guiding principle in designing the pulse sequences is that in each step one wants as few as possible near-resonant intermediate states.
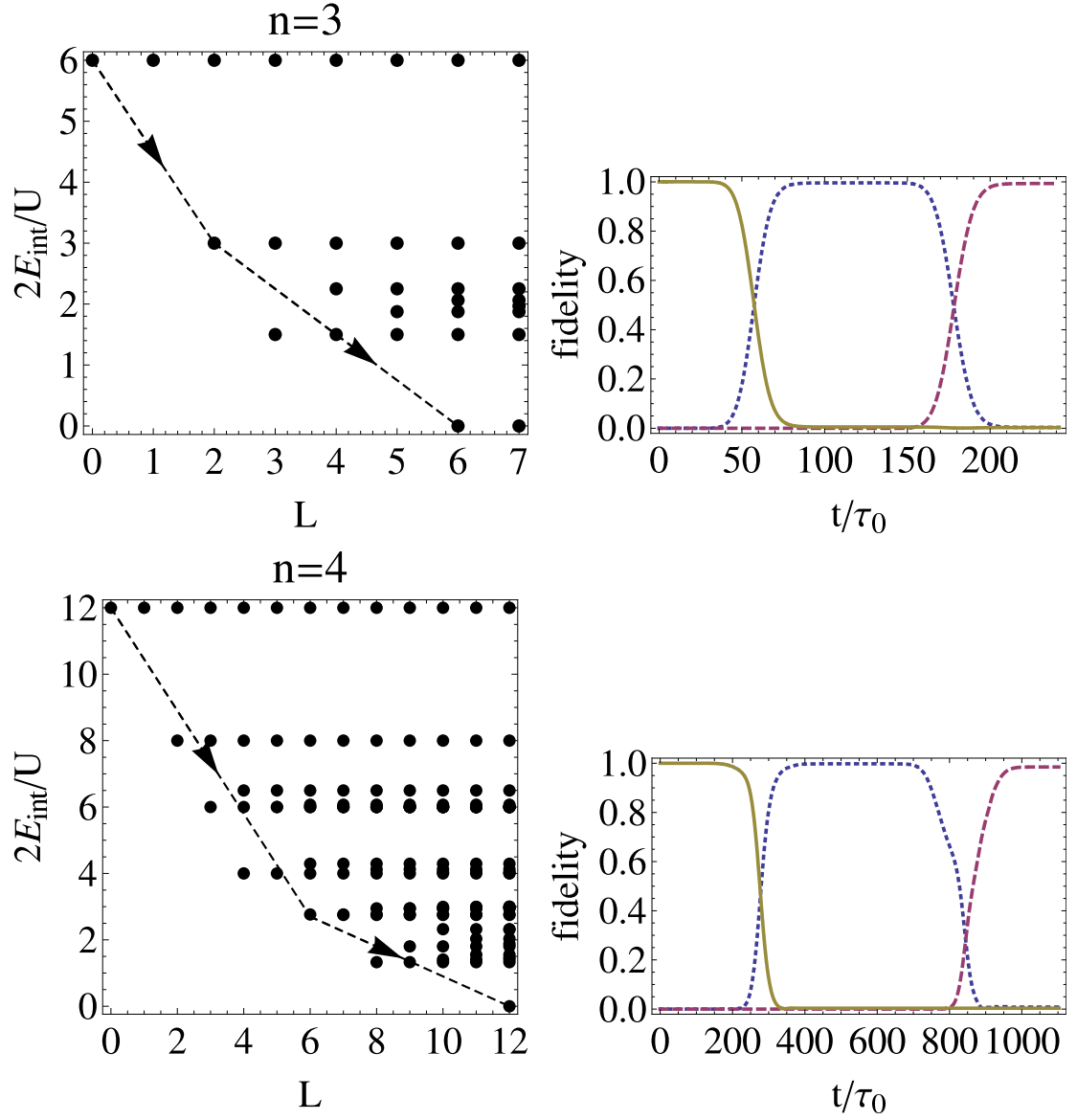
Figure 8.4: Transfering atoms using multiple pulses. Left: paths from initial to Laughlin states for $n = 3, 4$. Right: Solid line is the fidelity with the initial state, dotted with the intermediate $(L, E) = (2\hbar, 3(U/2))$ state, and the dashed line with the Laughlin state. All pulses are Gaussians. Despite using multiple pulses, this technique is faster than using a higher order $m = 2$ pulse. The frequencies (Ω_p), shape (m), and pulse times (τ) for the $N = 3$ sequence were $\hbar(\omega - \Omega_p)/(U/2) = 3.00, 3.035$, $m = 2, 4$, and $\tau/\tau_0 = 16.95, 19.2$. For both, $V_p = 0.05(U/2)$. For $N = 4$, using two pulses with $m = 2$ and $V_p = 0.2(U/2)$, we achieve $> 98\%$ fidelity after a total two-pulse sequences with $\hbar(\omega - \Omega_p)/(U/2) = 3.130, 1.0376$ and $\tau/\tau_0 = 82.5, 87.0$.

8.5 Conclusion

We have shown it is possible to use time dependent trap perturbations to coherently transfer boson clusters from nonrotating ground states to analogs of fractional quantum hall states. We achieve fidelity $f > 99\%$ for $n = 2, 3$ using very weak rotating $m = 2$ deformations, whose duration is of order tens of ms. Using a two-pulse sequence, we achieve similar results for $n = 4$. We find that smooth Gaussian pulses are much more effective than square pulses, and that further efficiency can be gained by using higher order perturbations of the form z^m with $m > 2$.

We briefly compare our technique with Ref. [3]'s proposal. While our approaches share the use of a rotating time-averaged optical lattice potential, our proposal offers significant differences and advantages. While Ref. [3] suggests an adiabatic evolution, we propose a coherent evolution – analogous to a Rabi oscillation – to the Laughlin state. This has the advantage of being faster, easier to implement, and more robust. For a slightly smaller perturbation relative to the adiabatic method, we achieve fidelity ~ 1 in contrast to the adiabatic method's 0.97 fidelity. Moreover, our method requires half the time. More importantly, the adiabatic method requires carefully navigating a path through possible rotating potential strengths and frequencies as a function of time. In contrast, our method requires only setting the pulse duration and strength, and is thus more easily implementable and less susceptible to small experimental errors.

This technique will allow the efficient creation of bosonic quantum Hall puddles – a state of matter which has not yet been observed. The clusters pro-

duced will be orbitally entangled, have strong interparticle correlations, have fractional excitations, and possess topological orders [1, 2, 3, 4]. Although current experiments, and the present theory, is focussed on the small-atom limit, it would be exciting to apply these techniques to larger collections of atoms, producing true analogs of fractional quantum Hall states. The main difficulty is that the spectra become dense as n increases, requiring one to set Ω_p to extremely high precision. By carefully choosing the trajectory, taking advantage of gaps in the spectrum, one might be able to overcome such difficulties.

Finally, we mention that our approach allows one to drive the system into almost arbitrary excited states. This may, for example, be important for using quantum hall puddles in a topological quantum computing scheme [12].

BIBLIOGRAPHY FOR CHAPTER 8

[1] N.K. Wilkin, J.M.F. Gunn, and R.A. Smith, Phys. Rev. Lett. **80**, 2265 (1998); N.R. Cooper and N.K. Wilkin, Phys. Rev. B **60**, R16279 (1999); S. Viefers, T.H. Hansson, and S.M. Reimann, Phys. Rev. A **62**, 053604 (2000); N.K. Wilkin and J.M.F. Gunn, Phys. Rev. Lett. **84**, 6 (2000); N.R. Cooper, N.K. Wilkin, and J.M.F. Gunn, Phys. Rev. Lett. **87**, 120405 (2001); B. Paredes, P. Fedichev, J.I. Cirac, and P. Zoller, Phys. Rev. Lett. **87**, 010402 (2001); J. Sinova, C. B. Hanna, and A. H. MacDonald, Phys. Rev. Lett. **89**, 030403 (2002); Susanne Viefers, J. Phys. Cond. Mat. **20**, 123202 (2008)

[2] J.W. Reijnders, F.J.M. van Lankvelt, K. Schoutens, and N. Read, Phys. Rev. Lett. **89**, 120401 (2002); B. Paredes, P. Zoller, and J.I. Cirac, Phys. Rev. A **66**, 033609 (2002); N. Regnault, and Th. Jolicoeur, Phys. Rev. Lett. **91**, 030402 (2003); Uwe R. Fischer, Petr O. Fedichev, Alessio Recati, J. Phys. B **37**, S301 (2004).

[3] M. Popp, B. Paredes, and J. I. Cirac, Phys. Rev. A **70**, 053612 (2004).

[4] T.-L. Ho and E. J. Mueller, Phys. Rev. Lett. **89**, 050401 (2002); N. Read and N. R. Cooper, Phys. Rev. A **68**, 035601 (2003)

[5] S. Chu, *private communications.*

[6] K. Bergmann, H. Theuer, and B. W. Shor, Rev. Mod. Phys **70**, 1003 (1998).

[7] W. Petrich, M. H. Anderson, J. R. Ensher, and E. A. Cornell, Phys. Rev. Lett. **74**, 3352 (1995).

[8] T. Kinoshita, T. Wenger, and D. S. Weiss, Phys. Rev. Lett. **95**, 190406 (2005); M. Junker, D. Dries, C. Welford, J. Hitchcock, Y. P. Chen, and R. G. Hulet, arXiv:0803.1167 (2008).

[9] M. O. Oktel, and L. S. Levitov, Phys. Rev. Lett. **83**, 6 (1999).

[10] D. Jaksch, C. Bruder, J.I. Cirac, C.W. Gardiner, and P. Zoller, Phys. Rev. Lett. **81**, 3108 (1998). .

[11] Holger Müller, Sheng-wey Chiow, and Steven Chu, *unpublished*.

[12] Yu. A. Kitaev, Annals Phys. **303** 1, 2 (2003).

[13] N. Gemlke, E. Sarajilic, and Steven Chu, arXiv:1007.2677v1 (2010).

[14] N. R. Cooper, Adv. Phys. **57**, 539 (2008)

CHAPTER 9

NONEQUILIBRIUM EFFECTS OF BOSONS IN OPTICAL LATTICES

*This chapter was adapted from "Two-body recombination in a quantum mechanical lattice gas: Entropy generation and probing of magnetic short-range correlation" by Stefan K. Baur and Erich J. Mueller, published in Physical Review A **82**, 023626 (2010).*

9.1 Motivation

Here we study the effects of two-body losses on lattice bosons. Losses are ubiquitous in experiments with ultracold gases, but often neglected in theoretical calculations. As these losses cause heating, they pose limits on what temperatures are achievable in experiments. When considering an uncorrelated state, such as a weakly interacting Bose gas, losing particles from the condensate does not seem to cause heating (as the condensate has zero entropy). The situation is different for Fermi gases and Mott insulators (MI), where losing particles creates holes in the Fermi sea/MI. The production of holes naturally is followed by an increase in entropy, for Fermi gases this was discussed in the early days by Timmermans (the so called "hole heating") [1]. With ever more advanced lattice gas experiments, approaching the regime of quantum magnetism, it is a natural question to ask what effect losses have on cold atoms in optical lattices. Another set of ideas were proposed by the groups of Cirac and Zoller where models are considered, that seem to become more correlated as particles are lost. Our study is motivated by Ref. [2], where a 1D lattice gas of bosonic molecules with strong nearest neighbor losses was considered (for bosonic molecules losses are large, because every collision between molecules allows for three-body recombination
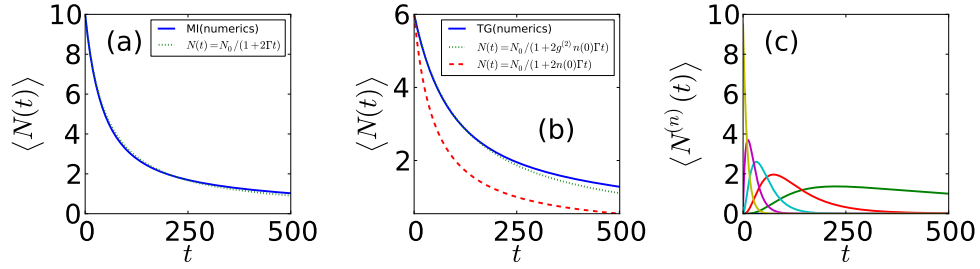
Figure 9.1: Left: Average particle number $\langle N \rangle = \sum_n n \operatorname{Tr} \rho^{(n)}$ as a function of time for an initial Mott insulator state on a $L = 10$ lattice. Solid line: numerical simulation; Dotted line: two-body decay law for an uncorrelated state $N(t) = N(0)/(1 + 2\Gamma t)$. Middle: Same, but for a Tonks-Girardeau gas initial state (ground state of a hard core lattice gas with $L = 10, N = 6$). Solid line: simulation. Green dashed curve: two-body decay law for an uncorrelated state. $N(t) = N(0)/(1 + 2\Gamma t)$, Dotted line: two-body decay low assuming time independent correlations $N(t) = N(0)/(1 + 2g^{(2)}(0)n(0)\Gamma t)$. Right: Average particle numbers in the different sectors $\langle N^{(n)}(t) \rangle = n \operatorname{Tr} \rho^{(n)}(t)$ for the Mott insulator initial state. The sum of all curves at a certain time gives the blue in the leftmost figure. All times measured in units of the inverse hopping J^{-1}.

of the atoms). The authors of Ref. [2] study two different experimental settings: a continuum model and a lattice experiment of bosonic molecules. We are interested in the lattice experiment, where the system is initially prepared in $n = 1$ Mott insulating state and one can ask what state is created after a large fraction of particles is lost. The basic questions we are asking are

- Beginning with MI, does one generate lower density coherent superfluid (or Tonks gas) after losing a large fraction of particles?

- If the losses create a state distinct from the superfluid, how much heating/entropy is generated?

- Can these losses be used as a tool? For example strong induced two-body losses should probe local correlation functions. Measuring such correlation functions could be valuable tool to detect magnetic order in optical lattices.

9.2 Abstract

We study entropy generation in a one-dimensional (1D) model of bosons in an optical lattice experiencing two-particle losses. Such heating is a major impediment to observing exotic low temperature states, and "simulating" condensed matter systems. Developing intuition through numerical simulations, we present a simple empirical model for the entropy produced in this 1D setting. We also explore the time evolution of one and two particle correlation functions, showing that they are robust against two-particle loss. Because of this robustness, induced two–body losses can be used as a probe of short range magnetic correlations.

9.3 Introduction

As cold gas experimentalists turn their attention towards more strongly correlated states (such as Mott insulators and fractional quantum Hall states) they find that equilibration times become large. This is problematic: inelastic processes limit the time over which one can conduct an experiment, and the experimentalists find themselves in a race. Can the system equilibrate before the entropy generated by the inelastic processes destroy the state of interest? A similar issue arises when the experimental protocol involves some sort of "adiabatic" change of parameters (such as ramping up the intensity of an optical lattice): can the adiabatic ramp be completed before inelastic processes take over? Here we explore a simple one dimensional (1D) model where one can quantitatively study the entropy generated by two-body losses. Within this model we find that the entropy produced by each recombination event is of order the logarithm of

the number of atoms, highlighting the difficulty faced by future experiments. We hope that quantitative studies of such inelastic processes can help overcome them – though we see no simple solution at this point and time. On a more positive note, we find that within our model the inter-atomic correlations are largely time independent, even in the presence of drastic atom loss. Thus even with atom loss one can confidently measure the inter-atomic correlations of an initial state of interest. While one hopes that this result is generic, it is possible that the robustness of the correlations is an artifact of 1D, where the dynamics are non-ergodic. To test this we have looked at small 2D clusters, finding nearly identical results. Extrapolating to more complex systems, we give an explicit example of how one could use losses to measure nearest neighbor antiferro-magnetic correlations in a two component Fermi gas.

The problem of heating due to atom losses goes back to the first attempts to experimentally create degenerate Fermi gases [3, 1]. Then it was pointed out that while atom losses are relatively benign in a Bose condensate, they have drastic consequences for a degenerate Fermi gas. Randomly removing particles from a Fermi sea generates large amounts of entropy.

Here we consider a version of a model introduced by Verstraete et al. [4]. This and related models were explored in a number of theoretical and experimental works [4, 5, 6, 7, 8, 9, 10, 2, 11]. The original model consists of a gas of bosons moving in a 1D lattice. Whenever two bosons are on the same site they recombine with rate Γ_0. The composite object which they form is then lost. This model could describe a gas of molecules (where a recombination mechanism always exists) or a gas of atoms (where light assisted collisions provide a re-combination mechanism). Most experiments are engineered to minimize these

two-body losses. They can intentionally be made stronger [12] and also occur in near-resonant optical traps, such as the blue-detuned lattices used by Schneider *et al.* [13].

When Γ_0 is sufficiently high, or in the presence of strong on-site interactions, one can integrate out the doubly occupied sites, producing a model with hard-core interactions and a nearest neighbor loss term. Mathematically the time evolution of this dissipative system is then given by a Master equation

$$\begin{aligned}
\frac{d\rho}{dt} &= -\frac{i}{\hbar}[H, \rho] \\
&+ \Gamma \sum_{\langle i,j \rangle} \left[a_i a_j \rho a_j^\dagger a_i^\dagger - \frac{1}{2} \left(n_i n_j \rho + \rho n_i n_j \right) \right],
\end{aligned} \tag{9.1}$$

where the conservative part of the dynamics are described by the Hamiltonian

$$H = -J \sum_{\langle i,j \rangle} a_i^\dagger a_j + a_j^\dagger a_i. \tag{9.2}$$

In these equations, a_i is the operator which annihilates an atom at site i, J is the tunneling matrix element, ρ is the density matrix, $\hbar$ is the reduced Planck's constant, $\langle i, j \rangle$ denotes nearest neighbor sites, $1/\Gamma$ is the time it takes for atoms at nearest neighbor sites to recombine. These equations implicitly assume that one works in a Hilbert space where each site is occupied by only zero or one particle. The remarkable result found in previous work is that Γ scales inversely Γ_0. Thus when $\Gamma_0 \to \infty$, the dynamics become conservative, coinciding with those of a hard-core gas of particles, a lattice Tonks-Girardeau gas.

We are interested in how entropy and correlations evolve with time in this model when $\Gamma \ll J$, but $\Gamma \neq 0$. For example, suppose one begins at time $t = 0$ in an N-particle Tonks state. As time evolves atoms are lost, until the system has $N' < N$ particles. Does the system adiabatically evolve into a N' particle Tonks gas (or an ensemble of such gases with a different particle numbers)? We

find that this is not the case. As we describe below, we find that the N' parti-cle system is better described by the initial N-particle Tonks state with random atoms removed. This is a high entropy state. Despite its highly non-equilibrium character, it inherits the two-particle correlations of the initial N-particle Tonks gas. These correlations, which are very different from what one expects for the N'-particle Tonks gas, are directly measurable, and greatly impact the behavior of the system.

9.4   Numerical Approach

To solve the Master equation in Eq. (9.1), we consider a small chain of length L. We numerate all 2^L possible many-body states in which no more than one particle sits on each site. We explicitly write the density matrix in this basis as a $2^L \times 2^L$ matrix, and express Eq. (9.1) as a coupled system of equations for the 2^{2L} matrix elements. Note the time evolution does not create coherences between states of different particle number. This lack of coherence represents the fact that recombination events at different places/time are in principle distinguish-able. Consequently the density matrix is block diagonal, and for even number of particles N can be written

$$\rho = \rho^{(0)} \oplus \rho^{(2)} \oplus \ldots \oplus \rho^{(N)} \tag{9.3}$$

where $\rho^{(n)}$ is the $\binom{L}{n}$-dimensional density matrix for the sector with n particles. We use a split-step method for our time evolution – alternating the exact Hamil-tonian dynamics with the exact dissipative dynamics. We vary our time step to verify that our results are independent of the time step. We find that it is im-practical to take $L > 12$, as the Hilbert space becomes too large. We typically
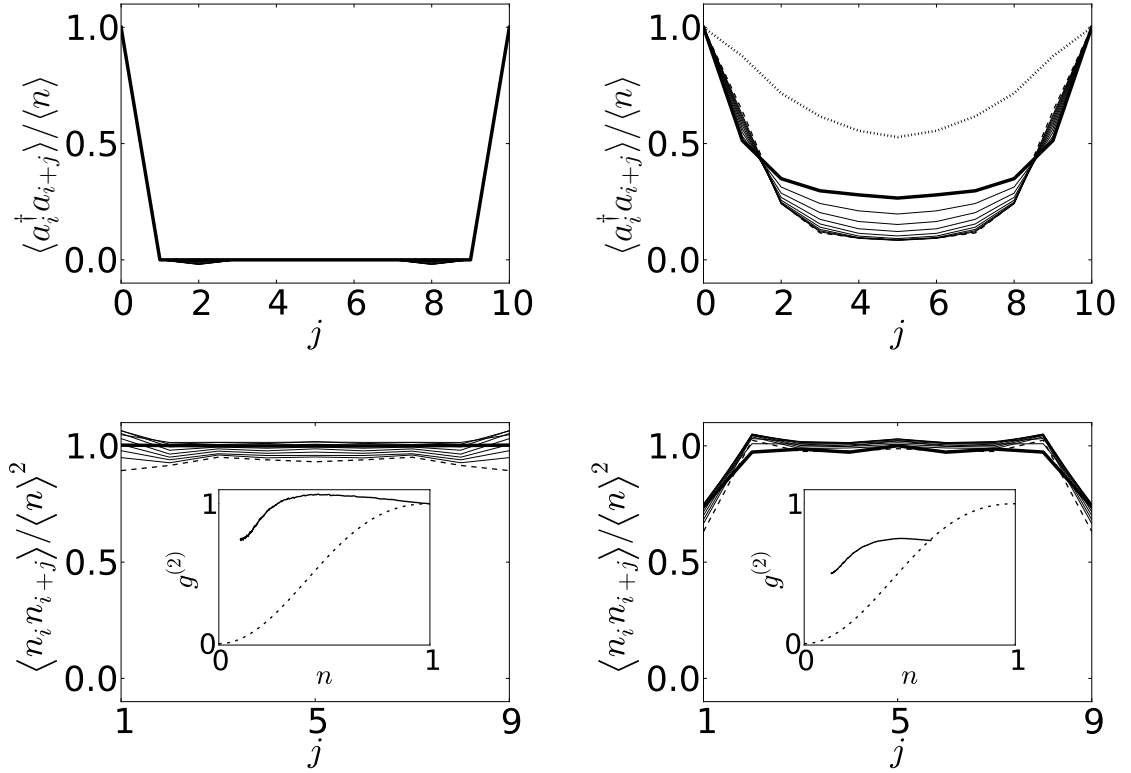
Figure 9.2: Time evolution of correlation functions starting from (left) the 10 particle Mott Insulator ($L = 10, N = 10$) or (right) the 6 particle Tonks-Girardeau state ($L = 10, N = 6$). Thick line: $t = 0$; Dashed line: $t = 200J^{-1}$; Thin lines: intermediate times separated by $20J^{-1}$; Dotted line: The single particle density matrix $\langle a_i^\dagger a_{i+j} \rangle$ one would expect if each of the n-particle sectors were in their ground state at $t = 200J^{-1}$. The insets of the lower-left and lower-right figures show $g^{(2)}$ as a function of density $n = N/L$ together with the analytic formula for an infinite hardcore boson system in the ground state at the same density $g_{\text{eq}}^{(2)}(n) = 1 - [\sin(\pi n)/(n\pi)]^2$.

quote results using $L = 10$ or $L = 12$.

Other approaches, such as the Density Matrix Renormalization Group can be applied to this problem [7], allowing one to consider larger systems, but making some observables more difficult to calculate

9.5 Time evolution of the density

As described by García-Ripoll et al. [7], the time evolution of the density in this model can be understood by a rather simple argument. One begins by noting that the rate of change of the number of atoms at a site only depends on the correlations between particles on nearby sites:

$$\frac{d\langle n_i \rangle}{dt} = -\Gamma \left[\langle n_i n_{i+1} \rangle + \langle n_i n_{i-1} \rangle \right] \tag{9.4}$$

Translational invariance implies that the two terms in brackets are equal to one-another, and one can write

$$\frac{dn}{dt} = -2\Gamma g^{(2)} n^2(t) \tag{9.5}$$

where $g^{(2)} = \langle n_i n_{i+1} \rangle / \langle n_i \rangle^2$ measures pair correlations and is related to the probability for finding two particles on neighboring sites. (Note: this differs from the definition of $g^{(2)}$ in [2].) For uncorrelated sites, such as one finds in the Mott insulator, one has $g^{(2)} = 1$. As we will directly illustrate in section 9.6, when $n < 1$, the exact ground state of H has $g^{(2)} < 1$, and these equilibrium correlations are strongly number dependent. Despite this behavior of the equilibrium correlations, the time evolution in Eq. (9.1) leaves the initial correlations nearly unchanged: $g^{(2)}(t) \approx g^{(2)}(t = 0)$. The degree to which this holds will be quantified below. If one treats the correlations as static one finds

$$n(t) = \frac{n(0)}{1 + 2t\Gamma n(0) g^{(2)}(0)}. \tag{9.6}$$

Variations on this equation have appeared in the literature [7, 2], which can be interpreted as different models for $g^{(2)}(t)$.

Figure 9.1 (a,b) compares the time evolution found from the Master equation with that from Eq. (9.6). Panel (a) shows the evolution beginning from a Mott

state (with $g^{(2)}(t=0)=1$), while panel (b) shows the decay of a correlated state. Panel (c) shows the weight in each of the different particle number channels.

Similar results for the decay of the Mott insulator were found in [2]. In particular, García-Ripoll et al. [7] used a Density Matrix Renormalization Group simulation to show that the observations in Fig. 1(a) are independent of system size. In the remainder of this paper we extend these results, directly analyzing the time dependence of correlations and entropy.

9.6 Time evolution of two-site observables

We quantify the time evolution of the correlations by studying two objects: the single particle density matrix $\langle a_i^\dagger a_{i+j}\rangle/\langle n\rangle$, and the density-density correlations function $\langle n_i n_{i+j}\rangle/\langle n\rangle^2$. The equilibrium value of the latter correlation function is efficiently calculated by performing a Jordan-Wigner transformation and mapping the hard-core Bose gas onto a gas of non-interacting Fermions. In particular, in the thermodynamic limit the equilibrium nearest neighbor density-density correlator at density n is

$$g_{\text{eq}}^{(2)}(n) = 1 - \left(\frac{\sin \pi n}{\pi n}\right)^2 \tag{9.7}$$

As already emphasized, we see large deviations from this equilibrium prediction.

Figure 9.2 shows the time dependence of the correlation functions for the two initial conditions previously explored. The two figures on the left show the behavior of the Mott state. Not only are the density correlations largely time independent, but so is the single-particle density matrix. One immediate

implication is that the atom momentum distribution (and hence a time-of-flight image) is unchanged by the loss. The inset of the lower left figure compares the $g^{(2)}$ extracted from our simulations to Eq. (9.7)

As shown by the two figures on the right, the dynamics from the Tonks state also leads to nearly time independent correlation functions. As time evolves there is a very slight drop in the nearest neighbor density correlations, and the single particle density matrix begins to fall off more rapidly with distance. This redistribution of the off-diagonal weight of the single particle density matrix corresponds to a shift of particles to larger momentum. Interestingly, this is the opposite of what one would expect if one instead modeled the dynamics as just an adiabatic change in the number of particles. The inset to the top-right figure shows the equilibrium single particle density matrix (corresponding to the number of particles are at time $t = 200 J^{-1}$). The slower slower spatial variation of the equilibrium $\langle a_i^\dagger a_{i+j} \rangle / \langle n \rangle$, corresponds to a lower occupation of large k states. This is intuitively sensible, since when $n = 1$ one should have only the $k = 0$ state occupied.

In addition to being conceptually important, these correlation functions are directly observable. For example a time of flight measurement of the momentum distribution (as was for example done in [14]) yields the Fourier transform of the single particle density matrix. The full density-density correlation function can be studied within experiments with single-site resolution such as [15]. Alternatively noise correlation measurements [16] or elastic light scattering [17] also probe this static structure factor.

9.7 Entropy

We now proceed to calculate the entropy

$$S(t) = -\operatorname{Tr}\rho(t)\ln\rho(t).\tag{9.8}$$

For ultra-cold atom experiments, where one is dealing with a small isolated system, the entropy is a more relevant than the temperature. This is especially true here, where the dynamics take one out of thermal equilibrium.
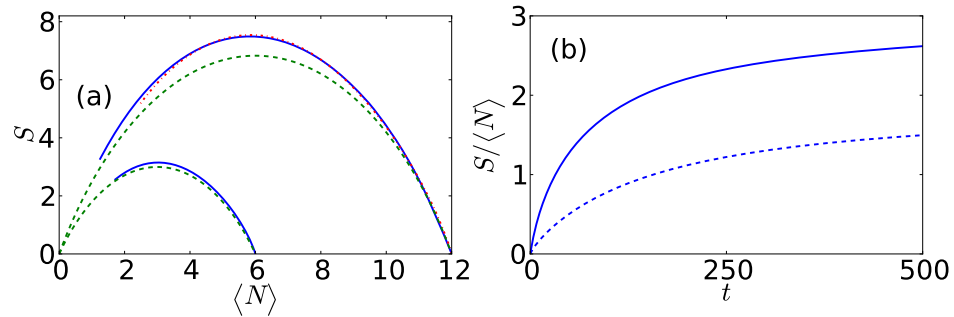
Figure 9.3: Left: Entropy S as a function of average particle number $\langle N\rangle$ during time evolution, starting from the (top, solid line) $L = 12, N = 12$ Mott insulator, (top, dashed-dotted line) 4×3, $N = 12$ (2D) Mott insulator and (bottom, solid line) $L = 12, N = 6$ Tonks-Girardeau initial states. Dashed line: analytic formula $S \sim \ln\binom{N(0)}{N}$. Right: Entropy per particle as a function of time starting from the (solid line) $L = 12$, $N = 12$ Mott Insulator and (dashed line) $L = 12$, $N = 6$ Tonks-Girardeau state with $\Gamma = 0.01J$.

It is convenient, as in Fig. 9.3, to parametrically plot $S(t)$ as a function of $N(t)$. For $\Gamma \ll J$ the resulting curve is then independent of Γ. We find that the entropy is well approximated by the simple law

$$S(N) \sim \ln\binom{N_0}{N},\tag{9.9}$$

where N_0 is the number of particles at $t = 0$.

There is a particularly simple interpretation of this result when one starts in the Mott insulating state. The entropy in Eq. (9.9) is what one would find if

one randomly punched holes in the Mott insulator. One would naively expect Eq. (9.9) to be an upper bound to the entropy, yet the numerical simulations find an entropy which is strictly above this curve. The extra entropy principally comes from the fact there is an indefinite number of particles. When the Mott insulator is depleted to half-filling the entropy is maximal and one has an entropy per particle of (for $L, N \to \infty$)

$$S/N \sim 2\ln(2) \approx 1.4. \tag{9.10}$$

A similar interpretation can be produced for the entropy of a depleted Tonks-Girardeau gas. There it is convenient to map the system onto a gas of non-interacting fermions via a Jordan-Wigner transform. The fermions initially occupy N_0 different momentum states. If one randomly removes fermions from momentum states one arrives at the entropy in Eq. (9.9). This is similar to the arguments of Timmermans, where a trapped noninteracting Fermi gas in three dimensions was considered [1]. Again, the simulation finds an entropy slightly larger than this estimate.

To understand the applicability of our results to higher dimensional systems, we have performed simulations of a two dimensional (2D) hardcore Bose gas on a rectangular square lattice geometry with a dimension of 4×3 sites and periodic boundary conditions. The result for entropy vs. particle number is also shown in Fig. 9.3 (a) and is almost identical to what we found in a 1D system with the same number of lattice sites.

9.8 Induced losses as a probe of local spin correlations

Our observation that initial correlations are preserved during time evolution makes two-body losses an extremely powerful probe of cold atoms. Losses have long been recognized as a probe of correlations, but have always been viewed as quite invasive [18, 2, 19, 20, 21, 11]. We find that two-body losses are a reliable way to learn about the *initial* correlations, even when a large fraction of the atoms are depleted.

As a particular example, we now describe how photoassociation induced losses [22, 18, 12] may be used to measure short-range magnetic correlations in two-species lattice bosons or fermions in the $n = 1$ Mott insulating phase [23]. This approach complements methods that detect long range order, such as noise correlations and light scattering [24, 17]. Section 9.8.1 will discuss the fermionic case, while section 9.8.2 will deal with bosons.

We wish to emphasize that this weak photassociation approach is very different from a *sudden* probe such as sweeping the system through a Feshbach resonance or photoassociating the system using a STIRAP protocol [13, 25]. In those latter approaches the signal size is limited by the instantaneous number of doubly occupied sites, which scales as J/U. For the weak probes used here, however, one can remove a large fraction of the atoms.

The nearest neighbor spin correlations are a smooth function of temperature [26], and represent an important precursor of the magnetic order which sets in on temperatures $T \sim J_s$, where J_s is the coupling constant in the effective spin model. Alternative approaches to measure these correlations use lattice modulation spectroscopy [27] or manipulation of double well potentials

combined with band mapping [28].

9.8.1 Two species fermions

We consider a two-species Fermi gas in a deep optical lattice that can be described by a Hubbard-model

$$H = -J \sum_{\langle i,j \rangle, \sigma=\uparrow,\downarrow} \left(c_{i\sigma}^\dagger c_{j\sigma} + c_{j\sigma}^\dagger c_{i\sigma} \right) + U \sum_i n_{i,\uparrow} n_{i,\downarrow} \tag{9.11}$$

We envision introducing a photoassociation laser which drives two atoms on the same site into a molecular state, which is lost from the system. The bare loss rate Γ_0, depends on the intensity of the photoassociation laser, as well as details of the atomic/molecular states. Integrating out the doubly-occupied sites produces a master equation similar to Eq. (9.1), which can formally be represented as a a complex Hamiltonian

$$H_F = \left(\tilde{J}_F + i4\Gamma \right) \sum_{\langle i,j \rangle} \left(\mathbf{S}_i \cdot \mathbf{S}_j - \frac{1}{4} n_i n_j \right) \tag{9.12}$$

with $\tilde{J}_F = 4J^2 U_0/(U_0^2 + (\Gamma_0/2)^2)$ and $\Gamma = J^2(\Gamma_0/2)/(U_0^2 + (\Gamma_0/2)^2)$. We envision letting the system equilibrate with the photoassociation lasers turned off ($\Gamma_0 = 0$). The lasers are then turned on at a low enough intensity that $\tilde{J}_F \approx J_F$. The subsequent density evolution will then be described by

$$\frac{dn}{dt} = -q\Gamma g_{\uparrow\downarrow}^{(2)} n^2(t) \tag{9.13}$$

where q is the number of nearest neighbors and the correlation function $g_{\uparrow\downarrow}^{(2)}$ is given by

$$g_{\uparrow\downarrow}^{(2)} = \langle n_i n_j - 4\mathbf{S}_i \cdot \mathbf{S}_j \rangle / \langle n_i \rangle^2 \tag{9.14}$$

The initial two-body loss coefficient is proportional to $g_{\uparrow\downarrow}^{(2)}(t=0) = 1 - 4\langle \mathbf{S}_i \cdot \mathbf{S}_j \rangle$ and provides a direct measure of nearest neighbor spin correlations.

9.8.2 Two species bosons

For an $n = 1$ Mott insulator of a two-species Bose gas one can similarly measure local spin correlation functions. Integrating out doubly occupied sites, the Hamiltonian of such a system is formally [29]

$$H_B = \sum_{\langle i,j \rangle} J_z S_i^z S_j^z - J_\perp \left(S_i^x S_j^x + S_i^y S_j^y \right) \tag{9.15}$$

$$+ \frac{h}{2} \left(S_i^z n_j + n_i S_j^z \right) - V n_i n_j.$$

In the absence of losses, the coupling constants are related to the hopping rate of the two species $(J_\uparrow, J_\downarrow)$, and the on-site interactions between same $(U_{\uparrow\uparrow}, U_{\downarrow\downarrow})$ and different $(U_{\uparrow\downarrow})$ species,

$$J_\perp = \frac{4 J_\uparrow J_\downarrow}{U_{\uparrow\downarrow}}; \quad h = 4 \left[\frac{J_\downarrow^2}{U_{\downarrow\downarrow}} - \frac{J_\uparrow^2}{U_{\uparrow\uparrow}} \right] \tag{9.16}$$

$$J_z = J_\uparrow^2 \left[\frac{2}{U_{\uparrow\downarrow}} - \frac{4}{U_{\uparrow\uparrow}} \right] + J_\downarrow^2 \left[\frac{2}{U_{\uparrow\downarrow}} - \frac{4}{U_{\downarrow\downarrow}} \right] \tag{9.17}$$

$$V = J_\uparrow^2 \left[\frac{1}{2 U_{\uparrow\downarrow}} + \frac{1}{U_{\uparrow\uparrow}} \right] + J_\downarrow^2 \left[\frac{1}{2 U_{\uparrow\downarrow}} + \frac{1}{U_{\downarrow\downarrow}} \right] \tag{9.18}$$

With a two species Bose gas one can selectively address three different photoassociation transitions($\uparrow\uparrow\to$molecule, $\uparrow\downarrow\to$molecule and $\downarrow\downarrow\to$molecule). This versatility may be used to measure a variety of nearest-neighbor spin-correlation functions. For example, driving a photoassociation resonance that converts an $\uparrow$- and a $\downarrow$-boson into a molecule can be formally described by substituting $U_{\uparrow\downarrow} \to U_{\uparrow\downarrow} - i\Gamma_{\uparrow\downarrow}^0/2$. Specializing to the case $J_\uparrow = J_\downarrow = J$, corresponding to a typical optical lattice setup, one has

$$H = \sum_{\langle i,j \rangle} \left[\tilde{J}_z S_i^z S_j^z - \tilde{J}_\perp \left(S_i^x S_j^x + S_i^y S_j^y \right) \right. \tag{9.19}$$

$$+ \frac{h}{2} \left(S_i^z n_j + n_i S_j^z \right) - \tilde{V} n_i n_j \Bigg]$$

$$- i4\Gamma_{\uparrow\downarrow} \sum_{\langle i,j \rangle} \left[\frac{1}{4} n_i n_j - S_i^z S_j^z + S_i^x S_j^x + S_i^y S_j^y \right]$$

where $\tilde{J}_\perp = 4J^2 U_{\uparrow\downarrow}/[U_{\uparrow\downarrow}^2 + (\Gamma_{\uparrow\downarrow}^0/2)^2]$, $\tilde{J}_z = 4J^2 U_{\uparrow\downarrow}/[U_{\uparrow\downarrow}^2 + (\Gamma_{\uparrow\downarrow}^0/2)^2] - 4J^2(1/U_{\uparrow\uparrow} + 1/U_{\downarrow\downarrow})$, $\tilde{V} = J^2/[U_{\uparrow\downarrow}^2 + (\Gamma_{\uparrow\downarrow}/2)^2] + J^2(1/U_{\uparrow\uparrow} + 1/U_{\downarrow\downarrow})$ and $\Gamma_{\uparrow\downarrow} = (\Gamma_{\uparrow\downarrow}^0/2)J^2/[U_{\uparrow\downarrow}^2 + (\Gamma_{\uparrow\downarrow}/2)^2]$. In this case two-body losses measure

$$g_{\uparrow\downarrow}^{(2)} = \langle n_i n_j - 4(S_i^z S_j^z - S_i^x S_j^x - S_i^y S_j^y)\rangle/\langle n_i\rangle^2 \tag{9.20}$$

where i, j are nearest neighbors. Alternatively one can photoassociate $\uparrow\uparrow\to$molecule to measure $g_{\uparrow\uparrow}^{(2)} = \langle n_i n_j + 4S_i^z S_j^z + 2(S_i^z n_j + n_i S_j^z)\rangle/\langle n_i\rangle^2$. Photoassociating $\downarrow\downarrow\to$molecule flips the sign of S_z, giving $g_{\downarrow\downarrow}^{(2)} = \langle n_i n_j + 4S_i^z S_j^z - 2(S_i^z n_j + n_i S_j^z)\rangle/\langle n_i\rangle^2$. Simultaneously photoassociating $\uparrow\uparrow$ and $\downarrow\downarrow$ at the same rate allows measurement of $(g_{\uparrow\uparrow}^{(2)} + g_{\downarrow\downarrow}^{(2)})/2 = \langle n_i n_j + 4S_i^z S_j^z\rangle$.

For a Mott insulating state of two species bosons, the expression in Eq. (9.20) simplifies to $g_{\uparrow\downarrow}^{(2)}(t = 0) = 1 - 4\langle S_i^z S_j^z - S_i^x S_j^x - S_i^y S_j^y\rangle$. Linear combinations of $g_{\uparrow\downarrow}^{(2)}, g_{\uparrow\uparrow}^{(2)}, g_{\downarrow\downarrow}^{(2)}$ probe $\langle \mathbf{S}_i \cdot \mathbf{S}_j\rangle$, $\langle S_i^z S_j^z\rangle$ and $\langle S_i^x S_j^x + S_i^y S_j^y\rangle$.

Generically, for both bosons and fermions, the spin correlations at low temperatures tend to increase the loss rate. The ferromagnetic super-exchange in a Bose system encourages same-species atoms to sit next to each other, which due to Bose enhancement leads to an increased probability of doubly-occupying a site. The antiferromagnetic super-exchange in a Fermi system enhances the probability of up-spins lying beside down-spins, increasing the chance that they will end up on the same site.

BIBLIOGRAPHY FOR CHAPTER 9

[1] Eddy Timmermans, Phys. Rev. Lett. **87**, 240403 (2001).

[2] N. Syassen, D. M. Bauer, M. Lettner, T. Volz, D. Dietze, J. J. Garcia-Ripoll, J. I. Cirac, G. Rempe, and S. Durr, Science **320**, 1329 (2008).

[3] B. DeMarco and D. S. Jin, Science **285**, 1703 (1999).

[4] F. Verstraete, J. J. García-Ripoll, and J. I. Cirac, Phys. Rev. Lett. **93**, 207204 (2004).

[5] B. Kraus, H. P. Büchler, S. Diehl, A. Kantian, A. Micheli, and P. Zoller, Phys. Rev. A **78**, 042307 (2008).

[6] S. Diehl, A. Micheli, A. Kantian, B. Kraus, H. P. Büchler, and P. Zoller, Nat. Phys. **4**, 878 (2008).

[7] J J García-Ripoll, S Dürr, N Syassen, D M Bauer, M Lettner, G Rempe, and J I Cirac, New Journal of Physics **11**, 013053 (2009).

[8] A. J. Daley, J. M. Taylor, S. Diehl, M. Baranov, and P. Zoller, Phys. Rev. Lett. **102**, 040402 (2009).

[9] S. Dürr, J. J. García-Ripoll, N. Syassen, D. M. Bauer, M. Lettner, J. I. Cirac, and G. Rempe, Phys. Rev. A **79**, 023614 (2009).

[10] A. Kantian, M. Dalmonte, S. Diehl, W. Hofstetter, P. Zoller, and A. J. Daley, Phys. Rev. Lett. **103**, 240401 (2009).

[11] M. Roncaglia, M. Rizzi, and J. I. Cirac, Phys. Rev. Lett. **104**, 096803 (2010).

[12] M. Junker, D. Dries, C. Welford, J. Hitchcock, Y. P. Chen, and R. G. Hulet, Phys. Rev. Lett. **101**, 060406 (2008).

[13] U. Schneider, L. Hackermuller, S. Will, Th. Best, I. Bloch, T. A. Costi, R. W. Helmes, D. Rasch, and A. Rosch, Science **322**, 1520 (2008).

[14] B. Paredes, A. Widera, V. Murg, O. Mandel, S. Foelling, I. Cirac, G. V. Shlyapnikov, T.W. Haensch, and I. Bloch, Nature **429**, 277 (2004).

[15] W. S. Bakr, J. I. Gillen, A. Peng, S. Fölling, and M. Greiner, Nature **462**, 74 (2009).

[16] A. Imambekov, I. E. Mazets, D. S. Petrov, V. Gritsev, S. Manz, S. Hofferberth, T. Schumm, E. Demler, and J. Schmiedmayer, Phys. Rev. A **80**, 033604 (2009).

[17] T. A. Corcovilos, S. K. Baur, J. M. Hitchcock, E. J. Mueller, and R. G. Hulet, Phys. Rev. A **81**, 013415 (2010).

[18] Toshiya Kinoshita, Trevor Wenger, and David S. Weiss, Phys. Rev. Lett. **95**, 190406 (2005).

[19] Gyu-Boong Jo, Ye-Ryoung Lee, Jae-Hoon Choi, Caleb A. Christensen, Tony H. Kim, Joseph H. Thywissen, David E. Pritchard, and Wolfgang Ketterle, Science **325**, 1521 (2009).

[20] M. Popp, B. Paredes, and J. I. Cirac, Phys. Rev. A **70**, 053612 (2004).

[21] Edina Sarajlic, Nathan Gemelke, Sheng-Wey Chiow, Sven Herrman, Holger Müller, and Steven Chu, in *Pushing the Frontiers of Atomic Physics: Proceedings of the XXI International Conference on Atomic Physics, Storrs, CT*, edited by R. Côté, P. L. Gould, M. Rozman, and W.W. Smith (World Scientific, Singapore, 2008), p. 34.

[22] Tim Rom, Thorsten Best, Olaf Mandel, Artur Widera, Markus Greiner, Theodor W. Hänsch, and Immanuel Bloch, Phys. Rev. Lett. **93**, 073002 (2004).

[23] David M. Weld, Patrick Medley, Hirokazu Miyake, David Hucul, David E. Pritchard, and Wolfgang Ketterle, Phys. Rev. Lett. **103**, 245301 (2009).

[24] Ehud Altman, Eugene Demler, and Mikhail D. Lukin, Phys. Rev. A **70**, 013603 (2004).

[25] Matt Mackie, Ryan Kowalski, and Juha Javanainen, Phys. Rev. Lett. **84**, 3803 (2000).

[26] Simone Chiesa, Christopher N. Varney, Marcos Rigol, and Richard T. Scalettar, Phys. Rev. Lett. **106**, 035301 (2011).

[27] C. Kollath, A. Iucci, I. P. McCulloch, and T. Giamarchi, Phys. Rev. A **74**, 041604 (2006).

[28] I. Bloch, 2010, (unpublished).

[29] A. B. Kuklov and B. V. Svistunov, Phys. Rev. Lett. **90**, 100401 (2003).